THE UNIVERSITY *of* EDINBURGH

A lattice QCD study of octet hyperon semi-leptonic decays

Ashley N. Cooke

Doctor of Philosophy
University of Edinburgh
2014

For my mother, Donna.

Declaration

I declare that this thesis was written by myself and that work was carried out by me, as a memeber of the QCDSF-UKQCD collaboration. The work presented within has not been submitted for any other degree or professional qualification.

Gauge configurations were generated by the collaboration and simulations were performed using the Chroma software suite. Analysis was carried out using code designed by myself and based upon previous collaboration software. Baryon masses were calculated previously by the collaboration and used in analysis here. I generated all propagators and correlation functions of the $24^3 \times 48$ lattice ensembles while all $32^3 \times 64$ data is courtesy of Dr. James Zanotti of the CSSM and QCDSF-UKQCD collaborations.

Determination of the terms appearing in the paramaterisation of $SU(3)$-symmetry breaking at first order was carried out by Dr. Paul Rakow of the QCDSF-UKQCD collaboration. Results presented here have also appeared in:

- A. N. Cooke et al. The effects of flavour symmetry breaking on hadron matrix elements. *PoS*, LATT2012:116, 2012. [arXiv:1212.2564 [hep-lat]].
- A. N. Cooke et al. $SU(3)$ flavour breaking and baryon structure. *PoS*, LATT2013:278, 2013. [arXiv:1311.4916 [hep-lat]].

Ashley N. Cooke

Acknowledgements

I would like to thank Roger Horsley and Brian Pendleton. I have been very lucky to have supervisors who put so much time and effort into my education. A big thanks to James Zanotti for my initial supervision and for always being willing to help, even after moving to the far side of the planet! I want to thank the QCDSF-UKQCD collaboration, especially Paul Rakow for stimulating discussion. Thanks to Vicent Mateu for his assistance and time spent answering our emails.

I am thankful to the PPT group in Edinburgh, especially to Tony Kennedy for his advice. Thanks to Richard Kenway and Peter Boyle for providing very helpful comments on my work throughout. Without the friendship of Nathan Hartland, Tom Metcalf and Eliana Lambrou I would not have stayed sane.

STRONGnet provided incredible opportunities and support structures for which I was exceptionally lucky to avail of. I would like to thank Rainer Schiel, my STRONGnet mentor, who gave invaluable advice, on more than one occasion. I have gained some life-long friends through STRONGnet and I am thankful to them all; Valentina, Nemanja, Dmitry, Elena, Axel, Ydalia, Graham, Eoin, Shane, Aoife, Christian and many others. Pol, Mario and Eric I count as three of my best friends and to whom I am indebted; until next time guys!

Lastly, I would like to thank my family and friends for their encouragement despite not having a clue what it is I do. A special thanks to my girlfriend Edel for her unwavering love and attention. Finally, I attribute any successes I have to my mother. Her single-handed commitment to my education gave me the chance to achieve what I want from life. Thank you Mum.

Abstract

We present a calculation of vector and axial-vector form factors for each of the octet hyperon semi-leptonic transition matrix elements by using the techniques of lattice QCD where simulations were performed with $N_f = 2 + 1$ flavours of dynamical $\mathcal{O}(a)$-improved Wilson fermions. We also study the electromagnetic form factors, axial charges and other properties of octet baryons. Errors due to extrapolation to zero transferred momentum are reduced by applying a twist to the boundary conditions on the lattice. Our form factor results compare favourably with experiment and other lattice QCD determinations. By considering an expansion about the $SU(3)$-flavour symmetric limit we seek to investigate and quantify the symmetry breaking effects in these matrix elements due to the mass splitting between the strange and light quarks. We find good agreement with the Ademollo-Gatto theorem for the vector form factor, a measurable amount of breaking in the axial-vector form factor and significant effects in the weak magnetism form factor. Knowledge of the parameterisation of $SU(3)$-flavour symmetry breaking allows for a series of constrained fits to be made to the form factor results which are used to arrive at a 'baryonic' estimation of the Cabibbo-Kobayashi-Maskawa matrix element $|V_{us}|$.

Lay Summary

The Standard Model (SM) of particle physics provides a comprehensive description of many of the forces of nature and is one of the most successful scientific theories to date. There are some aspects of the physical world which are not covered by the SM however, such as the persistent difficulty of incorporating gravity into the picture or no existing explanation of the nature of dark energy. It is suspected then that there exists physics beyond the SM which has yet to be discovered.

This project seeks to test the SM and investigate whether the theory can fully account for certain physical processes called *flavour changing semi-leptonic decays*. These decays involve particles called baryons, such as the proton and neutron, which are made up of fundamental constituents called quarks. The quarks can change from one type (or *flavour*) to several other types according to a certain probability predicted by the SM which is known as a *CKM matrix element*. Investigating whether measurements match these predictions thus provides one avenue for testing the SM.

Experimental physicists measure decay rates in laboratories but this is not yet enough information to evaluate CKM matrix elements. One must also have knowledge of how the quarks behave via the strong nuclear force during such decays. The strong force is described mathematically by the theory of *Quantum Chromodynamics* (QCD). Due to the incredibly complicated nature of the strong force it is impossible to solve the equations of QCD to arrive at exact solutions.

It is possible however, to simulate these strong interactions on a computer using the tools of lattice QCD.

Using large scale lattice QCD computer simulations we can calculate quantities called form factors which encapsulate information about the complex strong force interactions. This work involves both computational calculations and also the use of the mathematical techniques of group theory in order to arrive at a precision estimation of these form factors.

Group theory provides an elegant and powerful way of understanding the relationship between physical processes. It is a mathematical discipline that involves the study of symmetries. Within the context of particle physics it has many useful applications and one which we are particularly concerned with in this work is that of *flavour symmetry breaking*. This involves investigating to what extent physics would change if we were to swap one flavour of quark for another within a physical process. We use group theory arguments along with simulation results to quantify how large the effect of flavour symmetry breaking is in the semi-leptonic decays of baryons.

We focus on the decays involving a change from a quark of 'strange' flavour changing to one of 'up' flavour and calculate the associated form factors. Having quantified the strength of flavour symmetry breaking we then go on to combine the form factors with experimental decay rate results to arrive at a value for the relevant CKM matrix element.

Contents

List of Figures

List of Tables

"Tús maith, leath na hoibre."

"A good start is half the work"

— Old Irish Proverb

Chapter 1

Introduction

1.1 Motivation

Present day high-energy physics has been successfully described by the Standard Model, a theoretical construction which includes the fundamental building blocks of the universe. This set of quantum field theories provide the mathematical framework in which to describe the possible interactions between elements of the model. Though gravity has proven difficult to incorporate successfully into this picture, the Lagrangian of the Standard Model embodies the strong and electroweak processes found in nature.

Quantum Chromodynamics (QCD) is the field theory describing the strong interactions. It has an unbroken symmetry group, $SU(3)$, associated with the 'colour' charge of the massless gauge bosons of the theory, gluons, and of the fundamental spin 1/2 spinor fields, dubbed quarks, which bind together to form hadrons such as protons and neutrons, along with more exotic matter. QCD can only be tackled perturbatively at high energies as it is strongly coupled non-Abelian gauge theory; the gauge bosons also interact amongst themselves. For the low energy regime one must employ non-perturbative methods to calculate, for example, the QCD spectrum or hadron matrix elements.

Lattice QCD is a non-perturbative tool that has seen much development in the past forty years. It allows for first principle calculations of low energy hadronic quantities by adopting a Monte Carlo approach to the calculation of path integrals on a finite-volume discretised lattice of points approximating space-time. A discrete version of the QCD action is developed and placed on this lattice which allows for large-scale computer simulations, the outcome being numerical results for physical observables. Lattice QCD has provided remarkably precise measurements of low energy quantities and we aim to use its techniques to evaluate form factors which can be compared with existing experimental results.

The quarks of QCD come in six 'flavours', which are found to have different masses. Significantly so, in certain cases. The Lie group $SU(3)$ plays another role here as an approximate symmetry of the three lightest flavour of quarks: the 'up', 'down' (collectively, 'light') and 'strange' quarks. This symmetry is broken due to the mass splitting between these quarks. The effects of flavour symmetry breaking are of great theoretical interest and it is part of our aim to quantify these effects on the matrix elements of octet hyperons (baryons containing strange quarks). Obviously it is impossible to test the impact of different quark masses in the real world, as nature has already decided on specific values for us, but Lattice QCD has no such restrictions aside from computational expense at very low quark masses.

The Standard Model also describes the electroweak sector and it is the weak force in particular which is important in our study of symmetry breaking. The weak force, mediated by massive $W^{\pm}$ and Z bosons, is flavour violating and provides the mechanism for transition between quark flavours and thus between baryon states, such as in the familiar beta decay of the neutron. This 'quark mixing', is understood within the framework of the Cabibbo theory and the Cabibbo-Kobayashi-Maskawa (CKM) unitary matrix. Hyperon form factors, which can be measured by experiment or calculated non-perturbatively using

Lattice QCD, can be combined with decay rate data to estimate the elements of the CKM matrix.

The Standard Model contains a profusion of parameters which cannot be known a priori, which in and of itself has prompted interest in the investigation of physics beyond the Standard Model. The matrix element $|V_{us}|$ is one of four of these parameters stemming from the CKM matrix and is of particular interest as a precision calculation of its value would allow one to verify if, in fact, the CKM matrix is unitary. A violation of unitarity would indicate deficiencies in the Standard Model and could be evidence for new physics.

1.2 Project Outline

Broadly speaking this study of octet hyperon semi-leptonic decays can be split into three distinct areas. The first of these is the calculation of the vector and axial-vector form factors defined through these decays. This involves setting out the background theory that governs strong interactions and weak transitions within the framework of the Standard Model. The necessary techniques and tools of Lattice QCD are outlined and explored, which can be used to calculate such form factors non-perturbatively. Results can be compared with experimental measurements of the same quantities. This provides the majority of the work within the project.

Secondly, an analytic approach to $SU(3)$-flavour symmetry breaking is taken so as to numerically quantify the effects of flavour symmetry breaking on hyperon strangeness changing transition form factors. Some of these form factors are theoretically predicted to not display any leading order effects of mass-splitting. Others have no such constraints and symmetry breaking effects may lead to significant deviations from the $SU(3)$ symmetry limit. The use of 'fan plots' will be prevalent in this study as they are useful in depicting the magnitude of

symmetry breaking. Finally, the evaluation of the parameters of flavour symmetry breaking allow for a constrained fit to form factor data which can be used to provide a 'baryonic' route to evaluating the parameter $|V_{us}|$ of the Standard Model.

Chapter 2 seeks to introduce the constituent fundamental particles of the Standard Model, in particular those interacting via the strong force. A brief overview of the properties of Quantum Chromodynamics, the generally accepted theory of the strong interaction, will be given in this chapter. The symmetries of the strong force are discussed and the path integral formalism of quantum field theory is introduced in preparation for its discretisation in Chapter 3. The concepts of $SU(2)$ and $SU(3)$ flavour symmetry are to be introduced in this chapter along with the baryon octet and decuplet representations of $SU(3)$.

Chapter 3 provides a summary of the basics of Lattice QCD to the reader. These methods and techniques provide the tools with which hyperon form factors will be computed non-perturbatively. Discretisation of space-time and the Wick rotation to Euclidean space are outlined in order to provide a sensible mathematical scheme suitable for numerical evaluation. Lattice actions for the gauge and fermion parts will be outlined along with some discussion of improvement procedures. An outline of how a simulation is performed follows, including discussion of some of the technical aspects of Lattice QCD methods, such as implementing twisted boundary conditions. In this chapter, two and three-point correlation functions are discussed, while their relationship to hyperon form factors is left for later chapters. Finally, the simulation details of this study are included at the end of the chapter.

Following this synopsis of QCD, Chapter 4 seeks to provide a similar treatment for the weak sector. An understanding of the essentials of the weak force is important to understand the process of hyperon semi-leptonic decays. A description of how theories of this force evolved are followed by an introduction

to the modern understanding of the weak force through various experimental observations and theoretical developments. Quark mixing and the Cabibbo-Kobayashi-Maskawa (CKM) are discussed in the context of their historical development, ending with sections on the properties of the CKM matrix which is crucial for motivating the need to evaluate the CKM matrix element $|V_{us}|$.

Chapter 5 is a longer chapter which aims to familiarise the reader with some key concepts surrounding hyperon semi-leptonic decays and the matrix elements of vector and axial-vector currents which will be calculated using Lattice QCD techniques. The hyperon form factors are introduced and the long-standing Cabibbo theory outlined in some detail, with emphasis on particular aspects including the Ademollo-Gatto theorem and the $SU(3)$-flavour symmetric limit of axial form factors. The most up-to-date experimental results available are summarised for comparative purposes. The link between Lattice QCD correlation functions and hyperon form factors is explained along with the necessary technical details of their calculation, including the form factors' momentum dependence.

Results for these vector and axial-vector form factors, using the lattice ensembles outlined in Chapter 3, will then be shown in Chapter 6. Results are qualitatively compared with the Cabibbo theory in regards to the effects of flavour symmetry breaking. Both diagonal and off-diagonal form factor results are presented. Axial charge results will be compared with other Lattice QCD results and chiral perturbation theory estimates while isovector magnetic moment values analysed in conjunction with recent $32^3 \times 64$ Lattice QCD results. Baryon spin fraction results are reported with focus on that of the Λ baryon. Transition form factors are compared with the experimental values given in the previous chapter.

The effects of flavour symmetry breaking discussed up to that point will have been in a qualitative fashion. In Chapter 7 our goal is to quantify the effects of $SU(3)$-flavour symmetry breaking seen in the hyperon form factor results of the preceding chapter. This is done through the parameterisation of first order mass

splitting in hyperon transitions; unique values for each form factor but which share a common structure amongst transitions, dictated by the symmetry group. A graphical presentation of fits to these parameters, known as a 'fan plot', has been developed by the QCDSF-UKQCD collaboration and is used extensively throughout this chapter. First order constrained fits to these parameters are used to reconstruct the hyperon form factors and reduce error.

Chapter 8 aims to use the results obtained for the hyperon form factors combined with a better understanding of the effects of $SU(3)$-flavour symmetry breaking to predict a new estimate of $|V_{us}|$. This 'baryonic' way of determining $|V_{us}|$ is less precise than other approaches but provides for a complimentary evaluation. The existing values of $|V_{us}|$ are summarised and a discussion of the necessary modifications to the decay rate is included. We present our result for $|V_{us}|$ using our Lattice QCD derived form factors, taking into account first order flavour symmetry breaking effects.

The final part of this study, Chapter 9, concludes the project. Here the previous chapters' developments and outcomes are reflected upon. We remind the reader of the central goals of this study and then seek to evaluate our work. The shortcomings of the approaches taken are also discussed along with suggestion of future modifications that could be made, in order to improve upon our efforts.

"Three quarks for Muster Mark!
Sure he hasn't got much of a bark
And sure any he has it's all beside the mark."
— James Joyce, *Finnegan's Wake*

Chapter 2

Quantum Chromodynamics

The Standard Model (SM) of particle physics covers three of the four fundamental forces of nature: the electromagnetic, weak nuclear and strong nuclear forces. It has been a very successful theory, built over decades, as it accurately describes the interactions between all fundamental particles known to exist, excluding the gravitational force [1].

These fundamental particles are called the quarks and leptons, collectively known as fermions; they have spin-1/2. Their interactions are mediated by spin-1 gauge bosons, and transform under a local $SU(3)_c \otimes SU(2)_L \otimes U(1)_Y$ internal symmetry. The quarks bind via gluonic interactions to form the hadrons which make up everyday matter, which can be further subdivided into the mesons and the baryons.

2.1 QCD in the Standard Model

Quarks and leptons are the fundamental constituents of matter and obey Fermi-Dirac statistics. These particles and their mediating gauge bosons are shown in Figure 2.1. The quarks are the only fermions which can interact with gluons while the neutrinos only feel the weak nuclear force (W and Z bosons).

Otherwise interactions between all fermions and forces occur. All fermions have corresponding anti-particles which have opposite quantum numbers. Gauge bosons are so called as the forces they represent are gauge invariant. The spin-0 Higgs boson is also a critical part of the SM, which is responsible for generating the mass of the matter fields and was recently discovered in 2013 at the Large Hadron Collider (LHC) [2, 3].

Some of the most interesting physics arising from the SM is due to the strong force. The particles interacting via the strong force are quarks and gluons which combine to form *hadrons*. Crucially, these particular mediating gauge bosons are also self-interacting. The strong sector of the SM is governed by Quantum Chromodynamics (QCD) which is a relativistic quantum field theory that provides the mathematical framework of quark/gluon interactions and has symmetry group $SU(3)_c$.

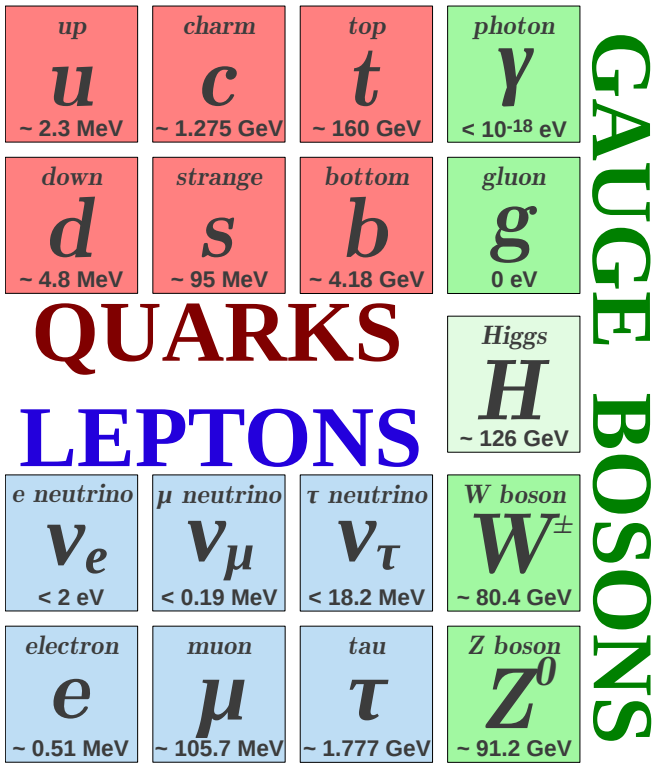

Figure 2.1: The particle content of the Standard Model of particle physics. Experimental particle masses are taken from PDG 2013 review [4].

The existence of quarks were first postulated in 1964 by Gell-Mann [5] and Zweig [6] independently of each other in order to explain the outcome of experiments performed in the '50s and '60s describing the low energy spectrum of hadronic states. Three quarks, the up (u), down (d) and strange (s), were originally hypothesised as a manifestation of flavour-$SU(3)$ as species of quarks are labelled by a 'flavour' naming convention. Experiments conducted at the Stanford Linear Accelerator Center (SLAC) confirmed that hadrons were indeed composite particles [7, 8].

Later, three more flavours of quark were discovered. Along with the charm (c) there were the bottom (b) and top (t) quarks. The quarks can be arranged into pairs of three *generations* where each pair has either electric charge $+\frac{2}{3}$ or $-\frac{1}{3}$:

$$\begin{pmatrix} u \\ d \end{pmatrix} \qquad \begin{pmatrix} c \\ s \end{pmatrix} \qquad \begin{pmatrix} t \\ b \end{pmatrix}$$

I II III.

We can refer to u, c and t ($Q = +\frac{2}{3}$) as *up-type* and d, s and b ($Q = -\frac{1}{3}$) as *down-type* quarks.

According to the Pauli exclusion principle it is impossible for fermions to have identical position and quantum states. To ensure the anti-symmetry of all observed hadron wavefuntions (Ψ), demanded by Fermi-Dirac statistics, it is necessary to introduce another quantum number [9] which was dubbed 'colour' (e.g. for the Δ^{++}). In Equation 2.1 $\Psi_{spatial}$ and $\Psi_{spin}\Psi_{flavour}$ can all be symmetric so an anti-symmetric Ψ_{colour} was required. Quarks have colour charge assignment red (r), green (g) or blue (b). Anti-particles have colour charge $\bar{r}$, $\bar{g}$ or $\bar{b}$.

$$\Psi_{total} = \Psi_{spatial}\Psi_{spin}\Psi_{flavour}\Psi_{colour} \tag{2.1}$$

Experiments have only found colour singlet states, meaning that gluons and quarks cannot exist as lone excitations; a phenomenon known as *confinement*.

These singlets typically manifest themselves as a quark anti-quark pair (meson) or three quarks (baryon) bound together once at sufficiently low energies. Baryons containing strange quarks can be referred to as *hyperons*. Some more exotic states of matter, such as tetraquarks are allowed by QCD but were not observed, however very recently a possible tetraquark signal was seen at the European Organization for Nuclear Research (CERN) [10]. Everyday matter consists mostly of hadrons made up of the three lighter quarks as the scale of QCD is larger than the masses of the lighter three quarks. The heavier quarks have negligible impact on low energy dynamics as they have significantly less time to form bound states before decaying into their lighter counterparts.

QCD is a non-Abelian gauge theory as the gluons also carry the colour charge and so they interact amongst themselves, in addition to the quarks. It is also the reason why the effective range of the strong force is not much larger than a few femtometres (fermi). The coupling constant of QCD, α_s, which denotes the strength of the attraction between colour-charged particles, decreases at high energies (asymptotic freedom [11,12]), which means that perturbative approaches only work at these energy scales. This is known as the *running* of the coupling. For the low energy sector of QCD, non-perturbative approaches such as Lattice QCD (LQCD) must be employed.

It should be pointed out that within the context of this work there are two kinds of $SU(3)$ symmetry which should not be confused: $SU(3)$-flavour and $SU(3)$-colour ($SU(3)_c$). Flavour $SU(3)$ symmetry, sometimes denoted $SU(3)_f$, is an approximate global symmetry arising from the near mass degeneracy of the u, d and s quarks. The $SU(3)$-colour symmetry is the gauge group of QCD and is a fundamental symmetry of the theory. The Lagrangian must thus be invariant under a local transformation of the quark colour charges.

2.2 QCD Lagrangian

The interactions of the strong force are governed by the QCD Lagrangian containing a Dirac part which describes the dynamics of the quarks ($\mathcal{L}_{\text{quark}}$) and an anti-symmetric field strength tensor term ($\mathcal{L}_{\text{gluon}}$) which is related to the interactions of the massless gauge bosons;

$$\begin{aligned}\mathcal{L}_{QCD} &= \mathcal{L}_{\text{quark}} + \mathcal{L}_{\text{gluon}} \\ &= \sum_{f=1}^{n_{\text{f}}} \bar{\psi}^f_\alpha (i\not{D}^\alpha_\beta - m^f)\psi^f_\beta - \frac{1}{4} F^\alpha_{\mu\nu} F^{\mu\nu}_\alpha,\end{aligned} \tag{2.2}$$

where ψ^f is a Dirac 4-spinor with flavour and colour components. Here we sum over the n_{f} quark flavours and the m^f refers to the mass of a particular quark flavour, the values of which are not known ab initio. The $\bar{\psi}^f = \psi^{f\dagger}\gamma^0$ is the adjoint spinor and along with ψ are anti-commuting Grassmann variables. The second term in Equation 2.2 is given later through definitions found in Equations 2.6 and 2.7. The Dirac operator $\not{D}$ is defined by

$$\not{D} = \gamma^\mu D_\mu = \gamma^\mu(\partial_\mu - igA_\mu), \tag{2.3}$$

where D_μ is the gauge covariant derivative, A_μ is the gluon field potential with Lorentz index ($\mu = 0, 1, 2, 3$) and g the dimensionless coupling constant of QCD, which is related to α_S by $\alpha_S = g^2/4\pi$. The γ^μ are known as the Dirac (or gamma) matrices and are given by the anti-commutation relations $\{\gamma_\mu, \gamma_\nu\} = 2g_{\mu\nu}$ (see Appendix A.1). The field potential, A_μ, is similar to the electromagnetic field but with an extra colour index, α,

$$A_\mu = \sum_{\alpha=1}^{8} T_\alpha A^\alpha_\mu, \tag{2.4}$$

with the generators of the $SU(3)$-colour group, $T_\alpha = \frac{\lambda_\alpha}{2}$, where λ_α are the *Gell-Mann* matrices. This group is an example of a *Lie group* and as such a *Lie algebra* for the $SU(3)$-colour group can be defined as

$$[T_\alpha, T_\beta] = i \sum_{\gamma=1}^{8} f_{\alpha\beta\gamma} T_\gamma, \tag{2.5}$$

where $f_{\alpha\beta\gamma}$ $(\alpha, \beta, \gamma = 1, ..., 8)$ are the structure constants of $SU(3)$ and they define the relationship between the commutators of the group generators. They are unique to the group. The structure constants, the generators and algebra of $SU(3)$ are further discussed in Appendix A.2.

Due to the non-abelian nature of the local gauge group of QCD the field strength tensor part must have a gluonic self-interacting term

$$F_{\mu\nu}(x) = \sum_{\alpha=1}^{8} T_\alpha F^\alpha_{\mu\nu}(x), \tag{2.6}$$

$$F^\alpha_{\mu\nu}(x) = \partial_\mu A^\alpha_\nu(x) - \partial_\nu A^\alpha_\mu(x) + g f^{\alpha\beta\gamma} A^\beta_\mu(x) A^\gamma_\nu(x). \tag{2.7}$$

Each individual flavour of quark couples to the gauge field in the same way, because the only difference between flavours, as far as the theory of QCD is concerned, is their mass.

A local $SU(3)$ gauge transformation of the field ψ is given by

$$\psi(x) \longrightarrow U\psi(x) = \exp\left[ig \sum_{\alpha=1}^{8} T_\alpha \theta^\alpha(x)\right] \psi(x), \tag{2.8}$$

where $\theta^\alpha(x)$ are real valued functions and parameterise rotations in $SU(3)$-colour space. The covariant derivative transforms in a similar way to the field ψ

$$D_\mu \psi \longrightarrow U D_\mu \psi. \tag{2.9}$$

The gluon fields transform infinitesimally as follows:

$$A^{\alpha}_{\mu} \longrightarrow A^{\alpha}_{\mu} - \frac{1}{g}\partial_{\mu}\theta^{\alpha} - \sum_{\beta,\gamma=1}^{8} f^{\alpha\beta\gamma}\theta^{\beta}A^{\gamma}_{\mu}, \tag{2.10}$$

which leads to the $SU(3)$ transformation

$$A^{\mu} \longrightarrow U(A_{\mu} - \frac{i}{g}\partial_{\mu})U^{\dagger}. \tag{2.11}$$

Finally the field strength tensor transforms as

$$F_{\mu\nu} \longrightarrow UF_{\mu\nu}U^{\dagger}. \tag{2.12}$$

The action of QCD, $\mathcal{S}_{QCD}$, is invariant under the discrete symmetries of charge conjugation (C), parity (P) and time reversal (T), along with products of these symmetries. The Lagrangian is invariant under Lorentz transformations and rotations in Minkowski space-time. An extra term can be included in $\mathcal{L}_{QCD}$ (equation 2.2), parameterised by an angle $\theta \in \{0, \pi\}$ that provides for the breaking of Charge Parity (CP) in the strong sector but experimentally it is found that $\theta \sim 0$ which has no theoretical underpinning. This is known as the *strong CP problem* [13].

It is useful to briefly introduce the functional integral, $\mathcal{Z}$, containing $\mathcal{S}_{QCD}$ which is central to the Feynman path integral formalism of QCD and critical to the calculations performed using LQCD which will be further discussed in Section 3.1;

$$\mathcal{Z} = \int \mathcal{D}[A, \bar{\psi}, \psi]e^{-i\int d^4x\mathcal{L}_{QCD}} = \int \mathcal{D}[A, \bar{\psi}, \psi]e^{-i\mathcal{S}_{QCD}}. \tag{2.13}$$

This formulation was developed by Feynman [14] and replaces the concept of a particle having a single trajectory in space-time with a functional integral which

posits that a particle takes infinitely many trajectories weighted by a complex phase containing the action. In a Quantum Field Theory (QFT), such as QCD, it is a central goal to compute expectation values of observables, which are operators made up of products of the fields of the theory. The expectation value of a physical observable, denoted by operator $\mathcal{O}$, is given by

$$\langle \mathcal{O} \rangle = \frac{1}{\mathcal{Z}} \int \mathcal{D}[A, \bar{\psi}, \psi] \mathcal{O}[A, \bar{\psi}, \psi] e^{-i\mathcal{S}_{QCD}}, \tag{2.14}$$

while the k-point *correlation function* (or *correlator*) of a set of time ordered operators can also be defined through the use of the path integral,

$$\langle T(\mathcal{O}_1 ... \mathcal{O}_k) \rangle = \frac{1}{\mathcal{Z}} \int \mathcal{D}[A, \bar{\psi}, \psi] \mathcal{O}_1[A, \bar{\psi}, \psi] ... \mathcal{O}_k[A, \bar{\psi}, \psi] e^{-i\mathcal{S}_{QCD}}. \tag{2.15}$$

QCD path integrals defined in Minkowski space can only be solved at high energy scales in perturbation theory.

2.3 Eightfold Way

Consider the case of QCD with a single quark field of mass m. The QCD Lagrangian has left-handed and right-handed pieces obtained through use of the chiral projectors, P_R and P_L, such that

$$\psi_R = P_{\mathrm{R}} \psi = \frac{1}{2}(1 + \gamma_5)\psi \quad \text{and} \quad \psi_L = P_{\mathrm{L}} \psi = \frac{1}{2}(1 - \gamma_5), \tag{2.16}$$

with $\psi = \psi_R + \psi_L$ and where the operators have the properties that $P_{\mathrm{R}} P_{\mathrm{L}} = 0$ and $P_{\mathrm{R/L}}^2 = P_{\mathrm{R/L}}$. The QCD Lagrangian (Equation 2.2) can be written as

$$\mathcal{L}_{QCD} = \bar{\psi}_L (i \not{D}) \psi_L + \bar{\psi}_R (i \not{D}) \psi_R - m \bar{\psi}_R \psi_L - m \bar{\psi}_L \psi_R - \frac{1}{4} F_{\mu\nu} F^{\mu\nu}, \tag{2.17}$$

where the mass term mixes chiral components. Under transformations that treat the left-handed and right-handed components independently,

$$\psi_R \longrightarrow e^{i\theta_R}\psi_R \quad \text{and} \quad \psi_L \longrightarrow e^{i\theta_L}\psi_L, \tag{2.18}$$

we see that the Lagrangian is only invariant in the limit of massless quarks. In that case the Lagrangian exhibits *chiral symmetry*.

For the case of two massless quarks $m_u = m_d = 0$ we say that $\mathcal{L}_{QCD}$ is symmetric under $U(2)_L \otimes U(2)_R$. This group can also be written as the direct product of the following groups:

$$U(2)_L \otimes U(2)_R = SU(2)_L \otimes SU(2)_R \otimes U(1)_V \otimes U(1)_A, \tag{2.19}$$

where $U(1)_V$ and $U(1)_A$ are *vector* and *axial* symmetries. The vector symmetry relates to the conservation of baryon number in QCD, however the axial symmetry is violated due to quantum effects; a phenomenon known as the *axial anomaly*.

Due to the dynamics of QCD the symmetry $SU(2)_L \otimes SU(2)_R$ is *spontaneously broken* down to $SU(2)_V \otimes U(1)_V$ even in the massless limit. This will result in massless excitations of the vacuum called *Goldstone bosons*. Due to the introduction of massive fermions, as seen in Equation 2.17, the chiral symmetry will be both spontaneously and *explicitly* broken, resulting in the pions π^+, π^0, π^- which have a small but non-zero mass and are *pseudo-Goldstone bosons*.

The $SU(2)$ group corresponds to the concept of isospin symmetry, I, which was originally introduced as an attempt to explain the difference between the mass of the proton and neutron long before the quark hypothesis. Under the strong force the two nucleons were considered different states of the same particles, thought at the time to be fundamental particles. This symmetry was not originally understood to be approximate within QCD but rather one that was violated only by the electromagnetic and weak forces.

Due to the similarity in mass between the u and d quarks it is still natural to group the hadrons together by their isospin because states with the same number of u and d quarks will have similar masses. More important than their near-degeneracy, that the masses of the u and d are much smaller than the scale of the strong interactions ensures that isospin is a good approximate symmetry of QCD. Isospin is often treated as an exact symmetry in LQCD.

This symmetry was further expanded into the $SU(3)$ approximate symmetry used today [15], with a $SU(2)$ isospin subgroup, when the quantum number of 'strangeness', S, was introduced into the model. This quantum number was devised to explain why certain hadrons decayed at a rate much lower than expected [16]. Strangeness is a property that is conserved by the strong force but not by the weak force.

The hadrons can be categorised according to electric charge, Q, strangeness, S, and the third component of isospin (or isospin projection number), I_3. This can be achieved as the strong force is *flavour-blind* and so does not distinguish between flavour. These quantities are related by the *Gell-Mann-Nishijima* relation,

$$Q = I_3 + \frac{1}{2}(\mathcal{Y}), \tag{2.20}$$

where B is the baryon number and we call $\mathcal{Y} = S + B$ the *strong hypercharge*. $SU(3)$ is a Lie group of rank 2 and thus its Cartan subalgebra consists of two of the eight generators of $SU(3)$. Two generators, T^3 and T^8 of $SU(3)$ are empirically related to I_3 and $\mathcal{Y}$ as follows

$$I_3 = T^3, \qquad \mathcal{Y} = \frac{2}{\sqrt{3}}T^8. \tag{2.21}$$

The tensor product of the appropriate number of quarks and anti-quarks can be decomposed into direct sums of irreducible multiplets of the Lie algebra of $SU(3)_f$ corresponding to the baryon and meson bound states. Theoretically

one could speak of $SU(6)$-flavour symmetry but this is very badly broken at low energies due to the large masses of the three heavier quarks; c, b and t. Discussion from this point onward, along with the work and results herein, will focus on the three lighter quarks: u, d and s.

The states will form *multiplets* which have the same isospin projection number which combine into *supermultiplets* and are defined by their spin, parity and baryon number: J^P (J is spin and the intrinsic parity is P). If we assign fundamental (triplet) representation 3 Dirac fields to the quarks we can decompose the baryons into decuplets, octets and singlets in the following way

$$3 \otimes 3 \otimes 3 = 10_S \oplus 8_M \oplus 8_M \oplus 1_A. \tag{2.22}$$

These multiplets have certain symmetry properties under flavour rotation and must be combined as in Equation 2.1 to create physical states. The decuplet is symmetric while the singlet state, however is totally anti-symmetric in flavour and corresponds to the Λ^1 baryon which does not exist in the ground state according to Fermi statistics. There is no way of creating a totally anti-symmetric spin wave-function from three quarks and thus $\Psi_{spin}\Psi_{flavour}$ will be anti-symmetric. The two octets are of mixed-symmetry and describe the same states. They are connected by a unitary transformation.

The $\frac{1}{2}^+$ baryon octet and the $\frac{3}{2}^+$ baryon decuplet are shown in Figure 2.2. By assigning fields in the conjugate representation $\bar{3}$ to the anti-quarks a meson octet and singlet can be constructed in a similar way (prompting Gell-Mann to first use the phrase 'Eightfold way' [17]), but the baryons are the focus of this work so mesons will not be further discussed here.

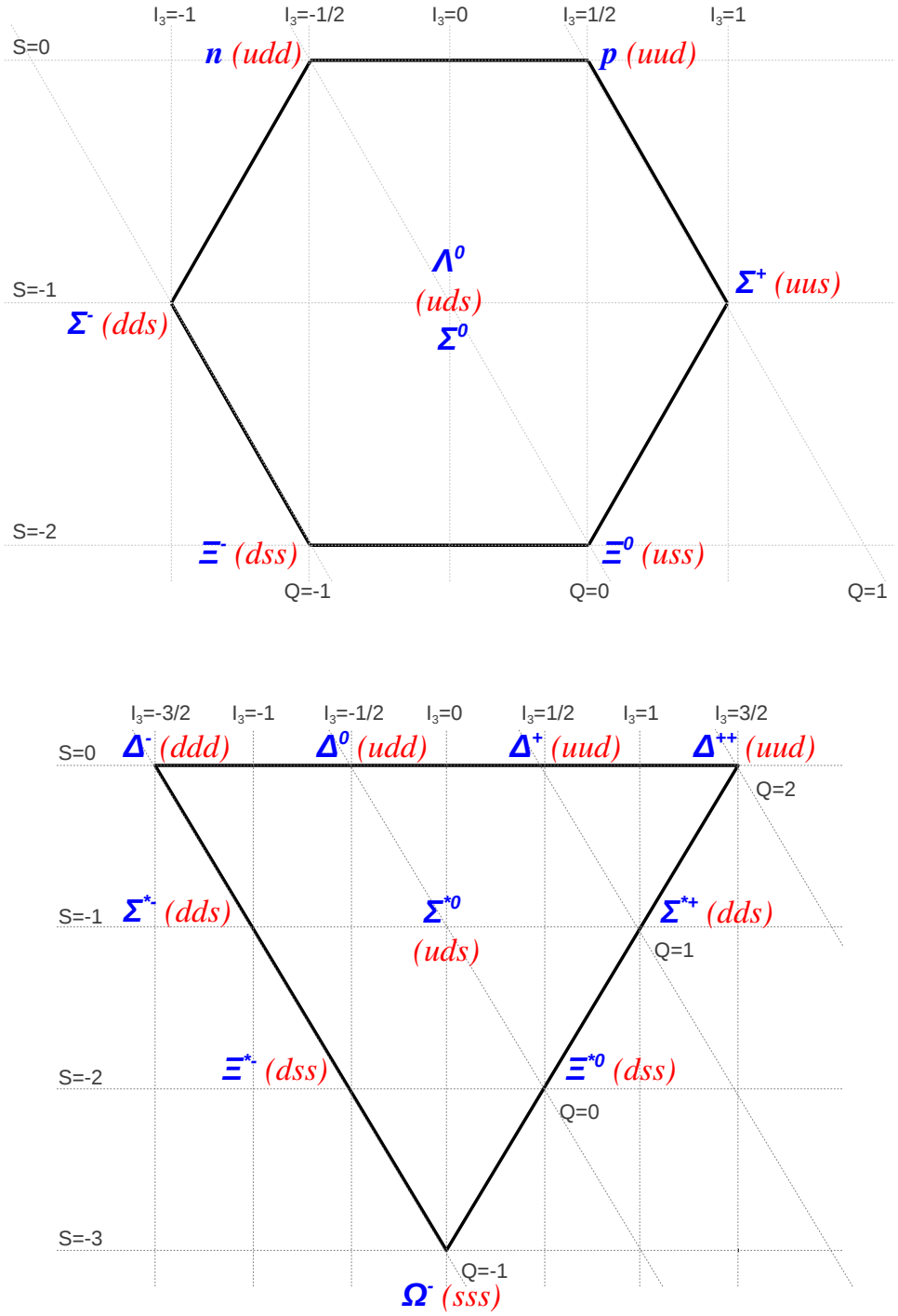

Figure 2.2: The baryon $\frac{1}{2}^+$ octet and $\frac{3}{2}^+$ decuplet.

"To err is human; to really foul things up requires a computer."

— Unknown

Chapter 3

Lattice QCD

To perform low energy calculations of QCD, when the coupling of the strong force, α_S, is large, it is necessary to introduce non-perturbative formulations such as LQCD, introduced by K. Wilson in 1974 [18]. Quantities of interest such as hadron matrix elements can only be calculated using tools like LQCD.

We perform a Wick rotation to move to Euclidean space and proceed by descretising space-time and putting the theory of QCD onto a hyper-cubic lattice of finite volume. The resulting form of the partition function contains the exponentiated Euclidean action which acts as a probability distribution comparable to a Boltzmann factor of statistical physics. As such it is possible to perform numerical simulations using Monte Carlo methods to calculate expectation values of quantities of interest. Several excellent texts cover the content of the following sections in much more detail for the interested reader [19–22].

3.1 Path Integrals in Lattice QCD

Within the context of a QFT the path integral is a central tool for calculating expectation values of observables. This was introduced at the end of Section 2.2.

The path integral of QCD is formulated in Minkowski space as it is a relativistic theory and has an oscillating exponential term containing the QCD action. This form does not allow for a numerical calculation however, as the phase is highly oscillatory.

In order to obtain a path integral which can be computed numerically it is necessary to move to *imaginary time*. This corresponds to a Euclidean formulation of the path integral approach to QCD. One can now write

$$\mathcal{Z} = \int \mathcal{D}[A, \bar{\psi}, \psi] e^{-\int d^4x \mathcal{L}^E_{QCD}} = \int \mathcal{D}[A, \bar{\psi}, \psi] e^{-\mathcal{S}^E_{QCD}}, \tag{3.1}$$

where the E superscript corresponds to quantities in Euclidean space. The Euclidean action, $\mathcal{S}^E_{QCD}$, is given by

$$\mathcal{S}^E_{QCD} = \int d^4x \sum_{f=1}^{n_f} \bar{\psi}^f (\not{D} + m_q) \psi^f + \frac{1}{4} \mathrm{Tr} \int d^4x F_{\mu\nu} F^{\mu\nu}. \tag{3.2}$$

$\mathcal{Z}$ now has the form of a partition function of statistical physics as the complex phase now becomes a damping factor similar to a Boltzmann factor. This is known as a *Wick rotation* and corresponds to the following replacements:

$$\begin{aligned} x_0 &\longrightarrow -i x_0^E \\ A_0 &\longrightarrow -i A_4^E \\ \partial_0 &\longrightarrow i \partial_4^E, \end{aligned} \tag{3.3}$$

along with the appropriate change to Euclidean Dirac matrices as outlined in Appendix A.1. The expectation value of a physical observable, $\mathcal{O}$, (see Equation 2.14) now becomes

$$\langle \mathcal{O} \rangle = \frac{\int \mathcal{D}[A, \bar{\psi}, \psi] \mathcal{O}[A, \bar{\psi}, \psi] e^{-\mathcal{S}^E_{QCD}}}{\int \mathcal{D}[A, \bar{\psi}, \psi] e^{-\mathcal{S}^E_{QCD}}}. \tag{3.4}$$

It is not possible to simulate an infinite number of degrees of freedom on a computer and so along with placing the theory on a finite volume lattice, we must also approximate the path integral by replacing it with a finite sum of gauge configurations on this lattice. The replacement of an integral with a finite sum will naturally have associated errors which will need to be accounted for in simulations.

3.2 Lattice Regularisation

Lattice QCD is a gauge invariant regulator of QCD which allows for a non-perturbative treatment. This regularisation cuts off higher momentum modes such that observables will now depend on a cut-off which is proportional to $1/a$. This a is the lattice spacing corresponding to the distance between neighbouring points in a 4-dimensional hypercubic grid, of dimension $L^3 \times T$ which approximates space-time, and onto which we place the theory of QCD. The momentum is confined to the Brillouin zone with a momentum cut-off $\frac{\pi}{a}$. Sending $a \longrightarrow 0$ allows one to obtain physically meaningful results. This step, known as taking the *continuum limit*, corresponds to the act of removing the regulator. In practice one simulates at several values of the lattice spacing and performs an extrapolation.

The symmetries of the theory are now significantly affected due to the introduction of the lattice regulator. For example space-time symmetries such as rotational invariance are now broken down to a discrete subgroup, but the more symmetries which can be maintained in the discretisation process helps to maintain the link between simulations and the continuum theory when the continuum limit is taken. The lattice does however, preserve gauge invariance. It will become apparent in later discussion that chiral symmetry will be broken in certain cases.

The space-time integral within the path integral is replaced by a sum over lattice sites,

$$\int d^4x \longrightarrow a^4 \sum \tag{3.5}$$

and it is now necessary to redefine the QCD action within the confines of this formulation. For the remainder of the chapter, the superscript E will be dropped and any action terms should be understood to be Euclidean. We consider first only the fermionic part of the action, with a single quark flavour,

$$\mathcal{S}_F = \bar{\psi}(x)(\not{D} + m)\psi(x) \tag{3.6}$$

where the fields are now defined exclusively on the lattice points, with $x = an$ and $n \in \mathbb{N}$ such that $L = aN$. We can now simply substitute

$$\psi(x) \longrightarrow \mathcal{U}(x)\psi(x) \quad \text{and} \quad \bar{\psi}(x) \longrightarrow \bar{\psi}(x)\mathcal{U}^{-1}(x), \tag{3.7}$$

where $\mathcal{U} \in SU(3)$, while taking the derivative to be a finite difference on the lattice, where $\hat{\mu}$ is the unit vector in the direction of μ,

$$\partial_\mu \psi(x) = \frac{1}{2a}(\psi(x + a\hat{\mu}) - \psi(x - a\hat{\mu})), \tag{3.8}$$

but one finds that the action is no longer gauge invariant. A discrete action is thus constructed such that gauge invariance is preserved.

This is achieved through the introduction of the parallel transporter $U_\mu(x)$ from lattice site x to site $x + a\hat{\mu}$ which is defined as

$$U_\mu(x) = U(x, x + a\hat{\mu}) = \mathcal{P}\text{exp}\left\{ i \int_x^{x+a\hat{\mu}} dx_\mu A_\mu(x) \right\}, \tag{3.9}$$

(with $\mathcal{P}$ indicating path ordering) which transforms under a local gauge transfor-

mation as

$$U_\mu(x) \longrightarrow \mathcal{U}(x)U_\mu(x)\mathcal{U}^{-1}(x+a\hat{\mu}). \tag{3.10}$$

As these are defined by orientation, it is also useful to introduce the notation

$$U_{-\mu}(x) = U^\dagger(x-a\hat{\mu}). \tag{3.11}$$

The quark fields are now defined exclusively on the lattice sites while the gauge fields exist on the connecting lines between sites, which are known as links. The gauge configurations mentioned in the previous section of this chapter are now understood as a collection of values for the gauge links on the lattice. It is the traces of closed loops (known as a 'Wilson loop') of link variables between lattice sites that are now the gauge invariant quantities.

The gauge invariant fermion action is

$$\mathcal{S}_F = \sum_{x,y} \bar{\psi}(x)M(x,y)\psi(y) \tag{3.12}$$

where

$$M(x,y) = m\delta_{x,y} + \frac{1}{2a}\sum_\mu \gamma_\mu \left[U_\mu(x)\delta_{x+a\hat{\mu},y} - U_\mu^\dagger(x-a\hat{\mu})\delta_{x-a\hat{\mu},y}\right]. \tag{3.13}$$

It is the matrix M that needs to be inverted to compute propagators on the lattice. The majority of the computational cost of LQCD calculations is involved in the inversion of these large and sparse matrices.

When taking the continuum limit, this naive discretisation of the fermion action results in extra species of fermion which are manifestly un-physical. This is known as the problem of *fermion doubling*, with the extra species being referred to as *doublers*. The Nielson-Ninomiya 'no-go' theorem [23, 24] in fact shows that these doublers are not just a result of the choice of discretisation but due to the very act of putting fermions on a lattice, even in the case of vanishing fermion

mass.

Ideally one would try to discretise the QCD fermion action on the lattice such that it retains the following properties:

- Locality of the $\not{D}$ operator, in that it only couples nearby sites.
- The matrix in Equation 3.12 is γ_5-Hermitian.
- Translational invariance.
- $\{\gamma_5, \not{D}\} = 0$, i.e., exact chiral symmetry.
- No doublers.

The Nielsen-Ninomiya theorem does not allow for such a formulation, and as such, one or more of these properties needs to be dropped in any discretisation of the fermionic part of the action. A number of solutions to this problem have been proposed with modifications that have their own separate advantages and drawbacks.

One straightforward change to the discretised action outlined here is to add what is known as a 'Wilson term' onto the fermion action. This new term is given by

$$\mathcal{S}_F^W = -a\frac{r}{2}\sum_x \bar{\psi}(x) \triangle \psi(x), \tag{3.14}$$

with r usually set to unity and where $\triangle$ is the discretised covariant lattice Laplacian given by

$$\triangle \psi(x) = \frac{1}{a^2}\sum_\mu (\psi(x + a\hat{\mu}) + \psi(x - a\hat{\mu}) - 2\psi(x)). \tag{3.15}$$

The fermion action becomes

$$\mathcal{S}_F + \mathcal{S}_F^W = \sum_{x,y} \bar{\psi}(x) M^W(x, y)\psi(y), \tag{3.16}$$

where

$$M^W(x,y) = \left(m + \frac{4}{a}\right)\delta_{x,y} - \frac{1}{2a}\sum_{\mu}\left[(1-\gamma_\mu)U_\mu(x)\delta_{x+a\hat{\mu},y} - (1+\gamma_\mu)U_\mu^\dagger(x-a\hat{\mu})\delta_{x-a\hat{\mu},y}\right], \tag{3.17}$$

which decouples the extra fermion species when the continuum limit is taken. This can be rewritten in terms of the *hopping parameter*, κ, under a reparameterisation $\psi \longrightarrow \sqrt{m+4/a}\psi$ and $\bar{\psi} \longrightarrow \sqrt{m+4/a}\bar{\psi}$, as

$$M^W(x,y) = 1 - \kappa H(x,y), \tag{3.18}$$

where $H(x,y)$ is the *hopping matrix* given by

$$H(x,y) = \sum_{\mu}\left[(1-\gamma_\mu)U_\mu(x)\delta_{x+a\hat{\mu},y} - (1+\gamma_\mu)U_\mu^\dagger(x-a\hat{\mu})\delta_{x-a\hat{\mu},y}\right], \tag{3.19}$$

and the hopping parameter is

$$\kappa = \frac{1}{2(am+4)}. \tag{3.20}$$

This strategy is not computationally costly but the inclusion of the Wilson term breaks chiral symmetry. A consequence of this is that the mass requires extra, additive, renormalisation which requires a fine tuning of the bare quark mass to compensate for [25]. There are alternative methods of constructing the fermion action which aim to preserve some chiral properties such as the staggered fermion formulation [26]. Fermion formulations satisfying the Ginsparg-Wilson relation [27] can be computationally expensive but retain some desirable properties. These other choices of fermion action will not be discussed further.

As discussed, the continuum limit is taken for a theory regularised on the lattice, but how quickly the continuum limit is reached depends on discretisation

effects. Such effects can be removed, order by order, through the use of Symanzik improvement program [28, 29]. In the case of Wilson fermions, its first order discretisation effects, $\mathcal{O}(a)$ are removed through the introduction of a counter-term, known as a *clover term*, with a parameter which can be tuned to ensure first order discretisation effects are cancelled [30]. This $\mathcal{O}(a)$-improved Wilson action is also known as a *clover action*. The clover part of the action is given by

$$\mathcal{S}_F^C = c_{sw} a^5 \sum_x \sum_{\mu,\nu} \bar{\psi}(x) \frac{1}{2} \sigma_{\mu\nu} F_{\mu\nu}(x) \psi(x), \tag{3.21}$$

where c_{sw} is the Sheikholeslami-Wohlert parameter, which for our gauge configurations, has been non-perturbatively determined [31]. A typical discretisation for the field strength tensor involves the notion of a *plaquette*, which is a square made up of link variables given by

$$U_{\mu\nu}(x) = U_\mu(x) U_\nu(x + a\hat{\mu}) U_\mu^\dagger(x + a\hat{\nu}) U_\nu^\dagger(x). \tag{3.22}$$

We then define

$$F_{\mu\nu}(x) = \frac{i}{8a^2}(Q_{\mu\nu}(x) - Q_{\nu\mu}(x)), \tag{3.23}$$

where

$$Q_{\mu\nu}(x) \equiv U_{\mu\nu}(x) + U_{\nu,-\mu}(x) + U_{-\mu-\nu}(x) + U_{-\nu,\mu}(x). \tag{3.24}$$

One can now use these gauge link variables and plaquette to construct the gauge part of the action. A simple formulation was introduced by Wilson, which is constructed around the plaquette, and thus preserves gauge invariance. It has $\mathcal{O}(a^2)$ corrections and is defined as

$$\begin{aligned} \mathcal{S}_G &= \beta \frac{1}{3} \sum_{x,\mu,\nu} Re\mathrm{Tr}\left[1 - U_\mu(x) U_\nu(x + a\hat{\mu}) U_\mu^\dagger(x + a\hat{\nu}) U_\nu^\dagger(x)\right] \\ &= \beta \frac{1}{3} \sum_{\text{plaquette}} Re\mathrm{Tr}\left[1 - U_{\text{plaquette}}\right], \end{aligned} \tag{3.25}$$

with the *inverse coupling*, $\beta = \frac{6}{g^2}$. This gauge action approaches the Yang-Mills action in the continuum limit.

Though this action has $\mathcal{O}(a^2)$ discretisation effects, an improved action can be constructed which will cancel some of these second order discretisation effects in order to reach the continuum limit more rapidly. This gauge action is given by

$$\mathcal{S}'_G = \beta \left\{ c_0 \sum_{\text{plaquette}} \frac{1}{3} Re\text{Tr}\left[1 - U_{\text{plaquette}}\right] + c_1 \sum_{\text{rectangle}} \frac{1}{3} Re\text{Tr}\left[1 - U_{\text{rectangle}}\right] \right\}, \tag{3.26}$$

where $\beta = \frac{6}{g^2} = \frac{10}{g^2}$ with $c_0 = \frac{20}{12}$ and $c_1 = -\frac{1}{12}$. This is the *tree-level Symanzik Improved* gauge action [32]. The second term in the action refers to the rectangular Wilson loop which is built in a similar manner to the plaquette but where the link variables follow the outline of a rectangle. The action can be generalised to multiple fermion flavours. The action used here will be written down in Section 3.5.

3.3 Lattice QCD Simulations

The expectation value of a physical observable $\mathcal{O}$ is now given by

$$\langle \mathcal{O} \rangle = \frac{\int \mathcal{D}[U, \bar{\psi}, \psi] \mathcal{O}[U, \bar{\psi}, \psi] e^{-\mathcal{S}_{lat}}}{\int \mathcal{D}[U, \bar{\psi}, \psi] e^{-\mathcal{S}_{lat}}}, \tag{3.27}$$

where the action is a choice of discretised QCD action. The integration measures are given by

$$\mathcal{D}[U, \bar{\psi}, \psi] = \prod_x \prod_{\alpha,a,f} \prod_\mu dU_\mu(x) d\bar{\psi}^{f,a}_\alpha(x) d\psi^{f,a}_\alpha(x), \tag{3.28}$$

where α, a, f, x and μ refer to Dirac, colour, flavour, co-ordinate and Lorentz indices respectively. As the fermion part of the lattice action is linear in ψ and $\bar{\psi}$ (or bilinear in fermion fields) these contributions can be integrated out

analytically through the use of source terms and the generating functional, which also avoids the issue of numerically simulating Grassmann numbers. This term is given by a Grassmann Gaussian integral which can be integrated to give

$$\mathcal{Z}_F = \int \mathcal{D}[\bar{\psi}, \psi] e^{-\mathcal{S}_F[U,\bar{\psi},\psi]} = \int \mathcal{D}[\bar{\psi}, \psi] e^{-\bar{\psi} M \psi} = \det(M). \tag{3.29}$$

It is computationally intensive to compute this non-local factor and as such in many LQCD calculations in the past a simplification known as the *quenched approximation* was implemented. This has the effect of neglecting the dynamical quark loops and is done by setting $\mathcal{Z}_F = 1$. The neglecting of the sea quarks introduces errors that are difficult to estimate and vary depending on the quantity being calculated. In most modern calculations (and in those computed as part of this work) this approximation has been abandoned, though it has been used in some of the studies with which we will compare our results.

This discretised version of the expectation value is still very time consuming to compute in practice even using supercomputers, due to the huge number of degrees of freedom in the path integral ($\mathcal{O}(10^6)$ to $\mathcal{O}(10^8)$ for typical lattices). As previously mentioned the use of techniques from statistical mechanics, such as Monte Carlo methods, can be of use here. In generating a set of gauge configurations, importance sampling algorithms were developed [33, 34] which would discard configurations of the gauge links that were not favoured by a probability density function which is weighted by the LQCD action. Simulations in this study which use dynamical fermions will use the Hybrid-Monte Carlo (HMC) and RHMC algorithms [35, 36].

These techniques involve using *Markov Chains* to generate the configurations. A starting configuration which is chosen randomly is conditionally updated in discrete simulation time steps according to some probability. At equilibrium the probability for changing from a configuration will be the same as changing into it. A simple example of this is the Metropolis algorithm wherein a gauge

configuration U is to be updated to configuration U' according to an acceptance probability given by

$$P = e^{\mathcal{S}[U]-\mathcal{S}[U']}, \tag{3.30}$$

where $\mathcal{S}$ is the action. If P is greater than unity the updated configuration is accepted. It is a Markov chain in the sense that the process is memory-less; the update depends only on the current state.

The quantity of interest in Equation 3.27 is now approximated by taking the average over the ensemble of gauge configurations as

$$\langle \mathcal{O} \rangle \approx \frac{1}{N_{\text{conf}}} \sum_{i=1}^{N_{\text{conf}}} \mathcal{O}[U_i], \tag{3.31}$$

where N_{conf} is the number of configurations. There are statistical errors associated with such an approximation and these generally decrease in proportion to $1/\sqrt{N_{\text{conf}}}$ so that the expectation value reaches its physical value in the limit of an infinite number of configurations. See Appendix B.1 for a discussion of the *bootstrap algorithm* which we use here to estimate statistical errors.

Simulations are performed in a finite volume typically of the order of a few fermi. Due to computational constraints, the largest volume lattices typically have lattice spacings which are more coarse (i.e. relatively large a), while the lattice spacing itself is an un-physical construct. The study of effects arising from lattice techniques come under the heading of *systematics* which can have varying impact on the calculation of different physical quantities.

Decreasing discretisation effects of the action through the Symanzik improvement program reduces the impact of a finite lattice spacing but generally, in order to understand these effects lattice calculations are carried out on several differing choices of spacing a and volume $L^3 \times T$. When the wavelength of a quantity of interest is comparable to the size of the lattice then finite volume effects can increasingly contribute. Work herein is performed only at one value of the lattice

spacing.

The fact that the simulation is confined to dimensions of finite length requires a choice of boundary conditions. Periodic boundary conditions are often chosen for the spatial extent so that

$$\psi(x + \hat{\mu}_i L) = \psi(x), \quad i \in 1, 2, 3, \tag{3.32}$$

along with a choice of anti-periodic boundary conditions for the temporal direction. As mentioned, the introduction of the finite spacing, a, places restrictions on the values of momenta that can be chosen. The lattice momentum is restricted to the first Brillouin zone which satisfies

$$p_i \in \left(-\frac{\pi}{a}, \frac{\pi}{a} \right] \tag{3.33}$$

for each component. The lattice momenta is thus discretised in units as follows:

$$p_i = \frac{2\pi}{L} n_i, \quad n_i = 1, 2, \ldots, L/a \tag{3.34}$$

One can choose to implement *twisted boundary conditions* as this allows for a fine tuning of the momentum of the lowest-lying state to an arbitrary value, though is costly as it requires separate inversions for each transition to be investigated.

The introduction of twisted boundary conditions modifies the quark fields at the boundary such that a continuous momentum spectrum (below the cut-off), between the usual Fourier modes, becomes accessible [37–39]. This can be expressed as

$$\psi(x + \hat{e}_i L) = e^{i\theta_i} \psi(x), \quad i \in 1, 2, 3, \tag{3.35}$$

so that the momentum is given by

$$p_i = \frac{2\pi}{L} n_i + \frac{\theta_i}{L}. \tag{3.36}$$

This 'twist' can be applied to any of the spatial directions, though often only one or two are chosen to simplify computation and limit any additional finite volume effects, which we expect to be small [40]. In this work twists will only be applied in the z-direction.

The primary difficulty in implementing twisted boundary conditions is that for each twist a new set of gauge configurations are required for each choice of twist. This is expensive to do and so one often employs *partially* twisted boundary conditions instead. This means that a twist is applied to the valence quarks but the usual periodic boundary conditions remain for the sea quarks. In practice this means computing propagators where the gauge links $\{U_i(x)\}$ are replaced with $\{e^{\frac{ia\theta_i}{L}}U_i(x)\}$ [41]. In this work the word 'partially' is sometimes omitted even when such techniques are being utilised. Any further discussion concerning twisted boundary conditions should be understood as applying a twist to the valence quarks only.

Another factor in performing simulations is that computational cost of matrix inversion is inversely proportional to the bare quark mass ($\propto 1/am$). Practically this means that these masses, especially light quark masses, are chosen to be heavier that their real world counterparts. An extrapolation in the limit of $am \longrightarrow 0$ is then required which depends on knowledge of a quantity's chiral behaviour. In the analysis performed here our data indicates linear trends and we simply adopt such linear fits in the chiral extrapolation.

A balance must thus be struck when carrying out a simulation, between using suitably large bare quark masses to ensure prompt matrix inversion and choosing masses close to the chiral limit to reduce the impact of extrapolation. As computing power increases, the choice of simulating at or near physical masses is becoming possible and more frequent [42, 43]. The number of quarks in a simulation is often restricted to the lighter variety. Neglecting heavier flavours should have only a small effect on quantities calculated in this work.

3.4 2pt and 3pt Correlation Functions

In order to calculate matrix elements, the core goal of this study, some detail is required on the structure of two-point (2pt) and three-point (3pt) correlation functions. Quantities such as hadron masses can be computed using 2pt correlation functions exclusively while matrix elements require 3pt functions. Discussion here will be restricted to correlation functions of the octet baryons. The correlation function, similar to that found in Equation 2.15, is written as

$$C^H_\Gamma(t;\vec{p}) = \Gamma_{\beta\alpha}\langle H_\alpha(t;\vec{p})\overline{H}_\beta(0;\vec{p})\rangle \tag{3.37}$$

for a 2pt correlation function with suitable baryon interpolators, where Γ is some Dirac structure. The interpolators correspond to Hilbert space operators creating and annihilating the appropriate baryon states. These operators are built from products of quark fields which will need to be integrated out before any averaging over gauge configurations can be performed. This 2pt function describes the creation of a baryon with momentum $\vec{p}$ initially and then the annihilation of that baryon at some later time. A useful aspect of the path integral formalism of a QFT is that one can switch between it, with the associated computational advantages, and the operator picture for convenience.

In order to construct an appropriate operator one must build it in such a way as to respect the symmetries of the baryon being considered. Baryons are three quark states so the operators must also have three quark fields. Conventionally the flavour index of a field is dropped and instead the field given a unique name, for example $\psi^u_\alpha(x)$ is relabelled $u_\alpha(x)$ The correct quantum numbers for charge C, parity P, and total spin J, must also be included. The baryons which are the focus of this work are those of the $J^P = \frac{1}{2}^+$ octet (see Figure 2.2) so there is a need to project out the positive parity state which is done by including a Dirac projection operator Γ as seen in Equation 3.37. For unpolarised baryons this is

done by taking $\Gamma = \frac{1}{2}(1+\gamma_4)$.

The spin $\frac{1}{2}$ operators which will be needed in this work are now defined, where the charge conjugation matrix $C = \gamma_2\gamma_4$ (see Dirac matrix representations of Appendix A.1) is chosen to encode the properties

$$C = -C^T = C^{-1} = C^+. \tag{3.38}$$

Only a single free Dirac index is required for the baryon so two of the quarks form a di-quark structure and the colour indices, given by Latin characters, are contracted with the three dimensional Levi-Civita tensor, ϵ^{abc}, so that the baryon is a colour singlet.

$$H^p_\alpha(t;\vec{p}) = \sum_{\vec{x}} e^{-i\vec{p}.\vec{x}}\epsilon^{abc}\left[u^b(\vec{x},t)^T C\gamma_5 d^c(\vec{x},t)\right] u^a_\alpha(\vec{x},t), \tag{3.39}$$

$$H^n_\alpha(t;\vec{p}) = \sum_{\vec{x}} e^{-i\vec{p}.\vec{x}}\epsilon^{abc}\left[d^b(\vec{x},t)^T C\gamma_5 u^c(\vec{x},t)\right] d^a_\alpha(\vec{x},t), \tag{3.40}$$

$$H^{\Sigma^+}_\alpha(t;\vec{p}) = \sum_{\vec{x}} e^{-i\vec{p}.\vec{x}}\epsilon^{abc}\left[u^b(\vec{x},t)^T C\gamma_5 s^c(\vec{x},t)\right] u^a_\alpha(\vec{x},t), \tag{3.41}$$

$$H^{\Sigma^-}_\alpha(t;\vec{p}) = \sum_{\vec{x}} e^{-i\vec{p}.\vec{x}}\epsilon^{abc}\left[d^b(\vec{x},t)^T C\gamma_5 s^c(\vec{x},t)\right] d^a_\alpha(\vec{x},t), \tag{3.42}$$

$$H^{\Lambda}_\alpha(t;\vec{p}) = \sum_{\vec{x}} e^{-i\vec{p}.\vec{x}}\epsilon^{abc}\left[u^b(\vec{x},t)^T C\gamma_5 d^c(\vec{x},t)\right] s^a_\alpha(\vec{x},t), \tag{3.43}$$

$$H^{\Xi^0}_\alpha(t;\vec{p}) = \sum_{\vec{x}} e^{-i\vec{p}.\vec{x}}\epsilon^{abc}\left[s^b(\vec{x},t)^T C\gamma_5 u^c(\vec{x},t)\right] s^a_\alpha(\vec{x},t), \tag{3.44}$$

$$H^{\Xi^-}_\alpha(t;\vec{p}) = \sum_{\vec{x}} e^{-i\vec{p}.\vec{x}}\epsilon^{abc}\left[s^b(\vec{x},t)^T C\gamma_5 d^c(\vec{x},t)\right] s^a_\alpha(\vec{x},t), \tag{3.45}$$

are the interpolators for the proton, neutron, Σ^+, Σ^-, Λ, Ξ^0 and Ξ^- respectively [44,45] with suppressed Dirac indices. The anti-proton interpolator is given by

$$\overline{H}^p_\alpha(t;\vec{p}) = \sum_{\vec{x}} e^{i\vec{p}.\vec{x}}\epsilon^{abc}\bar{u}^a_\alpha(\vec{x},t)\left[\bar{d}^b(\vec{x},t)C\gamma_5\bar{u}^c(\vec{x},t)^T\right], \tag{3.46}$$

with similar operators for the other anti-baryons.

The 2pt correlation function can now be written in terms of quark propagators with momentum $\vec{p}$ from a *source* to a *sink* at some later point. These are created by performing Wick contractions of the quark fields. The quark propagator is defined through

$$G^{q\bar{q}}(x;y)^{ab}_{\alpha\beta} = M^{-1}(x,y)^{ab}_{\alpha\beta} = \overbrace{q^a_\alpha(x)\bar{q}^b_\beta}(y), \tag{3.47}$$

for some quark of flavour q, with the Dirac fermion matrix M defined in Equation 3.13. In contrast with 2pt correlation functions of mesons there are no *disconnected* pieces for baryons, though they will contribute to 3pt functions. As an example, the 2pt correlator for the proton can be written in the following form,

$$\begin{aligned} C^p_\Gamma(t;\vec{p}) &= \Gamma_{\beta\alpha}\langle H^p_\alpha(t;\vec{p})\overline{H}^p_\beta(0;\vec{p})\rangle \\ &= \sum_{\vec{x}} e^{i\vec{p}.\vec{x}}\epsilon^{abc}\epsilon^{a'b'c'}\times \\ &(\mathrm{Tr}[\Gamma G^{u\bar{u}}(\vec{x},t;\vec{0},0)]\mathrm{Tr}[\widetilde{G}^{d\bar{d}}(\vec{x},t;\vec{0},0)G^{u\bar{u}}(\vec{x},t;\vec{0},0)] \\ &+ \mathrm{Tr}[\Gamma G^{u\bar{u}}(\vec{x},t;\vec{0},0)\widetilde{G}^{d\bar{d}}(\vec{x},t;\vec{0},0)G^{u\bar{u}}(\vec{x},t;\vec{0},0)]), \end{aligned} \tag{3.48}$$

with the definition $\widetilde{G} = (C\gamma_5 G\gamma_5 C)^T$. There are two trace terms within this expression deriving from the fact that there are two ways to contract the up flavour quark fields as indicated here by contraction lines above and below:

$$\overbrace{u^a_\alpha(\vec{x},t)\overbrace{u^b(\vec{x},t)^T C\gamma_5 \overbrace{d^c(\vec{x},t)\bar{d}^c}(\vec{0},0)C\gamma_5\bar{u}^b}(\vec{0},0)^T\bar{u}^a_\alpha}(\vec{0},0). \tag{3.49}$$

The 'upper' contractions refer to the first term in Equation 3.48.

The 3pt correlation functions are somewhat more complicated as disconnected diagrams can appear. One refers to the insertion of a current, $\mathcal{O}$, at some time τ which satisfies $0 \ll \tau \ll t$, where t is the time of annihilation of the baryon state

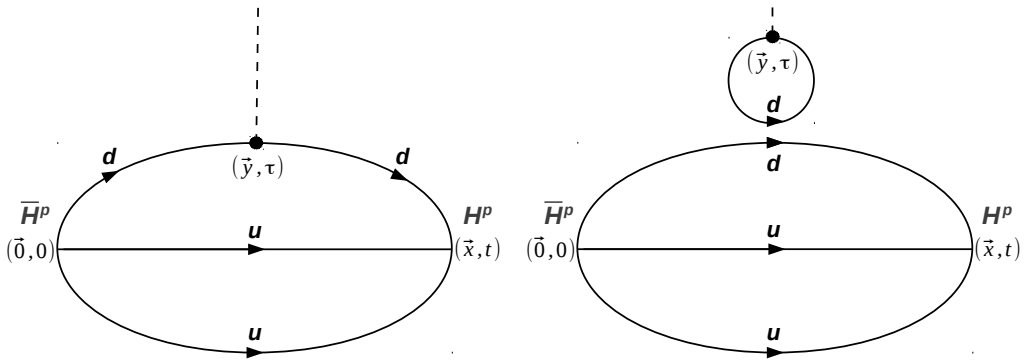

Figure 3.1: The three-point correlation function of the proton where at time τ, the current insertion $\bar{d}\Gamma d$ has some unspecified Dirac structure and is indicated by the dashed line. The left hand diagram is the connected piece while the quark line disconnected part is on the right. The latter is neglected in this study.

on the lattice. This current is some operator adequately reflecting the interaction which is to be simulated, for example this would be a vector current of the form $\bar{q}\gamma_\mu q$ for the electromagnetic current. The 3pt correlator can be written as

$$C_\Gamma^{HH'}(t,\tau;\vec{p},\vec{p}';\mathcal{O}) = \sum_{\alpha\beta}\Gamma_{\beta\alpha}\langle H_\alpha(t;\vec{p}')\mathcal{O}(\tau,\vec{q})\overline{H}_\beta(0;\vec{p})\rangle, \tag{3.50}$$

where $q = p - p'$. With this kind of current there are both connected and disconnected contributions as depicted in Figure 3.1 which will both affect the physics. The disconnected pieces are significantly more difficult to compute on the lattice, requiring propagators from all lattice sites to all other points (the so called 'all-to-all' propagators) [46]. These contributions will not be computed in this work, and where possible, quantities will be computed such that disconnected contributions cancel.

A current may also change the flavour of quark (see Chapter 4). Such currents are found in the weak interaction picture and will form a large part of the work carried out here. The transitions between baryon states will need to be computed and thus Wick contractions will need to be carried out first which differ depending

on the states being considered. An example of how to carry out this procedure is discussed in Appendix B.2 along with a list of the 3pt functions used in this work, in terms of quark propagators. The 3pt functions are calculated on the lattice using the sequential source technique which is briefly discussed in Appendix B.3.

3.5 Simulation Details

Simulations carried out in this work are run on a lattice of dimension $24^3 \times 48$ with a lattice spacing of $a \sim 0.078$ fm [47]. The gauge field configurations are generated with $N_f = 2 + 1$ flavours of dynamical fermions (i.e. two mass-degenerate light quarks and one strange quark) with a single step of mild stout smearing [48], utilising the tree-level Symanzik improved gauge action and non-perturbatively $\mathcal{O}(a)$ improved Wilson fermions [49].

Our action takes the form

$$\mathcal{S}^{\text{lat}} = \mathcal{S}'_G + \mathcal{S}^u_F + \mathcal{S}^d_F + \mathcal{S}^s_F, \tag{3.51}$$

with the gluon action of Equation 3.26 and each flavour, f, has a fermion action given by

$$\begin{aligned}\mathcal{S}^f_F = \sum_x \Bigg\{ \frac{1}{2} \sum_\mu \Big[& \bar{\psi}^f(x)(\gamma_\mu - 1)\tilde{U}_\mu(x)\psi^f(x + a\hat{\mu}) \\ & - \bar{\psi}^f(x)(\gamma_\mu + 1)\tilde{U}^\dagger(x - a\hat{\mu})\psi^f(x - a\hat{\mu}) \Big] \\ & + \frac{1}{2\kappa_f}\bar{\psi}^f(x)\psi^f(x) - \frac{1}{4}ac_{SW}\sum_{\mu\nu}\bar{\psi}^f(x)\sigma_{\mu\nu}F_{\mu\nu}(x)\psi^f(x) \Bigg\}.\end{aligned} \tag{3.52}$$

The $\tilde{U}$ terms refer to the stout smeared (or 'fat') links which are designed to smooth fluctuations in the gauge fields for the Dirac kinetic term and the Wilson term. Regular (or 'thin') links are used for the clover term [50]. The stout

smeared link is given by

$$\begin{aligned} \tilde{U}_\mu(x) &= \exp\{iQ_\mu(x)\}U_\mu(x), \\ Q_\mu &= \frac{\alpha}{2i}\left[V_\mu U_\mu^\dagger - U_\mu V_\mu^\dagger - \frac{1}{3}\mathrm{Tr}\left(V_\mu U_\mu^\dagger - U_\mu V_\mu^\dagger\right)\right], \end{aligned} \tag{3.53}$$

where we take $\alpha = 0.1$ and V_μ correspond to the sum of all staples around $U_\mu(x)$;

$$\begin{aligned} V_\mu(x) = \sum_{\nu\neq\mu}\Big(&U_\nu(x)U_\mu(x+a\hat{\nu})U_\nu^\dagger(x+a\hat{\mu}) \\ &+ U_\nu^\dagger(n-a\hat{\nu})U_\mu(n-a\hat{\nu})U_\nu(n-a(\hat{\nu}+\hat{\mu}))\Big). \end{aligned} \tag{3.54}$$

Whilst for masses the improvement of the action will result in $\mathcal{O}(a^2)$ discretisation effects, the operators here are not $\mathcal{O}(a)$ improved [51].

Five ensembles of configurations are used with $\sim 1750 - 2000$ trajectories for each transition computed. Errors are computed using the bootstrap method as outlined in Appendix B.1. Further details concerning these configurations and the lattice set up can be found in an article by the QCDSF-UKQCD collaboration [52]. The ensemble details, however, are given here in Table 3.1. Ensemble $\mathcal{E}_1$ corresponds to an 'inverse' world where the 'light' quarks are heavier than the strange.

Ensemble	κ_l	κ_s	M_π[MeV]
$\mathcal{E}_1$	0.12083	0.12104	481
$\mathcal{E}_2$	0.12090	0.12090	443
$\mathcal{E}_3$	0.12095	0.12080	414
$\mathcal{E}_4$	0.12100	0.12070	377
$\mathcal{E}_5$	0.12104	0.12062	350

Table 3.1: Outline of the five ensembles used here with corresponding pion mass. Here $\beta = 5.50$ corresponding to a lattice spacing of $a \sim 0.078$ on a $24^3 \times 48$ lattice.

The bare light quark masses are defined through the hopping parameter, κ_l,

which can be related via

$$am_l = \frac{1}{2}\left(\frac{1}{\kappa_l} - \frac{1}{\kappa_{0;c}}\right), \tag{3.55}$$

and this can then be used to calculate the bare strange mass as

$$\kappa_s = \frac{1}{\frac{3}{\kappa_0} - \frac{2}{\kappa_l}}, \tag{3.56}$$

where κ_0 corresponds to the flavour symmetric point. They are related in this way as in these simulations we choose to keep the singlet mass

$$\bar{m} = (m_u + m_d + m_s)/3 = (2m_l + m_s)/3 \tag{3.57}$$

fixed along the path to the physical point. This formulation allows for expansions around the symmetric point ($\kappa_l = \kappa_s$) where we define

$$\delta m_q = m_q - \bar{m}. \tag{3.58}$$

The value of $\kappa_{0;c} = 0.121099(4)$ is determined by finding where the quark mass vanishes along the symmetric line as discussed by the QCDSF-UKQCD collaboration [52]. More motivation for the choice of fixing the quark singlet quantity can be found in that discussion.

The scale, in results detailed later in this study, will be defined through the quantity M_π^2/X_π^2 [52], where

$$X_\pi^2 = \frac{1}{3}\left(2M_K^2 + M_\pi^2\right), \tag{3.59}$$

This is an invariant mass dimensionless ratio which has a corresponding experimentally measured value. This quantity has a value of unity at the *symmetric point* (i.e. ensemble $\mathcal{E}_2$), where the masses of the light and strange

quark are equal and $SU(3)$ symmetry is unbroken. The quantity X_π^2 is constructed such that first order breaking effects from M_K^2 and M_π^2 cancel, leaving the symmetric point pseudoscalar meson mass, M_0^2. This provides a useful way of describing how measurements change as these masses diverge (the subject of Chapter 7).

The interpolators used here are those outlined in Equations 3.39-3.45 with Jacobi smearing [53, 54] in order to improve overlap with the physical wavefunction. They are taken to have a non-relativistic (NR) projection which cuts matrix inversion time significantly. From the 2pt correlation functions one can determine the mass of each baryon on each of the ensembles. These are not calculated here but were determined by the QCDSF-UKQCD collaboration (Table 22 [52]) and those numerical values will be used later when required.

We choose to implement partially twisted boundary conditions herein and for simplicity, twists will only be applied to the active quark (i.e. the valence quark impinged upon by the inserted current). As hyperon form factors are usually evaluated around $q^2 = 0$, we wish to twist boundary conditions for each transition (and ensemble) to attain this value of momentum transfer and negate errors due to extrapolation from non-zero values. We also choose to have another point corresponding to $q^2 = (0.075)^2$ to assist with interpolation when required. Both of these choices will conveniently lead to additional points between the usual lattice momentum Fourier modes.

In order to evaluate which twist is required for an arbitrary q^2 for a transition between state $H(p)$ and $H'(p')$ we use:

$$\begin{aligned} q = p - p' &= (i(E_H - E_{H'}), \vec{p} - \vec{p}'), \\ \implies q^2 &= -(E_H - E_{H'})^2 + (\vec{p} - \vec{p}')^2 \\ &= 2E_H E_{H'} - (M_H^2 + M_{H'}^2) - 2\vec{p}.\vec{p}', \end{aligned} \tag{3.60}$$

and choose the case where state H' is at rest (i.e. $\vec{p}' = 0$) so that $\vec{q} = \vec{p}$. From

the previous argument we find

$$q^2 = 2M_{H'}\sqrt{M_H^2 + \vec{q}^{\,2}} - (M_H^2 + M_{H'}^2), \tag{3.61}$$

which can be rearranged to solve for

$$\vec{q}^{\,2} = \left(\frac{q^2 + (M_H^2 + M_{H'}^2)}{2M_{H'}}\right)^2 - M_H^2, \tag{3.62}$$

but as $\vec{q} = \vec{p}$ this means that

$$\vec{q}^{\,2} = \left(\frac{2\pi}{L}\vec{n} + \frac{\theta_H}{L}\right)^2 = \left(\frac{q^2 + (M_H^2 + M_{H'}^2)}{2M_{H'}}\right)^2 - M_H^2, \tag{3.63}$$

and by considering zero lattice momenta one can solve for θ_H to arrive at [55]

$$|\theta_H| = L\sqrt{\left(\frac{q^2 + (M_H^2 + M_{H'}^2)}{2M_{H'}}\right)^2 - M_H^2}. \tag{3.64}$$

The twist applied to the final state, $\theta_{H'}$, is taken to be zero. The twists used in this work are shown in Tables 3.2 and 3.3. This method has been applied successfully in several other lattice calculations of various quantities [56–58], such as pion and kaon form factors.

Finally, as the lattice has acted as a regulator for the theory of QCD, the bare quantities that are computed must also be renormalised in order to match results with experiment. The multiplicative renormalisation constants which need to be considered in this work are Z_V and Z_A for the vector and axial-vector currents, respectively. There are methods, including perturbative [59] and non-perturbative [60, 61], which can be used to compute these constants for a particular lattice but in this work these quantities are fixed by employing a conserved vector current and matching axial-vector computed quantities with the well known experimental measurement of the nucleon axial charge. Ratios

Transition	$\mathcal{E}_1$	$\mathcal{E}_2$	$\mathcal{E}_3$	$\mathcal{E}_4$	$\mathcal{E}_5$
$N \to N$	0.57458	0.57470	0.57475	0.57482	0.57497
$\Sigma \to \Sigma$	0.57471	0.57470	0.57465	0.57463	0.57467
$\Lambda \to \Lambda$	0.57466	0.57470	0.57471	0.57469	0.57470
$\Xi \to \Xi$	0.57479	0.57470	0.57461	0.57453	0.57452
$\Xi \to \Lambda$	0.58001	0.57470	0.59394	0.61835	0.62395
$\Sigma \to \Lambda$	0.57301	0.57470	0.58234	0.58497	0.57721
$\Lambda \to N$	0.57473	0.57470	0.57985	0.59941	0.65676
$\Xi \to \Sigma$	0.57433	0.57470	0.58089	0.59386	0.61383
$\Sigma \to N$	0.58087	0.57470	0.59206	0.62594	0.67050

Table 3.2: Twists, θ_H, applied to the active valence quark in the hyperon state, H, such that $q^2 = (0.075)^2$ for each transition within the five ensembles used. These are taken to be in the z-direction in each case. All values are in units of π.

Transition	$\mathcal{E}_1$	$\mathcal{E}_2$	$\mathcal{E}_3$	$\mathcal{E}_4$	$\mathcal{E}_5$
$\Xi \to \Lambda$	0.13496	N/A	0.11166	0.18792	0.20238
$\Sigma \to \Lambda$	0.05158	N/A	0.05930	0.07329	0.02530
$\Lambda \to N$	0.08833	N/A	0.04381	0.12987	0.27292
$\Xi \to \Sigma$	0.08456	N/A	0.05153	0.11241	0.17588
$\Sigma \to N$	0.13870	N/A	0.10382	0.20579	0.30016

Table 3.3: Similar to Table 3.2 but for the case of $q^2 = 0$. It is not necessary to apply twists to the diagonal matrix elements in this case as this is achieved naturally at $q^2 = q^2_{\mathrm{MAX}} = (M_H - M_{H'})^2$. This is also pertinent to transition matrix elements at the symmetric point.

where renormalisation constants cancel will also be used extensively.

Our calculations were performed using the Chroma software suite [62], employing the SSE optimised Dslash code [63] and Bluegene codes were optimised with the use of BAGEL [64].

"Appear weak when you are strong, and strong when you are weak."

— Sun Tzu, *The Art of War*

Chapter 4

Flavour Physics

Within the SM there are many free parameters that need to be fixed by experiment, some of which can be aided by computational efforts. In particular there are many parameters that relate to 'flavour changing interactions'. There are the six quark masses, three lepton masses, three quark mixing parameters and another complex parameter corresponding to CP violation. The number of parameters will increase if one allows for non-zero neutrino mass.

Flavour physics is a term that relates to interactions that can discriminate between flavour. Some of these processes are *flavour changing* where a particle changes flavour, whilst others are *flavour conserving*. QCD is *flavour-blind* as it does not distinguish between quark flavours, while the weak interaction is not so, as will be discussed in this chapter.

4.1 Weak Interactions

The quark and lepton masses are generated after the Higgs field gains a non-zero vacuum expectation value from the spontaneous symmetry breaking of electroweak interactions. Upon reparameterisation of the Higgs field one will find that three vector bosons have acquired mass within the Higgs component of

the SM Lagrangian. These are the electrically charged $W^{\pm}$ and the neutral Z^0 mediators of the weak force. These massive particles decay, leading to a short effective range for the weak force.

Weak interactions are the only type in the SM that allow the charge (C) and parity (P) symmetries to be violated. In QCD and Quantum Electrodynamics (QED) any processes are invariant under an interchange of a particle with its own anti-particle (charge) and upon spatial inversion (parity), whereas not all weak decays respect these two symmetries. It was shown experimentally that parity is not only violated in weak decays [65] but is *maximally* so. The weak force was also later shown to be not invariant under the combined symmetry, called CP, in 1964 by Cronin and Fitch [66]. CP violation is a direct consequence of a theory with three generations of quark, if *quark mixing* is allowed. These experiments showed that the weak theory is a *chiral theory* in contrast with other fundamental interactions as it displays this asymmetry.

In order to explain the process of nuclear beta decay $n \to pe\bar{\nu}_e$, Fermi [67], in 1934, originally developed a model which involved a 4-fermion point interaction. As this was a point interaction model there was no force mediating particle. This is now understood to be approximate as the force is short range and only gives an accurate tree-level description. A vector-vector amplitude can be written using this model:

$$\mathcal{M} = \frac{G_F}{\sqrt{2}}(\bar{u}_n \gamma_\mu u_p)(\bar{u}_e \gamma^\mu u_{\bar{\nu}_e}), \tag{4.1}$$

with external Dirac spinor fields and where G_F is known as the *Fermi constant*. This model was later displaced by the intermediate vector boson theory (IVB) which included force mediators in direct analogy with QED and QCD. Current-current forms of the interaction provide for a good low-energy effective description however.

At the quark level, in Figure 4.1, one can see that the W^- is responsible for the change of electric charge of the fermion line. As was mentioned in Section 2.3,

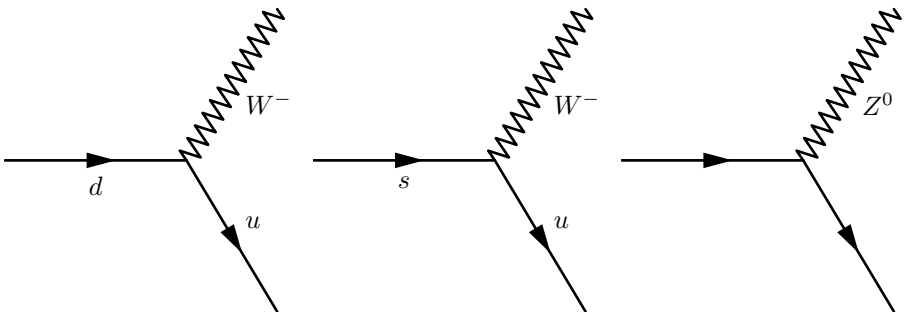

Figure 4.1: Example weak interactions involving the W^- and Z bosons. The first and second diagrams show a change in charge for the fermion. The solid lines in the third diagram can be any quark or lepton.

the weak force can violate strangeness. In the first diagram there is no change in the strangeness of the system; a strangeness conserving decay can be represented as $\Delta S = 0$. Similarly, $\Delta S = 1$ corresponds to a decay in which the strangeness quantum number of the system changes by one unit. An example would be the second diagram in Figure 4.1. Convention requires that the flavour quantum numbers have the same sign as their electric charge therefore $s \rightarrow u$ is a 'positive' change in strangeness. The empirical rule that $\Delta S = \Delta Q$ has been seen to hold in experiment for transitions which violate strangeness.

It could be possible in the SM to have an interaction where the neutral Z^0 changes the flavour of a quark (for example $s \rightarrow d$) which is known as a Flavour Changing Neutral Current (FCNC) though this sort of interaction is highly suppressed by the Glashow-Iliopoulos-Maiani (GIM) mechanism. In actuality it was the need to incorporate a suppressed FCNC into the SM that led to the concept of the charm quark being introduced, four years before it was discovered experimentally at the Brookhaven National Laboratory (BNL) and at SLAC [68–70].

Turning back to the current-current picture of nuclear beta decay we find Equation 4.1 does not provide for a modern understanding of parity and charge

conjugation violating weak processes and needs to be modified. It is possible to combine the gamma matrices in five different ways categorised by their transformation under the charge and parity operators. These combinations, with appropriate spinors, are known as *bilinear covariant fields* (or simply bilinears). The vector current seen in Equation 4.1 is one of these five which are all summarised in Table 4.1.

Name	Bilinear	Components	C	P	CP
Scalar	$\bar{u}_1 u_2$	1	$\bar{u}_2 u_1$	$\bar{u}_1 u_2$	$\bar{u}_2 u_1$
Pseudoscalar	$\bar{u}_1 \gamma_5 u_2$	1	$\bar{u}_2 \gamma_5 u_1$	$-\bar{u}_1 \gamma_5 u_2$	$-\bar{u}_2 \gamma_5 u_1$
Vector	$\bar{u}_1 \gamma_\mu u_2$	4	$-\bar{u}_2 \gamma_\mu u_1$	$\bar{u}_1 \gamma_\mu u_2$	$-\bar{u}_2 \gamma_\mu u_1$
Axial-Vector	$\bar{u}_1 \gamma_\mu \gamma_5 u_2$	4	$\bar{u}_2 \gamma_\mu \gamma_5 u_1$	$-\bar{u}_1 \gamma_\mu \gamma_5 u_2$	$-\bar{u}_2 \gamma_\mu \gamma_5 u_1$
Tensor	$\bar{u}_1 \sigma_{\mu\nu} u_2$	6	$-\bar{u}_2 \sigma_{\mu\nu} u_1$	$\bar{u}_1 \sigma_{\mu\nu} u_2$	$-\bar{u}_2 \sigma_{\mu\nu} u_1$

Table 4.1: Dirac bilinear covariant matrices with transformation properties under C and P. We have defined $\sigma_{\mu\nu} = \frac{i}{2}[\gamma_\mu, \gamma_\nu]$.

In order for the theory to adequately replicate properties found in nature and exhibit the symmetry violating behaviour seen in experiment it was necessary to replace the γ_μ in Equation 4.1 with a vector axial-vector (V-A) Lorentz structure $\gamma_\mu \to \gamma_\mu(1-\gamma_5)$ [71,72]. The vector and axial-vector currents transform in opposite ways under parity and thus provide for maximal parity violation. The term $(1-\gamma_5)$ ensures a weak force coupling to left-handed fermions. The amplitude thus becomes [73, 74]

$$\mathcal{M} = \frac{G_F}{\sqrt{2}}(\bar{u}_n \gamma_\mu (1-\gamma_5) u_p)(\bar{u}_l \gamma^\mu (1-\gamma_5) u_{\bar{\nu}_l}). \tag{4.2}$$

Nuclear beta-decay is an example of a *semi-leptonic decay* which will be discussed in more detail in Chapter 5. The vector current is also present in electromagnetic interactions while both the vector and the axial-vector structure is needed to calculate observables and for understanding the physics of hyperon semi-leptonic (HSL) decays.

4.2 Quark Mixing and the Cabibbo Model

The weak sector of the SM has symmetry group $SU(2)_L \otimes U(1)_Y$. The Lagrangian governing the coupling of the Higgs field to the fermions is given by the Yukawa interaction term

$$-\mathcal{L}^{\text{quark}}_{\text{Yukawa}} = Y^d_{ij}\bar{Q}^I_{Li}\phi d^I_{Rj} + Y^u_{ij}\bar{Q}^I_{Li}\tilde{\phi}u^I_{Rj} + \text{h.c.} \tag{4.3}$$

where ϕ is the Higgs doublet and $\tilde{\phi} = i\sigma_2\phi^*$. Q^I_{Li} are left-handed quark doublets for each generation and are expressed in the *interaction basis*, as emphasised by the I superscript. The d^I_{Rj} and u^I_{Rj} are singlets for down and up-type quarks while the $Y^{u/d}_{ij}$ are complex Yukawa matrices operating in flavour space. The Yukawa interaction with the Higgs condensate gives rise to both the quark masses and the mixing between flavours of quark. The masses are expressed in the interaction eigenbasis but can be transformed, through the use of unitary rotations, to be diagonal in the *mass eigenbasis*. It is the transformation between these two bases that allows for the mixing of quark flavours for charged $W^\pm$ interactions. Though flavour is violated, total quark number is conserved in weak interactions.

If we consider at first, a flavour-$SU(2)$ world, then the quarks will simply appear as a left-handed doublet, $(u, d)_L$, and two right-handed singlets, u_R and d_R. The *Cabibbo angle* [75], θ_C, parameterises the rotation from the mass eigenbasis into the weak interaction vector space. With the inclusion of the strange quark, s, we modify the doublet to be $(u, d')_L$ where d' is a mix of down type quarks that couple to the u quark via the flavour changing weak current, such that

$$\begin{pmatrix} u \\ d' \end{pmatrix}_L = \begin{pmatrix} u \\ d\cos\theta_C + s\sin\theta_C \end{pmatrix}_L . \tag{4.4}$$

Experiment suggested that the $\Delta S = 0$ coupling should be greater than that of the $\Delta S = 1$ coupling factor and so N. Cabibbo developed his model to

accommodate that observation. Indeed recent estimations are $\theta_C \sim 13.01°$ [76]. Upon including the charm quark, and thus the entire second generation, we can write the *Cabibbo matrix* as the unitary rotation matrix between the two bases.

$$\begin{pmatrix} d' \\ s' \end{pmatrix}_L = \begin{pmatrix} \cos\theta_C & \sin\theta_C \\ -\sin\theta_C & \cos\theta_C \end{pmatrix} \begin{pmatrix} d \\ s \end{pmatrix}_L . \tag{4.5}$$

The entries of the matrix relate to the probability of a down-type quark changing to a up-type quark. This can be made more clear in the form

$$\begin{pmatrix} \cos\theta_C & \sin\theta_C \\ -\sin\theta_C & \cos\theta_C \end{pmatrix} = \begin{pmatrix} V_{ud} & V_{us} \\ V_{cd} & V_{cs} \end{pmatrix} , \tag{4.6}$$

where, e.g., $|V_{cd}|^2$ and $|V_{cs}|^2$ are the relative probabilities of transitions between down and strange quarks to charm quarks.

4.3 Cabibbo-Kobayashi-Maskawa Matrix

The Cabibbo-Kobayashi-Maskawa (CKM) matrix is the generalisation of the Cabibbo model to the third generation of quarks. The third generation was postulated by Kobayashi and Maskawa in order to accommodate CP violation into the SM [77]. In a similar manner to the charm this occurred years before the third generation was discovered experimentally. The relation is now

$$D'_L = V_{CKM} D_L = V_{CKM} \begin{pmatrix} d \\ s \\ b \end{pmatrix}_L , \tag{4.7}$$

where D is the down-type quark triplet and

$$V_{CKM} = \begin{pmatrix} V_{11} & V_{12} & V_{13} \\ V_{21} & V_{22} & V_{23} \\ V_{31} & V_{32} & V_{33} \end{pmatrix} = \begin{pmatrix} V_{ud} & V_{us} & V_{ub} \\ V_{cd} & V_{cs} & V_{cb} \\ V_{td} & V_{ts} & V_{tb} \end{pmatrix}, \tag{4.8}$$

is the CKM matrix. It is a unitary matrix ($VV^\dagger = V^\dagger V = 1$) with 9, not all independent, complex elements. Normally a complex $N \times N$ matrix has $2N^2$ degrees of freedom but the CKM matrix is unitary and thus has N^2 constraints. These constraints can be explicitly written as

$$\sum_{j=1}^{3} |V_{ij}|^2 = \sum_{i=1}^{3} |V_{ij}|^2 = 1, \quad \text{for } i, j \in \{1, 2, 3\}, \tag{4.9}$$

which are known as the unitarity relations and

$$\sum_{k=1}^{3} V_{ki} V_{kj}^* = 0, \tag{4.10}$$

where $i \neq j$. The latter constraints are related to the orthogonality of the rows and columns of the matrix.

The CKM matrix should then have $2N^2 - N^2$ degrees of freedom, of which $N(N-1)/2$ are real rotation angles and $N(N+1)/2$ are complex phases. By a redefinition of the quark fields, $2N-1$ of these can be absorbed leaving $N^2-2N+1 = (N-1)^2$ parameters with $(N(N-3)+2)/2$ phases. In the 3×3 case removing these non-observable phases leaves just one complex phase factor. This phase is responsible for CP violation in the weak sector. The CKM matrix therefore has $(3-1)^2 = 4$ parameters of which the remaining three are real. In the case of Equation 4.6 the same line of reasoning would lead to just one parameter: the Cabibbo angle, θ_C.

The Cabibbo angle is a subset of the real parameters of the 3×3 case and

is usually identified with the angle θ_{12} in the standard parameterisation of the CKM matrix. The other two real parameters are θ_{13} and θ_{23} while the phase is usually denoted by δ. The standard parametrisation of V is given in full as

$$V_{CKM} = \begin{pmatrix} c_{12}c_{13} & s_{12}c_{13} & s_{13}e^{-i\delta} \\ -s_{12}c_{23} - c_{12}s_{23}s_{13}e^{-i\delta} & c_{12}c_{23} - s_{12}s_{23}s_{13}e^{-i\delta} & s_{23}c_{13} \\ s_{12}s_{23} - c_{12}c_{23}s_{13}e^{-i\delta} & -c_{12}s_{23} - s_{12}c_{23}s_{13}e^{-i\delta} & c_{23}c_{13} \end{pmatrix} \quad (4.11)$$

where $c_{ij} = \cos\theta_{ij}$ and $s_{ij} = \sin\theta_{ij}$. We can see from this that the relation between the Cabibbo model and the CKM matrix can be written as $\tan\theta_C = V_{us}/V_{ud}$. Given the value of θ_C we expect $s_{12} \sim 0.22$ while $c_{12} \sim c_{23} \sim c_{13} \sim 1$. Other factors such as s_{13} and s_{23} are significantly smaller and of magnitude 10^{-2} or less. This would imply that the certain flavour changes are much less likely than others and that transitions within generations are favoured.

The current status of the elements of the CKM matrix can be found in the most recent Particle Data Group (PDG) reviews [78,79]. They can be summarised as follows:

- $|V_{ud}| = 0.97425(22)$ from superallowed nuclear $0^+ \to 0^+$ beta decays.
- $|V_{us}| = 0.2253(14)$ from kaon decays, though determinations from hyperon and tau decays are an alternative approach.
- $|V_{ub}| = 4.15(49) \times 10^{-3}$ from exclusive and inclusive decays of the form $B \to X_u l\bar{\nu}$.
- $|V_{cd}| = 0.230(11)$ from semi-leptonic charm decays.
- $|V_{cs}| = 1.006(23)$ from semi-leptonic D or leptonic D_s decays.
- $|V_{cb}| = 40.9(1.1) \times 10^{-3}$ from inclusive and exclusive semi-leptonic decays of B mesons to charm.

- $|V_{td}| = 8.4(6) \times 10^{-3}$ from $B - \bar{B}$ oscillations or loop-mediated rare K and B decays.
- $|V_{ts}| = 42.9(2.6) \times 10^{-3}$ from the procedure as for $|V_{td}|$.
- $|V_{tb}| = 0.89(07)$ from top quark decays.

It is useful to display these numbers in matrix form to give a better understanding of the probability of certain transitions and of the relative level of uncertainty.

$$V_{CKM} = \begin{pmatrix} 0.97425(22) & 0.2246(12) & 4.15(49) \times 10^{-3} \\ 0.230(11) & 1.006(23) & 40.9(1.1) \times 10^{-3} \\ 8.4(6) \times 10^{-3} & 42.9(2.6) \times 10^{-3} & 0.89(07) \end{pmatrix}. \tag{4.12}$$

Immediately one can see that quarks usually mix within their own generation as diagonal entries are larger. It is also evident that particular matrix elements have significantly larger relative error in comparison with other entries within the same row or column. This will motivate the choice of matrix element we study.

Due to the size of $\sin\theta_{12}$ and the relative smaller sizes of $\sin\theta_{13}$ and $\sin\theta_{23}$ we use the small angle approximation ($\sin\psi \approx \psi$) to implement a different parametrisation called the Wolfenstein parametrisation [80], which is an expansion in the parameter λ which can be defined as $\lambda \approx |V_{us}| = \sin\theta_{12} \approx \theta_{12} \sim 0.22$. The other parameters are now A, ρ and η (representing the CP violating phase). This parametrisation, shown in Equation 4.13 helps to highlight the relative magnitudes of the mixing angles.

$$V_{CKM} = \begin{pmatrix} 1 - \frac{\lambda^2}{2} & \lambda & A\lambda^3(\rho - i\eta) \\ -\lambda & 1 - \frac{\lambda^2}{2} & A\lambda^2 \\ A\lambda^3(1 - \rho - i\eta) & -A\lambda^2 & 1 \end{pmatrix} + \mathcal{O}(\lambda^3). \tag{4.13}$$

One can parameterise the CKM matrix in many ways but it is useful to

note that a quantity, that is CP violating, can be constructed regardless of convention. This is known as the *Jarlskog* invariant [81] J, defined as $J \equiv \mathrm{Im}[V_{\alpha i}V_{\beta j}V^*_{\alpha j}V^*_{\beta i}] = c_{12}c^2_{23}s_{12}s_{13}s_{23}\sin\delta \approx \lambda^6 A^2\eta$. A primary consequence of this result can be expressed as

$$(m_u^2 - m_c^2)(m_c^2 - m_t^2)(m_t^2 - m_u^2)(m_d^2 - m_s^2)(m_s^2 - m_b^2)(m_b^2 - m_d^2)J \neq 0, \quad (4.14)$$

where m_x is the mass of a quark with flavour x. It is readily apparent from Equation 4.14 that CP violation will occur in weak interactions if there is no degeneracy in the up or down type quarks. If any of the mixing angles, or the phase angle, vanish then there will not be any CP violation.

The fits to the Wolfenstein parameters, as currently determined [79], are

- $\lambda = 0.22535(65)$
- $A = 0.811^{+0.022}_{-0.012}$
- $\bar{\rho} = 0.131^{+0.026}_{-0.013}$
- $\bar{\eta} = 0.345^{+0.013}_{-0.014}$

Here we have defined $\bar{\rho} = \rho(1 - \lambda^2/2)$ and similarly $\bar{\eta} = \eta(1 - \lambda^2/2)$.

It can be instructive to depict the current level of precision of these matrix elements in a graphical way. Consider the relation

$$V^*_{ub}V_{ud} + V^*_{cb}V_{cd} + V^*_{tb}V_{td} = 0, \quad (4.15)$$

arising from Equation 4.10. This equation can be represented as a triangle in the $\bar{\rho}$-$\bar{\eta}$ complex plane as shown in Figure 4.2. It is known as a *unitary triangle* and ensuring an accurate calculation of the parameters of this triangle, such as side lengths and angles, is an ongoing field of work in theoretical and experimental physics. The angles of the triangle can be related to the CKM matrix elements in the following way

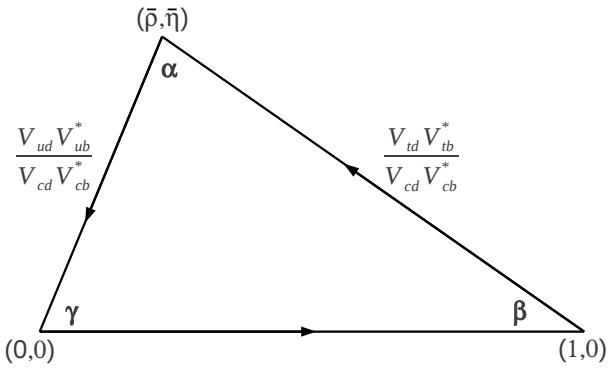

Figure 4.2: A typical example of a Unitary Triangle.

$$\alpha = \text{Arg}\left(-\frac{V_{td}V_{tb}^*}{V_{ud}V_{ub}^*}\right), \quad \beta = \text{Arg}\left(-\frac{V_{cd}V_{cb}^*}{V_{td}V_{tb}^*}\right), \quad \gamma = \text{Arg}\left(-\frac{V_{ud}V_{ub}^*}{V_{cd}V_{cb}^*}\right). \quad (4.16)$$

There are six such triangles, but all have equal area. The area itself is related to the level of CP violation. It is necessary to over-constrain this triangle to ensure that it does indeed respect unitarity. If this is not the case then this would strongly suggest the existence of physics beyond the standard model (BSM).

The various efforts to ascertain the parameters of the unitary triangle are regularly analysed by groups such as *CKMfitter*. Plots are created containing the constraints that all calculations and experiment to date have put on the parameters. An example, produced by *CKMfitter* [82], is shown in Figure 4.3.

We have introduced the CKM matrix and its individual elements, along with several parameterisations. As will be shown in Chapter 8, the form factors calculated in this study can be combined with the experimentally obtained decay rate data of weak processes to estimate entries of the CKM matrix, through the use of the non-perturbative methods of LQCD. Here we are particularly interested in studying the entry $|V_{us}|$ of the matrix as will be discussed later.

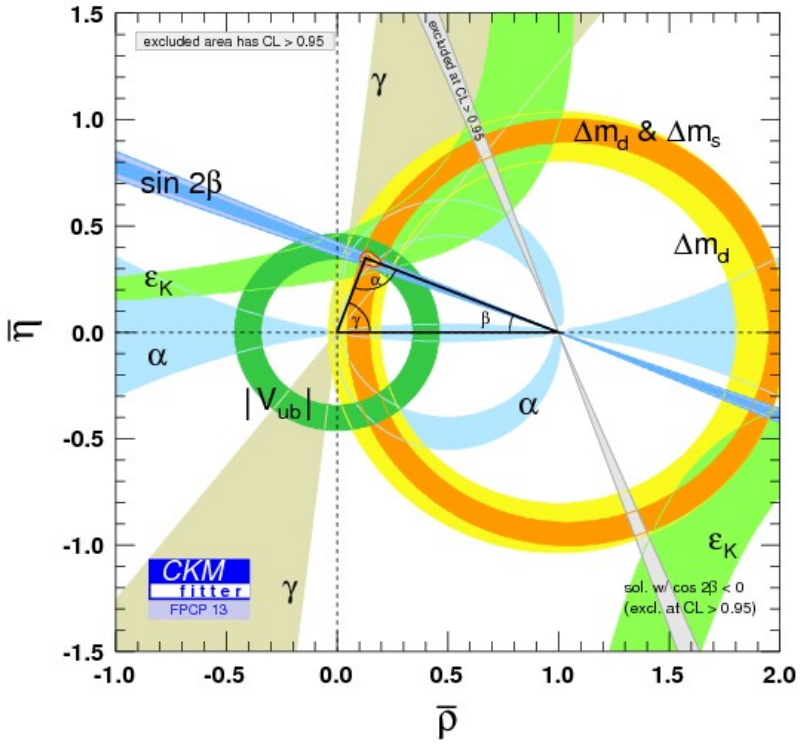

Figure 4.3: A fit produced by *CKMfitter* [82] showing a global fit to the constraints on the unitary triangle from available measurements. The apex of the triangle shows a small region that current measurement has yet to probe. If the triangle is unitary this region will converge on a single point.

"Why, sometimes I've believed as many as six impossible things before breakfast."

— Lewis Carroll, *Through the Looking Glass*

Chapter 5

Hyperon Form Factors

There have not been many recent efforts contributing to the calculation of the hyperon properties either theoretically or experimentally, despite being of enormous phenomenological interest. The lattice can be used to make estimates of hyperon properties such as charge and momentum distribution, magnetic moments, axial charges and other form factors [83–86]. Hyperon semi-leptonic (HSL) decays can be used as an alternative, 'baryonic', way of estimating CKM matrix elements such as $|V_{us}|$, which is normally calculated by considering kaon decays [87].

One can also examine the role of $SU(3)$-symmetry breaking effects in such decays. Cabibbo, Swallow and Winston argued in 2003 that it would take model-independent calculations of $SU(3)$ breaking effects, such as those using LQCD, to determine these effects [88]. As such, in this work we are particularly interested in transitions that are not strangeness preserving.

5.1 Hyperon Matrix Elements

In order to calculate hyperon form factors using LQCD it is first necessary to calculate matrix elements with the required current operator insertion between

states. The matrix elements take the form of

$$\langle H^i|\mathcal{O}^j|H^k\rangle, \tag{5.1}$$

where H^i and H^k are baryon octet states and $\mathcal{O}^j$ are operators containing various combinations of gamma matrices; $i, j, k \in \{1, 2, ..., 8\}$. Our choice of numbering convention is outlined in Table 5.1 and is arranged such that the use of operator number i corresponds to the same effect as the absorption of a meson with index i.

Index	Hyperon	Operator	Meson
1	n	$\bar{d}\Gamma s$	K^0
2	p	$\bar{u}\Gamma s$	K^+
3	Σ^-	$\bar{d}\Gamma u$	π^-
4	Σ^0	$\frac{1}{\sqrt{2}}(\bar{u}\Gamma u - \bar{d}\Gamma d)$	π^0
5	Λ^0	$\frac{1}{\sqrt{6}}(\bar{u}\Gamma u + \bar{d}\Gamma d - 2\bar{s}\Gamma s)$	η
6	Σ^+	$\bar{u}\Gamma d$	π^+
7	Ξ^-	$\bar{s}\Gamma u$	K^-
8	Ξ^0	$\bar{s}\Gamma d$	$\bar{K}^0$

Table 5.1: Index convention used in this work for labelling of states and operators. For example operator 2 can annihilate an s quark in Λ and create a u quark in order to transition to p. The V-A current structure is required here so Γ is chosen to be composed of the appropriate γ matrices, as discussed in Chapter 4.

As this work considers degenerate light quarks exclusively we need only calculate one amplitude within each isospin multiplet. All other amplitudes are calculated from isospin symmetry. For example, calculating the $\Xi \to \Sigma$ matrix element allows for a determination of the $\Xi^- \to \Sigma^0$, $\Xi^0 \to \Sigma^0$ and $\Xi^0 \to \Sigma^+$ amplitudes. Similarly knowing Σ^+ matrix elements also provides the Σ^0 and Σ^- matrix elements. When considering the $2 + 1$ case the following baryon naming convention will be understood: $\{p, n\} \to N$, $\{\Sigma^-, \Sigma^0, \Sigma^+\} \to \Sigma$ and $\{\Xi^-, \Xi^0\} \to \Xi$.

As was alluded to in Section 4.1 there are only certain physically permitted

decays, or transitions, within the baryon octet. Transitions of the form $s \to d$ are not permitted nor are those corresponding to $\Delta S = -\Delta Q$, which have never been observed. Within the octet the weak current will mediate these semi-leptonic transitions to the 'right' or 'upwards and right', examples of which are indicated in Figure 5.1.

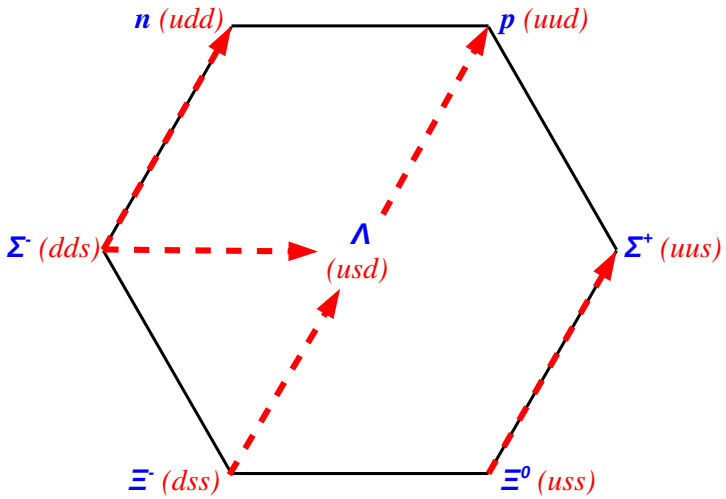

Figure 5.1: Example semi-leptonic transitions within the baryon octet corresponding to a weak current that preserve strangeness, indicated by the arrow to the right and those that do not, which are depicted by arrows pointing upwards and to the right. Arrows moving up and to the left are FCNC which are highly suppressed. We work in the isospin limit so the u and d quarks have the same masses but are still distinguished as different flavours. Σ^0 is not displayed as transitions involving it are related to those involving the other Σ baryons in the isospin limit. Transitions only occur between adjacent states in the octet.

Figure 5.1 also indicates all transitions between members of the set $\{N, \Sigma, \Lambda, \Xi\}$ which we wish to directly compute matrix elements for in this work, four with $\Delta S = 1$ and one where $\Delta S = 0$. Along with these five transition amplitudes we also wish to calculate seven possible diagonal matrix elements. These are the four $I = 0$ amplitudes, one for each element of the set but only three $I = 1$ amplitudes as $\Lambda^0 \to \Lambda^0$ with $I = 1$ is ruled out by isospin symmetry. These seven, of course, preserve strangeness. Thus, twelve V-A matrix elements are calculated in total.

I	Amplitude	Exact $SU(2)$
0	$\langle n\|\eta\|n\rangle$	$\mathcal{A}_{\bar{N}\eta N}$
0	$\langle p\|\eta\|p\rangle$	$\mathcal{A}_{\bar{N}\eta N}$
0	$\langle \Sigma^-\|\eta\|\Sigma^-\rangle$	$\mathcal{A}_{\bar{\Sigma}\eta\Sigma}$
0	$\langle \Sigma^0\|\eta\|\Sigma^0\rangle$	$\mathcal{A}_{\bar{\Sigma}\eta\Sigma}$
0	$\langle \Sigma^+\|\eta\|\Sigma^+\rangle$	$\mathcal{A}_{\bar{\Sigma}\eta\Sigma}$
0	$\langle \Lambda^0\|\eta\|\Lambda^0\rangle$	$\mathcal{A}_{\bar{\Lambda}\eta\Lambda}$
0	$\langle \Xi^-\|\eta\|\Xi^-\rangle$	$\mathcal{A}_{\bar{\Xi}\eta\Xi}$
0	$\langle \Xi^0\|\eta\|\Xi^0\rangle$	$\mathcal{A}_{\bar{\Xi}\eta\Xi}$

I	Amplitude	Exact $SU(2)$
1	$\langle n\|\pi^0\|n\rangle$	$-\mathcal{A}_{\bar{N}\pi N}$
1	$\langle p\|\pi^0\|p\rangle$	$\mathcal{A}_{\bar{N}\pi N}$
1	$\langle n\|\pi^-\|p\rangle$	$\sqrt{2}\mathcal{A}_{\bar{N}\pi N}$
1	$\langle p\|\pi^+\|n\rangle$	$\sqrt{2}\mathcal{A}_{\bar{N}\pi N}$
1	$\langle \Sigma^-\|\pi^0\|\Sigma^-\rangle$	$-\mathcal{A}_{\bar{\Sigma}\pi\Sigma}$
1	$\langle \Sigma^0\|\pi^0\|\Sigma^0\rangle$	0
1	$\langle \Sigma^+\|\pi^0\|\Sigma^+\rangle$	$\mathcal{A}_{\bar{\Sigma}\pi\Sigma}$
1	$\langle \Sigma^-\|\pi^-\|\Sigma^0\rangle$	$\mathcal{A}_{\bar{\Sigma}\pi\Sigma}$
1	$\langle \Sigma^0\|\pi^-\|\Sigma^+\rangle$	$-\mathcal{A}_{\bar{\Sigma}\pi\Sigma}$
1	$\langle \Sigma^0\|\pi^+\|\Sigma^-\rangle$	$\mathcal{A}_{\bar{\Sigma}\pi\Sigma}$
1	$\langle \Sigma^+\|\pi^+\|\Sigma^0\rangle$	$-\mathcal{A}_{\bar{\Sigma}\pi\Sigma}$
1	$\langle \Lambda^0\|\pi^0\|\Lambda^0\rangle$	0
1	$\langle \Xi^-\|\pi^0\|\Xi^-\rangle$	$-\mathcal{A}_{\bar{\Xi}\pi\Xi}$
1	$\langle \Xi^0\|\pi^0\|\Xi^0\rangle$	$\mathcal{A}_{\bar{\Xi}\pi\Xi}$
1	$\langle \Xi^-\|\pi^-\|\Xi^0\rangle$	$-\sqrt{2}\mathcal{A}_{\bar{\Xi}\pi\Xi}$
1	$\langle \Xi^0\|\pi^+\|\Xi^-\rangle$	$-\sqrt{2}\mathcal{A}_{\bar{\Xi}\pi\Xi}$

I	Amplitude	Exact $SU(2)$
1	$\langle \Sigma^-\|\pi^-\|\Lambda^0\rangle$	$\mathcal{A}_{\bar{\Sigma}\pi\Lambda}$
1	$\langle \Sigma^0\|\pi^0\|\Lambda^0\rangle$	$\mathcal{A}_{\bar{\Sigma}\pi\Lambda}$
1	$\langle \Sigma^+\|\pi^+\|\Lambda^0\rangle$	$\mathcal{A}_{\bar{\Sigma}\pi\Lambda}$

I	Amplitude	Exact $SU(2)$
1/2	$\langle n\|K^+\|\Sigma^-\rangle$	$\mathcal{A}_{\bar{N}K\Sigma}$
1/2	$\langle n\|K^0\|\Sigma^0\rangle$	$-\mathcal{A}_{\bar{N}K\Sigma}/\sqrt{2}$
1/2	$\langle p\|K^+\|\Sigma^0\rangle$	$\mathcal{A}_{\bar{N}K\Sigma}/\sqrt{2}$
1/2	$\langle p\|K^0\|\Sigma^+\rangle$	$\mathcal{A}_{\bar{N}K\Sigma}$
1/2	$\langle n\|K^0\|\Lambda^0\rangle$	$\mathcal{A}_{\bar{N}K\Lambda}$
1/2	$\langle p\|K^+\|\Lambda^0\rangle$	$\mathcal{A}_{\bar{N}K\Lambda}$
1/2	$\langle \Lambda^0\|K^+\|\Xi^-\rangle$	$\mathcal{A}_{\bar{\Lambda}K\Xi}$
1/2	$\langle \Lambda^0\|K^0\|\Xi^0\rangle$	$\mathcal{A}_{\bar{\Lambda}K\Xi}$
1/2	$\langle \Sigma^-\|K^0\|\Xi^-\rangle$	$\mathcal{A}_{\bar{\Sigma}K\Xi}$
1/2	$\langle \Sigma^0\|K^+\|\Xi^-\rangle$	$\mathcal{A}_{\bar{\Sigma}K\Xi}/\sqrt{2}$
1/2	$\langle \Sigma^0\|K^0\|\Xi^0\rangle$	$-\mathcal{A}_{\bar{\Sigma}K\Xi}/\sqrt{2}$
1/2	$\langle \Sigma^+\|K^+\|\Xi^0\rangle$	$\mathcal{A}_{\bar{\Sigma}K\Xi}$

Table 5.2: Isospin limit relations between all possible matrix elements corresponding to transitions within the baryon octet. For example the matrix element of the transition $\Xi^- \to \Sigma^-$ is equal to that of the $\Xi^0 \to \Sigma^0$ up to a factor of $-\frac{1}{\sqrt{2}}$, i.e., $\langle \Sigma^0|K^0|\Xi^0\rangle = -\frac{1}{\sqrt{2}}\mathcal{A}_{\bar{\Sigma}\eta\Xi} = -\frac{1}{\sqrt{2}}\langle \Sigma^-|K^0|\Xi^-\rangle$ in the isospin limit.

These twelve can be related to all possible allowed transitions matrix elements within the octet by $SU(2)$ isospin symmetry (which is exact in this $2+1$ world) and these relationships are outlined in Table 5.2. The matrix elements are labelled by $\mathcal{A}_{\bar{B}MH}$ and the complete set are thus

$$\mathcal{A}_{\bar{N}\eta N}, \quad \mathcal{A}_{\bar{\Sigma}\eta\Sigma}, \quad \mathcal{A}_{\bar{\Lambda}\eta\Lambda}, \quad \mathcal{A}_{\bar{\Xi}\eta\Xi} \tag{5.2}$$

and

$$\mathcal{A}_{\bar{N}\pi N}, \quad \mathcal{A}_{\bar{\Sigma}\pi\Sigma}, \quad \mathcal{A}_{\bar{\Xi}\pi\Xi}, \tag{5.3}$$

for the diagonal matrix elements. The off-diagonal matrix elements are

$$\mathcal{A}_{\bar{N}K\Lambda}, \quad \mathcal{A}_{\bar{N}K\Sigma}, \quad \mathcal{A}_{\bar{\Lambda}K\Xi}, \quad \mathcal{A}_{\bar{\Sigma}K\Xi}, \quad \mathcal{A}_{\bar{\Lambda}\pi\Sigma} \tag{5.4}$$

and together they make up the possible twelve amplitudes in the isospin limit. The coefficients in Table 5.2 are Clebsch-Gordan coefficients, relating the octet matrix elements in the basis of isospin.

A particular matrix convention for the octet baryon and meson matrices needs to be specified. In this work we follow the convention used widely in the chiral perturbation theory literature [89] such that the mesons are encoded in the matrix

$$M = \begin{pmatrix} \frac{1}{\sqrt{2}}\pi^0 + \frac{1}{\sqrt{6}}\eta & \pi^+ & K^+ \\ \pi^- & -\frac{1}{\sqrt{2}}\pi^0 + \frac{1}{\sqrt{6}}\eta & K^0 \\ K^- & \bar{K}^0 & -\frac{2}{\sqrt{6}}\eta \end{pmatrix}, \tag{5.5}$$

and similarly for the hyperon octet;

$$H = \begin{pmatrix} \frac{1}{\sqrt{2}}\Sigma^0 + \frac{1}{\sqrt{6}}\Lambda^0 & \Sigma^+ & p \\ \Sigma^- & -\frac{1}{\sqrt{2}}\Sigma^0 + \frac{1}{\sqrt{6}}\Lambda^0 & n \\ \Xi^- & \Xi^0 & -\frac{2}{\sqrt{6}}\Lambda^0 \end{pmatrix}, \tag{5.6}$$

$$\bar{H} = \begin{pmatrix} \frac{1}{\sqrt{2}}\bar{\Sigma}^0 + \frac{1}{\sqrt{6}}\bar{\Lambda}^0 & \bar{\Sigma}^- & \bar{\Xi}^- \\ \bar{\Sigma}^+ & -\frac{1}{\sqrt{2}}\bar{\Sigma}^0 + \frac{1}{\sqrt{6}}\bar{\Lambda}^0 & \bar{\Xi}^0 \\ \bar{p} & \bar{n} & -\frac{2}{\sqrt{6}}\bar{\Lambda}^0 \end{pmatrix}, \tag{5.7}$$

so that for some $SU(3)$ rotation matrix, $\mathcal{U}$, these three matrices transform as

$$M \to \mathcal{U}M\mathcal{U}^\dagger, \quad H \to \mathcal{U}H\mathcal{U}^\dagger \text{ and } \bar{H} \to \mathcal{U}\bar{H}\mathcal{U}^\dagger. \tag{5.8}$$

5.2 Hyperon Semi-leptonic Decays

Though it is not strictly a hyperon, discussion that follows will also pertain to the nucleon. The weak current operator J^W in the transition matrix element for a HSL decay, given generally as $H \to H'l\bar{\nu}_l$, is expressed in terms of hadronic J^h and leptonic J_l components [90]:

$$\begin{aligned} \mathcal{M}_{H\to H'l\bar{\nu}} &= \frac{G_F}{\sqrt{2}}\mathcal{C}\langle H'|J^h_\mu|H\rangle\langle l|J^\mu_l|\bar{\nu}_l\rangle \\ &= \frac{G_F}{\sqrt{2}}\mathcal{C}\langle H'|J^h_\mu|H\rangle l^\mu, \end{aligned} \tag{5.9}$$

where $l^\mu = \langle l|J^\mu_l|\bar{\nu}_l\rangle = \bar{u}_l\gamma^\mu(1-\gamma_5)v_{\bar{\nu}_l}$ is the matrix element describing the transition between lepton states, with external lepton Dirac spinors, and has a V-A structure. $\mathcal{C}$ is the relevant Cabibbo mixing-angle (e.g. V_{us} for $\Xi \to \Lambda$). In the case of only the three lightest quarks the hadron current can be expressed as

$$J^h_\mu = \cos\theta_C J^h_\mu(\Delta S = 0) + \sin\theta_C J^h_\mu(\Delta S = 1), \tag{5.10}$$

where $J^h_\mu(\Delta S = 0)$ and $J^h_\mu(\Delta S = 1)$ refer to the hadronic current for strangeness preserving and strangeness changing processes respectively. The angle, θ_C is the Cabibbo angle introduced in Chapter 4.

It is necessary to separate out both weak current components as the hadronic contribution to the amplitude is significantly modified by strong force effects.

Matrix elements of lepton-lepton processes, in contrast, are only affected by electroweak effects. The matrix element in that case $\mathcal{M} = \frac{G_F}{\sqrt{2}} l_\mu l^\mu$ described by the V-A structure does not suffer from the large perturbations arising due to strong effects that will be present for hadronic processes which require special treatment as a result.

The matrix element can be written so as to emphasise the separate contribution from the vector, V_μ, and the axial-vector, A_μ, components of the weak current,

$$\langle H'|J^h_\mu|H\rangle = \langle H'|V_\mu - A_\mu|H\rangle, \tag{5.11}$$

where $V_\mu = \bar{u}\gamma_\mu d$ and $A_\mu = \bar{u}\gamma_\mu\gamma_5 d$ for $\Delta S = 0$ and $V_\mu = \bar{u}\gamma_\mu s$ and $A_\mu = \bar{u}\gamma_\mu\gamma_5 s$ for $\Delta S = 1$ transitions.

This matrix element can be described in terms of three vector and three axial vector *form factors* through the decomposition of

$$\langle H'(\vec{p}', s')|J^h_\mu|H(\vec{p}, s)\rangle = \bar{u}_{H'}(\vec{p}', s')(\mathcal{V}_\mu(q) + \mathcal{A}_\mu(q))u_H(\vec{p}, s), \tag{5.12}$$

where we have defined the initial state H as having momentum $\vec{p}$ and spin s, while the final state has momentum $\vec{p}'$ and spin s'. The momentum transfer, $\vec{q}$, is given by $\vec{q} \equiv \vec{p} - \vec{p}'$. In Euclidean space one can write the matrix element of Equation 5.12 in terms of the six form factors as follows

$$\mathcal{V}_\mu(q^2) = \gamma_\mu f_1(q^2) - \sigma_{\mu\nu}q_\nu \frac{f_2(q^2)}{M_H + M_{H'}} - iq_\mu \frac{f_3(q^2)}{M_H + M_{H'}}, \tag{5.13}$$

$$\mathcal{A}_\mu(q^2) = \gamma_\mu\gamma_5 g_1(q^2) - \sigma_{\mu\nu}q_\nu\gamma_5 \frac{g_2(q^2)}{M_H + M_{H'}} - iq_\mu\gamma_5 \frac{g_3(q^2)}{M_H + M_{H'}}, \tag{5.14}$$

where M_H and $M_{H'}$ are the masses of the initial and final states and defining $\sigma_{\mu\nu} = \frac{i}{2}[\gamma_\mu, \gamma_\nu]$. Note other authors may use differing sign conventions to those used here [91, 92] or have a different $\sigma_{\mu\nu}$. The calculation involved in moving the matrix element from Minkowski to Euclidean space is outlined in detail in

Appendix C.1.

5.3 Semi-leptonic Form Factors

The form factors introduced in Equations 5.13 and 5.14 are known as the hyperon semi-leptonic decay *vector* and *axial-vector* form factors respectively. We will sometimes refer to the axial-vector form factors simply as the axial form factors. The form factors are real-valued functions of the Lorentz invariants only and do not depend on the initial and final spin states. The vector form factors are known as the *vector* $f_1(q^2)$, *weak magnetism* $f_2(q^2)$, and the *induced scalar* $f_3(q^2)$, form factors. The axial form factors are further sub-divided into the *axial* $g_1(q^2)$, *weak electricity* $g_2(q^2)$, and the *induced pseudoscalar* $g_3(q^2)$, form factors.

The vector $f_1(q^2)$ and axial $g_1(q^2)$ form factors are known as the vector and axial coupling constants $g_V \equiv f_1(0)$ and $g_A \equiv g_1(0)$ respectively when the transferred momentum between the initial and final state is zero. These are important phenomenological parameters that provide for a low-energy effective field theory description of the hyperons. Both of these form factors are critical for arriving at an estimation of CKM matrix elements as discussed in Chapter 8. When we consider diagonal hyperon matrix elements, where the final state is the same as that in the initial state, the form factors $f_3(q^2)$ and $g_2(q^2)$ are not present. In the $SU(3)$-symmetric limit these form factors will also vanish. In the Weinberg classification [93] they are known as *second-class* form factors.

The strong force is invariant under a rotation by π through the second component of isospin axis, I_2 and under charge conjugation. These transformations taken together are known as G-parity. Form factors which transform as

$$\begin{aligned} V_\mu &\longrightarrow V_\mu \\ A_\mu &\longrightarrow -A_\mu, \end{aligned} \tag{5.15}$$

under G-parity are known as *first class* form factors such as $f_1(q^2)$, $f_2(q^2)$ $g_1(q^2)$ and $g_3(q^2)$. The second class form factors transform with the opposite sign to those indicated in Equation 5.15 and thus vanish in the $SU(3)$ limit [94]. This occurs as states with definite G-parity transitioning to states with the same G-parity would require form factors of the vector current to transform without a sign change, and the opposite to hold for the axial current [95, 96].

In the Cabibbo theory [75] flavour-symmetry breaking effects are ignored and one can proceed to use the model to determine the six form factors. This is more appropriate for hyperon form factors than for meson form factors as the mass-splitting for the baryons is significantly smaller, though any deviations from the Cabibbo theory would indicate flavour-symmetry breaking effects.

Gaillard and Sauvage treat the Cabibbo theory thoroughly in their 1984 Annual Review of Nuclear Physics [94], part of which will be reviewed here as it is relevant to this discussion. Firstly, the primary assumption made by Cabibbo was that the vector and axial components of the weak current, itself a member of an $SU(3)$ octet, are also members of the same $SU(3)$ octet. Then Cabibbo noted that the matrix element of an $SU(3)$ octet operator between two octet states can be decomposed into the linear combination of two reduced matrix elements F_R and D_R (more about this in Chapter 7), so in general:

$$\langle H_i|\mathcal{O}_j|H_k\rangle = f_{ijk}F_R + d_{ijk}D_R. \tag{5.16}$$

Here f_{ijk} are the structure constants of $SU(3)$ and d_{ijk} are defined by $\{T_i, T_j\} = \frac{1}{3}\delta_{i,j} + 2d_{ijk}T_k$, with $SU(3)$ generators T_k . The three vector form factors, in the $SU(3)$-symmetric limit can then be expressed as

$$f_i(q^2) = A_{CG}F_i(q^2) + B_{CG}D_i(q^2) \tag{5.17}$$

and the axial form factors can be written in terms of

$$g_i(q^2) = A_{CG}F_{i+3}(q^2) + B_{CG}D_{i+3}(q^2), \tag{5.18}$$

with $i \in \{1, 2, 3\}$ and where each of these twelve $F_j(q^2)$ and $D_j(q^2)$ functions are different for each form factor, all of which the Cabibbo model attempts to determine. A_{CG} and B_{CG} are generalised Clebsch-Gordan coefficients for $SU(3)$.

If one assumes that the vector part of the weak current is conserved and further assumes that this part of the weak current is a member of the same octet as the electromagnetic current then one can directly relate these form factors to the known electromagnetic form factors of the proton and neutron. This part of the Cabibbo theory is known as the generalised conserved vector current (CVC) hypothesis. The vector component F_1 and D_1 can be expressed in terms of nucleon electromagnetic form factors at $q^2 = 0$, which are given by the electric charges so that trivially, $F_1(0) = 1$ and $D_1(0) = 0$, while $F_2(0)$ and $D_2(0)$ can be given in terms of the anomalous magnetic moments of the proton and neutron (see Table 5.3). The $f_3(q^2)$ form factor must vanish as previously mentioned, due to conservation of the electromagnetic current, so $F_3(0) = D_3(0) = 0$.

As the weak electricity form factor, $g_2(q^2)$, vanishes in the $SU(3)$ symmetric limit then we take $F_5^R(0) = D_5^R(0) = 0$. The form factors $f_3(q^2)$ and $g_3(q^2)$ are suppressed in decay amplitudes by a factor of $(M_l/(M_H + M_{H'}))^2$, where M_l is the lepton mass, making this factor small for the electron. Generally these form factors are ignored in the literature because of their negligible contribution to the transition amplitude [97, 98]. Another implication of this suppression factor is that experimental results for $f_3(q^2)$ and $g_3(q^2)$ are non-existent, at least until experiments involving heavier leptons are carried out as has been suggested [99].

The remaining form factor $g_1(q^2)$ is usually expressed in terms of parameters called F and D. The axial form factors for each transition can then be understood in terms of these two parameters. For nuclear beta decay we use the conventional

definition of $g_1(0) = F + D$ which fixes the values for the other transitions. F and D will appear in the chiral expansions of any baryon quantity so it is important to calculate these, especially as they have been seen to be poorly determined in general [94, 100].

Decay	$f_1(0)$	$g_1(0)$	$\frac{g_1(0)}{f_1(0)}$	$\frac{f_2(0)}{f_1(0)}$
$n \to pe^-\bar{\nu}$	1	$D+F$	$F+D$	$\frac{M_n+M_p}{2M_n}(\kappa_p-\kappa_n) = 3.70$
$\Xi^- \to \Xi^0 e^-\bar{\nu}$	-1	$D-F$	$F-D$	$\frac{M_{\Xi^-}+M_{\Xi^0}}{2M_n}(\kappa_p+2\kappa_n) = -2.85$
$\Sigma^\pm \to \Lambda e^\pm \nu$	0^*	$\sqrt{\frac{2}{3}}D$	$\sqrt{\frac{2}{3}}D$	$-\sqrt{\frac{3}{2}}\frac{M_{\Sigma^\pm}+M_\Lambda}{2M_n}\kappa_n = 2.88$
$\Xi^0 \to \Sigma^+ e^-\bar{\nu}$	1	$D+F$	$F+D$	$\frac{M_{\Xi^0}+M_{\Sigma^+}}{2M_n}(\kappa_p-\kappa_n) = 4.94$
$\Sigma^- \to ne^-\bar{\nu}$	-1	$D-F$	$F-D$	$\frac{M_{\Sigma^-}+M_n}{2M_n}(\kappa_p+2\kappa_n) = -2.31$
$\Lambda \to pe^-\bar{\nu}$	$-\sqrt{\frac{3}{2}}$	$-\frac{1}{\sqrt{6}}(D+3F)$	$F+\frac{D}{3}$	$\frac{M_\Lambda+M_p}{2M_n}\kappa_p = 1.96$
$\Xi^- \to \Lambda e^-\bar{\nu}$	$\sqrt{\frac{3}{2}}$	$-\frac{1}{\sqrt{6}}(D-3F)$	$F-\frac{D}{3}$	$-\frac{M_{\Xi^-}+M_\Lambda}{2M_n}(\kappa_p+\kappa_n) = 0.16$

Table 5.3: The $SU(3)$ symmetric limit value of octet hyperon form factors from the Cabibbo model. For $\Sigma^\pm \to \Lambda e^\pm \bar{\nu}$ the values quoted are for f_2 and g_1 instead of f_2/f_1 and g_1/f_1 as $f_1(0) = 0$ for this transition. Here the values of $\kappa_p = 1.793$ and $\kappa_n = -1.913$ are used for the anomalous magnetic moments. This table is in part a reproduction of Table 1 from Cabibbo, Swallow and Winston's review of semi-leptonic decays [101], with modifications due to differing definitions for $f_2(q^2)$. The amplitudes for the first three transitions are proportional to $|V_{ud}|$, while the rest to $|V_{us}|$.

In 1964 Ademollo and Gatto proved that first class vector form factors will be protected from first order $SU(3)$-flavour symmetry breaking effects and that any corrections will begin only at second order [102, 103]. This can be expressed as

$$\frac{f_1}{f_1^{SU(3)}} - 1 = \mathcal{O}(\delta m_l^2), \tag{5.19}$$

where $f_1^{SU(3)}$ is the value of f_1 in the flavour symmetric limit. While extrapolating to the chiral limit only $\sim (m_l - \bar{m})^2 = \delta m_l^2$ effects should be seen in LQCD calculations. This is known as the *Ademollo-Gatto theorem* [104]. The effect is present in semi-leptonic decays of both mesons and baryons [74, 105], but as it is not valid for axial-vector first class form factors, it makes the calculation

of hyperon amplitudes more involved. This is one of the primary reasons why lattice determinations of $|V_{us}|$ to date have relied on kaon decays [106]. The weak magnetism form factor f_2 will also not be protected from first order effects, though such effects have not yet been seen in experiment at current levels of precision [88]. Theoretical attempts have been made to quantify the effects of symmetry breaking in the f_2 form factor in addition to the Cabibbo theory. In 1979 A. Sirlin proposed several formula, now known as Sirlin's formulae, which express f_2 for the octet transitions in terms of the anomalous magnetic moments of octet baryons [107].

Given all of the above and as a 'baryonic' determination of $|V_{us}|$ is one of our aims, we focus our efforts on the form factors f_1 and g_1. As $SU(3)$ flavour symmetry breaking effects are large in the vector form factor f_2 we also calculate this form factor and present results for it. Additionally we find a poor signal-to-noise ratio for the second class form factors making any determination of their contributions to the matrix element difficult to determine.

The second class form factors, however, are often assumed to be small [88, 108, 109], as is their contribution to $|V_{us}|$. Furthermore, the form factor g_3 is also suppressed by the lepton mass in matrix elements as already discussed. Another motivation for focusing on the form factors f_1, g_1 and f_2 is the relative abundance of experimental data on them compared with the other form factors.

5.4 Diagonal Matrix Elements

As part of the CVC we have assumed the weak vector form factors are related to the electromagnetic form factors. This should not be surprising given the vector nature of the electromagnetic current and with a modern understanding of electroweak unification. As the vector and axial components of the weak current are separable and are computed independently on the lattice, the calculation

of weak hyperon matrix elements between the same initial and final states will include the calculation of *electromagnetic form factors*.

The expression for the diagonal matrix elements with a vector current will be similar to Equation 5.13 but with $f_3(q^2) = 0$. It is common in the literature to name these form factors the *Dirac*, $F_1(q^2)$, and the *Pauli*, $F_2(q^2)$, form factors. These form factors are related to the matrix element as

$$\langle H(\vec{p},s)|V_\mu|H(\vec{p},s)\rangle = \bar{u}(\vec{p},s)\left[\gamma_\mu F_1^q(q^2) + \sigma_{\mu\nu}\frac{q_\nu}{2M_H}F_2^q(q^2)\right]u(\vec{p},s), \tag{5.20}$$

where V_μ is a suitable vector current of the form $\bar{q}\gamma_\mu q$ for some quark flavour, q. The electromagnetic form factors are obtained through the use of the hadronic vector current which is given by

$$J_\mu^{EM} = e_u\bar{u}\gamma_\mu u + e_d\bar{d}\gamma_\mu d + e_s\bar{s}\gamma_\mu s, \tag{5.21}$$

with the electric charge, e_f, of the valence quark of flavour f in a particular hyperon. For example, to calculate the proton electromagnetic form factors with two u quarks and one d quark, we use $e_u = \frac{2}{3}$, $e_d = -\frac{1}{3}$ and $e_s = 0$. Other currents can also be chosen by substituting V_μ for the isovector current, $J_\mu^{V(u-d)} = \bar{u}\gamma_\mu u - \bar{d}\gamma_\mu d$, to obtain $F_{1,2}^v(q^2)$, or the isoscalar current $J_\mu^{V(u+d)} = \bar{u}\gamma_\mu u + \bar{d}\gamma_\mu d$, for $F_{1,2}^s(q^2)$ form factors. As we assume isospin symmetry the electromagnetic form factors can be decomposed into isovector and isoscalar components [110]. For the proton and neutron,

$$\begin{aligned} F_{1,2}^v(q^2) &= F_{1,2}^p(q^2) - F_{1,2}^n(q^2) = F_{1,2}^u(q^2) - F_{1,2}^d(q^2) \equiv F_{1,2}^{(u-d)}(q^2), \\ F_{1,2}^s(q^2) &= F_{1,2}^p(q^2) + F_{1,2}^n(q^2) = \frac{1}{3}\left(F_{1,2}^u(q^2) + F_{1,2}^d(q^2)\right) \equiv F_{1,2}^{(u+d)}(q^2), \end{aligned} \tag{5.22}$$

in the isospin limit.

The Dirac and Pauli form factors can be related to the *Sachs form factors*,

G_e and G_m, as seen below.

$$G_e(q^2) = F_1(q^2) + \frac{q^2}{4M_H^2} F_2(q^2), \tag{5.23}$$

$$G_m(q^2) = F_1(q^2) + F_2(q^2), \tag{5.24}$$

which as discussed previously, can be related to the electric charge and magnetic moment of a hyperon. As an example, for the proton, $G_e^{(p)}(0) = 1$ and $G_m^{(p)}(0) = 1 + \kappa^{(p)} = \mu^{(p)}$.

Similarly, for the axial current one can also describe the diagonal matrix elements in terms of axial form factors. The form factors in this case are often written as the axial form factor $G_A(q^2)$ (or $G_1(q^2)$), and the induced pseudo-scalar form factor $G_P(q^2)$ (or $G_2(q^2)$),

$$\langle H(\vec{p},s)|A_\mu|H(\vec{p},s)\rangle = \bar{u}(\vec{p},s)\left[\gamma_\mu\gamma_5 G_A(q^2) + \gamma_5 \frac{iq_\mu}{2M_H} G_P(q^2)\right] u(\vec{p},s). \tag{5.25}$$

The isovector and isoscalar axial currents $J_\mu^{A(u-d)}$, $J_\mu^{A(u+d)}$ are defined as

$$J_\mu^{A(u-d)} = \bar{u}\gamma_\mu\gamma_5 u - \bar{d}\gamma_\mu\gamma_5 d \tag{5.26}$$

and

$$J_\mu^{A(u+d)} = \bar{u}\gamma_\mu\gamma_5 u + \bar{d}\gamma_\mu\gamma_5 d. \tag{5.27}$$

The diagonal axial charges, found when $G_A(q^2 = 0)$, can be related to F and D in a similar manner to the transition matrix elements. The relations are $g_A^{NN} = F + D$, $g_A^{\Sigma\Sigma} = 2F$ and $g_A^{\Xi\Xi} = F - D$ in the $SU(3)$ limit. It will also be useful to define ratios of these constants because operator renormalisation

constants will cancel out. Following the lead of Reference [111] we note

$$\begin{aligned} \frac{g_A^{\Sigma\Sigma}}{g_A^{NN}} &= \frac{2F}{F+D}, \\ \frac{g_A^{\Xi\Xi}}{g_A^{NN}} &= \frac{F-D}{F+D}, \end{aligned} \tag{5.28}$$

along with conveniently combining the axial charges as follows

$$\begin{aligned} \frac{g_A^{NN} - g_A^{\Xi\Xi}}{g_A^{\Sigma\Sigma}} &= \frac{D}{F}, \\ \frac{g_A^{NN} + g_A^{\Xi\Xi}}{g_A^{\Sigma\Sigma}} &= 1, \end{aligned} \tag{5.29}$$

in the case of exact $SU(3)$.

By calculating the diagonal matrix elements with the axial current $\bar{q}\gamma_\mu\gamma_5 q$ with quark flavour q one can then use these values to determine the fraction of the hyperon's spin held by that particular flavour of quark (and anti-quark), usually denoted by Δq. Having defined the isovector axial coupling constant and introducing the notation that $g_A = \Delta u - \Delta d$ then one can also define the spin contribution of the valence quarks to a hyperon H, to be

$$\Sigma^H = \Delta u + \Delta d + \Delta s. \tag{5.30}$$

The spin fraction Δq of a hyperon, H, can be calculated from the axial vector current as

$$\frac{1}{2M_H}\langle H(p,s)|\bar{q}\gamma_\mu\gamma_5 q|H(p,s)\rangle = \Delta q s_\mu, \tag{5.31}$$

where s_μ is the covariant spin vector normalised as $s^2 = -1$.

The 'proton spin-crisis' first discovered by the European Muon Collaboration (EMC) [112] was the observation that most of the spin in the proton was not carried by its constituent quarks as was expected. There have been many suggestions as to the cause of this, including the effects of gluon exchange and

of chiral symmetry. Various models have been proposed to account for these findings (e.g. [113]) while LQCD can provide insight into the problem by non-perturbatively calculating the spin contributions to the proton, and to the other octet baryons, which can be compared with existing models. Though it is computationally intensive, a full analysis of the problem would involve calculating disconnected diagrams, which will not be done here.

Little work has been done in relation to the spin fractions of the Λ baryon in recent years. The Λ spin fractions are of interest for a variety of reasons such as examining the effects of $SU(3)$ symmetry breaking on the spin in comparison with that of the nucleon. It is also important for a variety of experimental reasons (cf. [114]).

5.5 Current Status of Form Factors

There have been limited theoretical and experimental investigations into the properties of the hyperon form factors in recent times though there has been some interest shown with several calculations from LQCD in the past.

Apart from nuclear beta decay, HSL decays represent less than a percent of the possible decay modes making them difficult to measure. Those experiments that have been performed to determine the hyperon form factors for transitions that are strangeness changing, $\Delta S = 1$, make the assumption that there is no $g_2(q^2)$ second class form factor away from the $SU(3)$ symmetric limit. No results are reported for $g_3(q^2)$ due to the small mass of the lepton in the decay process. The axial-vector and vector form factors are generally reported as a ratio $\frac{g_1}{f_1}$ with $q^2 \to 0$. There are limited experimental results for the weak magnetism form factor $f_2(q^2)$. These results are summarised here in Table 5.4.

Several $\Delta S = 0$ octet transitions are of interest to us in this study and have been measured experimentally. Of course, the most well known form factor

Decay Process	$\frac{g_1(0)}{f_1(0)_{\rm exp}}$	$\frac{f_2(0)}{f_1(0)_{\rm exp}}$	Branching Fraction (10^{-3})	Mean Lifetime (10^{-10}s)
$\Lambda \to p$ [4, 115]	0.718(15)	1.3(8)	8.34(14)	2.63(2)
$\Sigma^- \to n$ [4, 116]	−0.340(17)	−1.71(35)	10.17(34)	1.479(11)
$\Xi^- \to \Lambda$ [115]	0.25(5)		5.63(31)	1.639(15)
$\Xi^0 \to \Sigma^+$ [117]	1.3(2)	3.8(2.3)*	2.53(8)	2.90(9)

Table 5.4: Experimental results for $\Delta S = 1$ hyperon form factors $\frac{g_1(0)}{f_1(0)}$ and $\frac{f_2(0)}{f_1(0)}$ (where available). Decay rates for these transitions can be found by dividing the branching fraction by the mean lifetime of the parent hyperon. PDG [4] values are averaged over various experimental measurements. *A factor difference of $(M_H + M_{H'})/(M_H)$ exists between definitions.

quantity is that of $\frac{g_A}{g_V}$ for nuclear beta decay which is reported as an average of several measurements at $|\frac{g_A}{g_V}| = 1.2701(25)$ by the PDG [4]. It has been suggested that the precision of this measurement could potentially be improved upon in the near future at CERN [118]. The transition $\Sigma^- \to \Lambda$ has a vanishing $SU(3)$ symmetric limit value for $f_1(0)$ and as the vector form factor is protected from first order symmetry breaking effects the ratio is inverted; best estimates put $\frac{g_V}{g_A} = 0.01(10)$ [4].

The few LQCD studies of the hyperon form factors that exist [47, 97, 98, 119] have focused on the $\Sigma^0 \to n$ decay process, though one has involved $\Xi^0 \to \Sigma^+$. Several of these employ the quenched approximation, which often results in large systematic errors which are difficult to quantify. It is common in these studies to measure the 'lattice' form factors $f_0(q^2)$ (Equation 5.32) and $\tilde{g}_1(q^2)$ (Equation 5.33) due to the ratio of correlation functions used in those calculations. Their results will be discussed later, for comparative purposes, when calculations of form factors from this work are presented in Chapter 6. We define

$$f_0(q^2) \equiv f_1(q^2) + \frac{q^2}{M_H^2 - M_{H'}^2} f_3(q^2), \tag{5.32}$$

where f_0 is sometimes known as f_S, the scalar form factor, and

$$\tilde{g}_1(q^2) \equiv g_1(q^2) - \frac{M_H - M_{H'}}{M_H + M_{H'}} g_2(q^2). \tag{5.33}$$

5.6 Calculating Form Factors

The calculation of hyperon form factors requires information about their dependence on the transferred four-momentum. The four-momentum itself is determined from the energy of the hyperon state $E_H(p)$, $H \in \{N, \Sigma, \Lambda, \Xi\}$. The energy of a hyperon with momentum p is defined through the dispersion relation

$$E_H(p) = \sqrt{\vec{p}^2 + M_H^2}, \tag{5.34}$$

where momentum on the lattice is normally confined within the Brillouin zone of period 2π and $\vec{p} = (p_x, p_y, p_z) = \frac{2\pi}{L}(n_x, n_y, n_z)$ is the lattice momentum. In this work the boundary conditions are twisted such that the transferred four-momenta can take on values between the usual momentum modes of the lattice, such as corresponding to $q^2 = 0$ where the form factors are of most phenomenological interest. We will label the parameter governing this twist to zero by θ_0.

The calculation of the mass of each hyperon for the ensembles used has previously been performed by the QCDSF-UKQCD collaboration as discussed in Section 3.5. The twists are calculated using these values for hyperon masses as per Tables 3.2 and 3.3 and are unique to each of the twelve matrix elements. There is no need to calculate a twist to $q^2 = 0$ for the symmetric ensemble or for diagonal matrix elements as this occurs at lattice momenta $\hat{n} = (0, 0, 0)$ naturally. The second twist value we perform in all cases corresponds to a point between $\hat{n} = (0, 0, 0)$ and $\hat{n} = (1, 0, 0)$ (and equivalent permutations) at $q^2 = (0.075)^2$. This value is denoted θ_1.

The four-momentum transfer can then be calculated from

$$q = (q_4, \vec{q}) = (i(E_H(p) - E_{H'}), \vec{p}_T - \vec{p}'), \tag{5.35}$$

where $\vec{p}_T$ is compact notation for

$$\vec{p}_T = p_x\hat{x} + p_y\hat{y} + \left(p_z - \frac{\theta_i}{L}\right)\hat{z}, \tag{5.36}$$

which depends on the choice of twisting angle $\theta_i \in \{0, \theta_0, \theta_1\}$ which we have introduced in Section 3.3. We will always choose to twist in the z-direction so Equation 5.36 displays this discrimination. The final state will always be considered to be at rest (i.e. $\vec{p}' = 0$) so the calculations simplify. Simulations here consider all lattice momenta permutations (p_x, p_y, p_z), such that $n_i \in \{-1, 0, 1\}$. When no twist is present and $\hat{n} = (0, 0, 0)$ we call this value $q^2_{\text{MAX}} = (M_H - M_{H'})^2$, which is non-zero for off-diagonal matrix elements away from the symmetric point.

Consider now the 2pt (Equation 3.37) and 3pt (Equation 3.50) point correlation functions introduced in Section 3.4. In order to work towards calculating form factors using LQCD we must define an appropriate ratio of correlation functions. Building upon earlier definitions [120–122] we can write the following important ratio between correlation functions (which has proven to be useful for extracting form factors [123]):

$$\mathcal{R}_\Gamma(t, \tau; \vec{p}, \vec{p}'; \mathcal{O}) = \frac{C^{HH'}_\Gamma(t, \tau; \vec{p}, \vec{p}')}{C^{H'}_{\Gamma^{\text{unpol}}}(t; \vec{p}')} \sqrt{\frac{C^{H'}_{\Gamma^{\text{unpol}}}(\tau; \vec{p}') C^{H'}_{\Gamma^{\text{unpol}}}(t; \vec{p}') C^{H}_{\Gamma^{\text{unpol}}}(t - \tau; \vec{p})}{C^{H}_{\Gamma^{\text{unpol}}}(\tau; \vec{p}) C^{H}_{\Gamma^{\text{unpol}}}(t; \vec{p}) C^{H'}_{\Gamma^{\text{unpol}}}(t - \tau; \vec{p}')}}, \tag{5.37}$$

where $0 \ll \tau \ll t$ and τ is the time of current insertion between source, (0), and sink, (t). These conditions will ensure that this particular ratio will be independent of t and τ. The square root part will cancel any smearing from both the source and the sink. Only the quark line connected parts of the three-point functions are included in our analysis and disconnected contributions are ignored.

The index Γ refers to the chosen projection operator which takes on three forms in this work with Γ^{pol} taken in the x or z-directions and the unpolarised, Γ^{unpol}, case making the third option. In the following set of equations $i \in \{x, z\}$:

$$\Gamma \equiv \Gamma^{\text{unpol}} = \frac{1}{2}(1+\gamma_4) \quad \text{or} \quad \Gamma \equiv \Gamma^{\text{pol}} = \frac{1}{2}(1+\gamma_4)i\gamma_5\gamma_i n_i, \tag{5.38}$$

where n_i indicates direction of polarisation.

In order to obtain values from the ratio in Equation 5.37 we choose to take the middle one-third of the lattice time separation between source and sink, which are thirteen time-slices apart. This ratio should be relatively flat over this region in order to obtain a consistent result, an example of which is shown in Figure 5.2. Equation 5.37 can be simplified by our choice of kinematical setup and becomes

$$\mathcal{R}_\Gamma(t, \tau; \vec{p}, 0; \mathcal{O}) = \sqrt{\frac{E_H}{2(E_H + M_H)}} F(\Gamma, \mathcal{O}), \tag{5.39}$$

where we introduce the abbreviations E_H and $E_{H'}$ for the $E_H(\vec{p})$ and $E_H(\vec{p}')$ respectively, however in our case $E_{H'} = M_{H'}$. We also define

$$F(\Gamma, \mathcal{O}) = \frac{1}{4}\text{tr}\Gamma(1+\gamma_4)\mathcal{O}\left(\gamma_4 - i\frac{\vec{p}.\vec{\gamma}}{E_H} + \frac{M_H}{E_H}\right). \tag{5.40}$$

A more detailed description of how to arrive at Equation 5.39 can be found in Appendix C.2. Here the reader can also find full details about the effects of different choices of operator $\mathcal{O}$ on $F(\Gamma, \mathcal{O})$. The transferred four-momenta can be written as

$$q = (i(E_H - M_{H'}), \vec{p}_T). \tag{5.41}$$

We can now write the vector $\mathcal{V}_\mu$, and axial $\mathcal{A}_\mu$, components of the matrix

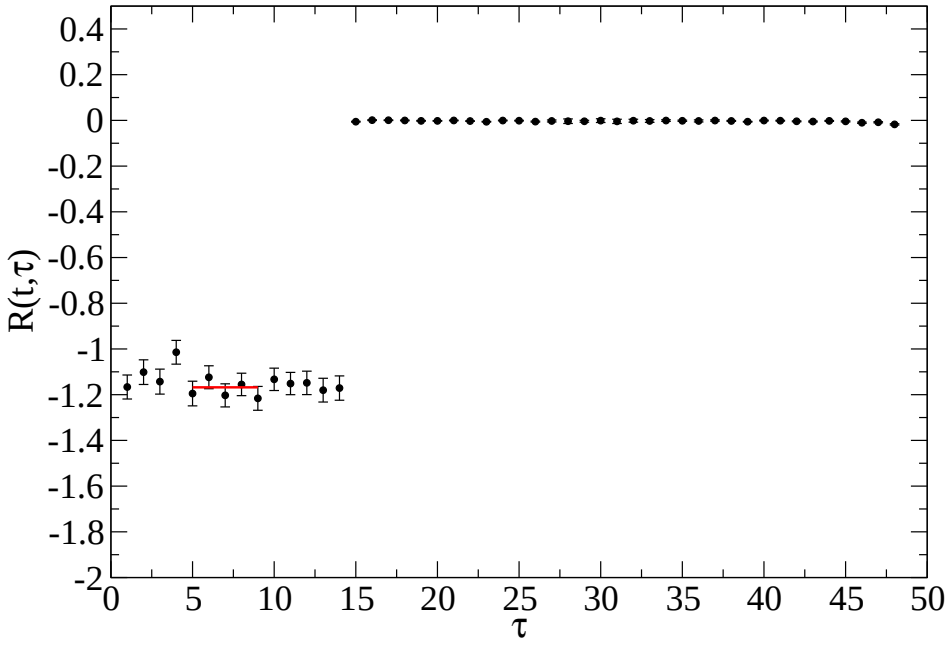

Figure 5.2: Unrenormalised ratio, $\mathcal{R}$, defined in Equation 5.37 choosing $F(\Gamma, \mathcal{O}) = F(\mathcal{V}_4, \Gamma^{\text{unpol}})$ (as per 5.40) with ensemble $\mathcal{E}_3$ for matrix element $\mathcal{A}_{\bar{\Sigma}K\Xi}$ and momentum $\hat{n} = (0, 0, 0)$ with no twist applied. Here τ varies as we have fixed the sink at $t = 13$.

element explicitly given our choice of kinematics. First, for the vector case,

$$\begin{aligned}\mathcal{V}_i &= \gamma_i f_1(q^2) - (\sigma_{ij}p_j + i\sigma_{i4}(E_H - M_{H'}))\frac{f_2(q^2)}{M_H + M_{H'}} - ip_i\frac{f_3(q^2)}{M_H + M_{H'}},\\ \mathcal{V}_4 &= \gamma_4 f_1(q^2) - \sigma_{4j}p_j\frac{f_2(q^2)}{M_H + M_{H'}} + i(E_H - M_{H'})\frac{f_3(q^2)}{M_H + M_{H'}},\end{aligned} \tag{5.42}$$

which upon choosing each of our three values of Γ will lead to the following result,

$$\begin{aligned}
&\mathcal{R}_{\Gamma^{\text{unpol}}}(t,\tau;\vec{p},0;\mathcal{O}_4^V) = \\
&\qquad \sqrt{\frac{E_H+M_H}{2E_H}}\left[f_1(q^2) - \frac{E_H-M_H}{M_H+M_{H'}}f_2(q^2) + \frac{E_H-M_{H'}}{M_H+M_{H'}}f_3(q^2)\right], \\
&\mathcal{R}_{\Gamma^{\text{unpol}}}(t,\tau;\vec{p},0;\mathcal{O}_i^V) = \\
&\qquad \frac{-ip_i}{\sqrt{2E_H(E_H+M_H)}}\left[f_1(q^2) - \frac{E_H-M_{H'}}{M_H+M_{H'}}f_2(q^2) + \frac{E_H+M_H}{M_H+M_{H'}}f_3(q^2)\right], \\
&\mathcal{R}_{\Gamma^{\text{pol}}}(t,\tau;\vec{p},0;\mathcal{O}_4^V) = 0, \\
&\mathcal{R}_{\Gamma^{\text{pol}}}(t,\tau;\vec{p},0;\mathcal{O}_i^V) = \frac{(\vec{p}\times\vec{n})_i}{\sqrt{2E_H(E_H+M_H)}}\left[f_1(q^2)+f_2(q^2)\right],
\end{aligned} \tag{5.43}$$

which relates the ratio to the vector part of the matrix element between two hyperon states. Superficially it may seem that the choice of x or z directions will result in the same ratio but as twisting is only applied in the z-direction, as seen in Equation 5.36, it is important to distinguish between the two. We will refer to Γ_x^{pol} or Γ_z^{pol} when wishing to be specific about direction of polarisation. We have $\hat{n}_i^2 = 1$ when our choice of polarisation is Γ_i^{pol} and zero otherwise.

It should be pointed out that even by twisting to $q^2 = 0$ it is not always possible to extract certain form factors such as $f_2(0)$ directly and extrapolation over q^2 will be required due to factors of $(E_H - M_H)$. If no twists were included the only non-zero ratio when $\hat{n} = (0,0,0)$ is

$$\mathcal{R}_{\Gamma^{\text{unpol}}}(t,\tau;0,0;\mathcal{O}_4^V) = \sqrt{\frac{E_H+M_H}{2E_H}}\left[f_1(q^2_{\text{MAX}}) + \frac{M_H-M_{H'}}{M_H+M_{H'}}f_3(q^2_{\text{MAX}})\right], \tag{5.44}$$

which makes a direct measurement of $f_1(0)$ impossible for transitions. This motivates the inclusion of twists which provides for the necessary number of equations to solve. Twists will also provide extra points between lattice momentum modes at higher q^2 which aids curve fitting; having one twist in between $\hat{n} = (0,0,0)$ and $\hat{n} = (\pm1,\pm1,\pm1)$ will provide nine extra q^2 values in

contrast with the usual four without twisting.

A similar procedure can be followed for the axial-vector components of the matrix elements,

$$\begin{aligned}\mathcal{A}_i &= \gamma_i\gamma_5 g_1(q^2) - \epsilon_{ijk}\left(p_j\sigma_{4k} - \frac{1}{2}\sigma_{jk}(E_H - M_{H'})\right)\frac{g_2(q^2)}{M_H + M_{H'}} - i\gamma_5 p_i\frac{g_3(q^2)}{M_H + M_{H'}},\\ \mathcal{A}_4 &= \gamma_4\gamma_5 g_1(q^2) - \frac{1}{2}\epsilon_{ijk}\sigma_{jk}p_i\frac{g_2(q^2)}{M_H + M_{H'}} + \gamma_5(E_H - M_{H'})\frac{g_3(q^2)}{M_H + M_{H'}}.\end{aligned} \tag{5.45}$$

In this case one can again choose the three values of Γ in the ratio to obtain

$$\begin{aligned}&\mathcal{R}_{\Gamma^{\text{unpol}}}(t,\tau;\vec{p},0;\mathcal{O}_4^A) = 0,\\ &\mathcal{R}_{\Gamma^{\text{unpol}}}(t,\tau;\vec{p},0;\mathcal{O}_i^A) = 0,\\ &\mathcal{R}_{\Gamma^{\text{pol}}}(t,\tau;\vec{p},0;\mathcal{O}_4^A) =\\ &\qquad\frac{\vec{p}.\vec{n}}{\sqrt{2E_H(E_H + M_H)}}\left[g_1(q^2) - \frac{E_H + M_H}{M_H + M_{H'}}g_2(q^2) + \frac{E_H - M_{H'}}{M_H + M_{H'}}g_3(q^2)\right],\\ &\mathcal{R}_{\Gamma^{\text{pol}}}(t,\tau;\vec{p},0;\mathcal{O}_i^A) =\\ &\qquad i\sqrt{\frac{E_H + M_H}{2E_H}}\Bigg[\left(g_1(q^2) - \frac{M_H - M_{H'}}{M_H + M_{H'}}g_2(q^2)\right)n_i\\ &\qquad\qquad - \left(g_2(q^2) - g_3(q^2)\right)\frac{\vec{p}.\vec{n}}{(E_H + M_H)(M_H + M_{H'})}p_i\Bigg],\end{aligned} \tag{5.46}$$

where the only surviving non-zero equation at zero lattice momenta with no twist is

$$\mathcal{R}_{\Gamma^{\text{pol}}}(t,\tau;\vec{p},0;\mathcal{O}_i^A) = i\left(g_1(q^2_{\text{MAX}}) - \frac{M_H - M_{H'}}{M_H + M_{H'}}g_2(q^2_{\text{MAX}})\right)n_i. \tag{5.47}$$

Being able to choose Γ_x^{pol} and Γ_z^{pol} is just as important for the axial current as will be shown.

In a similar fashion to Sasaki and Yamazaki [97] we will now define several dimensionless projected correlators, which we use as shorthand notation to make the calculation of form factors clearer. Note the difference in convention between

that work and the convention used here, for σ_{ij} along with opposite signs for $g_3(q^2)$ and $f_3(q^2)$.

There are three for the vector current, Λ^0, Λ^S and Λ^T and three for the axial current Λ^0, Λ^L, and Λ^T. For the vector case they are defined as

$$\Lambda^0(q^2) = \sqrt{\frac{2E_H}{E_H + M_H}}\mathcal{R}_{\Gamma^{\text{unpol}}}(t, \tau; \vec{p}, 0; \mathcal{O}_4^V), \tag{5.48}$$

$$\Lambda^S(q^2) = -\frac{\sqrt{2E_H(E_H + M_H)}}{ip_i}\mathcal{R}_{\Gamma^{\text{unpol}}}(t, \tau; \vec{p}, 0; \mathcal{O}_i^V), \tag{5.49}$$

$$\Lambda^T(q^2) = \frac{\epsilon_{ijk}\sqrt{2E_H(E_H + M_H)}\mathcal{R}_{\Gamma_k^{\text{pol}}}(t, \tau; \vec{p}, 0; \mathcal{O}_i^V)}{p_j}, \tag{5.50}$$

where an average is taken over non-zero combinations of equivalent momenta at each value of q^2. In the case of Λ^S the average over directions can also be taken (index i). The positive and negative signs of momenta, in each case, are also taken into account such that average is calculated correctly. For Λ^T an average is taken over the two cases of polarisation Γ_x^{pol} and Γ_z^{pol} (as these will be equivalent) along with direction. After averaging over permutations of momenta and directions, where appropriate, we obtain

$$\bar{\Lambda}^0(q^2) = f_1(q^2) - \frac{E_H - M_H}{M_H + M_{H'}}f_2(q^2) + \frac{E_H - M_{H'}}{M_H + M_{H'}}f_3(q^2), \tag{5.51}$$

$$\bar{\Lambda}^S(q^2) = f_1(q^2) - \frac{E_H - M_{H'}}{M_H + M_{H'}}f_2(q^2) + \frac{E_H + M_H}{M_H + M_{H'}}f_3(q^2), \tag{5.52}$$

$$\bar{\Lambda}^T(q^2) = f_1(q^2) + f_2(q^2), \tag{5.53}$$

where the bar notation indicates averaging.

For the axial current we can also define similar functions. These will be somewhat more complicated to calculate.

$$\Lambda^0(q^2) = -\frac{\sqrt{2E_H(E_H + M_H)}\mathcal{R}_{\Gamma_i^{\text{pol}}}(t, \tau; \vec{p}, 0; \mathcal{O}_4^A)}{p_i}, \tag{5.54}$$

$$\Lambda^L(q^2) = -i\sqrt{\frac{2E_H}{E_H + M_H}}\mathcal{R}_{\Gamma_i^{\rm pol}}(t, \tau; \vec{p}, 0; \mathcal{O}_i^A), \tag{5.55}$$

$$\Lambda^T(q^2) = \frac{(E_H + M_H)(M_H + M_{H'})}{p_i p_{i\neq j}}\mathcal{R}_{\Gamma_j^{\rm pol}}(t, \tau; \vec{p}, 0; \mathcal{O}_{i\neq j}^A). \tag{5.56}$$

For Λ^0 an average can be simply taken over both polarisation directions but Λ^L and Λ^T require a more careful treatment. The goal is to create three equations in a similar fashion to the vector case which will be written as

$$\bar{\Lambda}^0(q^2) = g_1(q^2) - \frac{E_H + M_H}{M_H + M_{H'}}g_2(q^2) + \frac{E_H - M_{H'}}{M_H + M_{H'}}g_3(q^2), \tag{5.57}$$

$$\bar{\Lambda}^L(q^2) = g_1(q^2) - \frac{M_H - M_{H'}}{M_H + M_{H'}}g_2(q^2), \tag{5.58}$$

$$\bar{\Lambda}^T(q^2) = g_2(q^2) - g_3(q^2), \tag{5.59}$$

after averaging, however there will be cases, where the ratio $\mathcal{R}_{\Gamma^{\rm pol}}(t, \tau; \vec{p}, 0; \mathcal{O}_i^A)$ will not simply give either one of $\bar{\Lambda}^L$ or $\bar{\Lambda}^T$.

At lower q^2 ($\hat{n} = (0, 0, 0)$ with twist θ_1, for example), the value of Equation 5.59 is impossible to determine due to the presence of p_i in $\mathcal{R}_{\Gamma^{\rm pol}}(t, \tau; \vec{p}, 0; \mathcal{O}_i^A)$ which can vanish identically. Having two choices of polarisation is important here as determining Equation 5.55 will result in a calculation of $\bar{\Lambda}^L$ as defined in Equation 5.58 for $\Gamma_x^{\rm pol}$ and a determination of all of the terms present in the definition of $\mathcal{R}_{\Gamma_z^{\rm pol}}(t, \tau; \vec{p}, 0; \mathcal{O}_3^A)$ (Equation 5.46) for the other choice of polarisation with factors proportional to $g_1(q^2)$, $g_2(q^2)$ and $g_3(q^2)$. Subtracting these two quantities, accounting for appropriate kinematical factors will result in the recovery of $\bar{\Lambda}^T$ as per 5.59.

Furthermore, at higher q^2 (using $\hat{n} = (\pm 1, \pm 1, \pm 1)$ with no twist as an example this time) $\bar{\Lambda}^T$ is easily obtainable, but calculating Equation 5.55 will not result in the desired correspondence to Equation 5.58 in this case. A subtraction between Λ^L and Λ^T in this case will allow one to arrive at the desired form of $\bar{\Lambda}^L$. Again, averaging over equivalent momentum permutations is performed in this work

where applicable.

We are now ready to finally write the form factors of interest in terms of quantities calculated on the lattice. This is done simply by solving the three simultaneous linear equations for both the vector (Equations 5.51-5.53) and axial cases (Equations 5.57-5.59) resulting in

$$f_1(q^2) = \frac{M_H + M_{H'}}{2M_{H'}}\left[\bar{\Lambda}^0(q^2) - \frac{E_H - M_{H'}}{E_H + M_H}\bar{\Lambda}^S(q^2) - \frac{M_H^2 + M_{H'}^2 - 2M_{H'}E_H}{(M_H + M_{H'})(E_H + M_H)}\bar{\Lambda}^T(q^2)\right], \tag{5.60}$$

$$f_2(q^2) = \frac{M_H + M_{H'}}{2M_{H'}}\left[-\bar{\Lambda}^0(q^2) + \frac{E_H - M_{H'}}{E_H + M_H}\bar{\Lambda}^S(q^2) + \frac{M_H + M_{H'}}{E_H + M_H}\bar{\Lambda}^T(q^2)\right], \tag{5.61}$$

$$f_3(q^2) = \frac{M_H + M_{H'}}{2M_{H'}}\left[-\bar{\Lambda}^0(q^2) + \frac{E_H + M_{H'}}{E_H + M_H}\bar{\Lambda}^S(q^2) + \frac{M_H - M_{H'}}{E_H + M_H}\bar{\Lambda}^T(q^2)\right], \tag{5.62}$$

for the vector form factors for all simulated values of q^2 and

$$g_1(q^2) = \frac{M_H + M_{H'}}{2M_{H'}}\left[\bar{\Lambda}^L(q^2) - \frac{M_H - M_{H'}}{M_H + M_{H'}}\left(\bar{\Lambda}^0(q^2) + \frac{E_H - M_{H'}}{M_{H'}}\bar{\Lambda}^T(q^2)\right)\right], \tag{5.63}$$

$$g_2(q^2) = \frac{M_H + M_{H'}}{2M_{H'}}\left[\bar{\Lambda}^L(q^2) - \bar{\Lambda}^0(q^2) - \frac{E_H - M_{H'}}{M_{H'}}\bar{\Lambda}^T(q^2)\right], \tag{5.64}$$

$$g_3(q^2) = \frac{M_H + M_{H'}}{2M_{H'}}\left[\bar{\Lambda}^L(q^2) - \bar{\Lambda}^0(q^2) - \frac{E_H + M_{H'}}{M_{H'}}\bar{\Lambda}^T(q^2)\right], \tag{5.65}$$

for the axial-vector form factors.

As can be seen from the above discussion there will often be ratios that are directly proportional to a very small p_i especially when $p_3 = 0$ and a twist is implemented. These ratios are extremely sensitive to small numerical fluctuations. As such these quantities, such as $\bar{\Lambda}^S$ and $\bar{\Lambda}^T$ for the vector current or $\bar{\Lambda}^T$ for the axial current, will have large uncertainties in these kinematical instances. This will impact on the calculation of certain form factors especially at $q^2 = 0$. Fortuitously, the form factors of primary phenomenological interest to

us, which are $f_1(0)$ and $g_1(0)$, will only depend on these quantities in a suppressed way as can be seen from Equations 5.60 and 5.63. As discussed at the beginning of the chapter we find our data too noisy to sucessfully extract results for the second class form factors.

The renormalised axial-vector form factors suffer from underestimation on the lattice in comparison with experimental results. This is something which has been seen in numerous lattice simulations in the past [124–128] and is no different in this work. Several reasons have been put forward to explain this discrepancy including finite volume effects, lattice spacing effects, excited state contamination and the methods of calculating operator renormalisation constants. These will not be examined in this work and often ratios of quantities of interest will be examined in order to avoid problems associated with operator renormalisation.

A final factor to consider is the behaviour of the form factors as transferred momentum is varied and how results depend on the model used to fit that behaviour. As simulations here are also computed directly with twist θ_0 it is possible to extract at $q^2 = 0$ directly from lattice calculations for most of the dimensionless projected correlators. For example, results for $F_2(0)$ from the diagonal matrix elements, however, are not possible to compute directly and a model must be introduced. It is useful to define, as done in many other studies, a dipole-like fit for some form factor F described by

$$F(q^2) = \frac{F(0)}{\left(1 + \frac{q^2}{M}\right)^2}, \tag{5.66}$$

where $F(0)$ and M are constants which need to be fitted.

"However beautiful the strategy, you should occasionally look at the results."

— Sir Winston Churchill

Chapter 6

Form Factor Results

Chapter 5 introduced hyperon form factors and outlined how to calculate them on the lattice. This chapter contains a report of these form factors as calculated on our $24^3 \times 48$ lattice and forms the basis of all results contained in this work. We will first examine results which are unrenormalised and then introduce both preliminary renormalisation constants and ratios of form factors which should result in renormalisation constant cancellation. Results will be compared to other lattice results when possible and also to experimental data where available.

First, results will be presented for the diagonal matrix elements before moving on to transitions. Several sample plots will be shown to indicate the q^2 dependence of the form factors, a chiral extrapolation to the physical point will then be performed on this data and renormalisation will be considered to arrive at our results.

6.1 Ratio Results: An Example

The dimensionless projected correlators introduced in Section 5.6 are worth examining before moving onto form factor results. As these were introduced by Sasaki and Yamazaki [97] for a calculation of the $\Xi \to \Sigma$ form factors it would

be prudent to look at the same transition in this case. Figures 1, 2 and 3 in that paper describe the ratios taken in their work. As can be seen there are at most five values of q^2 (and in most cases four or less) for each ratio whereas more values are accessible here due to twisting.

Before any comparison, it should also be noted that the ensembles used by Sasaki and Yamazaki are much further away from the physical pion mass than ensembles utilised here. The lattice volume and spacings in that case are different and the calculation is a quenched one. Though this will make any direct comparison between values difficult, an example of Λ^0, Λ^S and Λ^T, corresponding to the vector component, and Λ^L, Λ^0 and Λ^T for the axial-vector component, of the $\Xi \to \Sigma$ transition are shown in Figures 6.1 and 6.2. These can be compared with the results of Sasaki and Yamazaki in order to ascertain if the qualitative behaviour is similar, as it is. Though it is quite difficult to discern, there is an extra point for Λ^L and Λ^0 (vector) corresponding to q^2_{MAX} in these graphs.

As mentioned in the previous chapter, those ratios that are proportional to p_z (e.g. 5.46) are sensitive to the small value of momentum, when a twist is applied, and will result in large errors. For this reason it is necessary to drop the points where there is a twist along with zero lattice momentum for the axial Λ^T and Λ^0. A fit is then applied to the remaining points to determine a value for these quantities at $q^2 = 0$. This is not a problem encountered by Sasaki and Yamazaki as they cannot simulate at these values without twisting the boundary conditions.

The question remains as to which fit is best for these ratios in order to recover their values at $q^2 = 0$. As these ratios are comprised of form factors an attempt to estimate their momentum dependence using phenomenological arguments can be made. The ratio Λ^L is dominated by $g_1(q^2)$, which is often described by a dipole fit [122, 128, 129] in other studies of form factors and thus Λ^L is fitted with a dipole fit. Λ^T is the sum of $g_2(q^2)$, a second class form factor, and $g_3(q^2)$ which is expected to be non-zero and can have quite a strong momentum dependence.

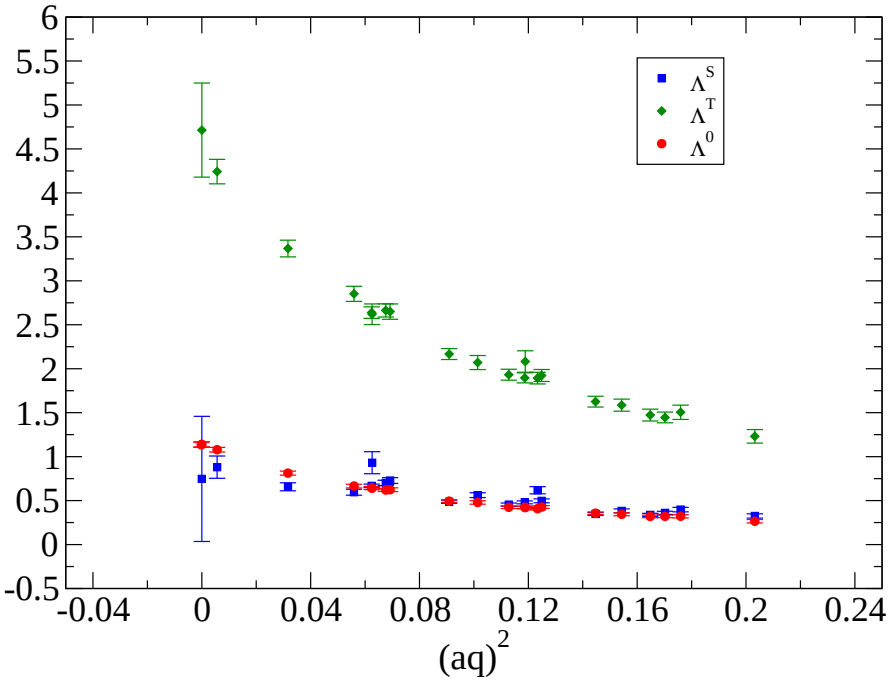

Figure 6.1: Dimensionless quantities Λ^0, Λ^S and Λ^T corresponding to the ratio of correlators of the vector component of current in the $\Xi \to \Sigma$ transition, for use in extracting vector hyperon form factors. Here the ensemble is $\mathcal{E}_4$.

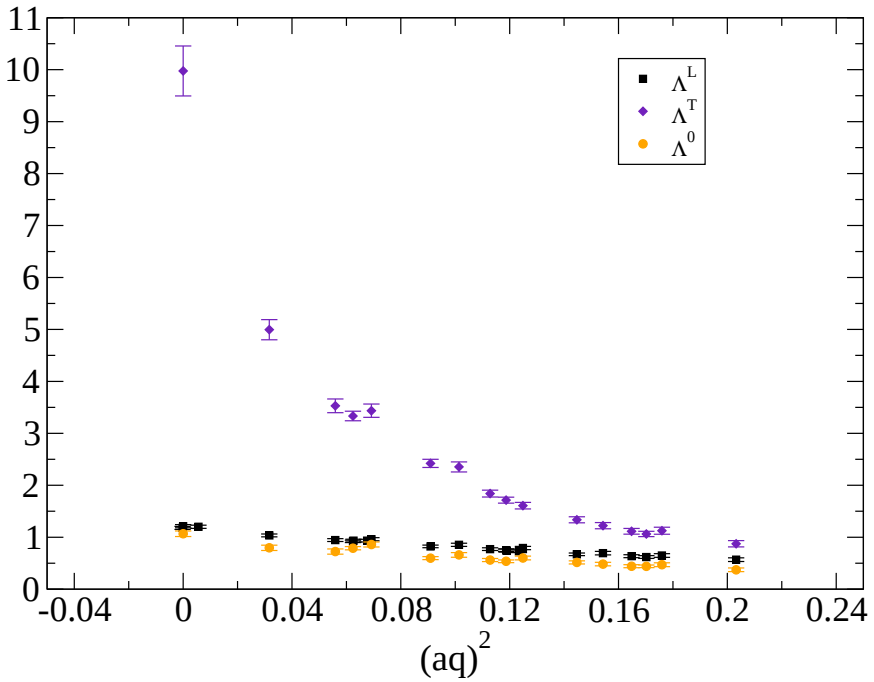

Figure 6.2: Dimensionless quantities Λ^L, Λ^0 and Λ^T corresponding to the ratio of correlators of the axial-vector component of current in the $\Xi \to \Sigma$ transition, for use in extracting axial hyperon form factors. Here the ensemble is $\mathcal{E}_4$. Points at $q^2 = 0$ for Λ^0 and Λ^T are found by extrapolation from other points.

The form factor $g_3(q^2)$ is expected to have what is known as a pion pole fit [97, 126, 128], which is proportional to $g_1(q^2)/(K + q^2)$, where K is a constant related to the pion mass. Sasaki and Yamazaki in particular find a chiral fit for $g_3(q^2)$ of the $\Xi \to \Sigma$ decay to be difficult to perform, but their data does support a pion pole fit. Combining this with our assumption that $g_1(q^2)$ is described by a dipole fit, our fit for Λ^T can therefore be described, in the most general form, as

$$\Lambda^T(q^2) = \frac{A}{1 + Bq^2 + Cq^4 + Dq^6}, \tag{6.1}$$

which is similar to a generalised fit to an arbitrary form factor as described by Kelly [130]. In our case, however, there is some degeneracy in the constants A, B, C and D, which is not shown here for simplicity, and which leaves us with three parameters to be fitted.

Away from $q^2 = 0$ the same behaviour is observed when comparing our ratios with those using similar methods [97, 126] such as those of Sasaki and Yamazaki. For the vector case (Figure 6.1) there is some noticeable noise in Λ^S (blue squares) and Λ^T (green diamonds) but these do not largely impact on the form factor results for the vector current so the lattice calculated values of these ratios are directly used to calculate form factors. The trend of Λ^0 (red circles) is quite clear and this makes the determination of $f_1(0)$ easier to perform as Λ^0 contributions dominate.

For the axial current (Figure 6.2) the trends of Λ^L (black squares) and Λ^0 (gold circles) are similar. This is to be expected, at least at $q^2 = 0$, where these will combine to give $g_2(0)$ which should be zero up to $SU(3)$-breaking effects. Again, Λ^L, is the singularly dominant term in the estimation of $g_1(0) = g_A$ and has a clear behaviour over varying q^2.

6.2 Transferred Momentum Dependence

In this chapter only a very small subset of the possible graphs showing the q^2 behaviour of the vector and axial form factors of the baryon octet will be given because of the large number of possible plots. In most cases it is not necessary to make a fit to our data to calculate form factor results at $q^2 = 0$ due to our twisting of the boundary conditions for each matrix element. It will be necessary for the form factor $F_2(q^2)$ of the diagonal matrix elements however, as simulating at zero transferred momenta is not possible in these cases.

Generally speaking it is this reduced fit model dependence that makes twisting desirable. In the case of HSL decays however, given our choice of kinematics, some model dependence is unavoidable for the axial form factors due to the presence of very small values of momenta suppressing certain ratios of correlation functions. This model dependence should be reduced for $g_1(q^2)$ however as the non-fitted ratio, Λ^L, dominates the estimation.

To fit $f_2(q^2)$ the dipole fit (Equation 5.66) is adopted as a function of the transferred momentum q^2. It should be highlighted that there is one important exception to this 'dipole-like' trend found in our calculations. The form factor $f_1(0) \sim 0$ for $\Sigma \to \Lambda$ is unique in that its trend could also be adequately described as linear in q^2. Again, this is not particularly important as one can simulate directly at $q^2 = 0$ in that case.

We know $|\frac{g_A}{g_V}| = 1.2701(25)$ from the PDG average value. This is a useful quantity one can use to fix Z_A, the axial multiplicative renormalisation constant, at the physical point. The value of $f_1(0)$ will, in effect, count the number of valence quarks in the baryon with the same flavour as those found in the current insertion. In a similar fashion, knowing this is useful in setting a value for Z_V. Ratios can of course also be examined where renormalisation constants should cancel.

6.3 Diagonal Vector Form Factors

The unrenormalised nucleon form factors $F_1(q^2)$ and $F_2(q^2)$ are first examined. $F_1(q^2)$ becomes the coupling constant g_V in the limit of $q^2 \to 0$ and this can be combined with $F_2(q^2)$ to make the Sachs form factors. It is also useful to examine the matrix element in terms of the isovector current $A^{(u-d)}$ (as discussed in Section 5.4); $\langle H|A^{(u-d)}|H\rangle$. We thus write $g_A = \Delta u - \Delta d$ for all matrix elements. In general the label $g_V^{XX;\bar{q}q}$ is given to the vector coupling of baryon X with current insertion contribution from quark flavour q.

The vector form factor $F_1(0) = g_V$ should be unity for the nucleon, N, when considering the isovector current $A^{(u-d)}$. Figures 6.3 and 6.4 show the unrenormalised results for this form factor. As can be seen there is a definite trend over q^2 that can be described by a dipole fit, however, as we can make use of the lattice calculated value exactly at $q^2 = 0$ we fix the form factor fit at $q^2 = 0$ to that value, leaving only one free parameter. We find at the physical point that $g_V^{NN} = 1.15(10)$. We utilise the results for $F_1(0)$ from all octet baryons (four in the isospin limit) and take an average to set $Z_V = 0.877(40)$.

We remind the reader that the x-axis scale is set via the parameter $X_\pi^2 = \frac{1}{3}(2M_K^2 + M_\pi^2)$ (Equation 3.59) which is equal to the square of the symmetric point pion mass up to second order flavour symmetry breaking corrections. A linear fit is also made to approach the physical point from our five ensembles. The chiral extrapolation is relatively flat which indicates good qualitative agreement with the Ademollo-Gatto theorem. One can attempt to quantify the effects of $SU(3)$ symmetry breaking in this form factor and others; this will be the subject of Chapter 7. The errors at the physical point were calculated by making fits to the bootstraps of each ensemble.

An example of $F_2(q^2)$ can be seen in Figure 6.5 for the Λ hyperon. As can be seen, it is necessary in this case to make a fit to the data in order to recover the value of the form factor at $F_2(0)$. A dipole fit is assumed as is done in similar

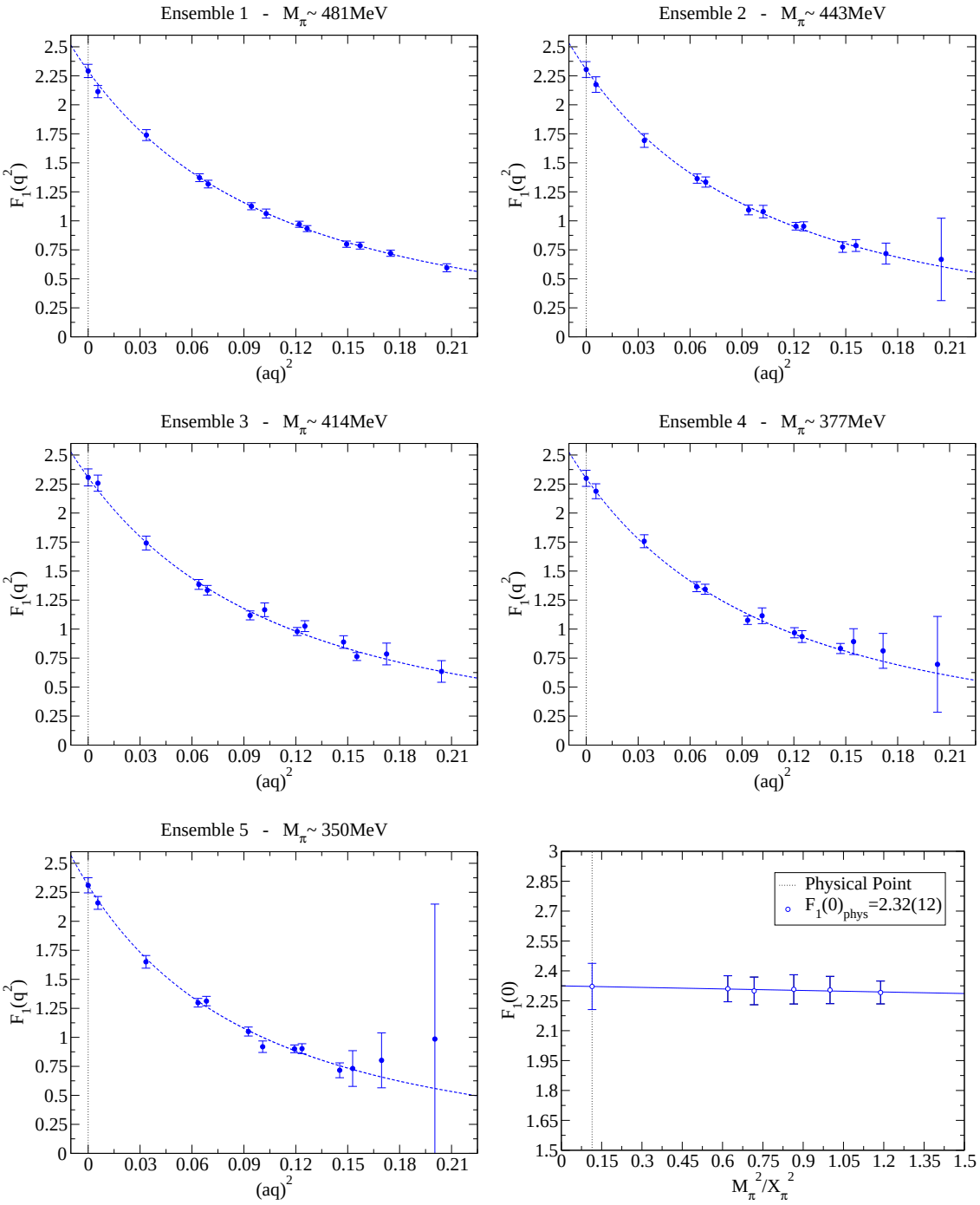

Figure 6.3: Unrenormalised vector form factor $F_1(q^2)$ of N for a $\bar{u}\gamma_\mu u$ current on all five ensembles, where the dotted line indicates $q^2 = 0$. A dipole fit has been made to the data with $F_1(0)$ fixed to the lattice calculated value. The bottom right graph is the linear chiral extrapolation to the physical limit, which is represented by a dashed line. Here $g_V^{NN;\bar{u}u} = 2.32(12)$.

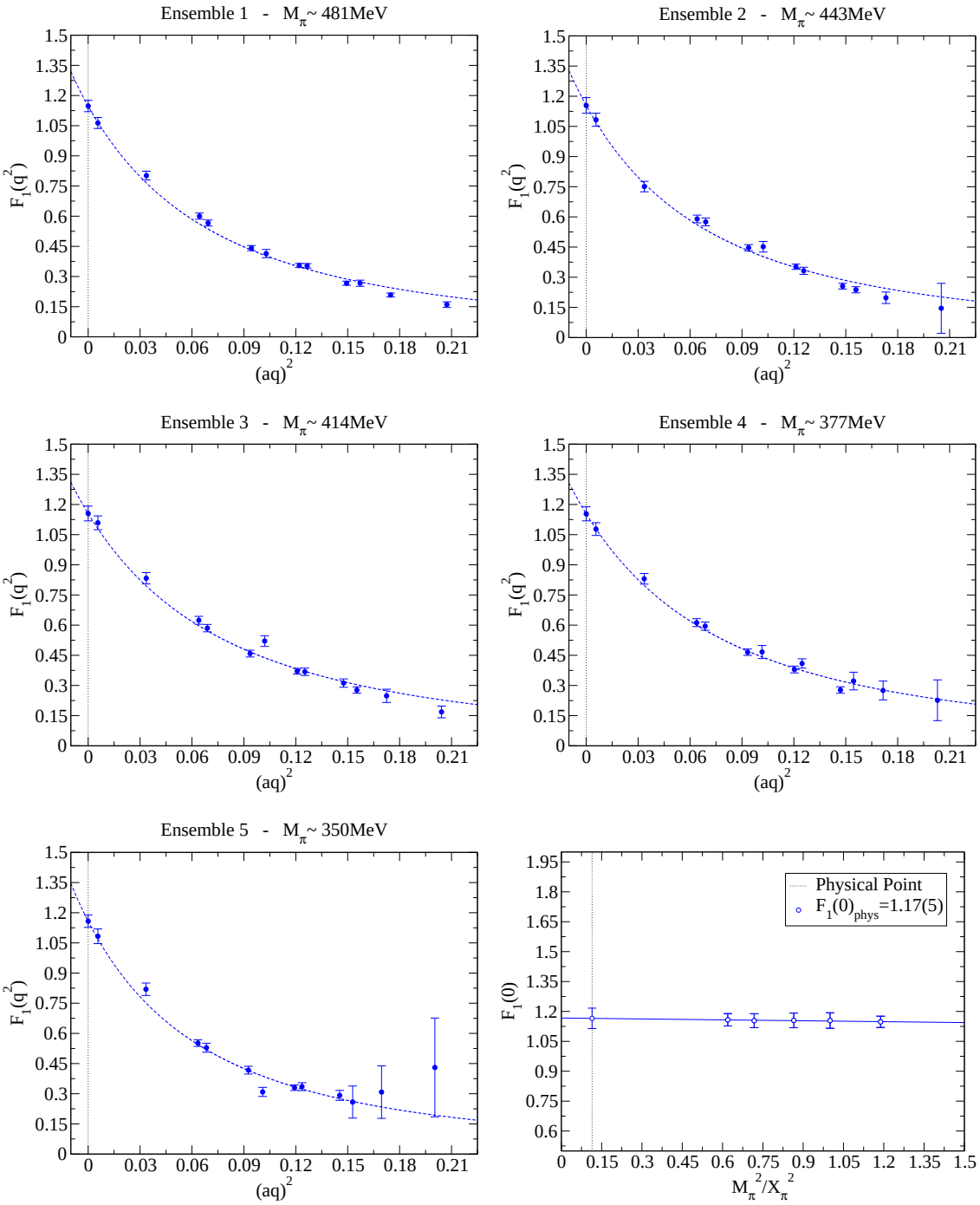

Figure 6.4: Unrenormalised vector form factor $F_1(q^2)$ of N for a $\bar{d}\gamma_\mu d$ current on all five ensembles, where the dotted line indicates $q^2 = 0$. A dipole fit has been made to the data with $F_1(0)$ fixed to the lattice calculated value. The bottom right graph is the linear chiral extrapolation to the physical limit, which is represented by a dashed line. Here $g_V^{NN;\bar{d}d} = 1.17(5)$.

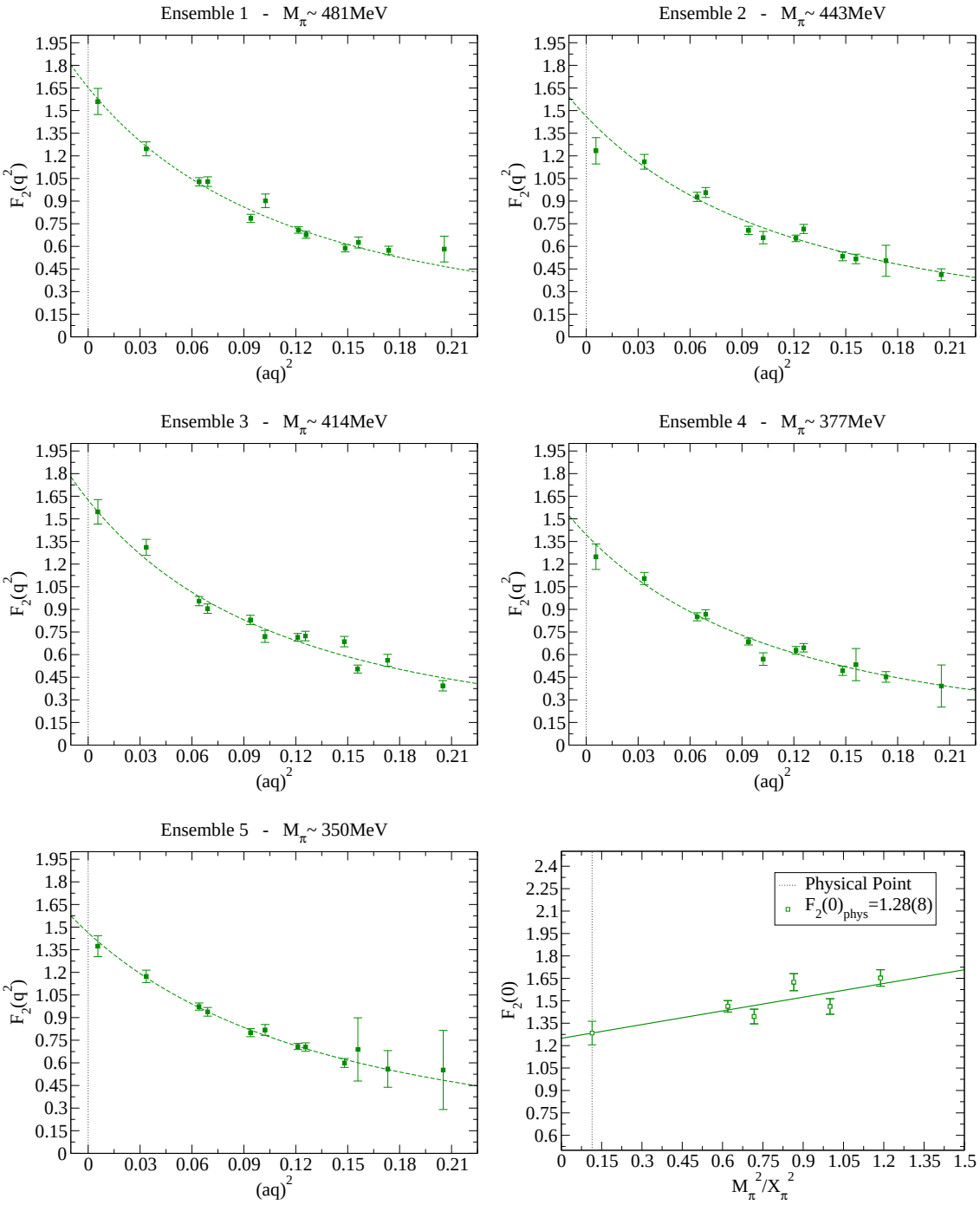

Figure 6.5: Unrenormalised vector form factor $F_2(q^2)$ of Λ for a $\bar{s}\gamma_\mu s$ current on all five ensembles, where the dotted line indicates $q^2 = 0$. A dipole fit has been made to the data over q^2 in each case. The bottom right graph is the linear chiral extrapolation to the physical limit, which is represented by a dashed line. The error on $F_2(0) = 1.28(8)$ at the physical point is calculated by the bootstrap method.

treatments of that form factor [131, 132], but as no value is measured $q^2 = 0$ in this case a second fit parameter $F_2(0)$, is introduced, in contradistinction to the $F_1(q^2)$ fit. The chiral extrapolation in this figure is indicative of a form factor that does not obey the Ademollo-Gatto theorem and has noticeable first order symmetry breaking effects.

By combining the result for $F_1(q^2)$ with the form factor $F_2(q^2)$ the numerical values for the Sachs form factors $G_e(0)$ and $G_m(0)$ as defined in Equations 5.23 and 5.24, can be determined. The results for the renormalised Sachs form factors $G_e^R(0)$ and $G_m^R(0)$ contributions from the singly and doubly represented quarks of the octet baryons are now given in Table 6.1. The form factor $G_e^R(0)$ is identical to $F_1^R(0)$ at $q^2 = 0$. The R superscript refers to a renormalised quantity. In order to compare with experiment and other LQCD calculations we can apply the isovector current to determine the baryon magnetic moments which has previously been defined as $\mu^{(H)} = G_m^R(0)$. The isovector magnetic moment is worth examining as disconnected quark loops cancel. Results from this work can be compared with those for the hyperons form factors calculated by Shanahan et al. [131] in Table 6.2.

H	$G_e^R(0)_{\mathcal{S}}$	$G_e^R(0)_{\mathcal{D}}$	$G_m^R(0)_{\mathcal{S}}$	$G_m^R(0)_{\mathcal{D}}$
N	1.021(65)	2.036(84)	−0.444(96)	3.14(15)
Σ	0.984(57)	2.037(93)	−0.509(75)	3.62(18)
Λ	0.978(57)	1.024(49)	2.12(13)	0.106(58)
Ξ	1.025(70)	1.958(90)	−0.640(85)	3.43(14)

Table 6.1: Renormalised values for $G_e^R(0)$ using lattice calculated values of $F_1^R(0)$. Results for the renormalised $G_m^R(0)$ are partly as a result of a dipole fit to the $F_2^R(0)$ data because it is the sum of $F_1^R(0)$ and $F_2^R(0)$. The $\mathcal{S}$ and $\mathcal{D}$ subscripts refer to the singly and doubly represented quarks respectively. In the case of the Λ hyperon the $\mathcal{D}$ subscript corresponds to either of the light quarks.

The isovector magnetic form factor results shown in Table 6.2 compare well with experiment for the Σ and Ξ hyperons and are in fact closer to the experimentally measured values than Shanahan et al. The result for the nucleon,

	$\mu^{(H)}$ (μ_N)		
H	P.E. Shanahan et al. [131]	Result	Experiment [4]
$n-p$	3.8(3)	3.6(2)	4.70(6)
$\Sigma^+ - \Sigma^-$	3.0(2)	3.6(2)	3.62(3)
$\Xi^0 - \Xi^-$	−0.51(8)	−0.64(9)	−0.60(1)

Table 6.2: Results for isovector magnetic moments along with experimental results and values determined from another study on a $32^3 \times 64$ lattice. The definition $G_m^R(0) = \mu^{(H)}$ has been used, where $G_m^R(0)$ is a combination of $F_1^R(0)$, which is directly calculated, and $F_2^R(0)$, which has been obtained from a dipole fit.

however, is slightly further away from the experimental value than the other lattice determination, but compares well with that lattice result suggesting that LQCD estimations may underestimate the $G_m(q^2)$ nucleon form factor.

It is worth noting that when considering the electromagnetic current (see Equation 5.21) we find that $G_m^R(0) = -0.63(5)$ for the Λ baryon which should be compared with the experimental PDG global average value of $\mu^{(\Lambda)} = -0.613(4)$ [4], though disconnected loops will contribute here.

6.4 Diagonal Axial Form Factors

The axial form factor of the diagonal matrix elements $G_1(q^2) = G_A(q^2)$ is not protected from first order symmetry breaking effects in contrast with the vector form factor $F_1(q^2)$. As before, we look at the isovector current as the axial coupling constant $g_A = G_A(0)$ has been defined in those terms, as per Equations 5.25 and 5.26. Again, a similar notation is adopted to the vector case with $g_A^{XX;\bar{a}a}$ being the contribution to the coupling constant of baryon X from the a flavour quark.

Repeating the analysis from the previous section we first examine the plots of the momentum dependence of the $G_1(q^2)$ form factor with the $\bar{u}\gamma_\mu u$ and $\bar{d}\gamma_\mu d$ contributions to the axial current for the nucleon in Figures 6.6 and 6.7. The

non-zero q^2 data for the axial form factors are generally noisier than their vector counterparts and this is evident in these figures. The error at $q^2 = 0$ is reduced thanks to our boundary condition twisting.

We continue to adopt a dipole trend and comment that our data is not precise enough to fix the momentum dependence of these form factors. Again, the value of $G_1(0)$ is fixed to that of the lattice calculated value as it is available to us from at the choice of zero lattice momentum. If we were to leave $G_1(0)$ as a free fit parameter this would only result in a change to the central value of g_A^{NN} of $\sim 1\%$, less than our level of precision, so we continue to constrain $G_1(0)$ in our fits.

As can be seen in the chiral extrapolation of $G_1(0)$ of Figure 6.7, there is a slight deviation from a constant fit. This suggests that the $SU(3)$ symmetry breaking effects for the nucleon are in fact quite small, though larger deviations are seen for other transitions. This will be confirmed in more detail in later analysis of the $G_1(0)$ form factor. We can determine g_A^{NN} from these extrapolations and we find $g_A^{NN} = 1.28(2)$ which will clearly underestimate the experimental value of g_A after renormalisation as one expects $Z_A < 1$. This is to be expected in some sense as it is consistently found to be the case, for a variety of possible reasons, when calculated using LQCD as discussed at the end of Section 5.6.

We will examine two ratios of the isovector axial coupling constants $\frac{g_A^{\Sigma\Sigma}}{g_A^{NN}}$ and $\frac{g_A^{\Xi\Xi}}{g_A^{NN}}$, where multiplicative renormalisation constants should cancel, in Figure 6.8. These unfortunately cannot be compared with experiment as little reliable data exists for $g_A^{\Xi\Xi}$ or $g_A^{\Sigma\Sigma}$. These ratios can be compared with results of other theoretical estimations from LQCD however, such as those calculated by Lin and Orginos [85]. The ratios defined in Equation 5.29 are also calculated and finally we can present one of the first lattice results of $G_A(0)$ for the Λ hyperon.

The only existing bounds upon $g_A^{\Sigma\Sigma}$ and $g_A^{\Xi\Xi}$ come from large-N_c calculations and chiral perturbation theory which are not at a particularly high level of

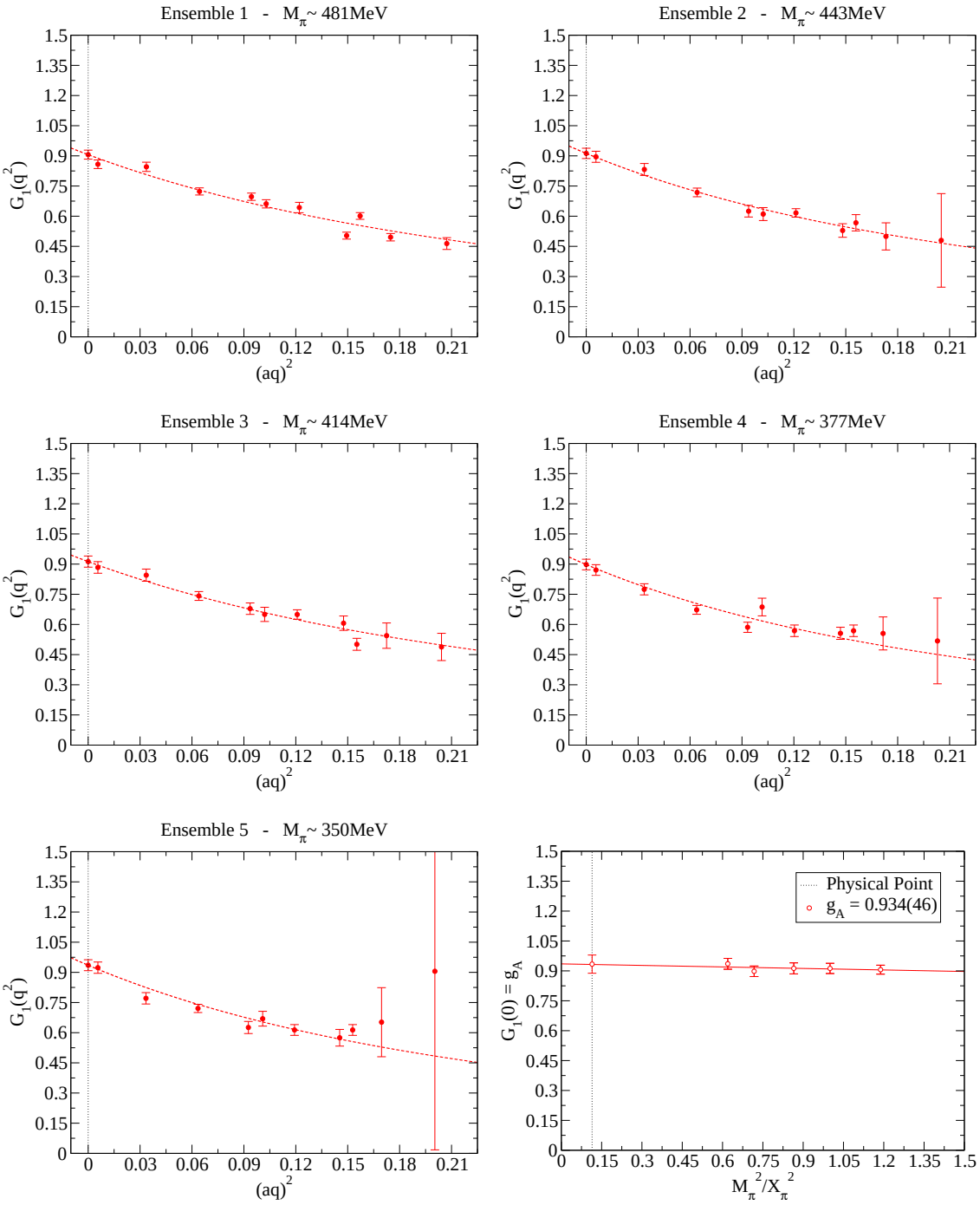

Figure 6.6: Unrenormalised axial form factor $G_1(q^2)$ of N for a $\bar{u}\gamma_\mu\gamma_5 u$ current on all five ensembles, where the dotted line indicates $q^2 = 0$. A dipole fit has been made to the data with $G_1(0)$ fixed to the lattice calculated value. The bottom right graph is the linear chiral extrapolation to the physical limit, which is represented by a dashed line. Here $g_A^{NN;\bar{u}u} = 0.934(46)$.

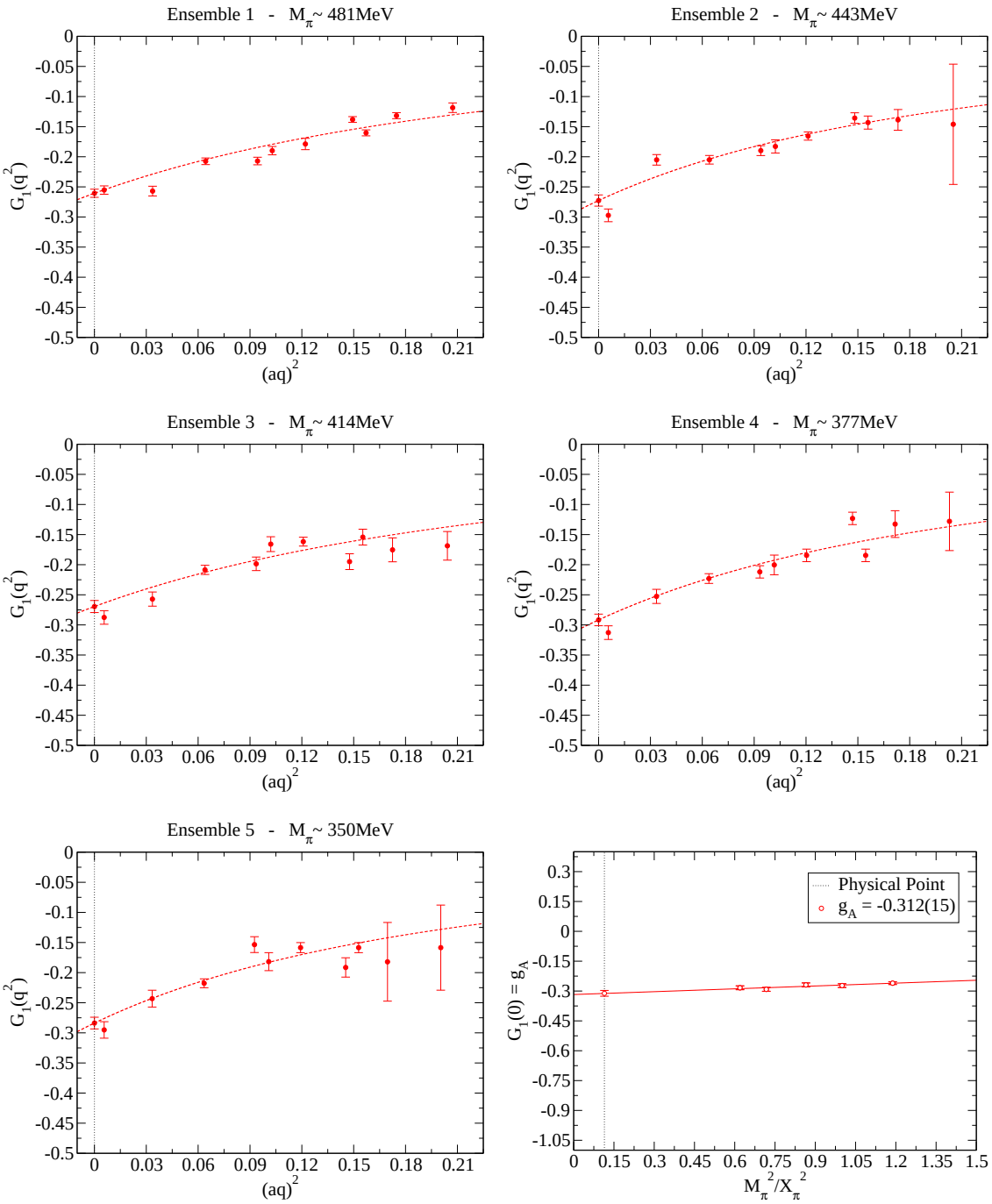

Figure 6.7: Unrenormalised axial form factor $G_1(q^2)$ of N for a $\bar{d}\gamma_\mu\gamma_5 d$ current on all five ensembles, where the dotted line indicates $q^2 = 0$. A dipole fit has been made to the data with $G_1(0)$ fixed to the lattice calculated value. The bottom right graph is the linear chiral extrapolation to the physical limit, which is represented by a dashed line. Here $g_A^{NN;\bar{d}d} = -0.312(15)$.

precision [74, 133]:

$$0.14 < -\frac{g_A^{\Xi\Xi}}{g_A^{NN}} < 0.28, \tag{6.2}$$

$$0.47 < \frac{g_A^{\Sigma\Sigma}}{g_A^{NN}} < 0.87, \tag{6.3}$$

which can be used as a rough comparison for our results from methods independent of LQCD. From Figure 6.8, with linear fits, we find that our calculations indicate

$$-\frac{g_A^{\Xi\Xi}}{g_A^{NN}} = 0.22(1), \tag{6.4}$$

$$\frac{g_A^{\Sigma\Sigma}}{g_A^{NN}} = 0.69(3), \tag{6.5}$$

which are in accordance with the estimations above, albeit with relatively large uncertainties. These results can also be compared with the lattice calculation by H-W. Lin and K. Orginos [85] who find $-\frac{g_A^{\Xi\Xi}}{g_A^{NN}} = 0.23(4)$ and $\frac{g_A^{\Sigma\Sigma}}{g_A^{NN}} = 0.76(10)$ which agree with our results within 1σ.

Finally for the axial coupling constants, two ratios of axial charges can be plotted, which are equal to unity and $\frac{D}{F}$ at the symmetric point respectively. These are

$$\frac{g_A^{NN} + g_A^{\Xi\Xi}}{g_A^{\Sigma\Sigma}} = 1 \tag{6.6}$$

and

$$\frac{g_A^{NN} - g_A^{\Xi\Xi}}{g_A^{\Sigma\Sigma}} = \frac{D}{F}. \tag{6.7}$$

Figure 6.9(a) should be equal to unity in the $SU(3)$ symmetric limit and we determine that ratio to be 1.01(4) at this point. The second ratio, Figure 6.9(b), can be compared with determinations of the F and D parameters. Savage and Walden [133] examine the available experimental data and make model independent estimates of the first order $SU(3)$ symmetry breaking effects so that they can then find $\frac{D}{F} = 1.7(3)$. Our result is $\frac{D}{F} = 1.60(5)$ which is in good agreement. Using the results from H-W. Lin and K. Orginos' work on the lattice

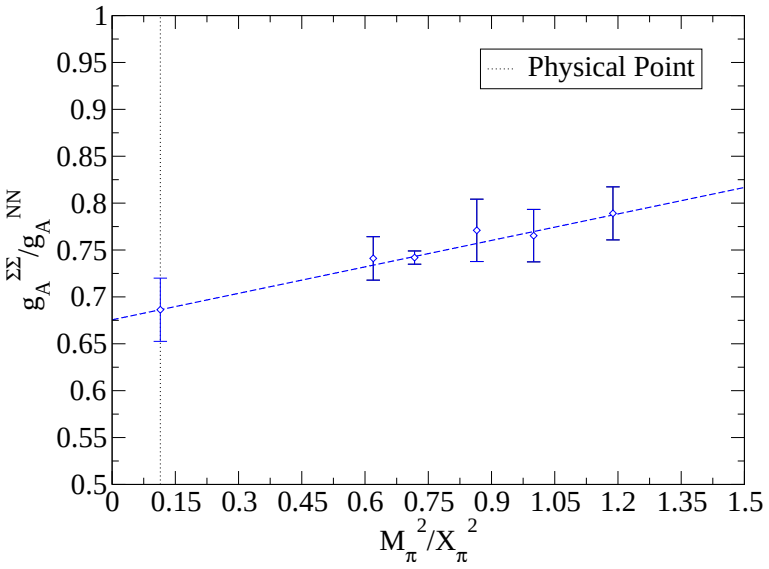

(a) Ratio of axial coupling for Σ with axial coupling of nucleon

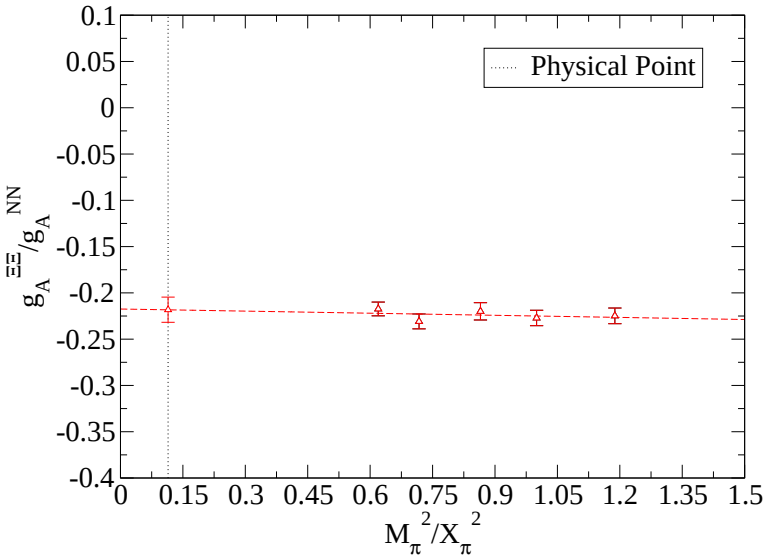

(b) Ratio of axial coupling for Ξ with axial coupling of nucleon

Figure 6.8: Ratio of axial coupling constants (a) $\frac{g_A^{\Sigma\Sigma}}{g_A^{NN}}$ and (b) $\frac{g_A^{\Xi\Xi}}{g_A^{NN}}$ along with chiral extrapolation to physical pion mass (dashed lines). All errors are calculated using the bootstrap error method.

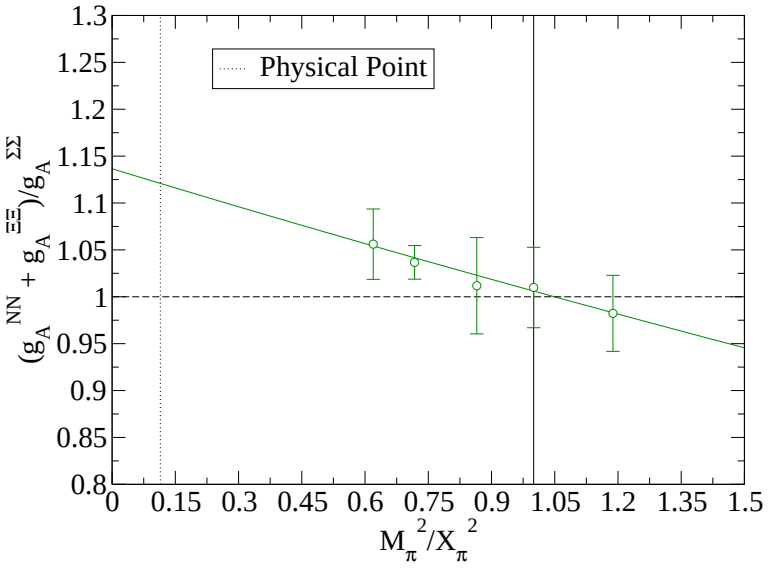

(a) Ratio $\frac{g_A^{NN}+g_A^{\Xi\Xi}}{g_A^{\Sigma\Sigma}}$ equal to unity (black dashed line) at the symmetric point (vertical black line in plot).

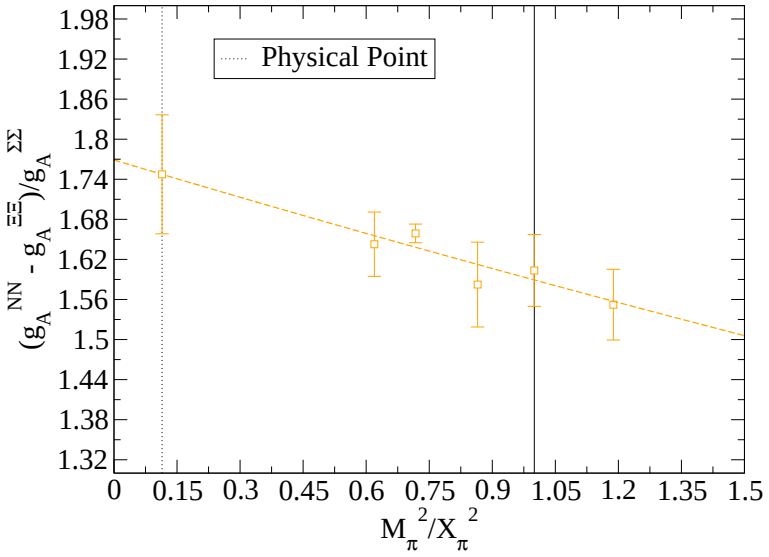

(b) Ratio $\frac{g_A^{NN}-g_A^{\Xi\Xi}}{g_A^{\Sigma\Sigma}}$ equal to $\frac{D}{F}$ at the symmetric point (vertical black line in plot).

Figure 6.9: Ratios of the axial coupling constants in the combinations (a) $\frac{g_A^{NN}+g_A^{\Xi\Xi}}{g_A^{\Sigma\Sigma}}$ and (b) $\frac{g_A^{NN}-g_A^{\Xi\Xi}}{g_A^{\Sigma\Sigma}}$, each with a chiral extrapolation to the physical point. Ratio (a) is notable as it should be equal to unity, at least at the symmetric point where $m_l = m_s$. All errors are calculated using the bootstrap error method.

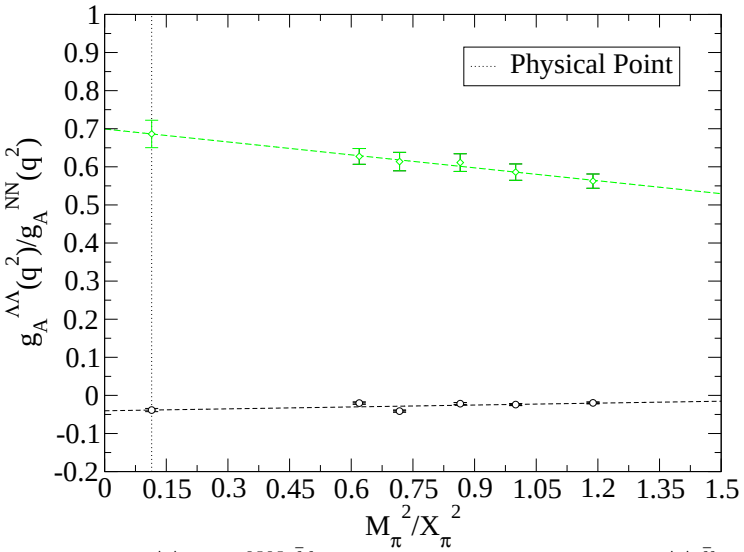

Figure 6.10: Ratios $g_A^{\Lambda\Lambda;\bar{s}s}/g_A^{NN;\bar{d}d}$(green diamonds) and $g_A^{\Lambda\Lambda;\bar{l}l}/g_A^{NN;\bar{u}u}$ (black circles). Also shown is chiral extrapolation to the physical point (represented by dotted black line). Errors are calculated using the bootstrap method.

would result in finding $\frac{D}{F} = 1.6(1)$. This is similar to the value found here as both calculations are performed at the symmetric point.

There are other calculations of the same quantity, where the authors neglect first order symmetry breaking effects, for example a two parameter fit has been made to find $\frac{D}{F} = 1.70(4)$ using available experimental results [74] or a similar calculation by Mateu and Pich [106] which finds $\frac{D}{F} = 1.75(3)$. Results are again in agreement if the value of this ratio is taken to be at the physical point where we find 1.75(9). It is important to point out that this ratio is not equal to $\frac{D}{F}$ now due the appearance of higher order effects away from the symmetric point. Both sets of authors report a poor fit due to the effects of $SU(3)$ symmetry breaking.

The axial coupling contributions to the Λ baryon from the light and strange quarks were also calculated in this work. The ratio of the strange contribution to the Λ axial coupling $g_A^{\Lambda\Lambda;\bar{s}s}$ to the axial coupling of the nucleon is taken. The same is done with the light quark component $g_A^{\Lambda\Lambda;\bar{l}l}$, to the nucleon axial coupling. These ratios are considered in Figure 6.10 where we show that $\frac{g_A^{\Lambda\Lambda;\bar{s}s}}{g_A^{NN}} = 0.69(4)$ and $\frac{g_A^{\Lambda\Lambda;\bar{l}l}}{g_A^{NN}} = -0.038(4)$.

6.5 Baryon Spin Fractions: An Aside

As the individual matrix elements $\langle H|\bar{q}\gamma_\mu\gamma_5 q|H\rangle$ with quark flavour q have been calculated one can relate this to the fraction of spin carried by the constituent quarks in a particular octet baryon as previously mentioned in Section 5.4. The analysis of the chiral extrapolation to the physical point can be somewhat involved and that will not be a focus here. We do however qualitatively compare our results for these spin fractions to those of Göckeler et al. [114] and Shanahan et al [134]. The former determined the spin fraction contributions of Δs and $\Delta u/d$ to the Λ baryon from a quenched calculation in 2002 while the latter calculates ratios of spin fractions of the Ξ and the Σ to that of the nucleon.

Our results, like those to be compared against, do not take into account the contributions from disconnected diagrams including the effect of strangeness contribution to the spin of the nucleon. This has been estimated to be anything from a value close to zero, in recent lattice calculations [135, 136], to a small, but in some cases significant, negative contribution of the order $\Delta s \approx -0.1$ [137], though these results have been disputed [138, 139]. Here only the effects of spin carried by the light quarks in the nucleon are considered.

Firstly, the spin fractions of the strange and light quarks in the Λ baryon will be examined. A graph showing a linear fit can be seen in Figure 6.11. Here the experimental value of g_A for the nucleon is used to set the relevant renormalisation constant. A linear fit is adopted as is done by Göckeler et al. and we find a value of $\Delta s = 0.867(5)$ and $\Delta u/d = -0.048(5)$ which can be compared with $\Delta s = 0.68(4)$ and $\Delta u/d = -0.02(4)$ of Göckeler et al. [114]. We can see that their result for $\Delta u/d$ is consistent with zero which is not the case here. Our result for Δs is also significantly larger than theirs. There are several possible reasons for this including the fact that the reference we compare with is a quenched calculation and that the chiral extrapolation depends only on three points, at much larger light quark masses than those computed in this study.

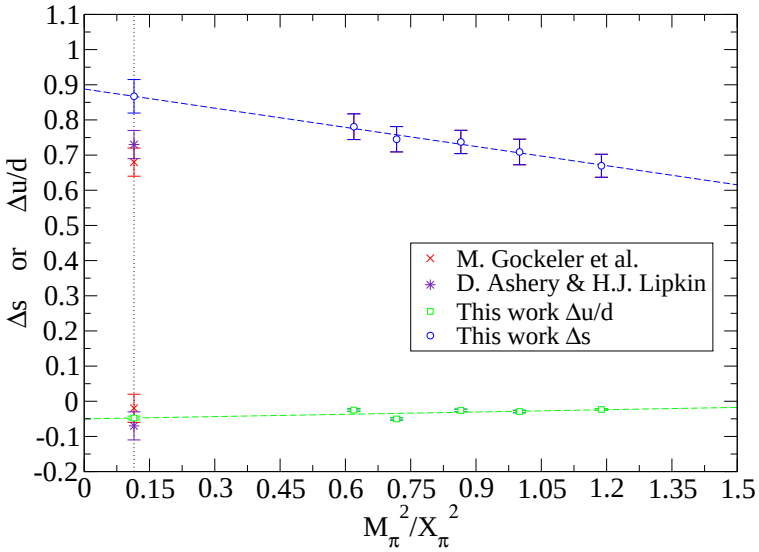

Figure 6.11: Δs (blue circles) and $\Delta u/d$ (green squares) spin contributions to the Λ baryon, excluding disconnected loop effects. A linear fit is made to the physical point which is represented by the black dotted line. Also included are results at physical point of M. Göckeler et al. [114](red crosses) and Ashery and Lipkin [140](purple stars) for comparison.

Another likely reason for this difference could arise from the choice of renormalisation constant Z_A. In that paper the value of Z_A was obtained non-perturbatively. A very recent study of octet spin fractions using a different procedure, known as the Feynman-Hellmann approach, was carried out by the CSSM and QCDSF-UKQCD collaborations [141]. Using the quoted value of $\Delta s = 0.68(4)$ along with their renormalisation factor (which is reported as being preliminary) results in a value of $\Delta s^{\text{latt}} = 0.80(1)$ for the unrenormalised version. Our value is $\Delta s^{\text{latt}} = 0.85(3)$, which is not within error of the other result but is closer than the renormalised case. This may be an indication of finite volume effects.

We can also compare with Ashery and Lipkin [140] who rely on models which assume $SU(3)$ symmetry of the sea to calculate spin contributions to the Λ. They find $\Delta s = 0.73(4)$, which again is a result smaller than ours, but to a lesser extent in this case, and $\Delta u/d = -0.07(4)$ which indicates a possible small non-zero value as we find. The naïve quark model predicts that the strange quark will carry all

of the spin of the Λ [140]; all results presented here disagree with that.

Apart from looking at the spin contribution of each flavour of quark we can also determine Σ^H which is the total spin contributed by the valence quarks of hyperon H. Here the ratio of spin in the Σ, Λ and Ξ to that of the nucleon, N, is calculated. Again, a simple linear fit for our chiral extrapolation is made, though more complicated parameterisations can be considered, such as those by Shanahan et al. [142]. We find the following results: $\frac{\Sigma^\Sigma}{\Sigma^N} = 0.87(6)$, $\frac{\Sigma^\Lambda}{\Sigma^N} = 1.3(1)$ and $\frac{\Sigma^\Xi}{\Sigma^N} = 1.3(1)$.

These values can be be roughly compared with those of Shanahan et al. [134] which involves a calculation with the same set of configurations used in this work. The chiral fit in that reference results in significantly large error bars, as they use a more complicated chiral extrapolation, though both set of results are consistent. Shanahan et al. find $\frac{\Sigma^\Sigma}{\Sigma^N} = 0.9(1)$ and $\frac{\Sigma^\Xi}{\Sigma^N} = 1.6(3)$. No result are presented for $\frac{\Sigma^\Lambda}{\Sigma^N}$.

6.6 Transition Vector Form Factors

This section and the one following, will outline our results for the transition matrix elements between octet hyperons. We first start with the vector form factors $f_1(q^2)$ and $f_2(q^2)$. As discussed earlier, the form factor $f_1(q^2)$ is protected from first order $SU(3)$ flavour symmetry breaking effects by the Ademollo-Gatto theorem. This is the only form factor considered here for which this is the case. Due to this theorem, final results extrapolated to the physical point should be quite similar to the value predicted by $SU(3)$ symmetry (see Table 5.3). The form factor $f_1(0)$ will be denoted g_V in what follows and the value found in Section 6.3 will be used to renormalise.

We find our results at the physical value are entirely consistent with the $SU(3)$ symmetric limit prediction for g_V. In fact within error, after making a linear fit,

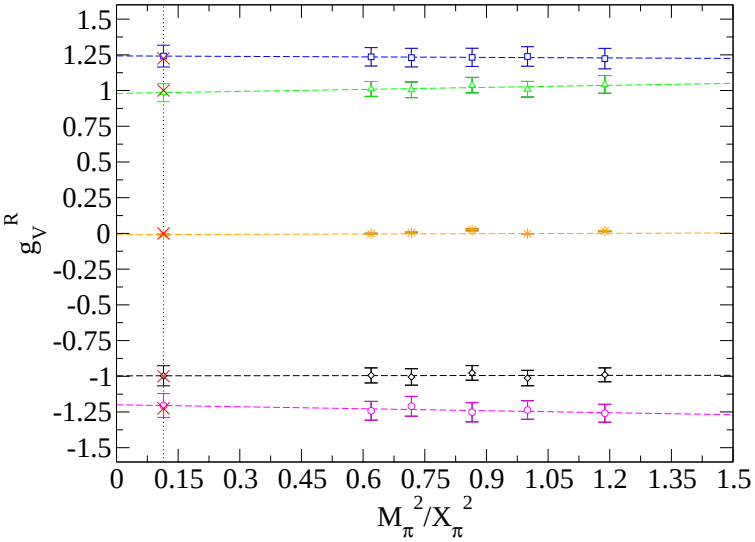

Figure 6.12: Renormalised g_V^R for the transition matrix elements of the baryon octet. The transitions are: $\Xi \to \Lambda$(blue squares), $\Xi \to \Sigma$(green triangles), $\Sigma \to \Lambda$(orange stars), $\Sigma \to N$(black diamonds) and $\Lambda \to N$(pink circles). A linear fit is made to the five ensembles to the physical point, which is represented by the dotted line. The $SU(3)$-flavour symmetric values (see Table 5.3) are also indicated by red crosses.

no discernible slope is found for any of the five transition matrix elements. It can be said that our simulations are not accurate enough to detect any second order symmetry breaking effects. Results for the vector form factor $f_1(0) = g_V^R$ are given in Table 6.3 and depicted in Figure 6.12.

Transition	g_V^R	$SU(3)$
$\Xi \to \Lambda$	1.24(7)	1.225
$\Xi \to \Sigma$	0.99(6)	1
$\Sigma \to \Lambda$	−0.008(8)	0
$\Sigma \to N$	−1.00(7)	−1
$\Lambda \to N$	−1.20(8)	−1.225

Table 6.3: Results for the renormalised form factor $f_1^R(0)$ (and thus vector coupling constant g_V^R) for the transition matrix elements between octet hyperons. The $SU(3)$ symmetric limit value is also shown in the rightmost column.

These results can also be compared with existing LQCD calculations available of hyperon semi-leptonic decays such as Sasaki [119] who finds $g_V^R = 0.973(8)$ for

the $\Xi \to \Sigma$ transition and $g_V^R = -0.97(2)$ for $\Sigma \to N$. Another quenched lattice calculation performed in 2006 by Guadagnoli et al. [98] finds $g_V^R = -0.99(7)$ for the transition $\Sigma \to N$. The results from Sasaki's calculation are more precise than ours and those of Guadagnoli et al. due to the ratio used, which would have been computationally expensive to use in our work. Clearly, all lattice calculations discussed here agree within error.

As before, only a sample of the plots of the q^2 dependency of the f_1 form factors are shown here. In this instance $\Xi \to \Lambda$ (Figure 6.13) and $\Lambda \to N$ (Figure 6.14) are chosen and a dipole fit fixed by the measured value at $q^2 = 0$ is plotted. These graphs show the unrenormalised lattice data. Again it can be seen that our data supports a dipole fit, though this is not very important for our purposes as we are interested in $q^2 = 0$. As two separate twists have been made for each transition matrix element ensemble (excepting the symmetric point) there will be more points in between the momentum Fourier modes than is seen for the diagonal matrix elements. These points are generally consistent within our fit.

The form factor $f_2(q^2)$ is best examined as a ratio to the vector form factor $f_1(q^2)$ as this is how it is measured in experiment. It is also the way in which other lattice authors often quote their results. For $\Sigma \to \Lambda$ the renormalised value of $f_2(q^2)$ is a more sensible way of presenting results due to the small value of $f_1(q^2)$ for this transition. The predictions of the Cabibbo theory for $\frac{f_2(q^2)}{f_1(q^2)}$ in the $SU(3)$ limit have already been outlined in Table 5.3. There are a few existing experimental results (Table 5.4) and LQCD calculations that can also be compared with.

As can be seen from Table 6.4 our results in general do not agree with the Cabibbo model but are closer to estimations using Sirlin's formula. This is something that is also acknowledged by S. Sasaki in his calculation of f_2 for $\Xi \to \Sigma$ [97]. Our results agree with those found in existing experimental and lattice calculations. This would suggest a weakness in the Cabibbo model for

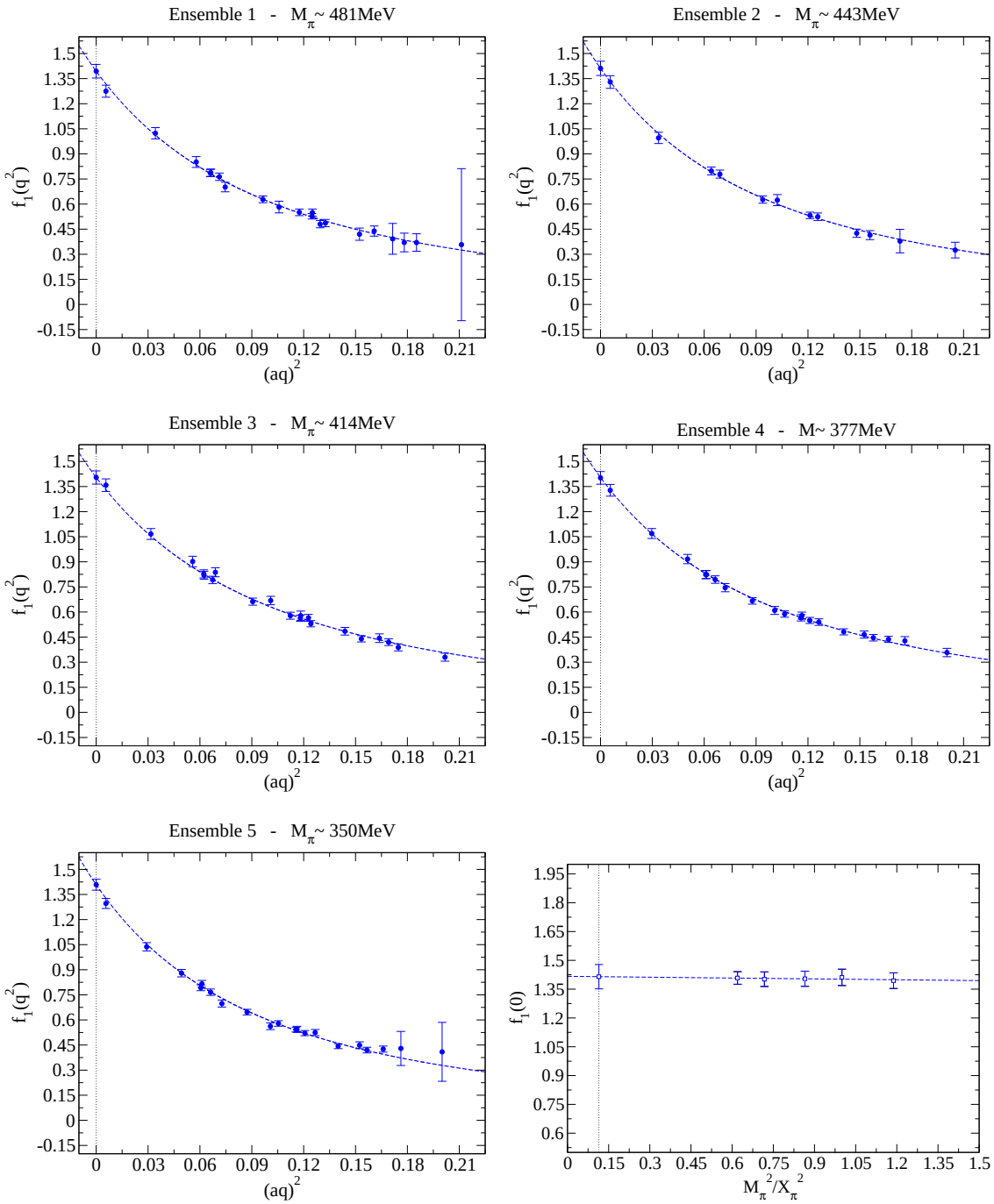

Figure 6.13: Unrenormalised vector form factor $f_1(q^2)$ for $\Delta S = 1$ transition $\Xi \to \Lambda$ on all five ensembles, where the dotted line indicates $q^2 = 0$. A dipole fit has been made to the data with $f_1(0)$ fixed to the lattice calculated value. The bottom right graph is the linear chiral extrapolation to the physical limit, which is represented by a dashed line. Here $g_V = 1.42(6)$.

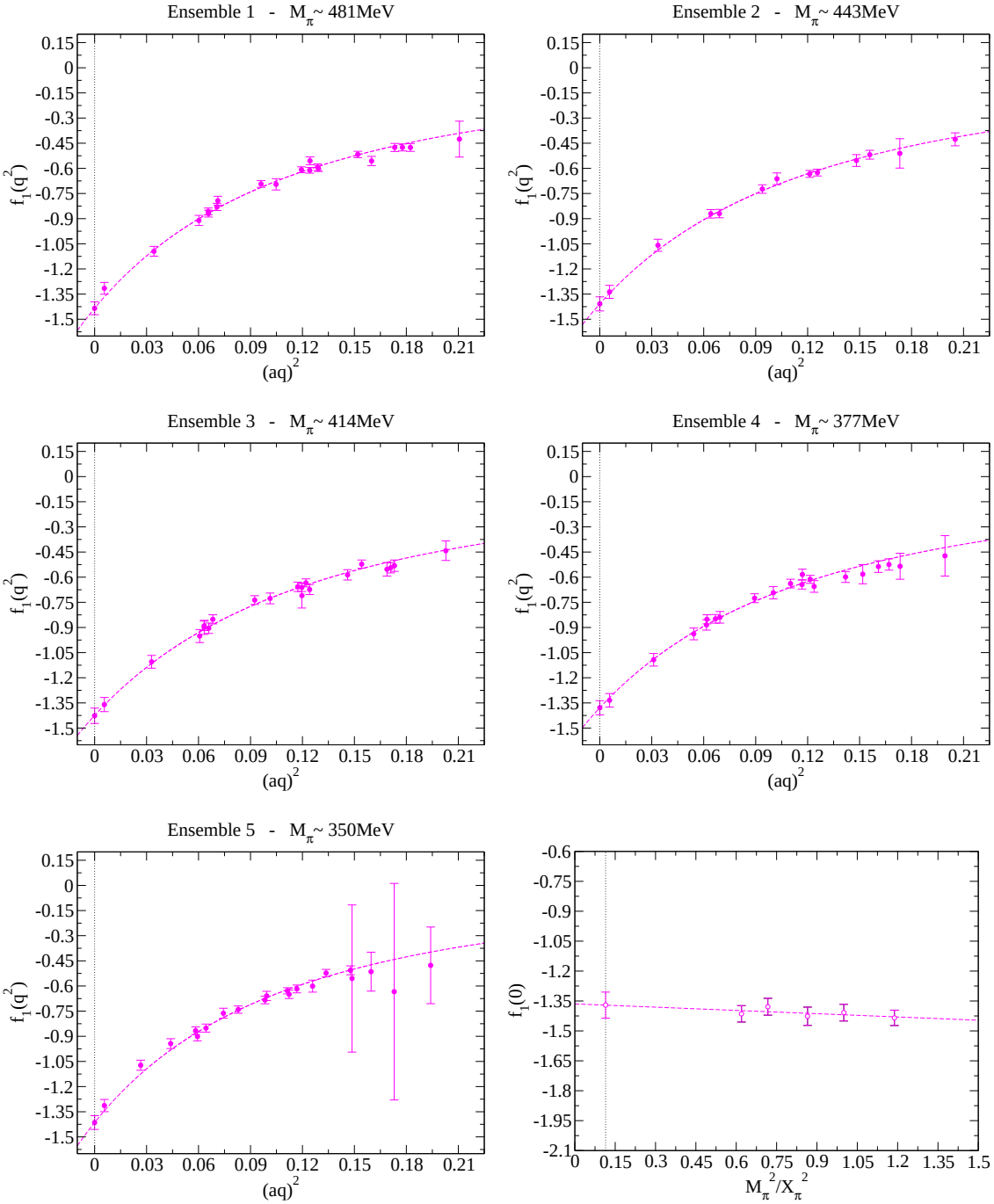

Figure 6.14: Unrenormalised vector form factor $f_1(q^2)$ for $\Delta S = 1$ transition $\Lambda \to N$ on all five ensembles, where the dotted line indicates $q^2 = 0$. A dipole fit has been made to the data with $f_1(0)$ fixed to the lattice calculated value. The bottom right graph is the linear chiral extrapolation to the physical limit, which is represented by a dashed line. Here $g_V = -1.37(7)$.

this form factor and that the $SU(3)$ flavour breaking effects are non-negligible. Figure 6.15 does indeed display linear fits resulting in a steeper slope, for some transitions, than those found in the equivalent plots for $f_1(0)$ (Figure 6.12). In this figure experimental results are not shown for clarity, due to their sizeable errors.

Transition	$\frac{f_2(0)}{f_1(0)}$	Cabibbo [101]	Sirlin [107]	Lattice	Experiment
$\Xi \to \Lambda$	0.01(1)	0.16	-0.03		
$\Xi \to \Sigma$	3.2(1)	4.94	2.50	3.3(2) [97]	2(1.3) [117]
$\Sigma \to \Lambda$	1.9(1)	2.88			
$\Sigma \to N$	$-1.46(7)$	-2.31	-1.66	-1.5(8) [98]	-1.71(35) [116]
$\Lambda \to N$	1.18(8)	1.96	1.40		1.3(8) [115]

Table 6.4: Results for $\frac{f_2(0)}{f_1(0)}$ (except for $\Sigma \to \Lambda$ where the quoted value is $f_2^R(0)$) as calculated from a linear fit to the five ensembles. Also shown are predictions using the Cabibbo theory and Sirlin's formula. Results from other lattice calculations and experimental determinations are presented, where available.

6.7 Transition Axial Form Factors

The final lattice results to present are those of the axial-vector form factor $g_1(q^2)$, which is one of the most important form factors calculated here; this form factor is sensitive to $SU(3)$-flavour symmetry breaking effects and contributes heavily toward calculating the CKM matrix element $|V_{us}|$, when combined with f_1 and experimental decay rates.

The q^2 behaviour is again described by a constrained dipole fit. As other lattice results are available for $\Xi \to \Sigma$ and $\Sigma \to N$ we plot $g_1(q^2)$ for these transitions in Figures 6.16 and 6.17 respectively. We find that the axial form factor g_1 has a slightly noisier q^2 dependency than its vector counterpart. Despite this, there is evidence of first order $SU(3)$ breaking effects for this form factor, at least for some of the transitions. The $\Xi \to \Sigma$ and $\Lambda \to N$ transitions in particular show stronger signs of such effects, as can be seen in Figure 6.18.

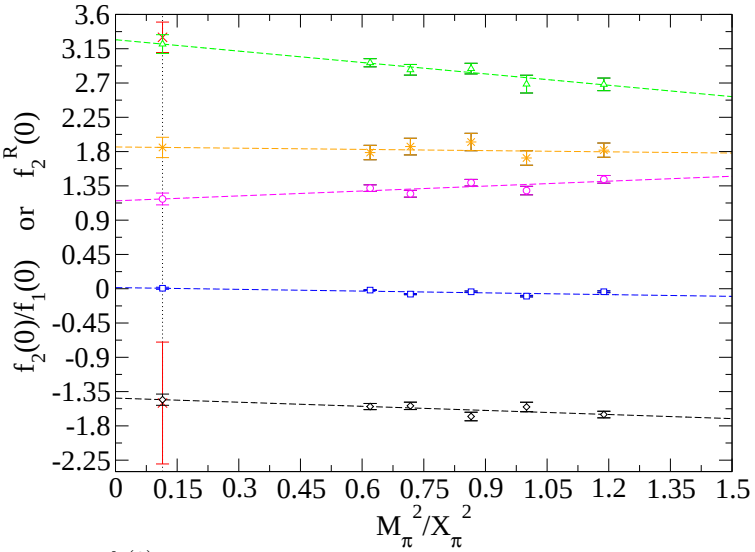

Figure 6.15: Ratio $\frac{f_2(0)}{f_1(0)}$ or $f_2^R(0)$ for $\Sigma \to \Lambda$ as $f_1 \sim 0$ for that transition. The transitions are: $\Xi \to \Lambda$(blue squares), $\Xi \to \Sigma$(green triangles), $\Sigma \to \Lambda$(orange stars), $\Sigma \to N$(black diamonds) and $\Lambda \to N$(pink circles). A linear fit is made to the five ensembles to the physical point, which is represented by the dotted line. The red crosses represent results by Sasaki and Yamazaki [97] ($\Xi \to \Sigma$) and Guadagnoli et al. [98] ($\Sigma \to N$).

We will briefly recap that the axial coupling $g_A = g_1(0)$ can be expressed in terms of two constants F and D in the $SU(3)$ symmetric limit as seen in Table 5.3. In Chapter 7 ratios of these constants will be determined using the values of g_A calculated here. For the moment, we compare results for g_A with the $SU(3)$ symmetry limit predictions by setting the values of F and D. Here we choose $F = 0.475(4)$ and $D = 0.793(5)$ from a study of the axial coupling constants [143]. The relevant combinations of F and D are then taken for each $\Delta S = 1$ transition. These are normalised by the Cabibbo theory prediction for $g_A^{\Sigma\Lambda}$, of the $\Delta S = 0$ transition, and are plotted in Figure 6.19.

As can be seen from these plots, this form factor deviates from the symmetric limit value as mass splitting increases. Our values for this ratio of axial charges, for each of the four transitions, indicate that the symmetric limit values do not provide an adequate prediction at the physical point. Of course comparison with Cabibbo theory values are naturally affected by the choice of F and D. One

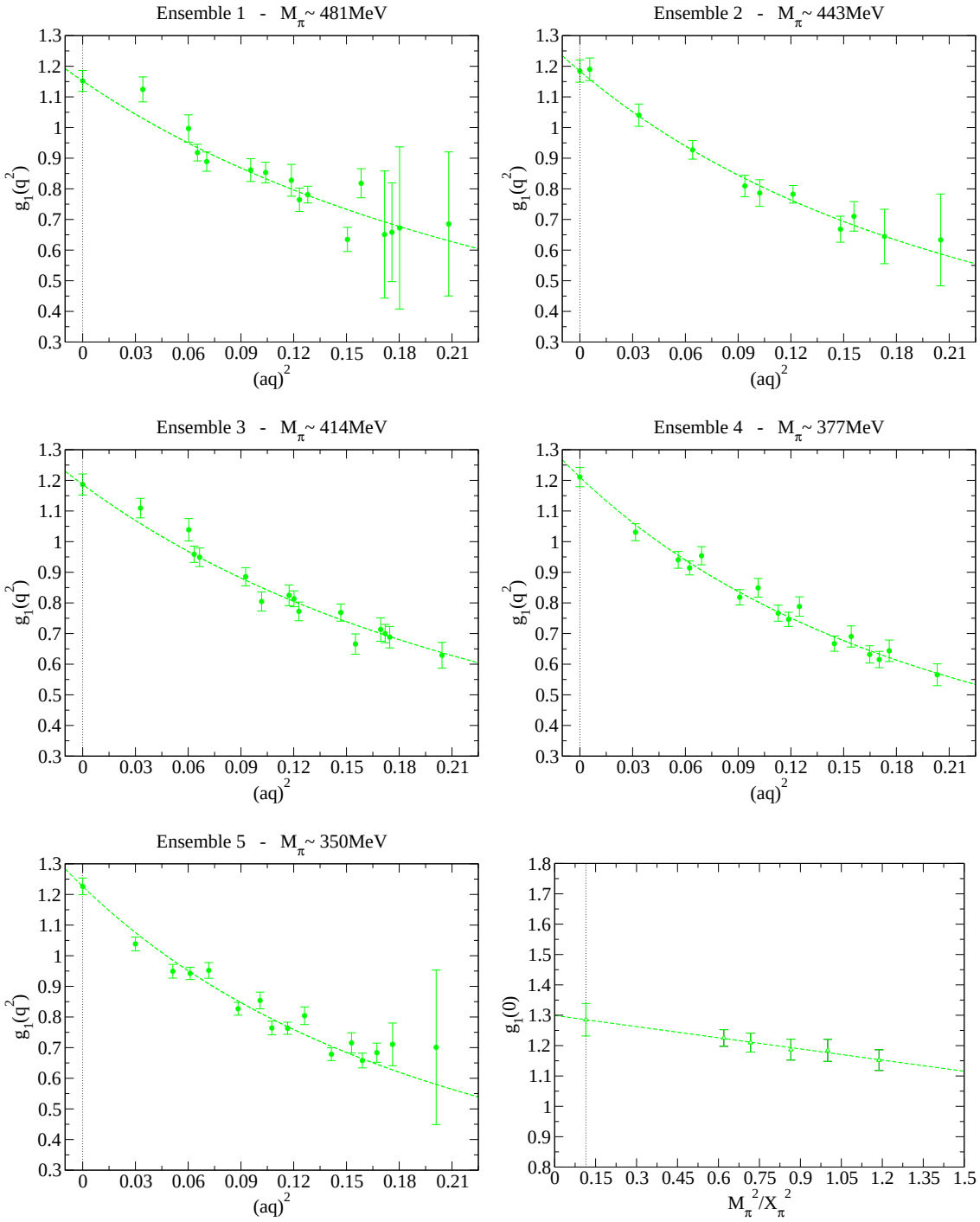

Figure 6.16: Unrenormalised axial-vector form factor $g_1(q^2)$ for $\Delta S = 1$ transition $\Xi \to \Sigma$ on all five ensembles, where the dotted line indicates $q^2 = 0$. A dipole fit has been made to the data with $g_1(0)$ fixed to the lattice calculated value. The bottom right graph is the linear chiral extrapolation to the physical limit, which is represented by a dashed line. Here $g_A = 1.30(5)$.

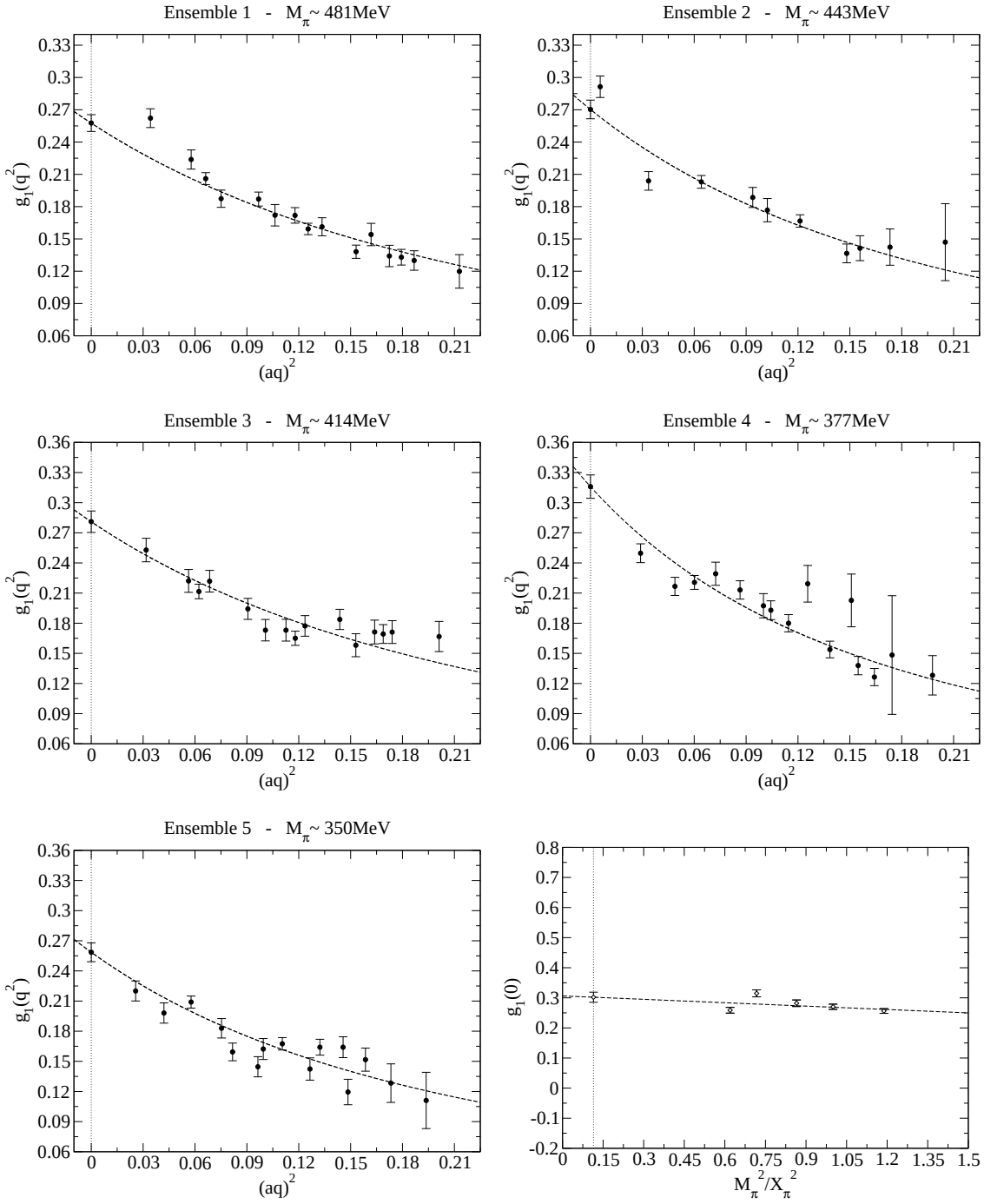

Figure 6.17: Unrenormalised axial-vector form factor $g_1(q^2)$ for $\Delta S = 1$ transition $\Sigma \to N$ on all five ensembles, where the dotted line indicates $q^2 = 0$. A dipole fit has been made to the data with $g_1(0)$ fixed to the lattice calculated value. The bottom right graph is the linear chiral extrapolation to the physical limit, which is represented by a dashed line. Here $g_A = 0.30(2)$.

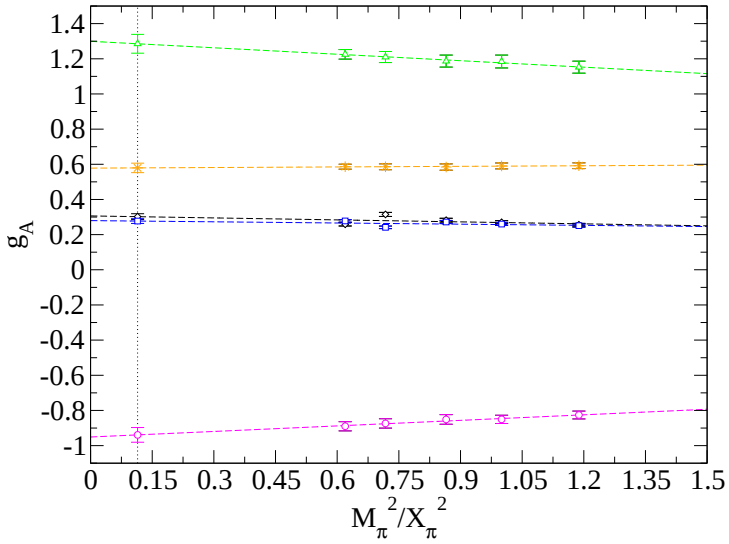

Figure 6.18: Unrenormalised results for $g_A^{\Xi\Lambda}$(blue squares), $g_A^{\Xi\Sigma}$(green triangles), $g_A^{\Sigma\Lambda}$(orange stars), $g_A^{\Sigma N}$(black diamonds) and $g_A^{\Lambda N}$(pink circles). A linear extrapolation (dashed lines) is made to the physical point (dotted line) in each case.

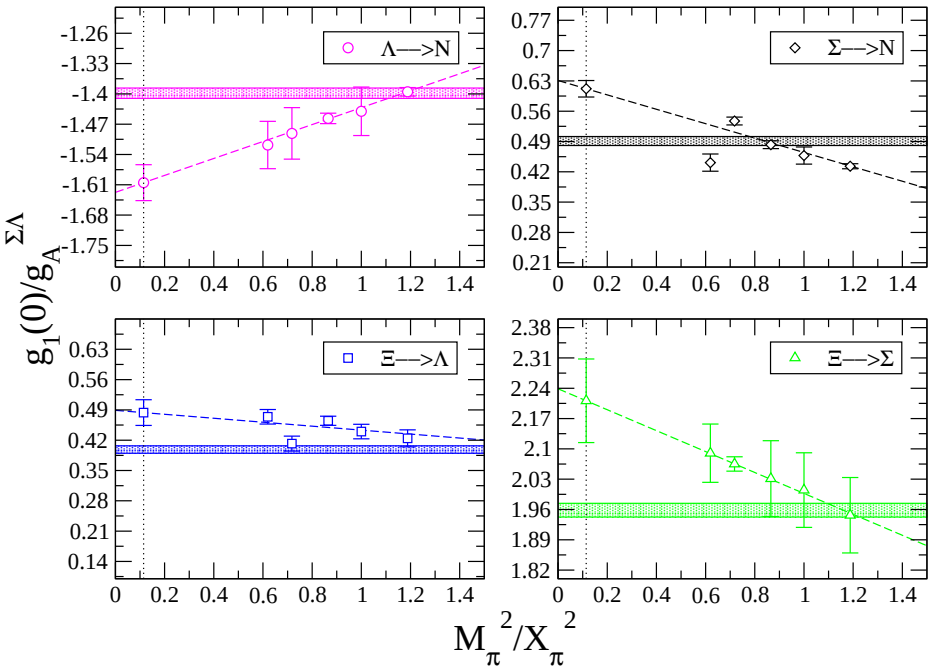

Figure 6.19: Ratio $\frac{g_A}{g_A^{\Sigma\Lambda}}$ for each of the following four transitions: $\Xi \to \Lambda$(blue squares), $\Xi \to \Sigma$(green triangles), $\Sigma \to N$(black diamonds) and $\Lambda \to N$(pink circles) with a linear chiral fit to the physical point (dotted lines). Also shown, including error, are the $SU(3)$ predictions for the ratios from the Cabibbo model (thick horizontal bars). We have used $F = 0.475(4)$ and $D = 0.793(5)$ [143].

can see that in some cases our symmetric point value ($M_\pi^2/X_\pi^2 = 1$) does not correspond to the Cabibbo model, even within error. To be thorough, we should also determine F and D. This is done in the following chapter.

It is also important to check the values of g_A for the transition matrix elements against what is known both theoretically and experimentally. Experiments, by necessity, measure $g_1(q^2)$ in terms of a ratio to the vector form factor $f_1(q^2)$ and as a result other lattice results are also presented as $\frac{g_1(0)}{f_1(0)}$. The same is done for results already outlined here where renormalisation is performed by fixing to the experimental result for g_A^{NN}. Results are summarised in Table 6.5 for the $\Delta S = 1$ transitions.

Transition	$\frac{g_1^R(0)}{f_1^R(0)}$	Lattice	Experiment
$\Xi \to \Lambda$	0.22(1)		0.25(5) [115]
$\Xi \to \Sigma$	1.33(6)	1.25(3) [97]	1.3(2) [117]
$\Sigma \to N$	−0.32(2)	−0.28(5) [98]	−0.34(2) [116]
$\Lambda \to N$	0.80(4)		0.72(2) [115]

Table 6.5: Results of ratio $\frac{g_1^R(0)}{f_1^R(0)}$ for four transitions within the baryon octet. Also shown are other lattice QCD results and experimental results for the same ratios, where available.

Three of the four ratios presented agree with both the experimental results and theoretical calculations. The only disagreement, in relation to $\Lambda \to N$ results and experimental measurement is marginal. This could be due to noise in the data or to finite size effects which are known to affect axial form factors [144], and which we do not determine, having calculated these form factors only on one set of lattice dimensions. Our choice of renormalisation would also impact upon these values. Results are also displayed graphically in Figure 6.20. Next we will examine, in the following chapter, the possibility of making simultaneous fits to lattice data in order to better constrain the chiral extrapolation.

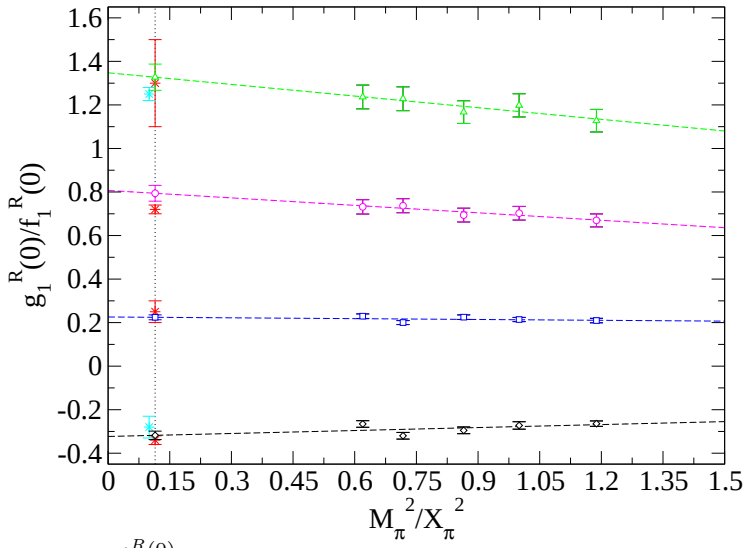

Figure 6.20: Ratio $\frac{g_1^R(0)}{f_1^R(0)}$ for $\Xi \to \Lambda$(blue squares), $\Xi \to \Sigma$(green triangles), $\Sigma \to N$(black diamonds) and $\Lambda \to N$(pink circles) with linear extrapolation to physical point (dotted line). Also included are experimental results (red stars) and other lattice QCD determinations (bright blue stars). Note the latter are displaced slightly along the x-axis for clarity.

"O day and night, but this is wondrous strange!"

— Shakespeare, *Hamlet*

Chapter 7

Flavour Symmetry Breaking

In the previous chapter, results were outlined such that individual linear fits were made for each diagonal and transition matrix element in isolation. This approach can be improved upon by utilising knowledge of $SU(3)$-flavour symmetry breaking in order to make improved fits to all of the available data simultaneously. The number of fit parameters in such constrained and simultaneous fits are therefore reduced.

The states in $SU(3)$ multiplets are only degenerate to about 25% so we can already understand the importance of quantifying the symmetry breaking effects in general. Earlier chapters have introduced the concept of $SU(3)$ symmetry and qualitatively discussed the effects of breaking this symmetry on the form factors of interest to us. We now wish to quantify those effects.

7.1 Parameterising Symmetry Breaking

In $SU(3)$ there is just one way of forming a singlet quantity from the direct product of two octets as seen here:

$$8 \otimes 8 = 1 \oplus 8 \oplus 8 \oplus 10 \oplus \overline{10} \oplus 27. \tag{7.1}$$

This product is useful for describing the $SU(3)$ breaking effects of the meson and baryon octet masses as previously carried out by Bietenholz et al. [52]. All $SU(3)$ breaking effects for these masses can be described in terms of singlet, octet, 10-plet and 27-plet quantities. A similar idea is used here to explore the symmetry breaking effects in matrix elements.

The size of $SU(3)$ breaking effects for hadron masses imply that they cannot only be the result of a force such as electromagnetism, but rather must be attributed to the strong force [145]. The hypothesis known as the *Gell-Mann-Okubo* ansatz states that $SU(3)$ breaking effects to the strong-interaction Hamiltonian appear as the eight component of an octet [146]. The Hamiltonian can thus be split into an $SU(3)$ singlet part and another part which explicitly breaks $SU(3)$ symmetry. We can extend this to $SU(2)$-breaking effects by including terms proportional to the third component of the same octet.

In the standard octet representation of $SU(3)$ the Gell-Mann matrices λ_3 and λ_8 are the Cartan (i.e. simultaneously diagonal) generators. The reasoning behind postulating that the symmetry breaking effects are proportional to λ_8 can be understood by noticing that members of an isodoublet or isotriplet within the hadron multiplets have the same masses (neglecting electromagnetic effects). One would thus demand that the symmetry breaking part of the Hamiltonian commute with the third component of isospin (the horizontal axis within $SU(3)$ multiplets). The only generator which can do this is λ_8, or hypercharge.

As the strong force is flavour blind the only differences between flavours comes from the quark mass matrix, if electromagnetic and weak interactions are ignored. As with the interaction Hamiltonian, the quark mass matrix can be written in terms of a singlet part and an octet part from which flavour symmetry effects

arise;

$$M = \begin{pmatrix} m_u & 0 & 0 \\ 0 & m_d & 0 \\ 0 & 0 & m_s \end{pmatrix} = \bar{m} \begin{pmatrix} 1 & 0 & 0 \\ 0 & 1 & 0 \\ 0 & 0 & 1 \end{pmatrix} + \frac{1}{2}(\delta m_u - \delta m_d) \begin{pmatrix} 1 & 0 & 0 \\ 0 & -1 & 0 \\ 0 & 0 & 0 \end{pmatrix} + \delta m_s \begin{pmatrix} -1 & 0 & 0 \\ 0 & -1 & 0 \\ 0 & 0 & 2 \end{pmatrix}, \tag{7.2}$$

where the final two matrices in this relation are simply λ_3 and λ_8 (neglecting normalisation factors). The notation used here is the same as that introduced in Section 3.5. In the isospin symmetry limit it should be clear that the term related to λ_3 will drop out.

The idea is to classify the matrix elements by their properties under $SU(2)$, $SU(3)$ and the subgroup S_3 (this approach was developed by P. E. L. Rakow and others of the QCDSF-UKQCD collaboration [147]) and then classify Taylor expansions of mass-splitting in the same way. Only polynomials which have symmetry matching that of the matrix elements can be considered as symmetry breaking terms. These reduced Taylor expansions result in the constraints mentioned at the start of this chapter.

The Cabibbo theory, as outlined in Section 5.3, assumes that the vector and axial-vector currents transform as an octet. As this work focuses on the octet baryons there will be three indices needed to label a hyperon matrix element, $\langle H^i|\mathcal{O}^j|H^k\rangle$ (as per Equation 5.1), with choices for the hyperons and operators displayed in Table 5.1. We thus need to classify the following direct product in

terms of $SU(3)$ multiplets:

$$\begin{aligned} 8 \otimes 8 \otimes 8 =& 1 \oplus 1 \oplus 8 \oplus 8 \oplus 8 \oplus 8 \oplus 8 \oplus 8 \oplus 8 \oplus 8 \\ & \oplus 27 \oplus 27 \oplus 27 \oplus 27 \oplus 27 \oplus 27 \oplus 64 \\ & \oplus 10 \oplus 10 \oplus 10 \oplus 10 \oplus \overline{10} \oplus \overline{10} \oplus \overline{10} \oplus \overline{10} \\ & \oplus 35 \oplus 35 \oplus \overline{35} \oplus \overline{35}, \end{aligned} \tag{7.3}$$

which can be arrived at using the intermediate result in Equation 7.1.

When hyperon matrix elements were introduced in Chapter 5 there was a discussion stemming from the fact that they could be written as the combination of two reduced matrix elements. These can now be understood as the two singlet representations found in the direct product of three $SU(3)$ octets as found in Equation 7.3. The Cabibbo theory assumes perfect $SU(3)$ symmetry, so in this case all higher representations than the singlets would vanish.

The Taylor expansion is more naturally performed around $\bar{m}$ and δm_q, for some quark of flavour q, in our work. This is because $\bar{m}$ is kept constant, and is thus a singlet, while δm_q is purely a symmetry breaking term. A Taylor expansion around some point $(m_u, m_d, m_s) = (m_0, m_0, m_0)$ will only have octet terms to first order in mass-splitting [52]. Other representations are only present at $(\delta m_q)^2$ and higher. By setting $m_u = m_d$ polynomial terms associated with the symmetry of the representations 10, $\overline{10}$, 35 and $\overline{35}$ will vanish, which is the case within the isospin symmetry limit [148].

The schematic pattern for the expansion of the hyperon matrix elements can be written as the sum of polynomials of known symmetry and rank 3 tensors containing integers and square roots of integers which encode how the matrix elements behave under the $SU(2)$ subgroups of isospin, V-spin and U-spin in particular representations. They can be thought of as three dimensional versions of 8×8 Gell-Mann matrices. Given that certain representations vanish in the isospin limit the general matrix element can be written as

$$\begin{aligned}\langle H^i|\mathcal{O}^j|H^k\rangle = &\sum(\text{singlet mass polynomial}) \times (\text{singlet tensor})^{ijk} \\ &+ \sum(\text{octet mass polynomial}) \times (\text{octet tensor})^{ijk} \\ &+ \sum(\text{27-plet mass polynomial}) \times (\text{27-plet tensor})^{ijk} \\ &+ \sum(\text{64-plet mass polynomial}) \times (\text{64-plet tensor})^{ijk} \\ &+ \ldots\end{aligned} \tag{7.4}$$

The task of matching polynomials by symmetry to tensor representations of $SU(3)$ becomes trivial at first order but should still indicate much about flavour symmetry breaking effects. Bietenholz et al. noted a large hierarchy between orders in mass splitting in their analysis [52]. By looking at combinations of decuplet baryon masses that only have contributions at particular orders they quantified this effect, as shown in Equation 7.5. Though not the same as matrix elements this indicates the potential benefit of quantifying symmetry breaking effects even up to only leading order effects;

$$\begin{aligned} 4M_\Delta + 3M_{\Sigma^*} + 2M_{\Sigma^*} + M_\Omega = 13.82\text{GeV} \quad &\propto \quad \mathcal{O}(\delta m_l)^0, \\ -2M_\Delta + M_{\Sigma^*} + M_\Omega = 0.742\text{GeV} \quad &\propto \quad \mathcal{O}(\delta m_l)^1, \\ 4M_\Delta - 5M_{\Sigma^*} - 2M_{\Sigma^*} + 3M_\Omega = -0.044\text{GeV} \quad &\propto \quad \mathcal{O}(\delta m_l)^2, \\ -M_\Delta + 3M_{\Sigma^*} - 3M_{\Sigma^*} + M_\Omega = -0.006\text{GeV} \quad &\propto \quad \mathcal{O}(\delta m_l)^3. \end{aligned} \tag{7.5}$$

If the analysis of $SU(3)$ symmetry breaking effects is restricted to first order in δm_q then eight parameters are needed to describe these effects. These eight parameters correspond to the eight octets arising in the direct product of three octets. Though they may seem numerous, some of the parameters will only contribute to the first class form factors of interest here. Additionally there are less parameters than there are amplitudes calculated in this work. The polynomial terms at first order would be 1, $(\bar{m} - m_0)$, $(\delta m_u - \delta m_d)$ and δm_s. In practice only

the 1 and δm_s terms remain. By working in the isospin limit with a fixed singlet mass quantity the other two terms will be zero. Equations 3.57 and 3.58 allow for the rewriting of δm_s in terms of δm_l, which will be the parameter used from here on to describe the first order symmetry breaking of hyperon matrix elements.

		singlet		octet							
I	$\mathcal{A}_{\bar{H}'MH}$	f	d	r_1	r_2	r_3	r_4	r_5	s_1	s_2	s_3
0	$\bar{N}\eta N$	$\sqrt{3}$	-1	1	0	0	0	0	0	-1	0
0	$\bar{\Sigma}\eta\Sigma$	0	2	1	0	$2\sqrt{3}$	0	0	0	0	0
0	$\bar{\Lambda}\eta\Lambda$	0	-2	1	2	0	0	0	0	0	0
0	$\bar{\Xi}\eta\Xi$	$-\sqrt{3}$	-1	1	0	0	0	0	0	1	0
1	$\bar{N}\pi N$	1	$\sqrt{3}$	0	0	-2	0	0	2	0	0
1	$\bar{\Sigma}\pi\Sigma$	2	0	0	0	0	0	0	-2	$\sqrt{3}$	0
1	$\bar{\Xi}\pi\Xi$	1	$-\sqrt{3}$	0	0	2	0	0	2	0	0
1	$\bar{\Sigma}\pi\Lambda$	0	2	0	1	$-\sqrt{3}$	1	0	0	0	0
1	$\bar{\Lambda}\pi\Sigma$	0	2	0	1	$-\sqrt{3}$	-1	0	0	0	0
$\frac{1}{2}$	$\bar{N}K\Sigma$	$-\sqrt{2}$	$\sqrt{6}$	0	0	$\sqrt{2}$	0	$\sqrt{2}$	$\sqrt{2}$	0	$\sqrt{6}$
$\frac{1}{2}$	$\bar{N}K\Lambda$	$-\sqrt{3}$	-1	0	1	0	1	$\sqrt{3}$	$-\sqrt{3}$	1	-1
$\frac{1}{2}$	$\bar{\Lambda}K\Xi$	$\sqrt{3}$	-1	0	1	0	-1	$-\sqrt{3}$	$\sqrt{3}$	-1	-1
$\frac{1}{2}$	$\bar{\Sigma}K\Xi$	$\sqrt{2}$	$\sqrt{6}$	0	0	$\sqrt{2}$	0	$-\sqrt{2}$	$-\sqrt{2}$	0	$\sqrt{6}$
$\frac{1}{2}$	$\bar{\Sigma}\bar{K}N$	$-\sqrt{2}$	$\sqrt{6}$	0	0	$\sqrt{2}$	0	$-\sqrt{2}$	$\sqrt{2}$	0	$-\sqrt{6}$
$\frac{1}{2}$	$\bar{\Lambda}\bar{K}N$	$-\sqrt{3}$	-1	0	1	0	-1	$-\sqrt{3}$	$-\sqrt{3}$	1	1
$\frac{1}{2}$	$\bar{\Xi}\bar{K}\Lambda$	$\sqrt{3}$	-1	0	1	0	1	$\sqrt{3}$	$\sqrt{3}$	-1	1
$\frac{1}{2}$	$\bar{\Xi}\bar{K}\Sigma$	$\sqrt{2}$	$\sqrt{6}$	0	0	$\sqrt{2}$	0	$\sqrt{2}$	$-\sqrt{2}$	0	$-\sqrt{6}$

Table 7.1: Coefficients for mass polynomials from Taylor expansion of hyperon matrix elements up to first order in $SU(3)$-flavour symmetry breaking. The set of matrix elements $\mathcal{A}_{\bar{H}'MH}$ were introduced in Section 5.1 (see Equations 5.2 to 5.4). Representations corresponding to $\mathcal{O}(\delta m_l)^2$ or higher are neglected. Parameters will be different for each form factor.

Table 7.1 displays the coefficients for each parameter of the Taylor expansion of the matrix elements in polynomials of singlet and octet $SU(3)$ representations. It should be emphasised that the numerical value for the parameters will be distinct for each form factor with only the relative differences between parameters remaining the same. The separating of the octet parameters into two distinct sets, of 's' and 'r' type are for reasons which will become more clear in the next section.

The singlet parameters are labelled f and d can be directly related to the F and D parameters introduced in earlier chapters for $g_1(0)$ as discussed later.

As can be seen, away from the symmetric point (which corresponds to the singlet parameters), the off-diagonal matrix elements can contain terms proportional to r_4, r_5 and s_3. This is due to the possible presence of second class form factors at first order in symmetry breaking, though we do not focus thereon in this analysis. The first class form factors are written in terms of f and d at the symmetric point while these terms vanish for second class form factors in accordance with the Cabibbo theory. The coefficients r_1, r_2, r_3, s_1 and s_2 will be sufficient to parameterise linear order $SU(3)$ symmetry breaking of the first class form factors f_1, f_2 and g_1 in our analysis [149].

Table 7.1 can be used to describe the hyperon matrix elements up to $\mathcal{O}(\delta m_l)$. As an example, neglecting higher order contributions, the first three matrix elements from Table 7.1 would be parameterised as

$$\begin{aligned}\langle N|\eta|N\rangle &= \sqrt{3}f - d + (r_1 - s_1)\delta m_l,\\ \langle \Sigma|\eta|\Sigma\rangle &= 2d + (r_1 + 2\sqrt{3}r_3)\delta m_l,\\ \langle \Lambda|\eta|\Lambda\rangle &= -2d + (r_1 + 2r_2)\delta m_l.\end{aligned} \tag{7.6}$$

One can also construct quantities which are equal at the symmetric point as many of the matrix elements are simply flavour permutations in $SU(3)$. As an example,

$$\frac{\sqrt{3}}{2}\langle p|\eta|p\rangle + \frac{1}{2}\langle p|\pi^0|p\rangle = \langle \Sigma^+|\pi^0|\Sigma^+\rangle = -\frac{\sqrt{3}}{2}\langle \Xi^0|\eta|\Xi^0\rangle + \frac{1}{2}\langle \Xi^0|\pi^0|\Xi^0\rangle = 2f, \tag{7.7}$$

is one such relation. This is more clearly seen by explicitly writing out the operators in the form $\bar{q}\Gamma q$ which gives

$$\frac{1}{\sqrt{2}}\langle p|\bar{u}\Gamma u - \bar{s}\Gamma s|p\rangle = \frac{1}{\sqrt{2}}\langle \Sigma^+|\bar{u}\Gamma u - \bar{d}\Gamma d|\Sigma^+\rangle = \frac{1}{\sqrt{2}}\langle \Xi^0|\bar{s}\Gamma s - \bar{d}\Gamma d|\Xi^0\rangle = 2f. \tag{7.8}$$

In each case the non-valence contributions to each diagonal matrix element have the same coefficient and will thus be equal at the symmetric point. The same can be said for the doubly represented quark in each; u in the proton, u in the Σ^+ and s in the Ξ^0. The pattern of doubly represented minus disconnected contributions repeats itself throughout the relation, explaining why these are equal at the symmetric point.

7.2 Fan Plots

Constructing quantities which are equal at the symmetric point can be presented in a useful graphical tool which we call *fan plots* as they will 'fan-out' from the symmetric point as the physical point is approached. This will allow the reader to understand the effects of $SU(3)$ symmetry breaking of matrix elements in an intuitive and visual way. This approach was first used by the QCDSF-UKQCD collaboration [52] to display the effects of flavour symmetry breaking for hadron masses.

We construct two sets of fan plots for the first class form factors exclusively in analysis performed here. Thus r_4, r_5 and s_3 are not required as previously discussed. Each fan plot will contain only one of the singlet parameters and will also contain a distinct set of octet parameters (hence the division between 'r' and 's' type). The reader should be aware that the fan plot elements labels shown here are not to be confused with the notation used previously for reduced matrix elements in Equation 5.17. The first fan plot which can be constructed will be

termed the *D-fan* which is $2d$ at the symmetric point and is made up of

$$\begin{aligned}
D_1 \equiv -(\mathcal{A}_{\bar{N}\eta N} + \mathcal{A}_{\Xi\bar{\eta}\Xi}) &= 2d - 2r_1\delta m_l, \\
D_2 \equiv \mathcal{A}_{\bar{\Sigma}\eta\Sigma} &= 2d + (r_1 + 2\sqrt{3}r_3)\delta m_l, \\
D_3 \equiv -\mathcal{A}_{\bar{\Lambda}\eta\Lambda} &= 2d - (r_1 + 2r_2)\delta m_l, \\
D_4 \equiv \frac{1}{\sqrt{3}}(\mathcal{A}_{\bar{N}\pi N} - \mathcal{A}_{\bar{\Xi}\pi\Xi}) &= 2d - \frac{4}{\sqrt{3}}r_3\delta m_l, \\
D_5 \equiv \mathcal{A}_{\bar{\Sigma}\pi\Lambda} &= 2d + (r_2 - \sqrt{3}r_3)\delta m_l, \\
D_6 \equiv \frac{1}{\sqrt{6}}(\mathcal{A}_{\bar{N}K\Sigma} + \mathcal{A}_{\bar{\Sigma}K\Xi}) &= 2d + \frac{2}{\sqrt{3}}r_3\delta m_l, \\
D_7 \equiv -(\mathcal{A}_{\bar{N}K\Lambda} + \mathcal{A}_{\bar{\Lambda}K\Xi}) &= 2d - 2r_2\delta m_l,
\end{aligned} \tag{7.9}$$

while the second one will be known as the *F-fan*,

$$\begin{aligned}
F_1 \equiv \frac{1}{\sqrt{3}}(\mathcal{A}_{\bar{N}\eta N} - \mathcal{A}_{\Xi\bar{\eta}\Xi}) &= 2f - \frac{2}{\sqrt{3}}s_2\delta m_l, \\
F_2 \equiv (\mathcal{A}_{\bar{N}\pi N} + \mathcal{A}_{\Xi\bar{\pi}\Xi}) &= 2f + 4s_1\delta m_l, \\
F_3 \equiv \mathcal{A}_{\bar{\Sigma}\pi\Sigma} &= 2f + (\sqrt{3}s_2 - 2s_1)\delta m_l, \\
F_4 \equiv \frac{1}{\sqrt{2}}(\mathcal{A}_{\bar{\Sigma}K\Xi} - \mathcal{A}_{\bar{N}K\Sigma}) &= 2f - 2s_1\delta m_l, \\
F_5 \equiv \frac{1}{\sqrt{3}}(\mathcal{A}_{\bar{\Lambda}K\Xi} - \mathcal{A}_{\bar{N}K\Lambda}) &= 2f + \frac{2}{\sqrt{3}}(\sqrt{3}s_1 - s_2)\delta m_l,
\end{aligned} \tag{7.10}$$

with elements which are all equal to $2f$ at the symmetric point.

We make a simultaneous fit to the various combinations of amplitudes as indicated in the fan plots shown in Equations 7.9 and 7.10 for the form factors f_1, f_2 and g_1 with $q^2 = 0$. The parameters d, f, r_1, r_2, r_3, s_1 and s_2 are determined by minimising the χ^2 values of the fan plots. We use the χ^2 test defined through

$$\chi^2 = \sum_{i=1}^{k} \left(\frac{F(x_i) - \mu(x_i)}{\sigma_i} \right)^2, \tag{7.11}$$

where $F(x_i)$ are form factors measurements with associated bootstrap error σ_i

at point x_i and μ_i are the values of the fan plot fitting functions at x_i. These parameters can then be used to reconstruct any particular matrix element of interest. Fits are made with the *Mathematica* software package [150].

It is also possible to normalise these fan plot elements by quantities which will not change, at least up to first order, as the quark masses are varied. We define

$$X_D = \frac{1}{10}(2D_1 + 2D_2 - 2D_3 + 2D_4 + 2D_5 + D_6 + 3D_7) = 2d + \mathcal{O}(\delta m_l)^2, \quad (7.12)$$

which can be used to normalise D-fan elements, along with

$$X_F = \frac{1}{8}(F_1 + F_2 + 2F_3 + 2F_4 + 2F_5) = 2f + \mathcal{O}(\delta m_l)^2, \quad (7.13)$$

which is the equivalent for the elements of the F-fan. Along with cancelling renormalisation constants, the expectation is that ratios of individual fan plot elements and either X_D or X_F will reduce the noise seen in data from LQCD simulations as was reported by W. Bietenholz et al. [52] for calculations involving hadron masses, such as with the quantity X_π which has been used throughout this study. Results within each ensemble are correlated so this procedure helps to cancel such effects. These choices for X_F and X_D are not unique and other combinations could also be used for normalisation.

7.3 Fan Plot Results

All plots shown in this section relate to form factors where the transferred momentum, q^2, has been determined at zero with the help of a suitable choice of twists. We begin by plotting X_D and X_F for the axial form factor $g_1(0)$. This form factor is chosen because a linear dependence is not excluded as would be the case with $f_1(0)$. This is performed in Figure 7.1 in order to see if these quantities are indeed flat as would be expected. Though this plot indicates that there is

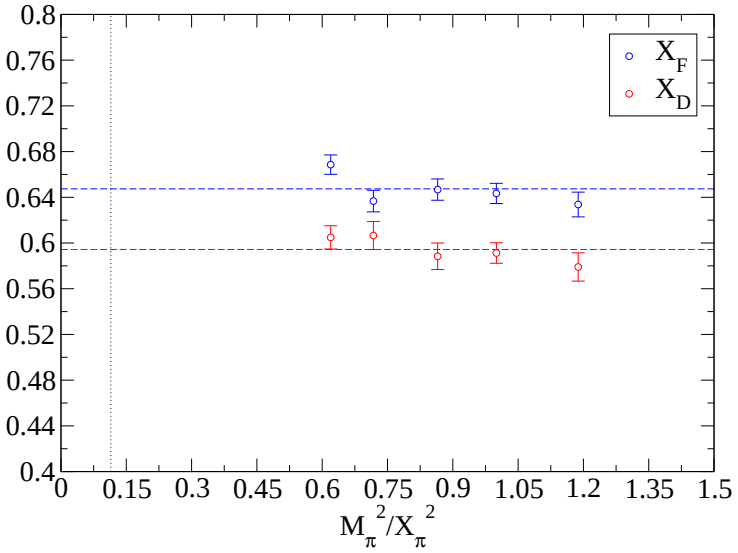

Figure 7.1: Combinations X_D and X_F of the axial form factor $g_1(0)$ for various hyperon amplitudes as defined in Equations 7.12 and 7.13 respectively. These quantities are expected to not show linear effects in δm_l. No matrix elements have been renormalised and fits are made to a constant. The physical point is represented by the black dotted line.

not much linear behaviour in both X_D and X_F though the data is still somewhat noisy. We do however, see reduction in noise once these quantities are used to normalise the fan plot elements.

Leaving aside $g_1(0)$ for the moment, we now examine the form factor $f_1(0)$, which should indicate negligible $SU(3)$ symmetry breaking effects at first order due to the Ademollo-Gatto theorem, and as such will provide a test of the polynomial expansion. As the vector current is conserved and simply counts the number of quarks for the diagonal matrix elements we can solve for f and d by assuming all δm_l contributions vanish at first order. Upon renormalisation one would then expect f^R and d^R to be

$$f^R = \frac{1}{\sqrt{2}} \sim 0.707 \quad \text{and} \quad d^R = 0, \tag{7.14}$$

which is indeed what we find: $f^R = 0.714(35)$ and $d^R = 0.0001(7)$ having renormalised by enforcing vector current conservation.

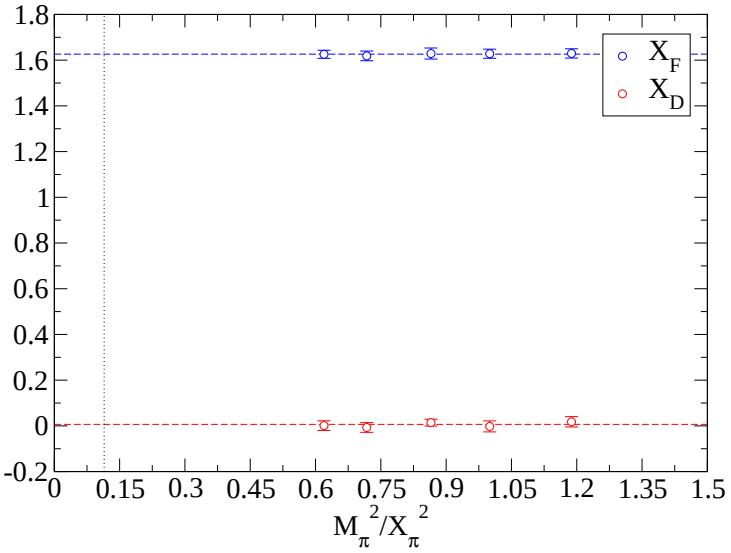

Figure 7.2: Combinations X_D and X_F of the vector form factor $f_1(0)$ for various hyperon amplitudes as defined in Equations 7.12 and 7.13 respectively. These quantities are expected to not show linear effects in δm_l. No matrix elements have been renormalised and fits are made to a constant. The physical point is represented by the black dotted line.

The fan plot for $f_1(0)$ will in fact not show many of the usual features of a fan plot as a result of the Ademollo-Gatto theorem. It is also not possible to normalise the D-fan by X_D for this form factor as this quantity would be very close to zero and result in an amplification of data noise (see Figure 7.2). The F-fan plot for the form factor $f_1(0)$, normalised by X_F is displayed in Figure 7.3, where each individual element of the plot has been separated out for convenience. Similarly the D-fan is plotted in Figure 7.4. In this case however, no normalisation (or operator renormalisation) has been performed. Renormalisation would have little effect on the D-fan.

Both fan plots are accompanied by fits. These fits are *not* made to the data sets of individual fan plot elements, rather they are made from a global fit to the data in an entire fan so that the fit parameters are solved for and then used to recreate linear fits as per Equations 7.9 and 7.10. The F-fan shows no $SU(3)$ flavour symmetry breaking effects within error at the physical point. Despite not being able to normalise in order to reduce fluctuations, the D-fan also shows

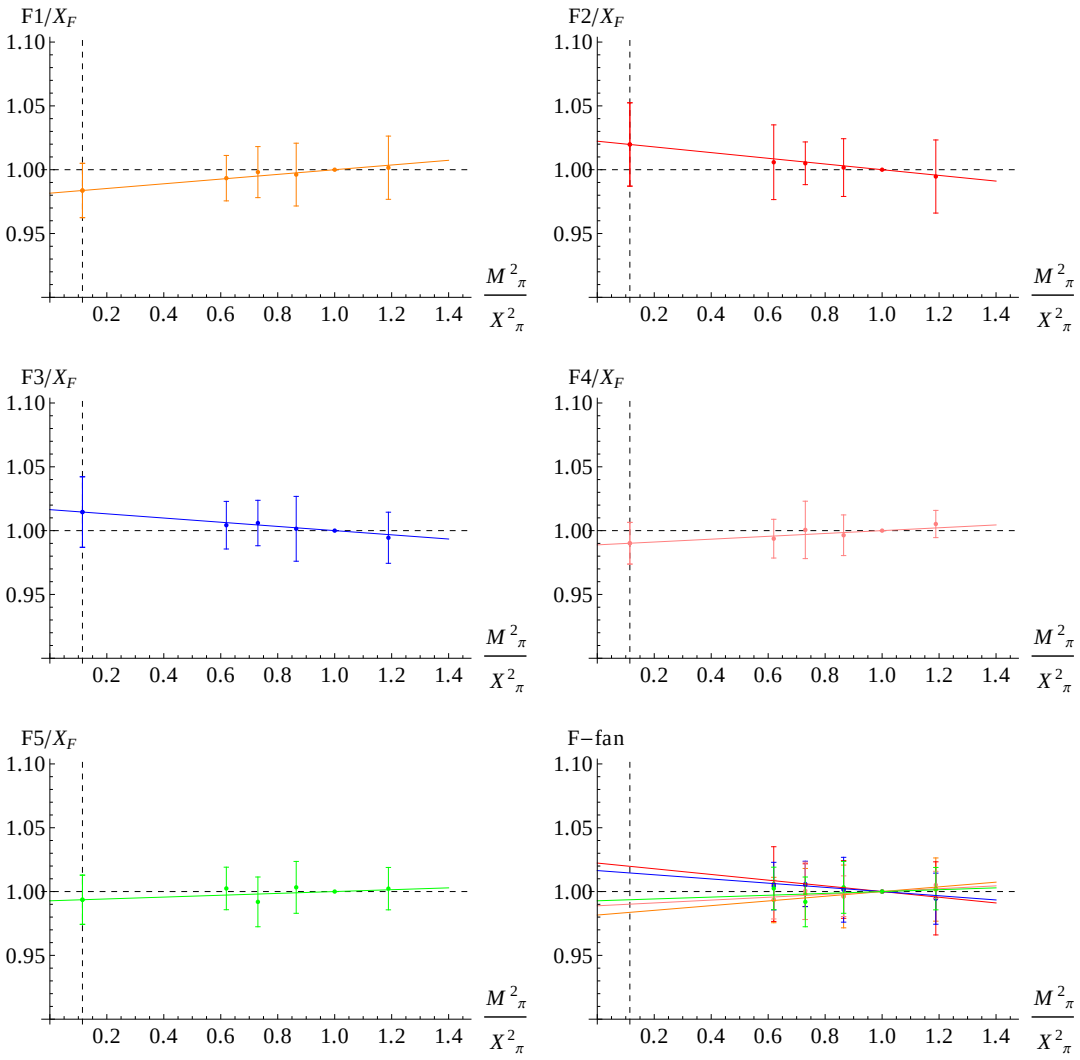

Figure 7.3: F-fan for the vector form factor $f_1(0)$ with each individual fan element displayed separately for clarity. A normalisation by X_F (Equation 7.13) has been applied to each element of the fan plot. Linear fits are global fits to the F-fan data following Equations 7.10. The vertical dashed line represents the physical point.

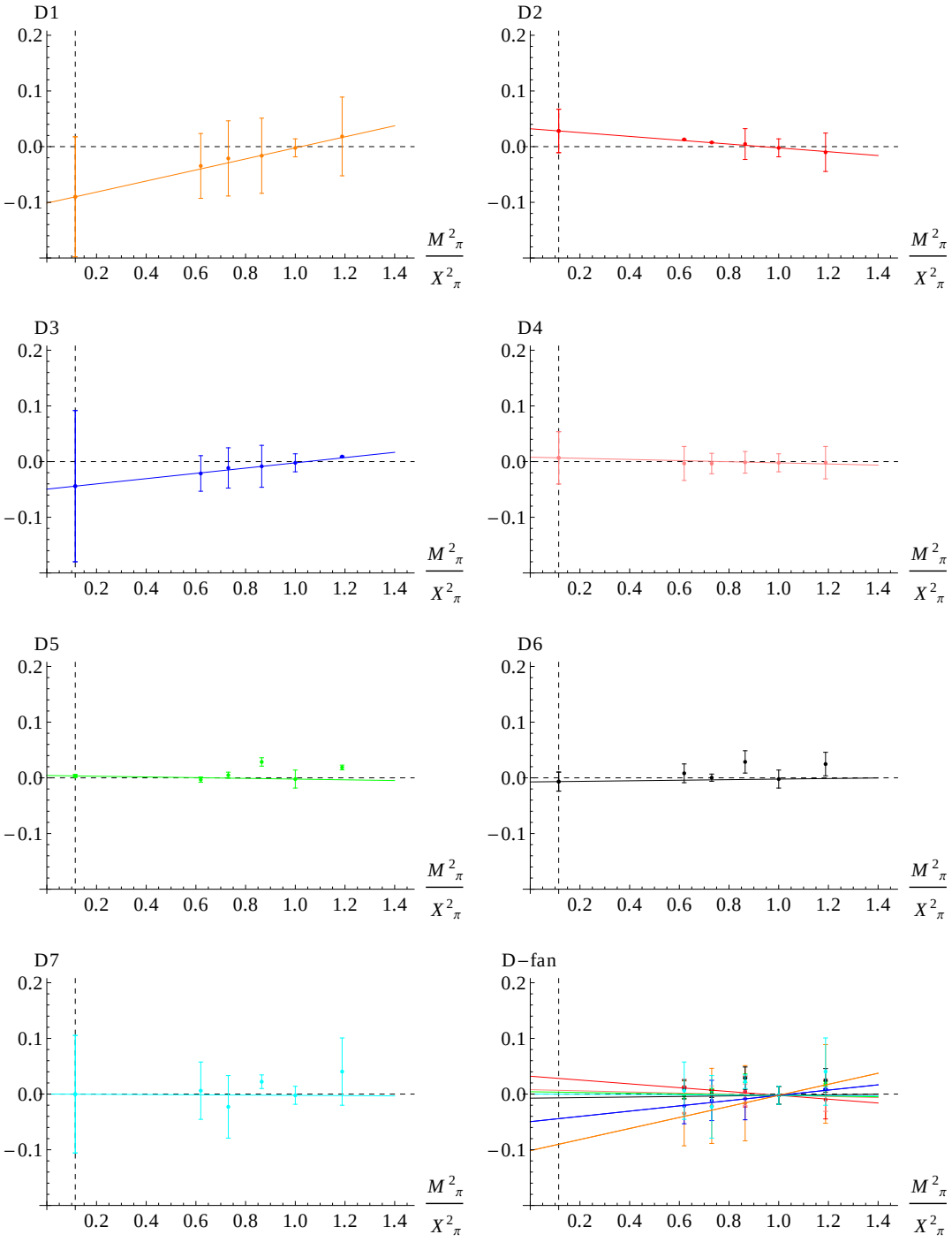

Figure 7.4: D-fan for the vector form factor $f_1(0)$ with each individual fan element displayed separately for clarity. No renormalisation has been performed in this case. Linear fits are global fits to the D-fan data following Equations 7.9. The vertical dashed line represents the physical point.

no symmetry breaking effects in our plots, albeit with larger errors in certain instances.

In Table 7.2 the slope parameters which contribute to both fan plots are given. All errors are calculated using the bootstrap method. This table also includes the values of each element of both fans at the physical point. With no deviation from unity at the physical point for the individual F-fan and D-fan elements we can say that there is no observable $SU(3)$ flavour symmetry breaking effects in this fan from our data. In fact, the calculated slope parameters all vanish within errors. Overall, results presented here show good agreement with the Ademollo-Gatto theorem.

	D-fan		F-fan
d	0.002(5)	f	0.813(5)
r_1	−0.050(50)	s_1	−0.009(15)
r_2	0.001(47)	s_2	−0.026(34)
r_3	0.004(13)		
D_1	−0.09(11)	F_1/X_F	0.984(21)
D_2	0.028(39)	F_2/X_F	1.020(33)
D_3	−0.04(14)	F_3/X_F	1.015(28)
D_4	0.007(47)	F_4/X_F	0.990(16)
D_5	0.003(3)	F_5/X_F	0.994(19)
D_6	−0.007(17)		
D_7	0.00(11)		

Table 7.2: Unrenormalised slope parameters for both the F and D-fans of $f_1(0)$ are given when the scale is given by $\frac{M_\pi^2}{X_\pi^2}$, which show little evidence of $SU(3)$ symmetry breaking to leading order. Also shown are the values of the individual fan elements at the physical point. The expectation is that the F elements should show no deviation from unity while the D elements should be zero. No renormalisation has been applied to the D-fan while the F-fan has been normalised by X_F (Equation 7.13). The accuracy of the D-fan fit is given by $\frac{\chi^2}{\text{d.o.f}} = 2.2$ and $\frac{\chi^2}{\text{d.o.f}} = 0.81$ for the F-fan.

A similar set of fan plots can be constructed for the weak magnetism form factor $f_2(0)$, but this time the form factor will not be protected from first order effects in δm_l. Here we find $f^R = 0.41(2)$ and $d^R = 0.88(4)$ so in this case it is

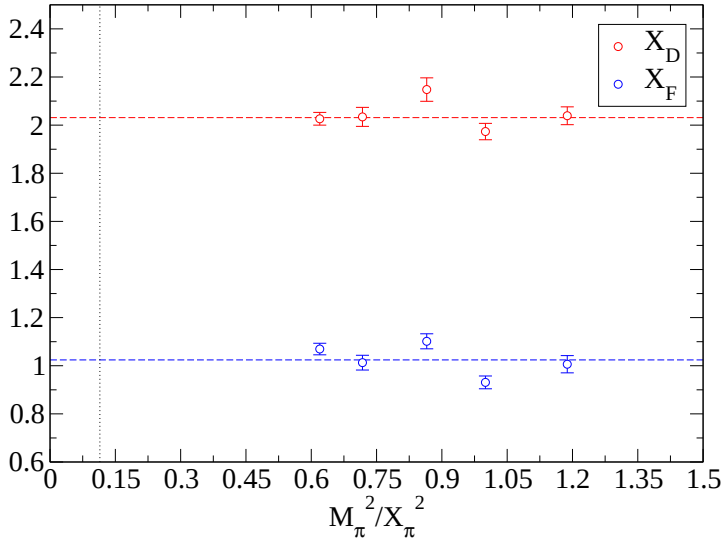

Figure 7.5: Combinations X_D and X_F of the vector form factor $f_2(0)$ for various hyperon amplitudes as defined in Equations 7.12 and 7.13 respectively. These quantities are expected to not show linear effects in δm_l. No matrix elements have been renormalised and fits are made to a constant. The physical point is represented by the black dotted line.

possible to normalise using both X_D and X_F. Both of these averaged quantities are plotted in Figure 7.5 and, as can be seen, $f_2(0)$ data is somewhat noisier than that of $g_1(0)$ which should be expected given the results presented in Chapter 6. There is no obvious linear trend in this plot however.

The fan plots for $f_2(0)$ do show significantly more splitting away from the symmetric point in comparison with the vector form factor $f_1(0)$ as seen in Figures 7.6 and 7.7. There are only a few fan plot elements which show small flavour symmetry breaking effects in this case. Generally speaking the original, unconstrained, data sits close to the linear fits created by finding the slope parameters, with the possible exception of F_1/X_F. The D-fan plot looks slightly more cluttered as the scale was chosen to be the same as that of the F-fan for comparative purposes. The F-fan shows significant splitting in many cases.

As before a table containing slope parameter results and values of fan plot elements at the physical point are included in Table 7.3. The fits themselves have a relatively large $\frac{\chi^2}{\text{d.o.f}}$, especially for the F-fan, which may point to large second

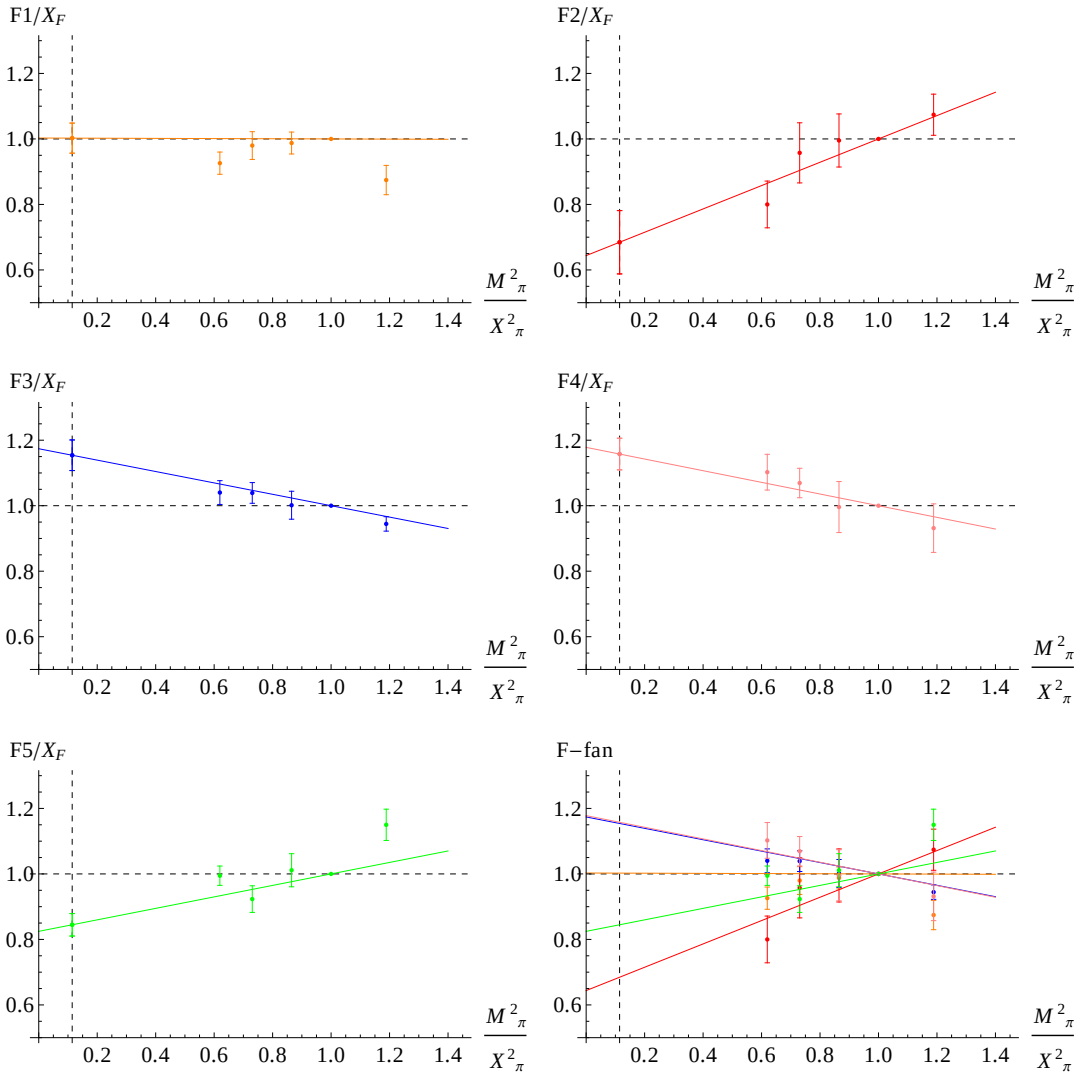

Figure 7.6: F-fan for the form factor $f_2(0)$ with each individual fan element displayed separately for clarity. A normalisation by X_F (Equation 7.13) has been applied to each element of the fan plot. Linear fits are global fits to the F-fan data following Equations 7.10. The vertical dashed line represents the physical point.

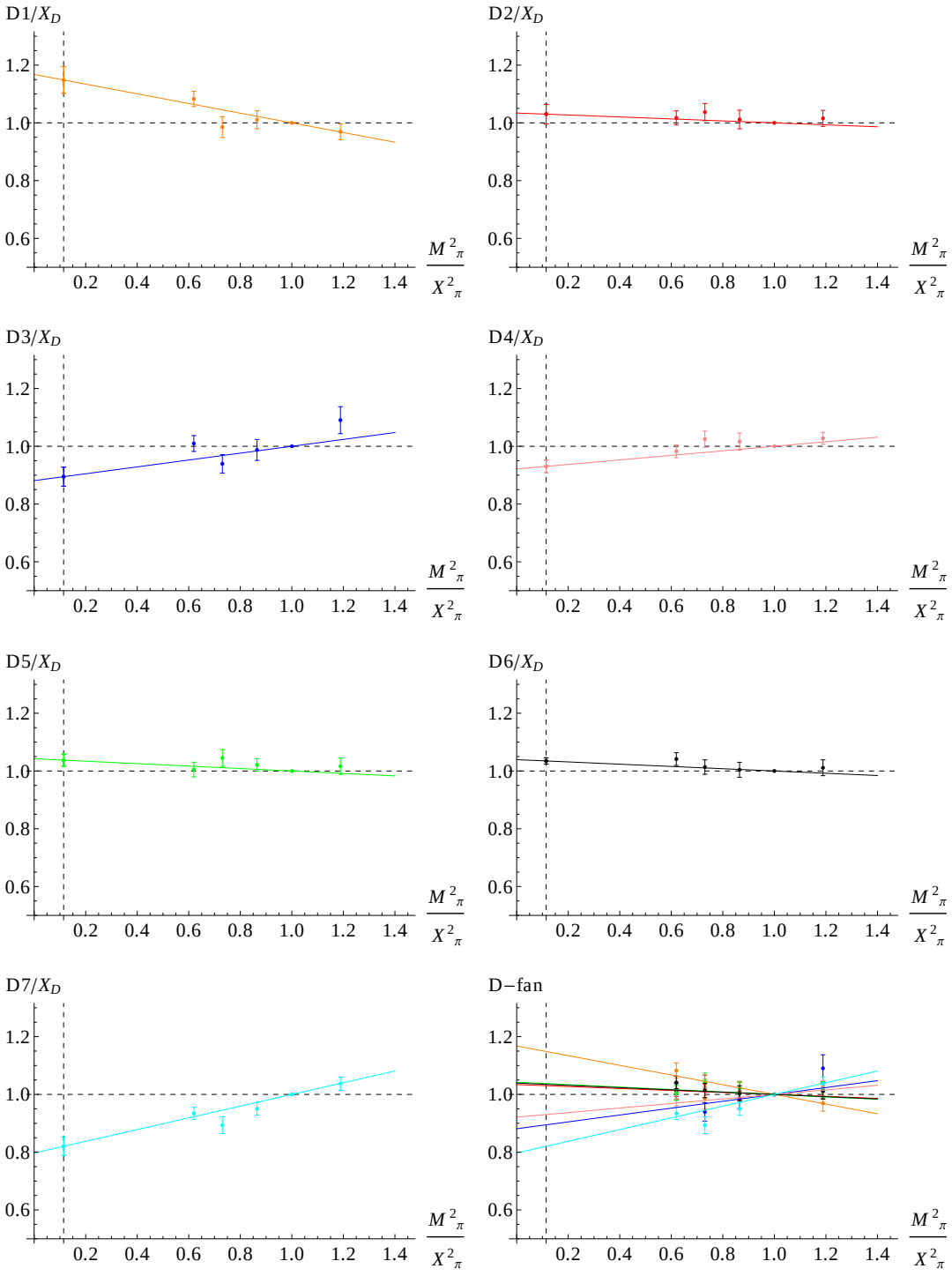

Figure 7.7: D-fan for the form factor $f_2(0)$ with each individual fan element displayed separately for clarity. A normalisation by X_D (Equation 7.12) has been applied to each element of the fan plot. Linear fits are global fits to the D-fan data following Equations 7.9. The vertical dashed line represents the physical point.

order effects in this form factor. The value of the parameters in both cases are the largest of the form factors examined in this work. The effects of $SU(3)$ symmetry breaking at leading order in mass splitting seem to be non-negligible according to results presented here.

For the $\Xi \to \Sigma$ transition at least, it was noted by Sasaki and Yamazaki [97] that the ratio $f_2(0)/f_1(0)$ had the largest symmetry breaking effects of the form factors they calculated; they found it to be $\sim 16\%$. We will also estimate this value for comparison later in this chapter, but will first move to the fan plots for the axial form factor $g_1(0)$.

	D-fan		F-fan
d	1.04(1)	f	0.513(9)
r_1	0.171(53)	s_1	0.095(28)
r_2	−0.206(37)	s_2	0.003(47)
r_3	−0.070(21)		
D_1/X_D	1.146(45)	F_1/X_F	1.003(47)
D_2/X_D	1.030(33)	F_2/X_F	0.673(99)
D_3/X_D	0.897(33)	F_3/X_F	1.158(48)
D_4/X_D	0.932(21)	F_4/X_F	1.163(50)
D_5/X_D	1.037(21)	F_5/X_F	0.840(36)
D_6/X_D	1.034(11)		
D_7/X_D	0.824(32)		

Table 7.3: Unrenormalised slope parameters for both the F and D-fans of $f_2(0)$ when the scale is given by $\frac{M_\pi^2}{X_\pi^2}$. Also shown are the values of the individual fan elements at the physical point. Both sets of fan plots elements have been normalised by either X_F (Equation 7.13) or X_D (Equation 7.12) as appropriate. The accuracy of the D-fan fit is given by $\frac{\chi^2}{\text{d.o.f}} = 1.60$ and $\frac{\chi^2}{\text{d.o.f}} = 2.06$ for the F-fan.

The axial-vector form factor $g_1(0)$ shows evidence of $SU(3)$ symmetry breaking effects in its fan plots, Figures 7.8 and 7.9. Again, the same scale is used in both sets of fan plots. The data in these plots is less noisy than that of the $f_2(0)$ fans and normalisation by X_D and X_F has significantly reduced fluctuations. All data points, but one, lie on global linear fit lines within uncertainty. In this case it is the D-fan which shows more splitting than the F-fan in contrast with

$f_2(0)$. This highlights that despite the equations governing the fan plots being the same, the values of parameters will vary significantly between form factors. These parameters are included in the leftmost columns of Table 7.5 for $g_1(0)$.

In addition to the $24^3 \times 48$ lattice data generated as part of this work, we will also introduce fan plot results made from $32^3 \times 64$ ensembles, generated by J. M. Zanotti of the QCDSF-UKQCD collaboration [148] for other projects. Some details of those configurations are given in Table 7.4. In general this data will have significantly smaller error bars than data on our lattice and will provide a good indication of the effectiveness of the fan plot approach. Though $g_1(q^2)$ itself is known to have finite size effects this comparison will utilise the normalisation of fan plot elements to reduce such sources of error.

κ_l	κ_s	M_π[MeV]
0.120900	0.120900	440
0.121040	0.120620	340
0.121095	0.120512	290

Table 7.4: Details of configurations for $32^3 \times 64$ lattice. Here $\beta = 5.50$ corresponding to a lattice spacing of $a \sim 0.078$.

Unfortunately only N, Σ and Ξ diagonal matrix elements are available from the $32^3 \times 64$ data, but this will still impact upon the combined fit as this extra data contributes two extra points to three elements in both the F-fan and the D-fan. To account for this we normalise using and X_D and X_F defined by

$$X_D = \frac{1}{6}\left(D_1 + 2D_2 + 3D_4\right) \tag{7.15}$$

and

$$X_F = \frac{1}{6}\left(3F_1 + F_2 + 2F_3\right). \tag{7.16}$$

This additional data will help to constrain the slope parameters further. These parameters do not deviate significantly from their central values as calculated

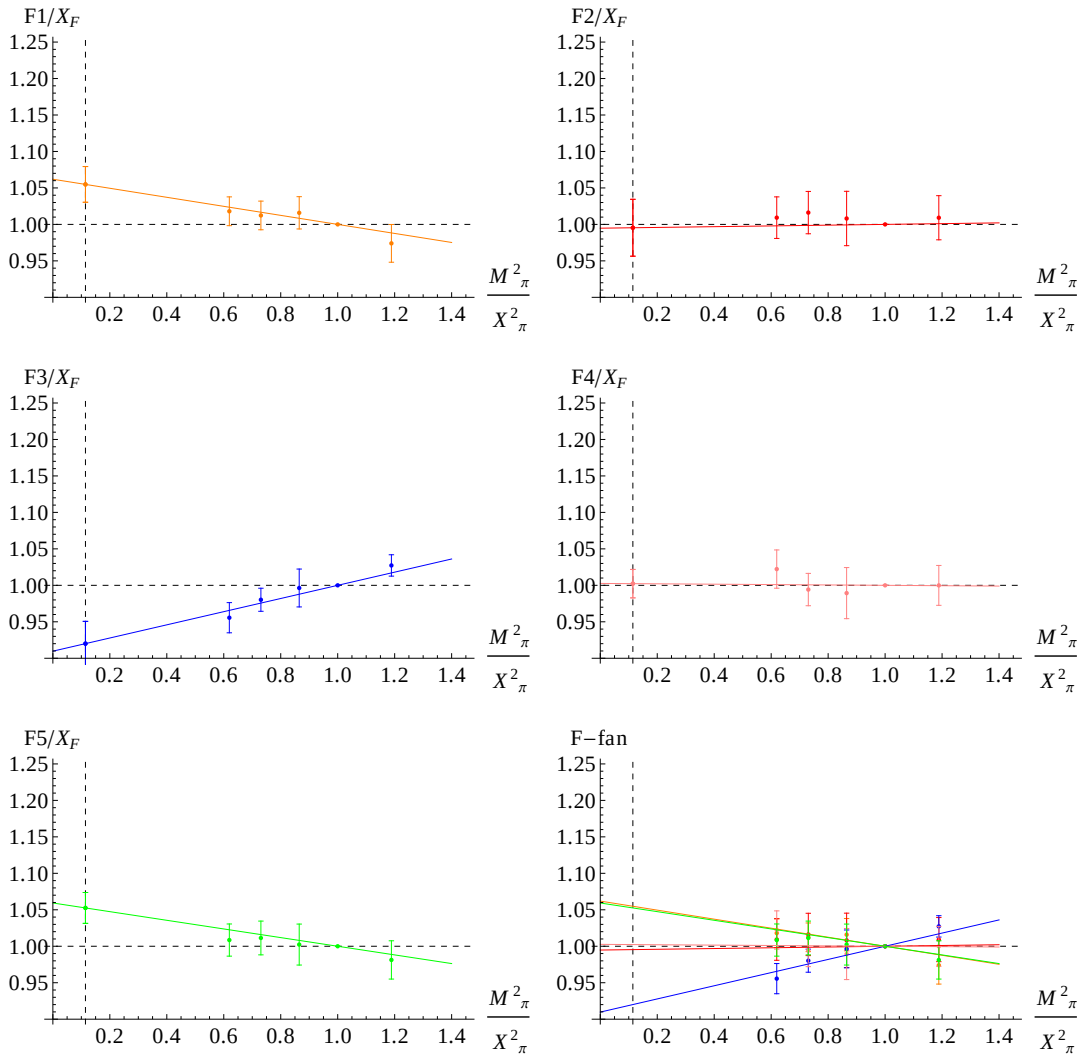

Figure 7.8: F-fan for the axial-vector form factor $g_1(0)$ with each individual fan element displayed separately for clarity. A normalisation by X_F (Equation 7.13) has been applied to each element of the fan plot. Linear fits are global fits to the F-fan data following Equations 7.10. The vertical dashed line represents the physical point.

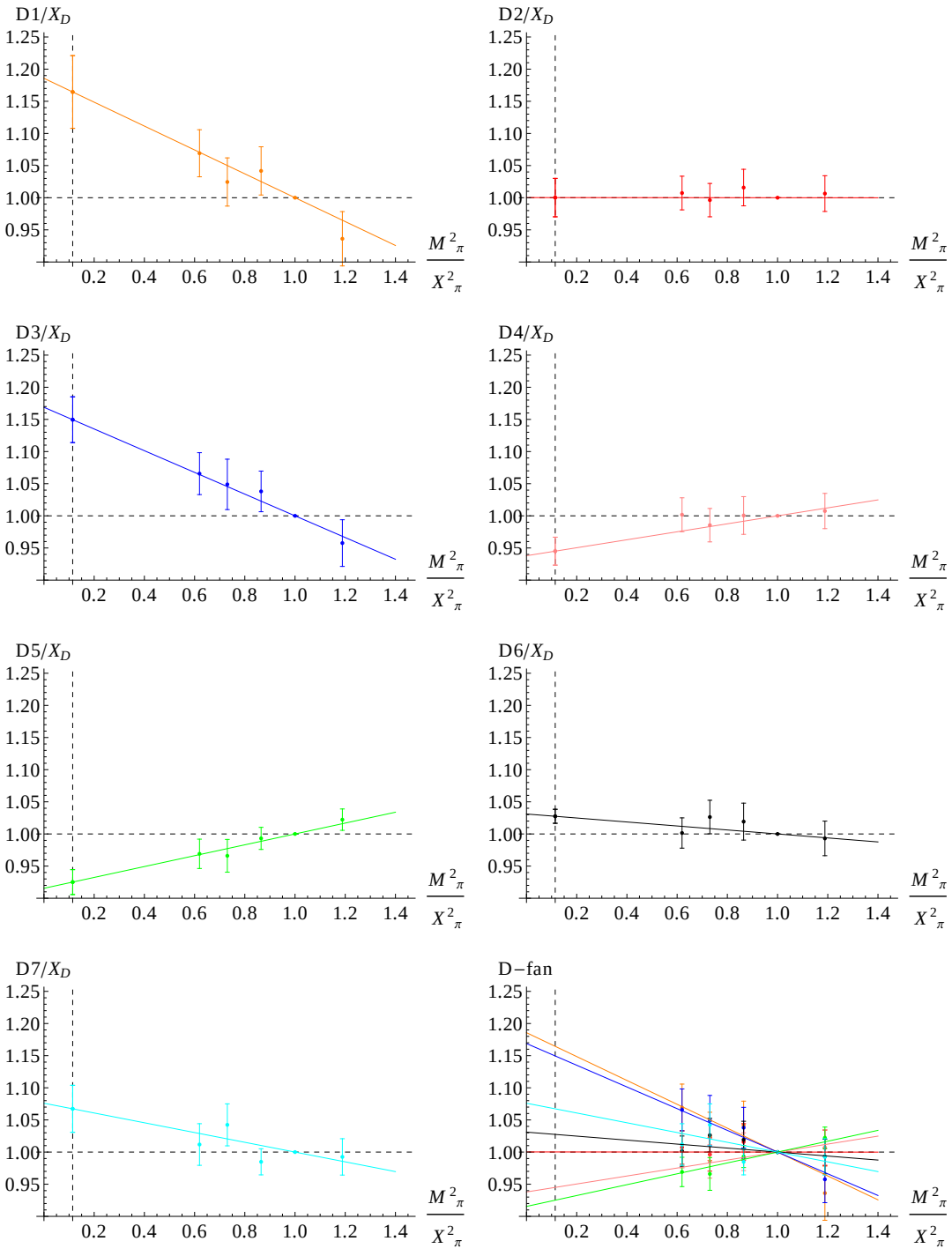

Figure 7.9: D-fan for the axial-vector form factor $g_1(0)$ with each individual fan element displayed separately for clarity. A normalisation by X_D (Equation 7.12) has been applied to each element of the fan plot. Linear fits are global fits to the D-fan data following Equations 7.9. The vertical dashed line represents the physical point.

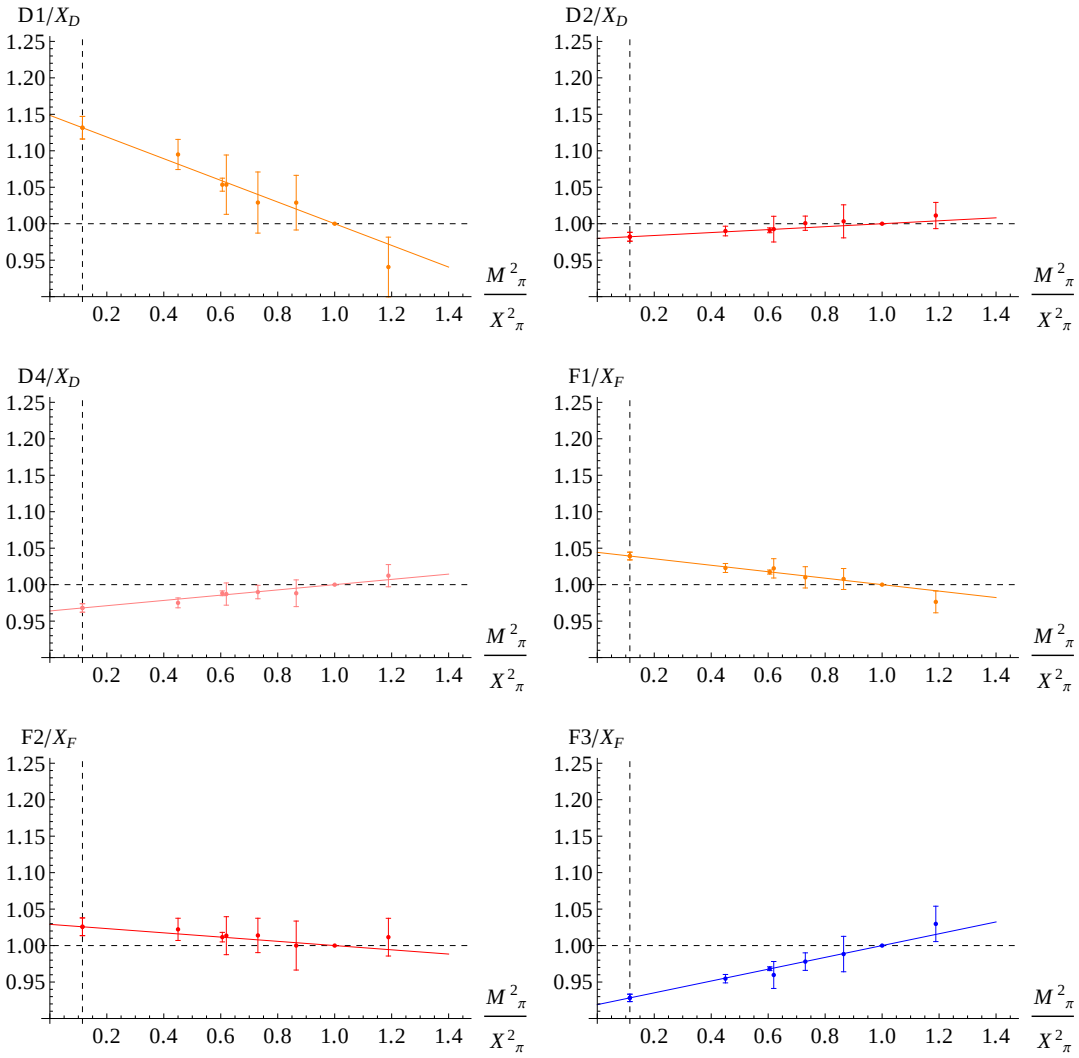

Figure 7.10: Fan plot elements for $g_1(0)$ with extra points contributed from $32^3 \times 64$ lattice data [148]. New points are the leftmost two points in each plot. These extra points result in smaller errors bars at the physical point (dotted line). Fits to other fan elements will change due to the introduction of the $32^3 \times 64$ data but these are not shown for brevity.

using only the $24^3 \times 48$ data but the errors are reduced significantly, indicating consistency in our fits. These parameters can be seen in Table 7.5 and plots of the fan plot elements that gain new points as a result of the new data are made in Figure 7.10. The parameters in both cases are quite small and indicate quite small, but non-negligible, symmetry breaking effects.

	D-fan	D-fan$^{(32)}$		F-fan	F-fan$^{(32)}$
d	0.297(2)	0.311(4)	f	0.323(2)	0.342(5)
r_1	0.055(19)	0.047(5)	s_1	0.002(71)	−0.005(2)
r_2	0.022(12)	0.027(11)	s_2	0.035(15)	0.026(3)
r_3	−0.016(6)	−0.010(2)			
D_1/X_D	1.164(57)	1.132(15)	F_1/X_F	1.055(25)	1.039(5)
D_2/X_D	1.000(30)	0.982(6)	F_2/X_F	0.995(39)	1.026(12)
D_3/X_D	1.150(36)	1.150(33)	F_3/X_F	0.920(31)	0.928(5)
D_4/X_D	0.945(22)	0.968(6)	F_4/X_F	1.002(20)	0.987(6)
D_5/X_D	0.925(20)	0.935(16)	F_5/X_F	1.053(21)	1.054(4)
D_6/X_D	1.027(11)	1.017(3)			
D_7/X_D	1.067(37)	1.080(33)			

Table 7.5: Unrenormalised slope parameters for both the F and D-fans of $g_1(0)$ when the scale is given by $\frac{M_\pi^2}{X_\pi^2}$. Also shown are the values of the individual fan elements at the physical point. Each fan has two columns: the left column are solely $24^3 \times 48$ results and the right hand columns (superscript '32') which comprise both $24^3 \times 48$ and $32^3 \times 64$ data. We choose normalisation factors X_D and X_F defined by Equations 7.15 and 7.16. The accuracy of the D-fan fit is given by $\frac{\chi^2}{\text{d.o.f}} = 1.02(1.04)$ and $\frac{\chi^2}{\text{d.o.f}} = 0.92(0.90)$ for the F-fan, where the first value is that for the $24^3 \times 48$ fit alone and the bracketed value is that for both data sets.

The parameters for this form factor and for both vector form factors can now be used to find all amplitudes within the baryon octet, at the physical point.

7.4 Reconstructing Form Factors

The form factors can be constructed at any desired choice of pion mass through the use of Equations 7.9 and 7.10 now that the slope parameters have been

determined. This section will conclude the chapter by determining a selection of the form factors at the physical point using those slope parameters.

The first quantity to be re-examined will be the electromagnetic $G_m^R(q^2)$ with $q^2 = 0$. The results for $G_e^R(q^2)$ are trivial and will not change significantly from results outlined in Chapter 6 as flavour symmetry breaking was found to be negligible for the form factor $f_1(q^2)$. As was discussed previously, results determined in this study can be compared with experimental results and with other lattice calculations. Using the slope parameters determined in the previous section the form factors $f_1^R(0)$ and $f_2^R(0)$ are calculated, again renormalising by assuming a conserved vector current.

Table 7.6 shows some differences from Table 6.2 now that the constrained fit slope parameters are used to find these form factors. The value for $\Xi^0 - \Xi^-$ moves exactly to the experimental point while $\Sigma^+ - \Sigma^-$ moves towards the other lattice determination. The $n - p$ magnetic moment moves away from both the lattice and experimental values, but is still within error of the lattice result. We also now start to see some splitting between the values of $\Sigma^+ - \Sigma^-$ and $p - n$ to show a similar hierarchy seen by Shanahan et al. [131]. Errors are reduced in general.

	$\mu^{(H)}$ (μ_N)		
H	P.E. Shanahan et al. [131]	New Fit	Experiment [4]
$n - p$	3.8(3)	3.5(1)	4.70(6)
$\Sigma^+ - \Sigma^-$	3.0(2)	3.43(8)	3.62(3)
$\Xi^0 - \Xi^-$	−0.51(8)	−0.6(1)	−0.60(1)

Table 7.6: Results for isovector magnetic moments, determined using constrained fit slope parameters. These are presented along with experimental results and values determined from another study on a $32^3 \times 64$ lattice. This table should be compared with Table 6.2.

A greater agreement with other lattice calculations is noticeable for the axial charges of the outer ring of octet baryons. In the case of the axial form factor, g_1, the slope values derived by including the $32^3 \times 64$ lattice are used in conjunction with the symmetric point values of the $24^3 \times 48$ lattice. In Section 6.4 results

for $\frac{g_A^{\Sigma\Sigma}}{g_A^{NN}}$ and $-\frac{g_A^{\Xi\Xi}}{g_A^{NN}}$ were presented along with similar estimations by Lin and Orginos [85]. As a reminder, their results were

$$-\frac{g_A^{\Xi\Xi}}{g_A^{NN}} = 0.23(4),$$

$$\frac{g_A^{\Sigma\Sigma}}{g_A^{NN}} = 0.76(10),$$

which can now be compared with new values of the same quantities obtained through the use of the constrained fit method. We find

$$-\frac{g_A^{\Xi\Xi}}{g_A^{NN}} = 0.200(5),$$

$$\frac{g_A^{\Sigma\Sigma}}{g_A^{NN}} = 0.722(7),$$

which is a significant improvement in resolution when comparing with our previous values given in Equations 6.4 and 6.5. These results agree well with those of Lin and Orginos and are of course within the predicted range from chiral perturbation theory estimates, also discussed in Section 6.4. We also now find $\frac{g_A^{\Lambda\Lambda}}{g_A^{NN}} = 0.71(2)$ which can be compared with our unconstrained result of $\frac{g_A^{\Lambda\Lambda}}{g_A^{NN}} = 0.69(4)$; a 50% reduction in error.

Equations 6.6 and 6.7 were both used previously to determine $\frac{D}{F}$, the ratio of $SU(3)$ axial constants and also to depict the effects of symmetry breaking. These can now be better understood through the use of Table 7.1 as can be described in terms of the determined slope parameters as

$$\frac{g_A^{NN} + g_A^{\Xi\Xi}}{g_A^{\Sigma\Sigma}} = \frac{2f + 4s_1\delta m_l + \mathcal{O}(\delta m_l^2)}{2f + (\sqrt{3}s_2 - 2s_1)\delta m_l + \mathcal{O}(\delta m_l^2)} \tag{7.17}$$

and

$$\frac{g_A^{NN} - g_A^{\Xi\Xi}}{g_A^{\Sigma\Sigma}} = \frac{2\sqrt{3}d - 4r_3\delta m_l + \mathcal{O}(\delta m_l^2)}{2f + (\sqrt{3}s_2 - 2s_1)\delta m_l + \mathcal{O}(\delta m_l^2)}, \tag{7.18}$$

so that when working in the limit of $\delta m_l \longrightarrow 0$ Equation 7.17 is unity and Equation 7.18 becomes $\frac{\sqrt{3}d}{f}$. The terms f and d can be related to the g_A axial

coupling constants F and D by

$$F = \sqrt{2}f \tag{7.19}$$

and

$$D = \sqrt{6}d. \tag{7.20}$$

The ratio $\frac{D}{F}$ can be considered so that renormalisation constants cancel. The new value from the constrained fit is now 1.592(6) at the symmetric point. This value has a similar central value as before but due to the input of parameters from a constrained fit the error has decreased significantly in comparison with our original result, 1.60(5). Calling upon Lin and Orginos' calculations again, this result can be compared with $\frac{D}{F} = 1.6(1)$. At the physical point Equation 7.18 is found to be 1.66(2).

The ratio 7.17 is identically equal to one using our fit parameters at the symmetric point, as seen in Figure 7.11. Finding its value at the physical point will indicate the strength of $SU(3)$ symmetry breaking. We find this value to indicate a breaking of 11(2)%. The relative error has decreased in comparison to that consisting of original lattice data, where symmetry breaking effects are 12(7)%. As can be seen the slope (magnitude of symmetry breaking) for this quantity has not changed significantly.

We now return briefly to the spin fraction of the Λ hyperon, and in particular to the quantity Δs, which we discussed in Section 6.5. We compared our unrenormalised result to that of Chambers et al. [141] and found slight disagreement. Before the constrained fit was carried out we had found $\Delta s^{\text{latt}} = 0.852(32)$, whereas now the result shifts to $\Delta s^{\text{latt}} = 0.837(24)$ which can be compared with the Chambers et al. result of $\Delta s^{\text{latt}} = 0.803(10)$. These results are now in better agreement, with the proviso that disconnected contributions have not been calculated in either case.

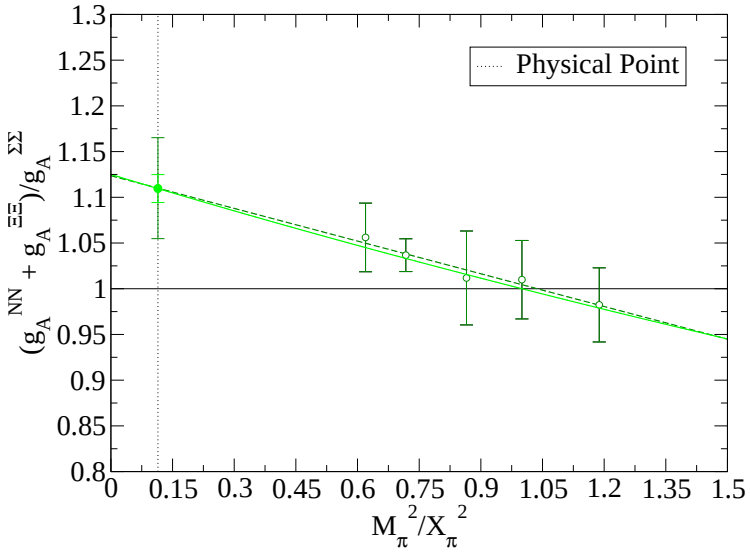

Figure 7.11: Ratio $\frac{g_A^{NN}+g_A^{\Xi\Xi}}{g_A^{\Sigma\Sigma}}$ with constrained fit physical point value calculated from constrained fit parameters of the axial-vector form factor $g_1(0)$. Both unconstrained (dashed) and constrained (solid) fit lines are included.

As we are working to first order in symmetry breaking effects we will not be expecting to see flavour symmetry breaking effects in transition matrix elements for the form factor $f_1(q^2)$. For the axial form factor $g_1(q^2)$ however, we can in practice see symmetry breaking effects. Though the mass splitting of the hyperons is of the order 10%, previous lattice calculations [97, 98] have found the flavour symmetry breaking effects to be considerably smaller when calculating hyperon transitions. The same is seen here.

Sasaki and Yamazaki [97] argue that the decay $\Xi \to \Sigma$ is best placed to measure flavour symmetry breaking effects as it is identical to the beta decay of a neutron but with the s quark interchanged with a u. Thus measuring the constant of proportionality from the following equation should measure the effect of $SU(3)$ symmetry breaking within hyperon transitions:

$$\left[\frac{g_1(0)}{f_1(0)}\right]_{\Xi\to\Sigma} \propto \left[\frac{g_1(0)}{f_1(0)}\right]_{n\to p}. \tag{7.21}$$

They report an effect of 5% in this particular transition though this does not

seem to account adequately for errors.

The axial to vector ratio of $\Xi \to \Sigma$ is reported to be 1.051(35) bigger than that of $n \to p$; the value of $\left[\frac{g_1(0)}{f_1(0)}\right]_{n\to p}$ used to find 5(4)% is thus 1.188(25) which was calculated earlier by the RIKEN-BNL-Columbia-KEK collaboration [151] using domain wall fermions. This number matches their determination of $Z_A g_A$ alone however, not $\frac{g_1(0)}{f_1(0)}$. The value of $\frac{g_1(0)}{f_1(0)}$ in that paper is reported to be 1.212(27). To account for this discrepancy a result of $g_A^R = 1.212 \pm 0.027(\text{stat}) \pm 0.024(\text{norm})$ is quoted. Instead, using the value of $\left[\frac{g_1(0)}{f_1(0)}\right]_{n\to p} = 1.212(27)$ along with the value given for $\left[\frac{g_1(0)}{f_1(0)}\right]_{\Xi\to\Sigma}$ would result in breaking effects of 3(3)%, i.e., no measurable symmetry breaking.

In either case the results outlined above point to small symmetry breaking effects for this ratio. Using our constrained fit parameters we can perform the same calculation to find an effect of 6(7)%. Our measurement of $n \to p$ is noisier than that of $\Xi \to \Sigma$, so instead we take the ratio of $\Xi \to \Sigma$ at the physical point to that of the symmetric point to find effects of 3(4)% which still has errors large enough to be unable to properly distinguish whether the correction is positive, though confirms that the breaking effects must be small. This is perhaps surprising given that model predictions indicate corrections from anything between 10% to 30% [74, 152, 153]. Corrections are consitently reported to be small, however, by the other lattice studies mentioned in this section.

If analysis is restricted to the axial form factor alone, flavour symmetry breaking can be determined to a greater precision. To measure its effects the ratio of the axial form factor at the physical point can be taken to the same form factor at the symmetric point. This should give a good indication of how strongly each particular transition is affected by symmetry breaking. The results in Equation 7.22 indicate that many of the transitions do indeed show measurable

symmetry breaking effects in this form factor, though all are smaller than $\sim 10\%$.

$$\begin{aligned}
\Xi \to \Lambda\text{:}\ & \frac{g_1(0)}{g_1^{sym}(0)} = 3(4)\%, \\
\Xi \to \Sigma\text{:}\ & \frac{g_1(0)}{g_1^{sym}(0)} = 0.5(4)\%, \\
\Sigma \to \Lambda\text{:}\ & \frac{g_1(0)}{g_1^{sym}(0)} = -4(2)\%, \\
\Sigma \to N\text{:}\ & \frac{g_1(0)}{g_1^{sym}(0)} = 7(1)\%, \\
\Lambda \to N\text{:}\ & \frac{g_1(0)}{g_1^{sym}(0)} = 6(1)\%.
\end{aligned} \tag{7.22}$$

There is disagreement between models of flavour symmetry breaking and some of these, outlined in detail in these references [108, 154, 155], support our results; R. Flores-Mendieta et al., for example, find $\Xi \to \Lambda$ $(0.3 - 7.2\%)$, $\Sigma \to N$ $(4 - 5.6\%)$ and $\Lambda \to N$ $(5 - 7.2\%)$, which indicate similar positive corrections as seen here.

In Chapter 5 we examined the Cabibbo model predictions of the form factor $g_1(0)$ by taking the ratio of the axial coupling for the four $\Delta S = 1$ transitions, to that of the $\Delta S = 0$, $\Sigma \to \Lambda$, transition. Symmetry breaking effects were manifest in our plots but the symmetric limit values did not always correspond to our symmetric ensemble results due to the values of the F and D coupling constants chosen in that case. Here, in Figure 7.12, we plot the same results but now with the added constrained fit lines and physical point values. The original, unconstrained, lattice data for the $\Sigma \to N$ transition was noisy and the constrained fit has now moved the physical point value down into the symmetric limit prediction. Apart from that, the other transitions all remain apart from the Cabibbo predictions at the physical point. Errors are also reduced in most cases.

To compare ratios of axial charges to experiment we consider $\Delta S = 1$ transitions over the nucleon axial charge. This can be done if full $SU(3)$ symmetry is assumed for the vector form factor $f_1(0)$ and experimental values for $\frac{g_1(0)}{f_1(0)}$ are used. This can be motivated given our lack of evidence for symmetry breaking

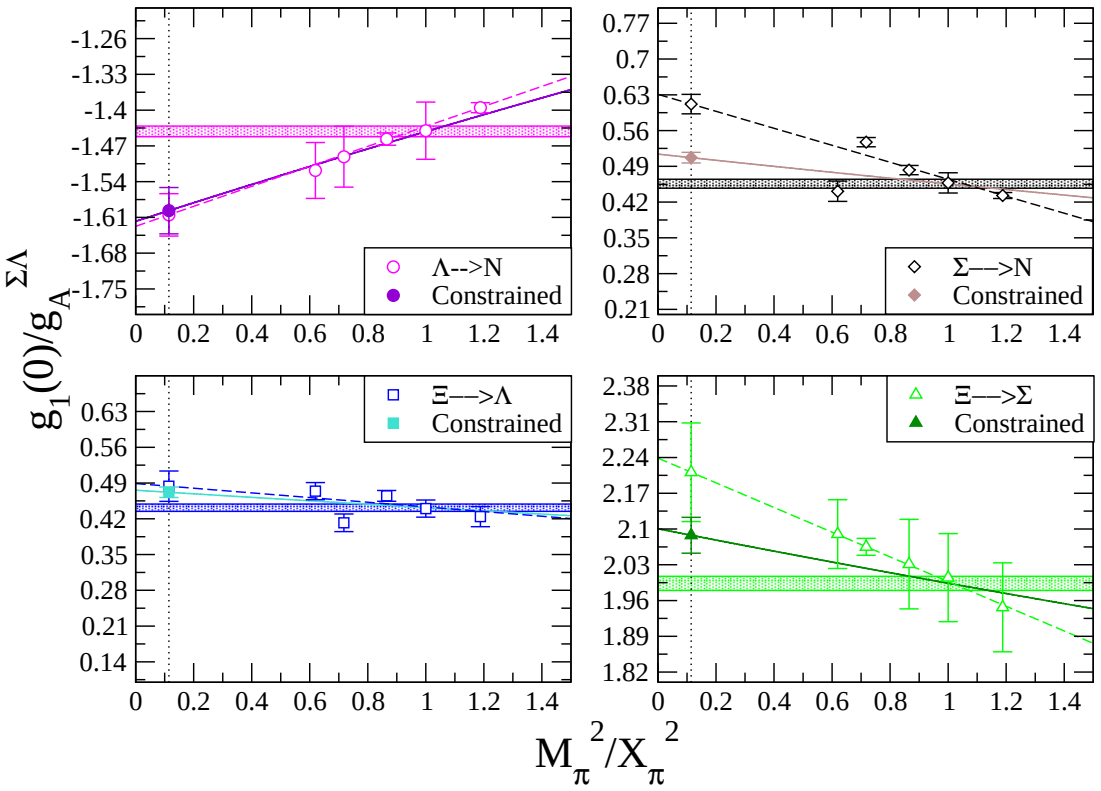

Figure 7.12: Ratio $g_1(0)/g_A^{\Sigma\Lambda}$ for the $\Delta S = 1$ hyperon transitions. Also indicated are the Cabibbo model predictions of the same quantities in the $SU(3)$ limit using F and D constants determined through a constrained fit using Table 7.1. Points away from the physical pion mass are the unconstrained lattice data. The solid lines are linear fits made using the slope parameters of the constrained fit. Dashed lines are linear fits to the original lattice data. Errors are calculated using the bootstrap method.

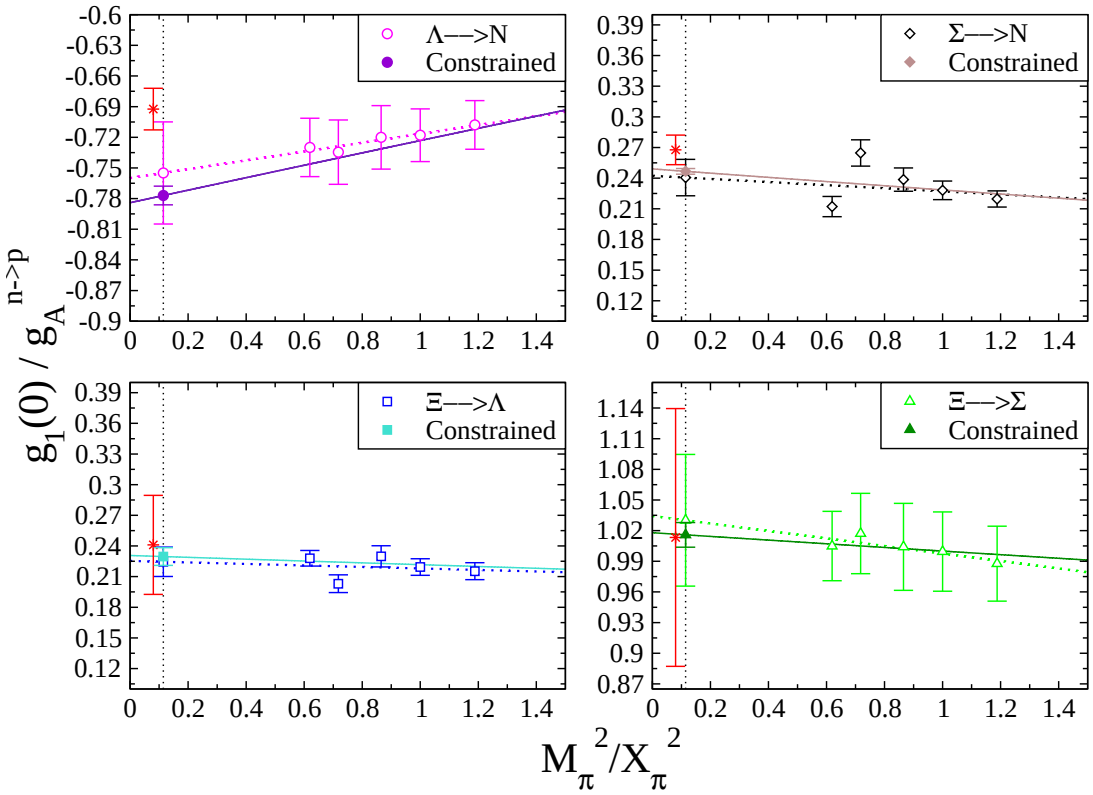

Figure 7.13: Ratio $g_1(0)/g_A^{np}$ for the $\Delta S = 1$ hyperon transitions. Also indicated are experimental results (red stars) which have been slightly shifted from the physical point (black dotted line) for clarity, and where $SU(3)$ symmetry has been assumed for the vector form factor $f_1(0)$. Points away from the physical pion mass are the unconstrained original lattice data. The solid lines are linear fits made using the slope parameters of Table 7.1 determined from a constrained fit. Dashed lines are linear fits to the original lattice data. Errors are calculated using the bootstrap method.

effects at first order for that form factor. These ratios are plotted in Figure 7.13. The solid linear fit line in each case is composed of values determined from the constrained fit while the dashed lines are linear fits to the original data.

Generally the new fits follow a similar trend to the originals, confirming the relationship between the transitions. The constrained fit proves its usefulness here as the error bars are noticeably reduced; in two cases a sixfold improvement. Unfortunately the value for $\Lambda \to N$ moves further away from the experimental value and there are few other LQCD evaluations to compare with. The other

values, however, move marginally closer to the central value of the experimental results in each case. This improves upon Figure 6.19.

	Transition	Constrained	Original	Lattice	Experiment
$\frac{g_1^R(0)}{f_1^R(0)}$ *	$\Xi \to \Lambda$	0.23(1)	0.22(1)		0.25(5)
	$\Xi \to \Sigma$	1.20(6)	1.33(6)	1.25(3)	1.3(2)
	$\Sigma \to \Lambda$	0.58(3)	0.59(4)		
	$\Sigma \to N$	−0.30(1)	−0.32(2)	−0.28(5)	−0.34(2)
	$\Lambda \to N$	0.75(5)	0.80(4)		0.72(2)

Table 7.7: $\frac{g_1^R(0)}{f_1^R(0)}$ (*or $g_1^R(0)$ in the case of $\Sigma \to \Lambda$) for flavour changing octet transitions. The 'Constrained' label refers to form factors reconstructed from simultaneous fits to lattice data. Also included are other Lattice QCD and experimental results where available. This table is, in part, a reproduction of Table 6.5.

Though the form factor ratio $\frac{g_1(0)}{f_1(0)}$ needs to be renormalised it will be an important quantity in the next chapter so it is worth estimating renormalisation factors by utilising the conserved vector current and fixing to the nucleon axial charge and updating our results using the constrained fit parameters. These results are now tabulated. There is a mixed effect; the errors do not significantly reduce as the fit for $f_1(0)$ is not very well constrained and $\Sigma \to N$ moves slightly away from the experimental result. The $\Lambda \to N$ point moves towards its experimental counterpart and $\Xi \to \Sigma$ changes quite significantly but stays within experimental error. Both results where other lattice determinations are available move closer to those points.

Finally we briefly comment on the flavour symmetry breaking effects in the weak magnetism form factor $f_2(0)$. By dividing the physical point value of $f_2(0)$ for a transition by the same quantity but at the symmetric point $f_2^{sym}(0)$ we can measure how strongly the form factor breaks $SU(3)$-flavour symmetry. These

results are presented below.

$$\begin{aligned}
\Xi \to \Lambda\text{:}\ & \frac{f_2(0)}{f_2^{sym}(0)} = -27(25)\% \\
\Xi \to \Sigma\text{:}\ & \frac{f_2(0)}{f_2^{sym}(0)} = 7(2)\% \\
\Sigma \to \Lambda\text{:}\ & \frac{f_2(0)}{f_2^{sym}(0)} = 9(2)\% \\
\Sigma \to N\text{:}\ & \frac{f_2(0)}{f_2^{sym}(0)} = -2(2)\% \\
\Lambda \to N\text{:}\ & \frac{f_2(0)}{f_2^{sym}(0)} = -17(3)\%.
\end{aligned} \tag{7.23}$$

One can see that in many cases flavour symmetry breaking effects at first order appear quite large. Errors are sometimes significant which makes definitive statements about the symmetry breaking of certain transitions difficult, such as that of $\Xi \to \Lambda$. Sasaki and Yamazaki [97] report a symmetry breaking effect of 16(11)% for f_2 of $\Xi \to \Sigma$ which shows the same positive sign of symmetry breaking effects as those seen here. As we found a better fan plot fit for f_1 and g_1 than for f_2 this may point to the relative importance of incorporating second order effects into this form factor. Aknowledging that caveat, we can still see in Table 7.8 that uncertainties reduce after the constrained fit and still agree with the results of Sasaki and Yamazaki and of Guadagnoli et al. [98].

Transition	Original	Constrained	Lattice
$\Xi \to \Lambda$	$-1.41(11)$	$-1.41(8)$	
$\Xi \to \Sigma$	1.46(12)	1.57(8)	1.5(8)
$\Sigma \to \Lambda$	1.85(13)	1.99(10)	
$\Sigma \to N$	3.19(21)	3.05(14)	3.30(24)
$\Lambda \to N$	0.013(17)	$-0.10(3)$	

Table 7.8: Renormalised results for weak magnetism form factor $f_2^R(0)$ with other Lattice QCD results where available. 'Original' refers to results from an unconstrained linear fit while 'Constrained' refers to results obtained from simultaneous fits to lattice data.

"Decay is inherent in all compounded things..."

— Siddhārtha Gautama, the Buddha

Chapter 8

Determination of $|V_{us}|$

Chapter 4 in part motivated the importance of determining the entries of the CKM matrix governing the relative probabilities of flavour violating transitions between hadrons. Confirming the predicted properties of the CKM matrix, through evaluating its elements, is a test of the SM and may present evidence for BSM physics. Providing for alternative avenues of calculating the elements is also an important consistency check on existing results.

Efforts in this study have thus far focused on determining the form factors of the octet hyperons including those of the $\Delta S = 1$ transitions, using the techniques of LQCD in order to compare with experimental data and measuring the effects of flavour symmetry breaking. Now these form factor results can be used to arrive at a hyperon derived estimation of one of the CKM matrix elements concerned with strangeness changing processes, $|V_{us}|$.

8.1 Status of $|V_{us}|$

The first row of the CKM matrix has three entries: V_{ud}, V_{us} and V_{ub}. As quarks are more likely to transition within their own generation the most dominant factor is V_{ud}, followed by V_{us}, while V_{ub} is orders of magnitude smaller than

V_{ud}. The elements within the matrix are determined to various levels of relative accuracy depending on how easy it is to probe those weak flavour changing processes both experimentally and theoretically. This means that at current levels of precision, certain parameters will dominate within the unitarity and orthogonality constraint relationships of the CKM matrix (see Equation 4.10). One such constraint is the equation

$$|V_{ud}|^2 + |V_{us}|^2 + |V_{ub}|^2 = 1 - \Delta, \tag{8.1}$$

where $\Delta = 0$ preserves unitarity. This relation contains some of the more easily accessible parameters of the matrix and has therefore received much attention.

The matrix element $|V_{ud}|$ is the best determined parameter of the CKM matrix due to the prevalence of first generation quarks in nature. The highest precision estimate of $|V_{ud}|$ comes from $0^+ \rightarrow 0^+$ superallowed nuclear decay [156, 157]. Neutron decay can also provide an avenue for this calculation, but as we have laid out in previous chapters, this is not a purely vector transition and requires a good evaluation of g_A. Radiative corrections and other theoretical uncertainties dominate the error of $|V_{ud}|$ determinations [158–160]. Other transitions such as $\pi^+ \rightarrow \pi^0 e^+ \nu$ result in a less precise, but consistent result [158].

Within the unitarity relation 8.1 the element $|V_{ub}|$ is significantly smaller ($|V_{ub}|^2 \sim 10^{-5}$) than the other two [161] and is negligible at current levels of precision [162]. It is therefore the error associated with $|V_{us}|$ that dominates this particular unitarity relation. There have been efforts over the past years, exploring various approaches, to reduce the error on this parameter. The three primary routes involve kaon semi-leptonic decays, tau decays and hyperon semi-leptonic decays.

Kaon semi-leptonic decays $K \rightarrow \pi l \bar{\nu}_l$, abbreviated as K_{l3}, can be simulated using the techniques of LQCD to arrive at a determination of the form factor $f_+(0)$ which is then combined with measurements of lifetimes [163] and branching

fractions from experiment (see PDG [4] or Flavianet [164] reviews of experimental results). Theoretical estimates of electroweak radiative radiative corrections are also required. Lattice calculations by Boyle et al. [56, 87, 165], which include the use of partially twisted boundary conditions, have given rise to very precise measurements of the $f_+(0)$ form factor and have significantly constrained the value of $|V_{us}|$ [166].

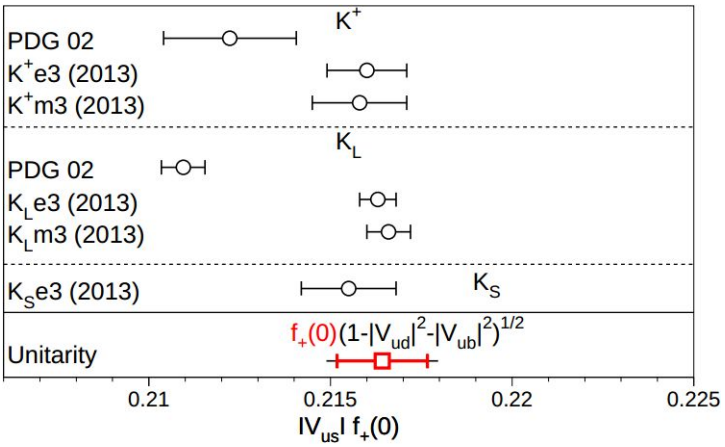

Figure 8.1: Results for $|V_{us}|f_+(0)$ using results from 2013 PDG review compared with the 2002 review. The unitarity condition is also imposed in this plot using calculated values of $|V_{ud}|$ and a lattice evaluation of $f_+(0)$ [165]. Inner (red) error bars on this prediction are due to errors on $f_+(0)$ while the outer (black) parts relate to uncertainties in $|V_{ud}|$ and $|V_{ub}|$. Figure taken from the 2013 PDG review of the CKM matrix [4].

The PDG takes the average of five results shown in Figure 8.1 (points labelled by '2013') to find $|V_{us}|f_+(0) = 0.2163(5)$ which leads to the following result:

$$|V_{us}| = 0.2253(14) \qquad \text{(kaon decays)}. \tag{8.2}$$

It should also be noted that the RBC/UKQCD collaboration had found $|V_{us}| = 0.2237^{+13}_{-8}$ using recent results for $f_+(0)$ from simulations involving near-physical pion masses [56]. Lattice calculations of kaon and pion decay constants, f_K and f_π respectively, are an alternative to K_{l3} decays, once experimental results for

the pion and kaon radiative inclusive decay rates are known [167,168]. Finally we mention that examining strangeness changing tau decays are another approach to constraining $|V_{us}|$ [169–172]. Using this process puts the estimate of $|V_{us}|$ at

$$|V_{us}| = 0.2202(15) \qquad \text{(tau decays)}. \tag{8.3}$$

8.2 $|V_{us}|$ from Hyperon Semi-leptonic Decays

The third approach mentioned previously as a means to determining $|V_{us}|$, is that of combining hyperon semi-leptonic decay form factors with experimental decay rates. As outlined previously this has generally been found to be less precise than methods involving meson strangeness changing decays primarily due to the fact that the axial-vector current includes first order flavour symmetry breaking effects.

To evaluate $|V_{us}|$ using this method, values for both the vector and axial-vector form factors, $f_1^R(0)$ and $g_1^R(0)$ are required. Non-perturbative theoretical approaches such as LQCD have provided an alternative to the use of experimental results, many of which were performed several years ago and have significant uncertainty. Another area where theory is required is for estimating electroweak radiative corrections to decay rates [173, 174]. These radiative corrections are important for reducing the deviations between theory and experiment [175, 176].

In order to calculate $|V_{us}|$, the theoretically derived results for form factors are combined with experimental measurements of total decay rates. These decay rates are calculated by dividing the PDG branching fraction by the mean lifetime for each particular decay channel. The four $\Delta S = 1$ branching fractions and mean lifetimes are given in Table 5.4, and are used in the analysis of the following section. The decay rates are given in Table 8.1.

The equation for the decay rate can be given at different orders of mass splitting [177] and an outline of its derivation, up to second order, is given in

Transition	Decay Rate (μsec^{-1})
$\Sigma \to N$	6.88(24)
$\Xi \to \Sigma$	0.872(39)
$\Xi \to \Lambda$	3.44(19)
$\Lambda \to N$	3.161(58)

Table 8.1: Decay rates used in analysis here for $\Delta S = 1$ hyperon semi-leptonic decays.

Appendix D. Here we state the result at first order in δ,

$$\Gamma = \frac{G_F^2 \Delta^5 |V_{us}|^2}{60\pi^3}(1-3\delta)\left[f_1^2 + 3g_1^2\right], \tag{8.4}$$

and at second order,

$$\begin{aligned}\Gamma = \frac{G_F^2|V_{us}|^2}{60\pi^3}\Delta^5\Bigg[&\left(1-3\delta+\frac{45}{7}\delta^2\right)f_1^2 + 3\left(1-3\delta+\frac{37}{7}\delta^2\right)g_1^2 \\ &+ \frac{12}{7}\delta^2 f_1 f_2 + \frac{4}{7}\delta^2 f_2^2 + \frac{4}{7}\delta^2 f_1^2\lambda_f + \frac{20}{7}\delta^2 g_1^2\lambda_g\Bigg].\end{aligned} \tag{8.5}$$

where we take the form factors at zero momentum transfer and with Δ defined through

$$\Delta = M_H - M_{H'} \tag{8.6}$$

and

$$\delta = \frac{\Delta}{M_H + M_{H'}}. \tag{8.7}$$

Note that conventions vary and one can also define $\delta = \Delta/M_H$. The decay rate expression includes an approximation of vanishing lepton mass and form factors are assumed to be renormalised quantities. Any terms due to g_2 are usually assumed to be negligible in analysis of hyperon decays [88, 106, 178]. Terms containing f_2 only begin to appear at second order (see Appendix D). As our analysis of $SU(3)$ symmetry breaking was to first order we will first consider the decay rate to this same order. If the assumption is made that second order

effects are small for the form factors $f_1(0)$ and $g_1(0)$ then we can proceed to use Equation 8.5.

In order to evaluate $|V_{us}|$ through the use of experimental decay rates, one includes terms related to the phase space momentum because measurements vary over a small range of momentum transfer [106, 173, 179]. These terms occur at second order and above, so are not present at first order. These terms, given as λ_f and λ_g in Equation 8.5 are fixed by experimental measurement and written as $\lambda_f = 2M_H^2/M_V^2$ and $\lambda_g = 2M_H^2/M_A^2$. Gaillard and Sauvage [94] discuss the sensitivity of the form factors to a variation of M_A and M_V and find it to be small so we simply take $M_V = 0.98(5)$GeV and $M_A = 1.25(9)$GeV following those authors. As an example, a change of 10% in both of these values would result in a $\sim 0.5\%$ effect on the value of $|V_{us}|$.

The electroweak radiative corrections which must be applied to the decay rate include both model dependent, α_d and model independent, α_i, parts [173, 180], along with a Coulomb correction, α_c due to the interaction of the daughter hyperon with the charged lepton. There have been various attempts to quantify the radiative corrections which manifest as constants, specific to each decay channel, which can be absorbed by the form factors within the matrix element as $|M|^2 \longrightarrow |M|^2(1+\alpha_c)(1+\alpha_i)(1+\alpha_d)^2 = |M|^2(1+\delta_{RC})$ [94, 181].

Sirlin first calculated these corrections for neutron beta decay [180, 182] through a method which was then applied to hyperon decays [173, 183]. The model independent terms for each transition (see Garcia and Kielanowski [173]) along with a standard determination of the model dependent correction were found to be $\alpha_d = 0.021$ which is used in analysis here, and in many other studies of hyperon decays. Other estimates of the model-independent part have also been performed [184, 185]. In the analysis here, we follow the lead of Mateu and Pich [186] and use the total decay rate radiative corrections as outlined in Table 8.2.

Transition	δ_{RC}
$\Sigma \to N$	0.0186
$\Xi \to \Sigma$	0.0442
$\Xi \to \Lambda$	0.0196
$\Lambda \to N$	0.0422

Table 8.2: Radiative corrections to hyperon total decay rates. Multiply by one hundred to obtain percentage radiative corrections.

The review of HSL decays carried out by Gaillard and Sauvage [94] includes an evaluation of $|V_{us}|$. By using the available experimental data they calculate $|V_{us}| = 0.231(3)$. This determination has been improved upon in recent times. The value of $|V_{us}|$ derived from HSL decays as quoted by the PDG is from a comprehensive analysis performed by Cabibbo, Swallow and Winston [101], twenty years after Gaillard and Sauvage reviewed the state of hyperon decay experiments. Experimental results of $\frac{g_1(0)}{f_1(0)}$ had improved in the intervening years [116, 187] which confirmed some predictions of the Cabibbo theory and allowed for an updated calculation of $|V_{us}|$. Cabibbo et al. used the $SU(3)$ symmetric limit and model values for the form factors $f_1(0)$ and $f_2(0)$ and found

$$|V_{us}| = 0.2250(27). \tag{8.8}$$

The authors acknowledged that symmetry breaking effects of second order in the vector form factor would likely push this value slightly higher. This value is a weighted average of the four $\Delta S = 1$ octet transitions, so a separate evaluation of $|V_{us}|$ for each was also determined [88] which are summarised in Table 8.3.

A similar analysis was performed by Flores-Mendieta [178] shortly following the Cabibbo et al. paper. This work also considered the decay $\Xi^- \to \Sigma^0 e^- \bar{\nu}_e$ which is indistinguishable in our case in the isospin limit within which we work. The author analyses the $SU(3)$ symmetry breaking effects for both the $f_1(q^2)$ and $g_1(q^2)$ form factors to calculate these effects from fits to experimental data,

Transition	$\lvert V_{us}\rvert$
$\Sigma \to N$	0.2282(49)
$\Xi \to \Sigma$	0.209(27)
$\Xi \to \Lambda$	0.2367(99)
$\Lambda \to N$	0.2224(34)

Table 8.3: $|V_{us}|$ for the octet hyperon $\Delta S = 1$ transitions by Cabibbo et al. [88, 101] where experimental $\frac{g_1(0)}{f_1(0)}$ results for have been combined with Cabibbo theory predictions of $f_1(0)$ and $f_2(0)$.

and while taking the model $SU(3)$ limit prediction for $f_2(0)$ and assuming no contribution from $g_2(0)$, deduces that

$$|V_{us}| = 0.2199(26), \tag{8.9}$$

which is similar to that found from tau decay results (Equation 8.3) and narrowly agrees with the previous hyperon decay estimation.

An analysis of systematic errors, including those arising from $SU(3)$ symmetry breaking effects by Mateu and Pich [106] followed, in order to explain the difference between the previous two estimates which differ despite relying on the same experimental data. A reliable estimate of second order effects to both the vector form factor and to the ratio $\frac{g_1(0)}{f_1(0)}$ was found by these authors to be difficult to perform within the constraints of existing experimental data. Fits to data at second order [186], performed using $1/N_C$ expansions in a similar manner to Flores-Mendieta, result in an increase in the uncertainty of $|V_{us}|$;

$$|V_{us}| = 0.226(5). \tag{8.10}$$

Finally, as mentioned, independent LQCD calculations of the form factors necessary to determine $|V_{us}|$ present an alternative approach. Lattice calculations of hyperon form factors performed by Sasaki [97, 119, 188] for the $\Xi \to \Sigma$ and $\Sigma \to N$ transitions have been compared with our results in previous chapters. In

regards to $|V_{us}|$, the author calculates $|V_{us}|$ through the use of experimental results which measure $|f_1(0)V_{us}|$ [117] and a calculation of $f_1(0)$ through a different ratio of correlation functions to that used in this work, which is computationally more expensive. The advantage of this method is that symmetry breaking effects are contained within the experimental results for the axial-vector form factor and need not be estimated. Of course this depends on accurate experimental results and the result presented within that study, for $\Xi \to \Sigma$,

$$|V_{us}| = 0.219(27)_{\text{exp}}(4)_{\text{theory}}, \tag{8.11}$$

contains sizeable uncertainty related to experiment.

8.3 $|V_{us}|$ Results

Our approach will be to use the constrained fit form factor results presented in Chapter 7 and directly insert these into the corrected hyperon decay rate discussed in the previous section. These results are constrained up to first order in flavour symmetry breaking which enters into the form factors $g_1(0)$ and $f_2(0)$. Radiative corrections as outlined in Table 8.2 are used in our analysis. The experimental decay rates can be calculated using Table 5.4 (note a different decay rate for $\Xi \to \Sigma$ as compared with N. Cabibbo et al. due to updated branching ratio values [189]) and are displayed in Table 8.2.

We present our results for $|V_{us}|$ at both first and second order in δ in Table 8.4. For a full treatment at $\mathcal{O}(\delta^2)$, a second order constrained fit would need to be made to the form factors f_1 and g_1, while first order is sufficient for f_2. Our weighted average results at both orders are within error of Mateu and Pich's result. The second order results agree with both PDG kaon and τ-decay estimates. In fact, the combined second order result is consistent with all other estimates of $|V_{us}|$ that have been highlighted in this chapter, which can be seen in Figure 8.2.

Transition	$f_1^R(0)$	$g_1^R(0)$	$f_2^R(0)$	$\lvert V_{us}\rvert$ - $\mathcal{O}(\delta)$	$\lvert V_{us}\rvert$ - $\mathcal{O}(\delta^2)$
$\Sigma \to N$	$-0.99(5)$	0.30(1)	1.57(8)	0.260(16)	0.233(14)
$\Xi \to \Sigma$	1.01(6)	1.22(5)	3.05(14)	0.228(11)	0.223(11)
$\Xi \to \Lambda$	1.21(7)	0.27(1)	$-0.10(3)$	0.254(17)	0.239(16)
$\Lambda \to N$	$-1.21(8)$	$-0.93(4)$	$-1.41(8)$	0.227(11)	0.215(11)
Combined	N/A	N/A	N/A	0.237(7)	0.225(6)

Table 8.4: $|V_{us}|$ results using constrained fit form factors f_1^R, f_2^R and g_1^R, which are also listed. Results are presented using the semi-leptonic decay rate formula with terms up to $\mathcal{O}(\delta)$ and $\mathcal{O}(\delta^2)$. A weighted average of the values of $|V_{us}|$ is also taken for results at both orders.

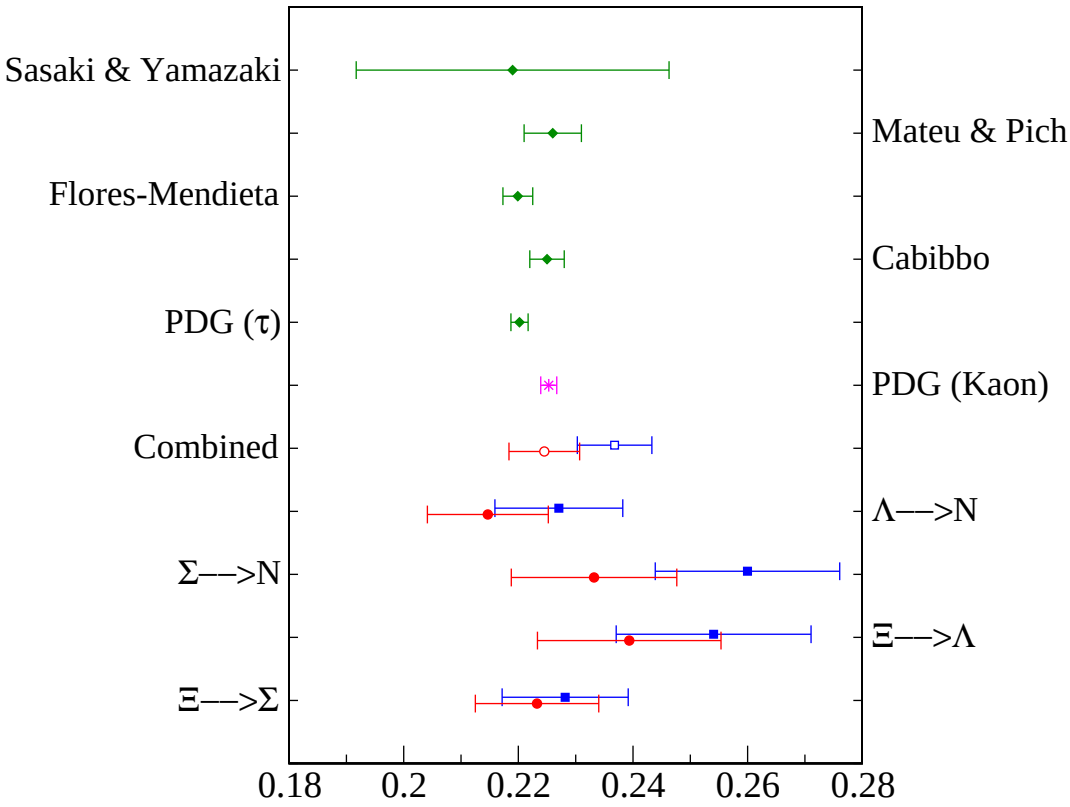

Figure 8.2: $|V_{us}|$ result for each $\Delta S = 1$ decay (filled circles and squares) along with weighted averages (empty circle and square) at both $\mathcal{O}(\delta)$ (blue squares) and $\mathcal{O}(\delta^2)$ (red circles). Also shown are estimates of $|V_{us}|$ from kaon decays, τ decays and other studies of octet hyperon semi-leptonic decays.

Encouragingly, our results and errors, at second order, are quite similar to those of Mateu and Pich, with whom we share values of radiative corrections. In

contrast with our methods however, along with using experimental results their decay rate formula was computed at $\mathcal{O}(\delta^5)$ [186]. Higher order effects should slightly shift our second order result towards their result (i.e. to the right in the plot). The constrained fit form factors were used to calculate this result for $|V_{us}|$ and it is worth noting that the unconstrained form factors would give rise to a result of $|V_{us}| = 0.219(8)$ at second order; an increase in relative error of $\sim 30\%$.

Our results for individual decay channels within the octet differ from the results of Cabibbo et al. in some respects. Differences may arise due to the fact that we do not use the symmetric limit value for f_2, nor do we use Cabibbo model estimates of that form factor. As was discussed at length by Mateu and Pich, there is disagreement between results of Cabibbo et al. and those of Flores-Mendieta despite both studies effectively using the same experimental data set. Indeed Flores-Mendieta argues his results support those found through τ decays whilst Cabibbo et al. found results more consistent with those of kaon decays.

We also point out that by changing the renormalisation constants, our result for $|V_{us}|$ would also change. We renormalised by fixing to the experimental value of g_A in the case of Z_A, and by using the conserved vector current for Z_V. For example, a variation by 5% in the value of Z_A would result in a change of between 0.5% and 4.5% in $|V_{us}|$ depending on the transition concerned, and similarly for Z_V. The underestimation of axial form factors is often seen in lattice calculations when using a non-perturbatively determined Z_A [190], and could significantly impact upon our results.

At the start of this chapter and in Chapter 4 we motivated a calculation of $|V_{us}|$ as a way of testing the unitarity constraints of the CKM matrix. If we use the PDG values for $|V_{ud}|$ and $|V_{ub}|$ we can test to see how our estimates of $|V_{us}|$ impact on unitarity relation of Equation 8.1. Working with the first order result we find

$$\Delta = 1 - |V_{ud}|^2 + |V_{us}|^2 + |V_{ub}|^2 = 0.005(3), \tag{8.12}$$

and at second order

$$\Delta = 1 - |V_{ud}|^2 + |V_{us}|^2 + |V_{ub}|^2 = -0.0004(30). \tag{8.13}$$

Though a 1.5σ deviation from unitarity is seen at first order, it disappears at the next order order. At second order this corresponds to a Cabibbo angle of $\theta_C = 13.0(4)^\circ$. Our approach results in larger relative errors than those of kaon decays, but provides an alternative avenue to test unitarity through the use of hyperon form factors determined non-perturbatively.

"It's the end of the world as we know it, and I feel fine."

— Michael Stipe, *R.E.M.*

Chapter 9

Conclusions

This work has focused on the calculation of octet hyperon semi-leptonic form factors of the vector and axial-vector currents. This was done for phenomenological interest in the form factors in isolation but also to explore the effects of $SU(3)$-flavour symmetry in the $SU(2)$ isospin limit and to estimate the CKM matrix element $|V_{us}|$. Our approach involved calculating hyperon transitions using the techniques and tools of Lattice QCD in order to determine matrix elements, both diagonal and off-diagonal. At all stages we compared our results with the theoretical work of others and measurements obtained through experiment. Our main result for $|V_{us}|$ is shown in Figure 8.2.

Early on we introduced the core concepts of Quantum Chromodynamics so that the technicalities surrounding the discretisation of the theory on the lattice could be understood. Our lattice action was discussed along with an overview of the techniques used in this study. In particular the partial 'twisting' of boundary conditions was presented as a means to eliminating errors due to extrapolation. Implementing twists did indeed reduce errors for the first class form factors of primary interest to us, however twisted points were unreliable for certain kinematical set-ups. Future work could look to expand on the choice of kinematics by implementing twists in more than one direction. One could also consider

having non-zero momenta for both initial and final state hyperons, though this would be computationally costly.

In order to obtain renormalised results for the vector and axial-vector form factors one should calculate the appropriate renormalisation constants, Z_V or Z_A. In general we sought to take ratios of quantities with the same renormalisation constants so that these unknown factors would cancel and this proved to be quite effective. In certain instances however, such as in the estimation of $|V_{us}|$, this was not possible. By fixing to the measured axial coupling constant, g_A, of the nucleon and relying on conservation of the vector current we could set these values. Further work towards a non-perturbative determination of Z_A, in particular, is on-going. After Z_A is found in this manner we would expect this to alter our results for $|V_{us}|$ significantly. The resolution of the problem relating to the underestimation of axial-form factors remains important. A further future objective would be to compute the form factors with different lattice spacings in order to take the continuum limit. Though it is not a consideration for transition matrix elements, a full computation of disconnected diagrams should also be considered for certain diagonal matrix elements.

The Cabibbo model, containing the V-A theory of weak interactions, is remarkably robust and provides an excellent theoretical platform from which to study hyperon form factors. The vector form factor f_1 was found to have no discernible symmetry breaking effects in our work, in good agreement with the Cabibbo model and the Ademollo-Gatto theorem. This form factor is important for an estimation of $|V_{us}|$ and in fact some authors have suggested relying on theoretical estimates of this form factor alone, in conjunction with experimental results for g_1/f_1, to calculate the CKM matrix element. The ratio of correlation functions used by Sasaki to determine f_1, involving only 3pt correlators, could also be considered in future work though this would be more expensive to implement in the case of several transitions. This also requires more precise experimental

work.

The axial form factor g_1 and the weak magnetism form factor f_2 were shown to display noticeable symmetry breaking effects which we quantified by parameterising the effects of $SU(3)$ breaking to first order. The results for g_1 were shown to be in good agreement with experimental results for those form factors in general, albeit those experimental results often suffer from large errors. We also chose lattice quark masses so that we could display the effects of symmetry breaking in what we call 'fan' plots. Making a constrained fit to determine the parameters of symmetry breaking showed the effectiveness of this group theoretic method, especially in the case of the axial charges where it helped to reduce error bars significantly. For the axial-vector case, results had noticeably smaller errors than the available experimental data. Our fits to the weak magnetism form factor f_2 may indicate that second order effects are large in this form factor.

By calculating all possible matrix elements in the $2 + 1$ case within the baryon octet we also calculated other quantities of phenomenological interest such as baryon spin fractions and baryon axial charges. We can also calculate the electromagnetic form factors in the process of calculating V-A current matrix elements. The spin fractions, axial charges and magnetic moments compared well with other theoretical estimates and experimental values with only some small disagreement. Our constrained fit resulted in an increase in precision of these quantities as all were seen to display some first order symmetry breaking effects.

The inclusion of $32^3 \times 64$ diagonal results for octet outer-ring diagonal matrix elements provided extra points with which to perform this constrained fit. Our $24^3 \times 48$ data did not have sufficient resolution to determine second order effects in flavour symmetry, even with this extra data. This indicates that possible future work would be to compute off-diagonal and Λ matrix elements on larger lattice volumes so that second order flavour symmetry breaking effects might be determined.

This would also assist in the calculation of $|V_{us}|$ at second order, though these effects would be suppressed by the factor δ^2 in the decay rate formula so would most likely be quite small. Our value of $|V_{us}|$, though not competitive with that from kaon form factors does agree with both kaon and τ decay PDG global estimates. We argue this shows the importance of calculating $|V_{us}|$ through several different methods, including hyperon decays. Our result is also comparable to that found by Mateu and Pich whose work is one of the most recent comprehensive studies into the topic. In the future, the effect of including a possible contribution from the g_2 form factor, due to symmetry breaking effects, could also be explored.

Our work, presented in this thesis, shows that hyperon form factors can be calculated with good precision using lattice QCD and that our calculated form factors compare favourably with experimental results. Few Lattice QCD calculations of these transition form factors exist and those that do often rely on the quenched approximation and focus on one particular transition alone. We have provided a comprehensive calculation of all transition matrix elements. We have shown that hyperon form factors provide an important way of studying flavour symmetry breaking and how this can be achieved. Our constrained fit approach resulted in more precise determinations of phenomenologically interesting quantities. We furnished evidence that $|V_{us}|$, as determined through hyperon decays, provides an important complimentary approach to kaon and τ decays, in probing the Standard Model by testing unitarity. Our hope is that further publication of our research will help to generate interest in future investigation of hyperon semi-leptonic form factors, through both theoretical and experimental means.

Appendix A

Conventions

A.1 Dirac Matrices

In this section superscripts will refer to the space in which we are considering; these are usually suppressed for brevity. In Euclidean space, E, the metric is denoted $g^E_{\mu\nu}$ and has a signature $(1,1,1,1)$, meaning $g^E_{\mu\nu} = \delta_{\mu\nu}$, in familiar notation. The Dirac (or gamma) matrices are given in the chiral representation so that

$$\gamma^E_i = \begin{pmatrix} 0 & -i\sigma_i \\ i\sigma_i & 0 \end{pmatrix} \quad \text{and} \quad \gamma^E_4 = \begin{pmatrix} 0 & -\mathbb{I}_{2\times 2} \\ -\mathbb{I}_{2\times 2} & 0 \end{pmatrix}, \tag{A.1}$$

where σ_i are the Pauli spin matrices given, through the use of the Kronecker delta, by

$$\sigma_i = \begin{pmatrix} \delta_{i3} & \delta_{i1} - i\delta_{i2} \\ \delta_{i1} + i\delta_{i2} & -\delta_{i3} \end{pmatrix}. \tag{A.2}$$

The Dirac matrices satisfy the Clifford algebra,

$$\{\gamma^E_\mu, \gamma^E_\nu\} = 2\delta_{\mu\nu}\mathbb{I}_{4\times 4}, \tag{A.3}$$

along with

$$\gamma_\mu^E = \gamma_\mu^{E\dagger} = (\gamma_\mu^E)^{-1}. \tag{A.4}$$

One may also define a 'fifth' Dirac matrix, given by $\gamma_5^E = \gamma_1^E\gamma_2^E\gamma_3^E\gamma_4^E$, meaning that explicitly

$$\gamma_5^E = \begin{pmatrix} \mathbb{I}_{2\times 2} & 0 \\ 0 & -\mathbb{I}_{2\times 2} \end{pmatrix}, \tag{A.5}$$

which anti-commutes past the other Dirac matrices and satisfies $\gamma_5^2 = \mathbb{I}_{4\times 4}$ and $\gamma_5^\dagger = \gamma_5$. The charge conjugation matrix, C, will be necessary to create baryon interpolators. It is defined as $C = \gamma_2^E\gamma_4^E$.

The rotation to Minkowski space, $\mathcal{M}$, changes the signature to $(1, -1, -1, -1)$. Any 4-vectors are related between Euclidean and Minkowski spaces via

$$A_i^{\mathcal{M}} = -A_i^E \quad \text{and} \quad A_4^{\mathcal{M}} = -iA_0^E, \tag{A.6}$$

while the Dirac matrices can be similarly related in the following way:

$$\gamma_i^{\mathcal{M}} = -i\gamma_i^E \quad \text{and} \quad \gamma_4^{\mathcal{M}} = \gamma_0^E. \tag{A.7}$$

The $\gamma_5^{\mathcal{M}}$ matrix is defined as

$$\gamma_5^{\mathcal{M}} = i\gamma^{\mathcal{M}0}\gamma^{\mathcal{M}1}\gamma^{\mathcal{M}2}\gamma^{\mathcal{M}3} = i\gamma_0^E(i\gamma_1^E)(i\gamma_2^E)(i\gamma_3^E) = -\gamma_5^E. \tag{A.8}$$

The algebra which the Minkowski versions of the Dirac matrices obey is given by the anti-commutation relations

$$\{\gamma_\mu^{\mathcal{M}}, \gamma_\nu^{\mathcal{M}}\} = 2g_{\mu\nu}^{\mathcal{M}}\mathbb{I}_{4\times 4} \tag{A.9}$$

and

$$\gamma_0^{\mathcal{M}}\gamma_\mu^{\mathcal{M}}\gamma_0^{\mathcal{M}} = \gamma_\mu^{\mathcal{M}\dagger}. \tag{A.10}$$

Covariant and contravariant indices Dirac matrices are related through

$$\gamma^{\mathcal{M}0} = \gamma_0^{\mathcal{M}} \quad \text{and} \quad \gamma^{\mathcal{M}i} = -\gamma_i^{\mathcal{M}} \tag{A.11}$$

in Minkowski space. Finally,

$$\sigma^{\mathcal{M}0j} = \frac{i}{2}\left[\gamma^{\mathcal{M}0}, \gamma^{\mathcal{M}j}\right] = \frac{i}{2}\left[\gamma_4^E, i\gamma_j^E\right] = i\sigma_{4j}^E, \tag{A.12}$$

$$\sigma^{\mathcal{M}ij} = \frac{i}{2}\left[\gamma^{\mathcal{M}i}, \gamma^{\mathcal{M}j}\right] = \frac{i}{2}\left[i\gamma_i^E, i\gamma_j^E\right] = -\sigma_{ij}^E. \tag{A.13}$$

A.2 The Special Unitary Group, $SU(N)$

The special unitary groups are integral to describing the physical interactions of theories of the strong and weak nuclear forces. The special unitary groups are given by the set of $N \times N$ complex matrices with a determinant of unity [191]. For $G \in SU(3)$,

$$GG^\dagger = \mathbb{I}_{N\times N} \quad \text{and} \quad \det(G) = 1. \tag{A.14}$$

This distinguishes them from the group $U(N)$ which has a similar definition but with no constraint on the determinant sign. Thus $SU(N) \subset U(N) \subset GL(N, \mathbb{C})$, where $GL(N, \mathbb{C})$ is the general linear group of invertible $N \times N$ matrices over the complex field.

The Lie algebra of $SU(N)$ is denoted as $su(N)$. For $SU(N)$ there will be a set of $N^2 - 1$ generators for the group. Any element of the group, $G \in SU(3)$ can be expressed in terms of the generators of the group, $T^i \in su(N)$, meaning

$$G = e^{-i\vec{c}.\vec{T}}, \tag{A.15}$$

with $\vec{c} \in \mathbb{R}^N$. The generators of a group are defined through their Lie algebra as

$$[T^i, T^j] = ic_{ijk}T^k, \tag{A.16}$$

where $c_{ijk} = -c_{jik}$ are the structure constants of $SU(N)$. The generators are traceless and Hermitian. Non-Abelian groups, such as $SU(N)$ correspond to those with $c_{ijk} \neq 0$ for at least one structure constant. Any set of matrices which satisfy the Lie algebra count as generators of the group and constitute a representation of the group. The structure constants will remain the same for different representations. The *rank* of a group is given by the number of generators which can be simultaneously diagonalised.

Important physical cases include $N = 2$ (e.g. isospin symmetry or quantum mechanical spin) and $N = 3$ (e.g. gauge group of QCD or $SU(3)$ flavour symmetry). For $SU(2)$ the generators simply satisfy the Lie algebra

$$[T^i, T^j] = i\epsilon_{ijk}T^k, \tag{A.17}$$

for $i, j, k \in \{1, 2, 3\}$, where the ϵ_{ijk} is the usual totally anti-symmetric Levi-Civita symbol. The generators are often written in terms of the Pauli spin matrices seen in Equation A.2, where

$$T^i = \frac{1}{2}\sigma^i. \tag{A.18}$$

For the case of $N = 3$ there will be $3^2 - 1 = 8$ generators and in particle physics

contexts are usually written in terms of the *Gell-Mann matrices*, $\lambda^i = 2T^i$, where

$$\lambda^1 = \begin{pmatrix} 0 & 1 & 0 \\ 1 & 0 & 0 \\ 0 & 0 & 0 \end{pmatrix}, \quad \lambda^2 = \begin{pmatrix} 0 & -i & 0 \\ i & 0 & 0 \\ 0 & 0 & 0 \end{pmatrix}, \quad \lambda^3 = \begin{pmatrix} 1 & 0 & 0 \\ 0 & -1 & 0 \\ 0 & 0 & 0 \end{pmatrix},$$
$$\lambda^4 = \begin{pmatrix} 0 & 0 & 1 \\ 0 & 0 & 0 \\ 1 & 0 & 0 \end{pmatrix}, \quad \lambda^5 = \begin{pmatrix} 0 & 0 & -i \\ 0 & 0 & 0 \\ i & 0 & 0 \end{pmatrix}, \tag{A.19}$$
$$\lambda^6 = \begin{pmatrix} 0 & 0 & 0 \\ 0 & 0 & 1 \\ 0 & 1 & 0 \end{pmatrix}, \quad \lambda^7 = \begin{pmatrix} 0 & 0 & 0 \\ 0 & 0 & -i \\ 0 & i & 0 \end{pmatrix}, \quad \lambda^8 = \frac{1}{\sqrt{3}} \begin{pmatrix} 1 & 0 & 0 \\ 0 & 1 & 0 \\ 0 & 0 & -2 \end{pmatrix},$$

though the group can be defined in terms of its structure constants, independently of its representation. In the case of $SU(3)$ these are

$$[T^i, T^j] = i f_{ijk} T^k, \tag{A.20}$$

where the structure constants can be found through the use of the Gell-Mann matrices. Explicitly they are

$$\begin{gathered} f_{123} = 1, \\ f_{147} = f_{165} = f_{246} = f_{257} = f_{345} = f_{376} = \frac{1}{2}, \\ f_{458} = f_{678} = \frac{\sqrt{3}}{2}, \end{gathered} \tag{A.21}$$

and unless related by anti-symmetric permutation of indices, are zero otherwise. One may also define the d_{ijk} through

$$\{T_i, T_j\} = \frac{1}{3}\delta_{i,j} + 2 d_{ijk} T_k \tag{A.22}$$

where explicitly the values are

$$\begin{aligned} d_{118} = d_{228} = & d_{388} = -d_{888} = \frac{1}{\sqrt{3}}, \\ d_{448} = d_{558} = & d_{668} = d_{778} = -\frac{1}{2\sqrt{3}}, \\ d_{146} = d_{157} = -d_{247} = d_{256} = & d_{344} = d_{355} = -d_{366} = -d_{377} = \frac{1}{2}, \end{aligned} \tag{A.23}$$

and zero otherwise.

Appendix B

Lattice QCD Methodology

An overview of some of the technical details of the lattice calculations which are performed in this study.

B.1 Bootstrap Algorithm

To provide an estimate of statistical errors the use of the *bootstrap* algorithm is used throughout this study. This is a re-sampling technique where out of a set of measurements, say N, a number of bootstrap samples or boots, N_B are generated by randomly selecting N times from the original set of measurements by sampling with replacement. The average of each boot, θ_j, is calculated and the standard deviation formula

$$\delta = \sqrt{\left(\frac{1}{N_B - 1}\right) \sum_{j=1}^{N_B} (\theta_j - \bar{\theta})^2}, \tag{B.1}$$

is used to calculate the error, δ, where the average of the original set of measurements is used as the central value, $\bar{\theta}$. In this work we take $N_B = 200$. When combining quantities, the separate boots for each can be combined in the same way as a means to estimate the error in the new quantity. A similar approach can be adopted, for example, when performing extrapolations.

B.2 Wick Contractions

This section will provide an example of how to arrive at a 3pt correlation function explicitly in terms of quark propagators. A full list of correlation functions will be provided for each transition relevant to this study of hyperon matrix elements. The baryon interpolators are given in Section 3.4 and will be used here. The charge conjugation matrix, C, is given in Section A.1 of this appendix. Note however that this choice of C is not unique and once the properties of the matrix are obeyed (i.e. Equation 3.38) then the following results will hold.

We shall consider a general operator insertion at time τ, with colour indices f and f' as

$$\begin{aligned}\mathcal{O}(\tau,\vec{q}) &= \sum_{\vec{y}} e^{i\vec{q}.\vec{y}}\mathcal{O}(\vec{y},\tau) \\ &= \sum_{\vec{y},v,w} e^{i\vec{q}.\vec{y}}\bar{q}_{\rho}^{f'}(v)O^{f'f}(v,w;\vec{y},\tau)_{\rho\sigma}q_{\sigma}^{f}(w),\end{aligned} \tag{B.2}$$

where we sum over all lattice sites v, w and where ρ and σ are spin indices. The 3pt correlator can be written as

$$C_{\Gamma}^{HH'}(t,\tau;\vec{p},\vec{p}';\mathcal{O}) = \sum_{\gamma\gamma'}\Gamma_{\gamma'\gamma}\langle H_{\gamma}(t;\vec{p}')\mathcal{O}(\tau,\vec{q})\overline{H}_{\gamma'}(0;\vec{p})\rangle. \tag{B.3}$$

As an example we shall choose the transition $\Lambda \to p$ so the 3pt correlation function is

$$C_{\Gamma}^{\Lambda p}(t,\tau;\vec{p},\vec{p}';\mathcal{O}^{\Lambda p}) = \sum_{\gamma\gamma'}\Gamma_{\gamma'\gamma}\langle H_{\gamma}^{p}(t;\vec{p}')\mathcal{O}^{\Lambda p}(\tau,\vec{q})\overline{H}_{\gamma'}^{\Lambda}(0;\vec{p})\rangle \tag{B.4}$$

and the $\Delta S = 1$ operator which changes an s quark to a u quark is given by

$$\mathcal{O}^{\Lambda p}(\tau,\vec{q}) = \sum_{\vec{y},v,w} e^{i\vec{q}.\vec{y}}\bar{u}_{\rho}^{f'}(v)O^{f'f}(v,w;\vec{y},\tau)_{\rho\sigma}s_{\sigma}^{f}(w). \tag{B.5}$$

This specific case can be written in terms of quark fields with explicit colour and Dirac indices. We make the choice that the final state is at rest and that, as

we are averaging over gauge fields, the source is located at $(\vec{0}, 0)$. This gives

$$\begin{aligned} C_{\Gamma}^{\Lambda p}(t,\tau;\vec{p},\vec{p}\,';\mathcal{O}^{\Lambda p}) = \sum_{\vec{y},v,w}\sum_{\vec{x}} e^{-i\vec{p}.\vec{x}}\epsilon^{abc}\epsilon^{a'b'c'}\sum_{\gamma\gamma'}\Gamma_{\gamma'\gamma}\times \\ \left[u_{\alpha}^{a}(\vec{x},t)^{T_D}(C\gamma_5)_{\alpha\beta}d_{\beta}^{b}(\vec{x},t)\right]u_{\gamma}^{c}(\vec{x},t)\times \\ \bar{u}_{\rho}^{f'}(v)O^{f'f}(v,w;\vec{y},\tau)_{\rho\sigma}s_{\sigma}^{f}(w)\times \\ \bar{s}_{\gamma'}^{c'}(\vec{0},0)\left[\bar{d}_{\alpha'}^{a'}(\vec{0},0)^{T_D}(C\gamma_5)_{\alpha'\beta'}\bar{u}_{\beta'}^{b'}(\vec{0},0)\right]. \end{aligned} \tag{B.6}$$

To make this expression easier to deal with we will suppress the transposes and the time dependency which will be reintroduced later. Considering only the quark fields the two possible combinations of Wick contractions are

$$\mathcal{W}_1 = \overbrace{u_{\alpha}^{a}(\vec{x})\underbrace{d_{\beta}^{b}(\vec{x})\overbrace{u_{\gamma}^{c}(\vec{x})\bar{u}_{\rho}^{f'}}(v)\underbrace{s_{\sigma}^{f}(w)\bar{s}_{\gamma'}^{c'}}(\vec{0})\bar{d}_{\alpha'}^{a'}}(\vec{0})\bar{u}_{\beta'}^{b'}(\vec{0})} \tag{B.7}$$

and

$$\mathcal{W}_2 = \overbrace{u_{\alpha}^{a}(\vec{x})\underbrace{d_{\beta}^{b}(\vec{x})\overbrace{u_{\gamma}^{c}(\vec{x})\bar{u}_{\rho}^{f'}}(v)\underbrace{s_{\sigma}^{f}(w)\bar{s}_{\gamma'}^{c'}}(\vec{0})\bar{d}_{\alpha'}^{a'}}(\vec{0})\bar{u}_{\beta'}^{b'}}(\vec{0}). \tag{B.8}$$

Permuting the quark fields will introduce an overall minus sign into these terms.

Reintroducing the charge conjugation matrix and unspecified Dirac structure operator, the first Wick contracted term (B.7), in terms of quark propagators, becomes

$$\begin{aligned} \mathcal{W}_1 =& (-1)G_u^{cb'}(\vec{x};\vec{0})_{\gamma\beta'}(C\gamma_5)_{\alpha'\beta'}G_d^{ba'}(\vec{x};\vec{0})_{\beta\alpha'}(C\gamma_5)_{\alpha\beta}\times \\ & G_u^{af'}(\vec{x};v)_{\alpha\rho}O^{f'f}(v,w;\vec{y})_{\rho\sigma}G_s^{fc'}(w;\vec{0})_{\sigma\gamma'}, \end{aligned} \tag{B.9}$$

with quark propagator subscript indicating the quark flavour. The second term (B.7) is

$$\begin{aligned} \mathcal{W}_2 =& G_u^{cf'}(\vec{x};v)_{\gamma\rho}O^{f'f}(v,w;\vec{y})_{\rho\sigma}G_s^{fc'}(w;\vec{0})_{\sigma\gamma'}\times \\ & G_u^{ab'}(\vec{x};\vec{0})_{\alpha\beta'}(C\gamma_5)_{\alpha'\beta'}G_d^{ba'}(\vec{x};\vec{0})_{\beta\alpha'}(C\gamma_5)_{\alpha\beta}. \end{aligned} \tag{B.10}$$

The Dirac indices may now be dropped with the use of Γ and the sum over Dirac

indices γ and γ' leading to

$$\mathcal{W}_1 = -Tr_D\{\Gamma G_u^{cb'}(\vec{x};\vec{0})\widetilde{G}_d^{ba'}(\vec{x};\vec{0})G_u^{af'}(\vec{x};v)O^{f'f}(v,w;\vec{y})G_s^{fc'}(w;\vec{0})\} \tag{B.11}$$

and

$$\mathcal{W}_2 = Tr_D\{\Gamma G_u^{cf'}(\vec{x};v)O^{f'f}(v,w;\vec{y})G_s^{fc'}(w;\vec{0})\}Tr_D\{G_u^{ab'}(\vec{x};\vec{0})\widetilde{G}_d^{ba'}(\vec{x};\vec{0})\}, \tag{B.12}$$

where we have used the definition $\widetilde{G} = (C\gamma_5 G\gamma_5 C)^T$. In order to match up colour indices we relabel and then permute the $\mathcal{W}_1$ term's colour indices by $\epsilon^{abc}\epsilon^{a'b'c'} \longrightarrow \epsilon^{abc}\epsilon^{b'a'c'} = -\epsilon^{abc}\epsilon^{a'b'c'}$ and the second term's with $\epsilon^{abc}\epsilon^{a'b'c'} \longrightarrow \epsilon^{cba}\epsilon^{b'a'c'} = \epsilon^{abc}\epsilon^{a'b'c'}$. The final expression for this 3pt function in terms of quark propagators is

$$C_\Gamma^{\Lambda p}(t,\tau;\vec{p},\vec{p}';\mathcal{O}^{\Lambda p}) = \sum_{\vec{y},v,w}\left\langle Tr\left\{\Sigma_\Gamma^{\Lambda p}(\vec{0},0;v;\vec{p},t)O^{\Lambda p}(v,w;\vec{y},t)G_s(w;\vec{0},0)\right\}\right\rangle_{\{U\}}, \tag{B.13}$$

where the trace is over colour and Dirac indices and with

$$\Sigma_\Gamma^{\Lambda p}(\vec{0},0;v;\vec{p},t) = \sum_{\vec{x}} S_\Gamma^{\Lambda p}(\vec{x},t;\vec{0},0,\vec{p})G_u(\vec{x},t;v) \tag{B.14}$$

and

$$\begin{aligned} S_\Gamma^{\Lambda p}(\vec{x},t;\vec{0},0,\vec{p}) = &-e^{-i\vec{p}.\vec{x}}\epsilon^{abc}\epsilon^{a'b'c'}\times \\ &Tr\{G_u(\vec{x},t;\vec{0},0)\widetilde{G}_d(\vec{x},t;\vec{0},0)\}\Gamma + \Gamma G_u(\vec{x},t;\vec{0},0)\widetilde{G}_d(\vec{x},t;\vec{0},0). \end{aligned} \tag{B.15}$$

The other four transitions relevant to this project can now be given by specifying the function S for each, though in the case of $\Sigma \to \Lambda$ there is also a need to specify a change due to the presence of a different current operator. In that case

$$G_s(w;\vec{0},0) \longrightarrow G_d(w;\vec{0},0), \tag{B.16}$$

but for the other three transitions the formulation outlined above remains valid.

The five transition 3pt correlation functions between octet states are thus given by:

- $\Lambda \to p$

$$\begin{aligned} S_{\Gamma}^{\Lambda p}(\vec{x},t;\vec{0},0,\vec{p}) &= -e^{-i\vec{p}.\vec{x}}\epsilon^{abc}\epsilon^{a'b'c'}\times \\ & Tr\{G_u(\vec{x},t;\vec{0},0)\widetilde{G}_d(\vec{x},t;\vec{0},0)\}\Gamma + \Gamma G_u(\vec{x},t;\vec{0},0)\widetilde{G}_d(\vec{x},t;\vec{0},0). \end{aligned} \tag{B.17}$$

- $\Sigma^- \to \Lambda$

$$\begin{aligned} S_{\Gamma}^{\Sigma\Lambda}(\vec{x},t;\vec{0},0,\vec{p}) &= -e^{-i\vec{p}.\vec{x}}\epsilon^{abc}\epsilon^{a'b'c'}\times \\ & \widetilde{G}_s(\vec{x},t;\vec{0},0)\widetilde{\Gamma}\widetilde{G}_d(\vec{x},t;\vec{0},0) + \Gamma G_s(\vec{x},t;\vec{0},0)\widetilde{G}_d(\vec{x},t;\vec{0},0). \end{aligned} \tag{B.18}$$

- $\Sigma^- \to n$

$$\begin{aligned} S_{\Gamma}^{\Sigma n}(\vec{x},t;\vec{0},0,\vec{p}) &= -e^{-i\vec{p}.\vec{x}}\epsilon^{abc}\epsilon^{a'b'c'}\times \\ & Tr\{\Gamma G_d(\vec{x},t;\vec{0},0)\}\widetilde{G}_d(\vec{x},t;\vec{0},0) + \widetilde{G}_d(\vec{x},t;\vec{0},0)\widetilde{\Gamma}\widetilde{G}_d(\vec{x},t;\vec{0},0). \end{aligned} \tag{B.19}$$

- $\Xi^- \to \Lambda$

$$\begin{aligned} S_{\Gamma}^{\Xi\Lambda}(\vec{x},t;\vec{0},0,\vec{p}) &= -e^{-i\vec{p}.\vec{x}}\epsilon^{abc}\epsilon^{a'b'c'}\times \\ & Tr\{\Gamma G_s(\vec{x},t;\vec{0},0)\}\widetilde{G}_d(\vec{x},t;\vec{0},0) + \Gamma G_s(\vec{x},t;\vec{0},0)\widetilde{G}_d(\vec{x},t;\vec{0},0). \end{aligned} \tag{B.20}$$

- $\Xi^0 \to \Sigma^+$

$$\begin{aligned} S^{\Xi\Sigma}(\vec{x},t;\vec{0},0,\vec{p}) &= -e^{-i\vec{p}.\vec{x}}\epsilon^{abc}\epsilon^{a'b'c'}\times \\ & \widetilde{G}_u(\vec{x},t;\vec{0},0)\widetilde{\Gamma}\widetilde{G}_s(\vec{x},t;\vec{0},0) - Tr\{G_u(\vec{x},t;\vec{0},0)\widetilde{G}_s(\vec{x},t;\vec{0},0)\}\Gamma - \\ & \widetilde{G}_u(\vec{x},t;\vec{0},0)G_s(\vec{x},t;\vec{0},0)\Gamma - \Gamma G_u(\vec{x},t;\vec{0},0)\widetilde{G}_s(\vec{x},t;\vec{0},0). \end{aligned} \tag{B.21}$$

We have expanded the tilde notation here to mean $\widetilde{G_2\Gamma G_1} = (C\gamma_5 G_1 \Gamma G_2 \gamma_5 C)^T$.

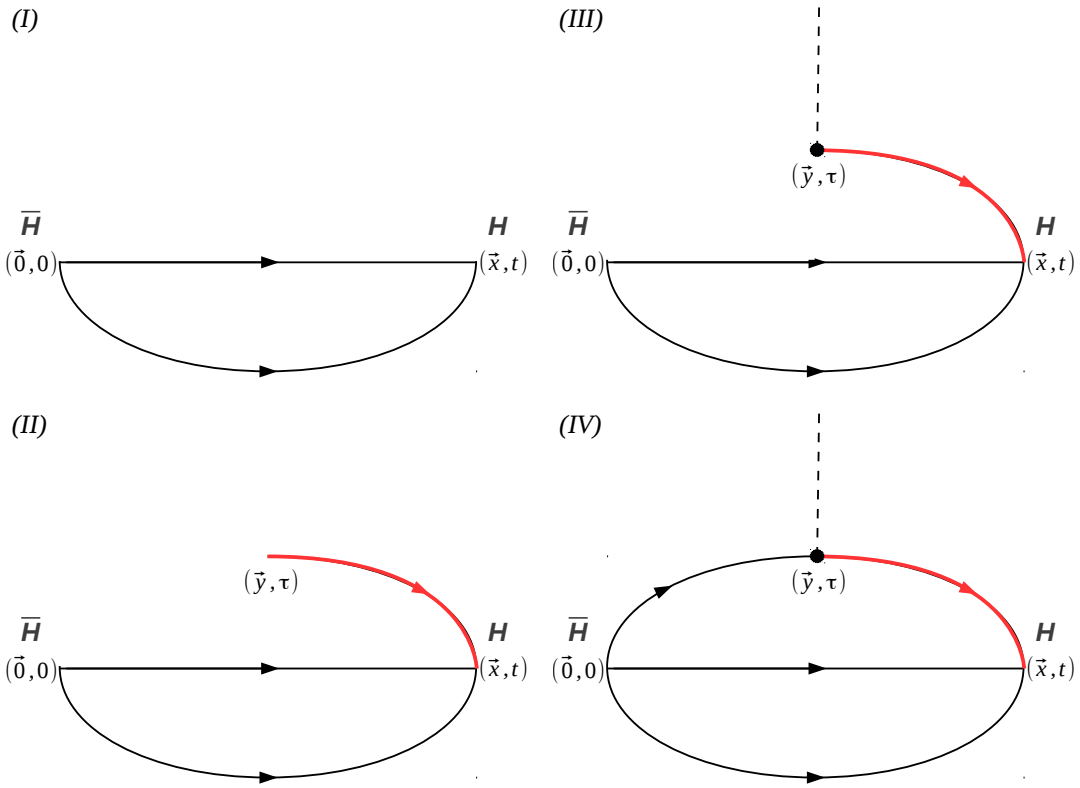

Figure B.1: Depiction of the construction order for a 3pt correlation function using the sequential source method. Ordering follows Roman enumeration.

B.3 Sequential Source Methods

The final part to this appendix will outline the 'fixed sink' sequential source method for calculating the connected piece of a 3pt functions on the lattice. The explanation for this technique will use Figure B.1 as a guide. A quark propagator is computed as per Equation 3.47. This is rewritten as a system of linear equations where one wishes to solve for the propagator of flavour q,

$$\sum_{w} M(x;w)G^{q}(w;y) = \delta_{xy}, \tag{B.22}$$

which is used in the first part of this method (I); two ordinary quark propagators from point $(\vec{0},0)$ to any point $\vec{x}$ at time t are computed.

From Section B.2 we see that one must find $\Sigma_\Gamma^{HH'}(\vec{0},0;v;\vec{p},t)$ through the use of

$$\sum_v \Sigma_\Gamma^{HH'}(\vec{0},0;v;\vec{p},t)M(v;v') = S_\Gamma^{HH'}(\vec{v}',t;\vec{0},0,\vec{p})\delta_{v_4'y}, \tag{B.23}$$

which needs to be put into a similar form to Equation B.22 through $M^{ab}_{\alpha\beta}(x;y) = (\gamma_5 M^*(y;x)^{ba}\gamma^5)_{\beta\alpha}$ and rewritten as

$$\sum_v M(v';v)\gamma_5\Sigma_\Gamma^{HH'\dagger_{CD}}(\vec{0},0;v;\vec{p},t) = \gamma_5 S_\Gamma^{HH'\dagger_{CD}}(\vec{v}',t;\vec{0},0,\vec{p})\delta_{v_4'y}. \tag{B.24}$$

This means that $\Sigma_\Gamma^{HH'}(\vec{0},0;v;\vec{p},t)$ acts a sequential propagator (II) based on a source $S_\Gamma^{HH'}(\vec{v}',t;\vec{0},0,\vec{p})$ which itself is made of the two ordinary quark propagators. This requires a second stage of inversion. The sequential propagator is distinguished by the red propagators in Figure B.1. We must then insert the current operator $\mathcal{O}(\tau,\vec{q})$ as in part (III). Finally another regular quark propagator is added (IV) to complete the 3pt correlation function.

There are several advantages to this approach of computing the correlator including having the ability to choose operator which will be inserted and also the total momentum transferred. This makes it particularly suited to the computation of form factors and structure functions and is thus the ideal choice for this work. The method is costly in certain respects. A separate matrix inversion is required for each choice of hyperon, polarisation and sink momentum. Instead one can compute the correlation function with the 'fixed current' method but this is not used here and we refer the reader to the literature for more information [20].

Appendix C

Matrix Elements in Lattice QCD

C.1 Matrix Element Euclideanisation

In Minkowski space (see Appendix A.1) the matrix element 5.11 can be written in terms of vector and axial-vector contributions;

$$\langle H'(\vec{p}',s')|V^{\mathcal{M}\mu}(x)+A^{\mathcal{M}\mu}(x)|H(\vec{p},s)\rangle = \bar{u}_{H'}(\vec{p}',s')\left(\mathcal{V}^{\mathcal{M}\mu}(q)+\mathcal{A}^{\mathcal{M}\mu}(q)\right)u_H(\vec{p},s)e^{iq.x} \tag{C.1}$$

with

$$\mathcal{V}^{\mathcal{M}\mu}(q^2) = \gamma^{\mathcal{M}\mu}f_1(q^2) - i\sigma^{\mathcal{M}\mu\nu}q_\nu^{\mathcal{M}}\frac{f_2(q^2)}{M_H+M_{H'}} + q^{\mathcal{M}\mu}\frac{f_3(q^2)}{M_H+M_{H'}}, \tag{C.2}$$

$$\mathcal{A}^{\mathcal{M}\mu}(q^2) = \left(\gamma^{\mathcal{M}\mu}g_1(q^2) - i\sigma^{\mathcal{M}\mu\nu}q_\nu^{\mathcal{M}}\frac{g_2(q^2)}{M_H+M_{H'}} + q^{\mathcal{M}\mu}\frac{g_3(q^2)}{M_H+M_{H'}}\right)\gamma_5^{\mathcal{M}}, \tag{C.3}$$

and defining $q^{\mathcal{M}} = p^{\mathcal{M}} - p'^{\mathcal{M}} = (E_H(\vec{p}) - E_{H'}(\vec{p}'), \vec{p}-\vec{p}')$. All possible Lorentz structures are given by this decomposition in terms of the spinors, Dirac matrices and momentum terms. The form factors are functions of the Lorentz invariant, q^2, only. We have defined

$$\sigma^{\mathcal{M}\mu\nu} = \frac{i}{2}\left[\gamma^{\mathcal{M}\mu},\gamma^{\mathcal{M}\nu}\right], \tag{C.4}$$

with the corresponding Minkowski version given in Appendix A.1. We also Euclideanise momenta, so that from

$$q^{\mathcal{M}} = p^{\mathcal{M}} - p'^{\mathcal{M}} = (E_H(\vec{p}) - E_{H'}(\vec{p}'), \vec{p} - \vec{p}'), \tag{C.5}$$

we find

$$q^{E} = p^{E} - p'^{E} = (i(E_H(\vec{p}) - E_{H'}(\vec{p}')), \vec{p} - \vec{p}'), \tag{C.6}$$

and do similar to $\gamma_5^{\mathcal{M}}$ (see Equation A.5);

$$\gamma_5^{\mathcal{M}} = i\gamma_0^{\mathcal{M}}\gamma_1^{\mathcal{M}}\gamma_2^{\mathcal{M}}\gamma_3^{\mathcal{M}} = \gamma_4^E\gamma_1^E\gamma_2^E\gamma_3^E = -\gamma_1^E\gamma_2^E\gamma_3^E\gamma_4^E = -\gamma_5^E. \tag{C.7}$$

The Minkowski vector operator is related to the Euclidean counterparts through the Dirac matrices as

$$\begin{aligned} V^{\mathcal{M}\mu} &= (V^{\mathcal{M}0}, V^{\mathcal{M}i}) \\ &= (\bar{q}'\gamma^{\mathcal{M}0}q, \bar{q}'\gamma^{\mathcal{M}i}q) \\ &= (\bar{q}'\gamma_0^E q, \bar{q}' i\gamma_i^{\mathcal{M}} q) \\ &= (V_0^E, iV_i^E) \end{aligned} \tag{C.8}$$

and similarly for the axial-vector current,

$$A^{\mathcal{M}\mu} = -(A_0^E, iA_i^E). \tag{C.9}$$

For the time component of Equation C.2, and suppressing the momentum

dependence of the form factors, we see

$$\begin{aligned}\mathcal{V}^{\mathcal{M}0} &= \gamma^{\mathcal{M}0} f_1 - i\sigma^{\mathcal{M}0\nu} q_\nu^{\mathcal{M}} \frac{f_2}{M_H + M_{H'}} + q^{\mathcal{M}0} \frac{f_3}{M_H + M_{H'}} \\ &= \gamma_4^E f_1 - i(i\sigma_{4j}^E)(-q_j^E) \frac{f_2}{M_H + M_{H'}} + (-iq_4^E) \frac{f_3}{M_H + M_{H'}} \\ &= \gamma_4^E f_1 - \sigma_{4j}^E q_j^E \frac{f_2}{M_H + M_{H'}} - iq_4^E \frac{f_3}{M_H + M_{H'}} \\ &= \mathcal{V}_4^E,\end{aligned} \tag{C.10}$$

and also

$$\begin{aligned}\mathcal{V}^{\mathcal{M}i} &= \gamma^{\mathcal{M}i} f_1 - i(\sigma^{\mathcal{M}i0} q_0^{\mathcal{M}} + \sigma^{\mathcal{M}ij} q_j^{\mathcal{M}}) \frac{f_2}{M_H + M_{H'}} + q^{\mathcal{M}i} \frac{f_3}{M_H + M_{H'}} \\ &= i\gamma_i^E f_1 - i(i\sigma_{i4}^E(-iq_4^E) + (-\sigma_{ij}^E)(-q_j^E)) \frac{f_2}{M_H + M_{H'}} + q_i^E \frac{f_3}{M_H + M_{H'}} \\ &= i(\gamma_i^E f_1 - \sigma_{ij}^E q_j^E \frac{f_2}{M_H + M_{H'}} - iq_4^E \frac{f_3}{M_H + M_{H'}}) \\ &= i\mathcal{V}_i^E.\end{aligned} \tag{C.11}$$

The vector part Euclidean matrix element can now be written by using the appropriate terms in Equation C.1 and substituting the Minkowski terms for Euclidean ones given the findings of Equations C.8, C.10 and C.10. The the matrix element is

$$\langle H'(\vec{p}', s')|V_\mu^E(x) + A_\mu^E(x)|H(\vec{p}, s)\rangle = \bar{u}_{H'}(\vec{p}', s')(\mathcal{V}_\mu^E(q) + \mathcal{A}_\mu^E(q))u_H(\vec{p}, s)e^{iq.x}, \tag{C.12}$$

where the vector component is

$$\mathcal{V}_\mu^E(q) = \gamma_\mu^E f_1(q^2) - \sigma_{\mu\nu}^E q_\nu^E \frac{f_2(q^2)}{M_H + M_{H'}} - iq_\mu^E \frac{f_3(q^2)}{M_H + M_{H'}}. \tag{C.13}$$

The axial component is no more difficult and the only difference between the given outline of Euclideanisation for the vector and that of the axial parts is that for each term in the decomposition the $\gamma_5^{\mathcal{M}}$ becomes a $-\gamma_5^E$ and thus contributes

an overall minus sign which can be cancelled with the one found in Equation C.9. Thus the axial-vector component of Equation C.12 is

$$\mathcal{A}_\mu^E(q) = \gamma_\mu^E \gamma_5^E g_1(q^2) - \sigma_{\mu\nu}^E \gamma_5^E q_\nu^E \frac{g_2(q^2)}{M_H + M_{H'}} - i q_\mu^E \gamma_5^E \frac{g_3(q^2)}{M_H + M_{H'}}. \tag{C.14}$$

C.2 Correlation Function Ratio

The 2pt and 3pt correlation functions given in Chapter 3 are reproduced here,

$$C_\Gamma^H(t;\vec{p}) = \Gamma_{\beta\alpha}\langle H_\alpha(t;\vec{p})\overline{H}_\beta(0;\vec{p})\rangle, \tag{C.15}$$

$$C_\Gamma^{HH'}(t,\tau;\vec{p},\vec{p}';\mathcal{O}) = \sum_{\alpha\beta}\Gamma_{\beta\alpha}\langle H_\alpha(t;\vec{p}')\mathcal{O}(\tau,\vec{q})\overline{H}_\beta(0;\vec{p})\rangle. \tag{C.16}$$

In the transfer matrix formalism we define a transfer matrix $\hat{S}$ as

$$\hat{S} \equiv e^{-\hat{\mathcal{H}}}, \tag{C.17}$$

which can act on a state $|m\rangle$ as

$$\hat{S}|m\rangle = e^{-E_m}|m\rangle \quad \text{where} \quad E_0 = 0, \tag{C.18}$$

while the normalisation is

$$|0\rangle\langle 0| + \sum_{m\neq 0}\frac{|m\rangle\langle m|}{2E_m} = 1, \tag{C.19}$$

with

$$\langle m|n\rangle = 2E_m\delta_{mn}, \quad \langle 0|0\rangle = 1. \tag{C.20}$$

For an arbitrary operator $\hat{O}(t)$ one can shift this in the temporal direction by

using the translation operator

$$\hat{O}(t) = \hat{S}^{-t}\hat{O}(0)\hat{S}^{t} = e^{-\hat{H}t}\hat{O}(0)e^{\hat{H}t}. \tag{C.21}$$

Using the transfer matrix one can now write the 2pt and 3pt correlation functions (Equations C.15 and C.16) as

$$C_{\Gamma}^{H}(t;\vec{p}) = Tr\Gamma\left[\hat{S}^{T-t}\hat{H}(0;\vec{p})\hat{S}^{t}\hat{\bar{H}}(0;\vec{p})\right], \tag{C.22}$$

$$C_{\Gamma}^{HH'}(t,\tau;\vec{p},\vec{p}';\mathcal{O}) = Tr\Gamma\left[\hat{S}^{T-t}\hat{H}(0;\vec{p})\hat{S}^{t-\tau}\mathcal{O}(0,\vec{q})\hat{S}^{t}\hat{\bar{H}}(0;\vec{p})\right], \tag{C.23}$$

where the temporal extent is restricted by the finite dimensions of the lattice. For use later we will define the following matrix elements in terms of spinors:

$$\begin{aligned}
\langle 0|\hat{H}_{\alpha}(\vec{0})|H,\vec{p},\vec{s}\rangle &= \sqrt{Z_H}u_{H\alpha}(\vec{p},\vec{s}),\\
\langle H,\vec{p},\vec{s}|\hat{\bar{H}}_{\alpha}(\vec{0})|0\rangle &= \sqrt{Z_{\bar{H}}}\bar{u}_{H\alpha}(\vec{p},\vec{s}),\\
\langle \bar{H},\vec{p},\vec{s}|\hat{H}_{\alpha}(\vec{0})|0\rangle &= \sqrt{Z_H}v_{H\alpha}(\vec{p},\vec{s}),\\
\langle 0|\hat{\bar{H}}_{\alpha}(\vec{0})|\bar{H},\vec{p},\vec{s}\rangle &= \sqrt{Z_{\bar{H}}}\bar{v}_{H\alpha}(\vec{p},\vec{s}),\\
\langle 0|\hat{H}_{\alpha}(\vec{0})|\bar{H},\vec{p},\vec{s}\rangle &= \sqrt{Z_H}v_{H\alpha}(\vec{p},\vec{s}),\\
\langle \bar{H},\vec{p},\vec{s}|\hat{\bar{H}}_{\alpha}(\vec{0})|0\rangle &= \sqrt{Z_{\bar{H}}}\bar{v}_{H\alpha}(\vec{p},\vec{s}),\\
\langle H,\vec{p},\vec{s}|\hat{H}_{\alpha}(\vec{0})|0\rangle &= \sqrt{Z_H}u_{H\alpha}(\vec{p},\vec{s}),\\
\langle 0|\hat{\bar{H}}_{\alpha}(\vec{0})|H,\vec{p},\vec{s}\rangle &= \sqrt{Z_{\bar{H}}}\bar{u}_{H\alpha}(\vec{p},\vec{s}),
\end{aligned} \tag{C.24}$$

where the Euclideanised spin is given by

$$s = \left(i\frac{\vec{s}.\vec{p}}{E_H},\vec{s}\right), \tag{C.25}$$

with

$$\vec{s}(\vec{p}) = \vec{e} + \frac{\vec{e}.\vec{p}}{M_H(E_H+M_H)}, \quad \vec{e} = \sigma M_H\vec{n} \quad \text{and} \quad \sigma = \pm 1. \tag{C.26}$$

We now can write

$$\begin{aligned} u_H(\vec{p},\vec{s})\bar{u}_H(\vec{p},\vec{s}) &= (-i\not{p}+M_H)\frac{1}{2}\left(1+i\gamma_5\frac{\not{s}}{M_H}\right) \\ &= (E_H\gamma_4 - i\vec{p}.\vec{\gamma}+M_H)\frac{1}{2}\left(1-\gamma_5\gamma_4\frac{\vec{p}.\vec{s}}{E_H M_H}+i\gamma_5\frac{\vec{\gamma}.\vec{s}}{M_H}\right), \\ v_H(\vec{p},\vec{s})\bar{v}_H(\vec{p},\vec{s}) &= (-i\not{p}-M_H)\frac{1}{2}\left(1+i\gamma_5\frac{\not{s}}{M_H}\right) \\ &= (E_H\gamma_4 - i\vec{p}.\vec{\gamma}-M_H)\frac{1}{2}\left(1-\gamma_5\gamma_4\frac{\vec{p}.\vec{s}}{E_H M_H}+i\gamma_5\frac{\vec{\gamma}.\vec{s}}{M_H}\right). \end{aligned} \tag{C.27}$$

Using the definition of the 2pt correlation function given in Equation C.22 and inserting the identity, twice as indicated, and using completeness, one can write

$$\begin{aligned} C^H_\Gamma(t;\vec{p}) &= \mathrm{Tr}\Gamma I\left[\hat{S}^{T-t}\hat{H}(0;\vec{p})I\hat{S}^t\hat{\bar{H}}(0;\vec{p})\right] \\ &= \Gamma_{\beta\alpha}\Bigg[\langle 0|\hat{H}_\alpha|0\rangle\langle 0|\hat{\bar{H}}_\beta|0\rangle \\ &\quad + \sum_{n\neq 0}\frac{1}{2E_n}\langle 0|\hat{H}_\alpha|n\rangle\langle n|\hat{\bar{H}}_\beta|0\rangle e^{-E_n t} \\ &\quad + \sum_{m\neq 0}\frac{1}{2E_m}\langle m|\hat{H}_\alpha|0\rangle\langle 0|\hat{\bar{H}}_\beta|m\rangle e^{-E_m(T-t)} \\ &\quad + \sum_{m,n\neq 0}\frac{1}{2E_n 2E_m}\langle m|\hat{H}_\alpha|n\rangle\langle n|\hat{\bar{H}}_\beta|m\rangle e^{-E_n t - E_m(T-t)}\Bigg], \end{aligned} \tag{C.28}$$

$$\begin{aligned} C^H_\Gamma(t;\vec{p}) = \sum_{\vec{s}}\Gamma_{\beta\alpha}\Bigg[&\frac{1}{2E_H}\langle 0|\hat{H}_\alpha|H,\vec{p},\vec{s}\rangle\langle H,\vec{p},\vec{s}|\hat{\bar{H}}_\beta|0\rangle e^{-E_H t} \\ &+ \frac{1}{2E_H}\langle \bar{H},\vec{p},\vec{s}|\hat{H}_\alpha|0\rangle\langle 0|\hat{\bar{H}}_\beta|\hat{H},\vec{p},\vec{s}\rangle e^{-E_H(T-t)} + ...\Bigg], \end{aligned} \tag{C.29}$$

where a complete set of states has been inserted. We have also used $\langle 0|\hat{H}_\alpha|0\rangle = 0$ and only kept the lowest lying state of interest and neglect excited states. Using

Equations C.24 we write

$$C_\Gamma^H(t;\vec{p}) = \frac{\sqrt{Z_H Z_{\bar{H}}}}{2E_H} \sum_{\vec{s}} \left\{ \bar{u}_H(\vec{p},\vec{s})\Gamma u_H(\vec{p},\vec{s}) e^{E_H t} + \bar{v}_H(\vec{p},\vec{s})\Gamma v_H(\vec{p},\vec{s}) e^{E_H(T-t)} \right\}. \tag{C.30}$$

Now we use the following

$$\Gamma \equiv \Gamma^{\text{unpol}} = \frac{1}{2}(1+\gamma_4), \quad \text{or} \quad \Gamma \equiv \Gamma^{\text{pol}} = \frac{1}{2}(1+\gamma_4) i\gamma_5 \vec{\gamma}\vec{s}, \tag{C.31}$$

to write

$$\begin{aligned} \sum_{\vec{s}} \bar{u}_H(\vec{p},\vec{s})\Gamma^{\text{unpol}} u_H(\vec{p},\vec{s}) &= 2(E_H + M_H), \\ \sum_{\vec{s}} \bar{v}_H(\vec{p},\vec{s})\Gamma^{\text{unpol}} v_H(\vec{p},\vec{s}) &= 2(E_H - M_H). \end{aligned} \tag{C.32}$$

which can then be used as

$$C_\Gamma^H(t;\vec{p}) = \sqrt{Z_H Z_{\bar{H}}} \left[\left(\frac{E_H + M_H}{E_H} \right) e^{-E_H t} + \left(\frac{E_H - M_H}{E_H} \right) e^{-E_H(T-t)} \right]. \tag{C.33}$$

In the relevant regime $0 \leq t \leq \frac{T}{2}$ this is

$$C_\Gamma^H(t;\vec{p}) = \sqrt{Z_H Z_{\bar{H}}} \left(\frac{E_H + M_H}{E_H} \right) e^{-E_H t}. \tag{C.34}$$

For the 3pt correlator, in the case where $t > \tau$, we can similarly write

$$\begin{aligned}
C_\Gamma^{HH'}(t,\tau;\vec{p},\vec{p}\,') &= \mathrm{Tr}\Gamma I\left[\hat{S}^{T-t}\hat{H}'(0;\vec{p})I\hat{S}^{t-\tau}\hat{O}(0)\hat{S}^{\tau}I\hat{\bar{H}}(0;\vec{p})\right] \\
&= \Gamma_{\beta\alpha}\Bigg[\langle 0|\hat{H}_\alpha|0\rangle\langle 0|\hat{O}|0\rangle\langle 0|\hat{\bar{H}}_\beta|0\rangle \\
&\quad + \sum_{m\neq 0}\frac{1}{2E_m}\langle m|\hat{H}_\alpha|0\rangle\langle 0|\hat{O}|0\rangle\langle n|\hat{\bar{H}}_\beta|m\rangle e^{-E_m(t-T)} \\
&\quad + \sum_{n\neq 0}\frac{1}{2E_n}\langle 0|\hat{H}_\alpha|n\rangle\langle n|\hat{O}|0\rangle\langle 0|\hat{\bar{H}}_\beta|0\rangle e^{-E_n(t-\tau)} \\
&\quad + \sum_{k\neq 0}\frac{1}{2E_k}\langle 0|\hat{H}_\alpha|0\rangle\langle 0|\hat{O}|k\rangle\langle k|\hat{\bar{H}}_\beta|0\rangle e^{-E_k\tau} \\
&\quad + \sum_{m,n\neq 0}\frac{1}{2E_m 2E_n}\langle m|\hat{H}_\alpha|n\rangle\langle n|\hat{O}|0\rangle\langle 0|\hat{\bar{H}}_\beta|m\rangle e^{-E_m(T-t)-E_n(t-\tau)} \\
&\quad + \sum_{m,k\neq 0}\frac{1}{2E_m 2E_k}\langle m|\hat{H}_\alpha|0\rangle\langle 0|\hat{O}|k\rangle\langle k|\hat{\bar{H}}_\beta|m\rangle e^{-E_m(T-t)-E_k\tau} \\
&\quad + \sum_{n,k\neq 0}\frac{1}{2E_n 2E_k}\langle 0|\hat{H}_\alpha|n\rangle\langle n|\hat{O}|k\rangle\langle k|\hat{\bar{H}}_\beta|0\rangle e^{-E_n(T-\tau)-E_k\tau} \\
&\quad + \sum_{m,n,k\neq 0}\frac{1}{2E_k 2E_n 2E_k}\langle m|\hat{H}_\alpha|n\rangle\langle n|\hat{O}|k\rangle\langle k|\hat{\bar{H}}_\beta|m\rangle e^{-E_m(T-t)-E_n(t-\tau)-E_k\tau}\Bigg],
\end{aligned} \tag{C.35}$$

giving

$$\begin{aligned}
C_\Gamma^{HH'}(t,\tau;\vec{p},\vec{p}\,') &= \sum_{\vec{s},\vec{s}'}\Gamma_{\beta\alpha}\times \\
&\Bigg[\frac{1}{2E_H 2E_{H'}}\langle 0|\hat{H}'_\alpha|H',\vec{p}\,',\vec{s}'\rangle\langle H',\vec{p}\,',\vec{s}'|\hat{O}(\vec{q})|H,\vec{p},\vec{s}\rangle\langle H,\vec{p},\vec{s}|\hat{\bar{H}}_\alpha|0\rangle\times \\
&\qquad\qquad e^{-E_{H'}(t-\tau)-E_H\tau}+\ldots\Bigg],
\end{aligned} \tag{C.36}$$

where we assume that t and $t-\tau$ are large enough so that excited state

contributions are negligible.

$$C_{\Gamma}^{HH'}(t,\tau;\vec{p},\vec{p}\,') = \\ \frac{\sqrt{Z_{H'}Z_{\bar{H}}}}{2E_{H'}2E_{H}}\sum_{\vec{s},\vec{s}'}\bar{u}_{H}(\vec{p},\vec{s})\Gamma u_{H'}(\vec{p}\,',\vec{s}\,')\langle H',\vec{p}\,',\vec{s}\,'|\hat{O}(\vec{q})|H,\vec{p},\vec{s}\rangle e^{-E_{H'}(t-\tau)-E_{H}\tau}. \tag{C.37}$$

By defining

$$\langle H',\vec{p}\,',\vec{s}\,'|\hat{O}(\vec{q})|H,\vec{p},\vec{s}\rangle = \bar{u}_{H'}(\vec{p}\,',\vec{s}\,')\mathcal{O}(\vec{q})u_{H}(\vec{p},\vec{s}), \tag{C.38}$$

one can then write the 3pt correlation function as

$$C_{\Gamma}^{HH'}(t,\tau;\vec{p},\vec{p}\,') = \sqrt{Z_{H'}Z_{H}}F(\Gamma,\mathcal{O})e^{-E_{H'}(t-\tau)-E_{H}\tau}, \tag{C.39}$$

where

$$\begin{aligned} F(\Gamma,\mathcal{O}) &= \frac{1}{2E_{H}2E_{H'}}\sum_{\vec{s},\vec{s}'}\mathrm{Tr}\Gamma u_{H'}(\vec{p},\vec{s})\bar{u}_{H'}(\vec{p},\vec{s})\mathcal{O}u_{H}(\vec{p},\vec{s})\bar{u}_{H}(\vec{p},\vec{s}) \\ &= \frac{1}{2E_{H}2E_{H'}}\mathrm{Tr}\Gamma\left(E_{H'}\gamma_{4}-i\vec{p}\,'.\vec{\gamma}+M_{H'}\right)\mathcal{O}\left(E_{H}\gamma_{4}-i\vec{p}.\vec{\gamma}+M_{H}\right). \end{aligned} \tag{C.40}$$

We now wish to construct an appropriate ratio of correlation functions which will cancel the unknown wave-functions. The ratio we use is that found in Equation 5.37. Considering two parts of this ratio separately,

$$\frac{C_{\Gamma}^{HH'}(t,\tau;\vec{p},\vec{p}\,')}{C_{\Gamma^{unpol}}^{H'}(t;\vec{p}\,')} = \frac{Z_{\bar{H}}}{Z_{\bar{H}'}}\frac{E_{H'}}{E_{H'}+M_{H'}}F(\Gamma,\mathcal{O})e^{(E_{H'}-E_{H})\tau} \tag{C.41}$$

and

$$\frac{C_{\Gamma^{unpol}}^{H'}(\tau;\vec{p}\,')C_{\Gamma^{unpol}}^{H'}(t;\vec{p}\,')C_{\Gamma^{unpol}}^{H}(t-\tau;\vec{p})}{C_{\Gamma^{unpol}}^{H}(\tau;\vec{p})C_{\Gamma^{unpol}}^{H}(t;\vec{p})C_{\Gamma^{unpol}}^{H'}(t-\tau;\vec{p}\,')} = \frac{Z_{H'}Z_{\bar{H}'}}{Z_{H}Z_{\bar{H}}}\frac{E_{H}}{E_{H'}}\frac{E_{H'}+M_{H'}}{E_{H}+M_{H}}e^{-2(E_{H'}-E_{H})\tau}, \tag{C.42}$$

which are combined to make

$$\begin{aligned}\mathcal{R}_\Gamma(t,\tau;\vec{p},\vec{p}';\mathcal{O}) &= \frac{C_\Gamma^{HH'}(t,\tau;\vec{p},\vec{p}')}{C_{\Gamma^{unpol}}^{H'}(t;\vec{p}')}\sqrt{\frac{C_{\Gamma^{unpol}}^{H'}(\tau;\vec{p}')C_{\Gamma^{unpol}}^{H'}(t;\vec{p}')C_{\Gamma^{unpol}}^{H}(t-\tau;\vec{p})}{C_{\Gamma^{unpol}}^{H}(\tau;\vec{p})C_{\Gamma^{unpol}}^{H}(t;\vec{p})C_{\Gamma^{unpol}}^{H'}(t-\tau;\vec{p}')}} \\ &= \left(\frac{Z_{H'}Z_{\bar{H}}}{Z_H Z_{\bar{H}'}}\right)^{\frac{1}{4}}\sqrt{\frac{E_H E_{H'}}{(E_H+M_H)(E_{H'}+M_{H'})}}F(\Gamma,\mathcal{O}).\end{aligned} \tag{C.43}$$

If we take $Z_{\bar{H}} = Z_H$ and $Z_{\bar{H}'} = Z'_H$ then these cancel in the ratio, assuming $0 \ll \tau \ll t \ll T/2$, and taking the particular kinematical case of $\vec{p}' = 0$ then the ratio can be given as

$$\mathcal{R}_\Gamma(t,\tau;\vec{p},\vec{p}';\mathcal{O}) = \sqrt{\frac{E_H}{2(E_H+M_H)}}F(\Gamma,\mathcal{O}), \tag{C.44}$$

where

$$F(\Gamma,\mathcal{O}) = \frac{1}{4}\mathrm{Tr}\Gamma(1+\gamma_4)\mathcal{O}\left(\gamma_4 - i\frac{\vec{p}.\vec{\gamma}}{E_H} + \frac{M_H}{E_H}\right), \tag{C.45}$$

with

$$q = (q_4,\vec{q}) = (i(E_H - M_H),\vec{p}). \tag{C.46}$$

A list of kinematical factors can be obtained through explicit choices of Γ and $\mathcal{O}$ for Equation C.45.

$$\begin{aligned}F(\Gamma^{unpol},I) &= \frac{E_H+M_H}{E_H} \\ F(\Gamma^{unpol},\gamma_4) &= \frac{E_H+M_H}{E_H} \\ F(\Gamma^{unpol},\vec{\gamma}) &= -i\frac{\vec{p}.\vec{n}}{E_H} \\ F(\Gamma^{unpol},\gamma_5) &= 0 \\ F(\Gamma^{unpol},\gamma_4\gamma_5) &= 0 \\ F(\Gamma^{unpol},\vec{\gamma}\gamma_5) &= 0 \\ F(\Gamma^{unpol},\sigma_{4i}) &= \frac{p_i}{E_H} \\ F(\Gamma^{unpol},\sigma_{ij}) &= 0,\end{aligned} \tag{C.47}$$

with $\Gamma^{unpol} = \frac{1}{2}(1+\gamma_4)$ and

$$\begin{aligned}
F(\Gamma^{pol}, I) &= 0 \\
F(\Gamma^{pol}, \gamma_4) &= 0 \\
F(\Gamma^{pol}, \vec{\gamma}) &= \frac{\vec{p}\times\vec{n}}{E_H} \\
F(\Gamma^{pol}, \gamma_5) &= -\frac{\vec{p}.\vec{n}}{E_H} \\
F(\Gamma^{pol}, \gamma_4\gamma_5) &= -\frac{\vec{p}.\vec{n}}{E_H} \\
F(\Gamma^{pol}, \vec{\gamma}\gamma_5) &= i\frac{E_H+M_H}{E_H}\vec{n} \\
F(\Gamma^{pol}, \sigma_{4i}) &= \frac{\epsilon_{ijk}p_j n_k}{E_H} \\
F(\Gamma^{pol}, \sigma_{ij}) &= -\frac{E_H+M_H}{E_H}\epsilon_{ijk}n_k,
\end{aligned} \tag{C.48}$$

with $\Gamma^{pol} = \frac{1}{2}(1+\gamma_4)i\gamma_5\vec{\gamma}.\vec{n}$.

Appendix D

Hyperon Decay Rate

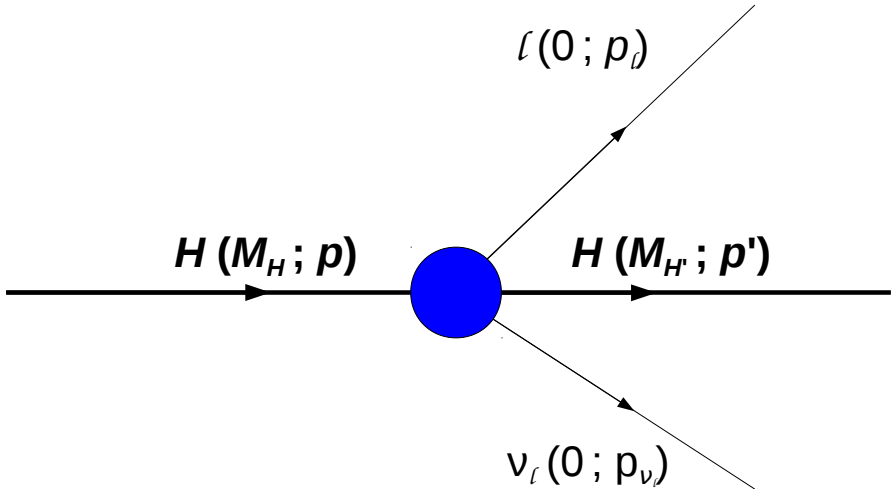

Figure D.1: Depiction of three body decay with incoming parent hyperon, H, daughter hyperon, H', and lepton, l, and neutrino, $\bar{\nu}_l$, decay particles. Here the lepton and neutrino are both taken in the massless limit.

The differential decay rate for a three-body decay, such as that shown in Figure D.1, is given by

$$d\Gamma = \frac{1}{2M_H}|\mathcal{M}_{H\longrightarrow H'l\bar{\nu}}|^2 d\Phi_3, \tag{D.1}$$

where the three-body phase space $d\Phi_3$ is

$$d\Phi_3 = (2\pi)^4\delta^{(4)}(p - p' - p_e - p_{\bar{\nu}_l})\frac{d^3p'}{(2\pi)^3 2E_{H'}}\frac{d^3p_l}{(2\pi)^3 2E_l}\frac{d^3p_{\bar{\nu}_l}}{(2\pi)^3 2E_{\bar{\nu}_l}}, \tag{D.2}$$

with the energies of the daughter hyperon given by $E_{H'}$, the lepton by E_l and the neutrino by $E_{\bar{\nu}_l}$. As before $q^2 = (p - p')^2$. The rest frame of the parent hyperon is considered here. Carrying out integration over p' gives

$$d\Phi_3 = \frac{1}{2^3(2\pi)^5}\delta(M - E_{H'} - E_l - E_{\bar{\nu}_l})\frac{d^3p_l d^3p_{\bar{\nu}_l}}{E_{H'}E_l E_{\bar{\nu}_l}}, \tag{D.3}$$

and defining Ω_l as the solid angle in the direction of $\vec{p_l}$ and $\Omega_{\bar{\nu}_l}$ as a solid angle for $\vec{p}_{\bar{\nu}_l}$ with respect to $\vec{p_l}$ the phase space becomes

$$d\Phi_3 = \frac{1}{2^3(2\pi)^5}\delta(M - E_{H'} - E_l - E_{\bar{\nu}_l})\frac{p_l^2 dp_l d\Omega_l p_{\bar{\nu}_l}^2 dp_{\bar{\nu}_l} d\Omega_{\bar{\nu}_l}}{E_{H'}E_l E_{\bar{\nu}_l}}. \tag{D.4}$$

Integrate now over the solid angles to find

$$d\Phi_3 = \frac{1}{4(2\pi)^3}\delta(M - E_{H'} - E_l - E_{\bar{\nu}_l})\frac{p_l^2 dp_l p_{\bar{\nu}_l}^2 dp_{\bar{\nu}_l} d(cos\theta_{l\bar{\nu}_l})}{E_{H'}E_l E_{\bar{\nu}_l}}, \tag{D.5}$$

where $\theta_{l\bar{\nu}_l}$ is the angle between the lepton and neutrino. Noting $E_i^2 = p_i^2 + m_i^2 \implies dE_i E_i = dp_i p_i$ Equation D.5 becomes

$$d\Phi_3 = \frac{1}{4(2\pi)^3}\delta(M - E_{H'} - E_l - E_{\bar{\nu}_l})\frac{p_l dE_l p_{\bar{\nu}_l} dE_{\bar{\nu}_l} d(cos\theta_{l\bar{\nu}_l})}{E_{H'}}, \tag{D.6}$$

which upon using $E_{H'} = p_l^2 + p_{\bar{\nu}_l}^2 + 2|\vec{p_l}||\vec{p_{\bar{\nu}_l}}|cos\theta_{l\bar{\nu}_l} + m_{H'}^2$, becomes

$$d\Phi_3 = \frac{1}{4(2\pi)^3}\delta(M - E_{H'} - E_l - E_{\bar{\nu}_l})dE_{H'}dE_l dE_{\bar{\nu}_l}. \tag{D.7}$$

Upon integration of the δ function this becomes

$$d\Phi_3 = \frac{1}{4(2\pi)^3} dE_{H'} dE_l. \tag{D.8}$$

Now define the invariant mass, m_{ij}, of particles i and j as

$$\begin{aligned} m_{ij}^2 = p_{ij}^2 &= (p_i + p_j)^2 \\ &= M_H^2 + m_k^2 - 2M_H E_k, \end{aligned} \tag{D.9}$$

such that

$$m_{H'e}^2 + m_{H'\bar{\nu}_l}^2 + m_{l\bar{\nu}_l}^2 = M_H^2 + M_{H'}^2 + M_l^2 + M_{\bar{\nu}_l}^2 = M_H^2 + M_{H'}^2, \tag{D.10}$$

as $M_{\bar{\nu}_l} = M_l = 0$ in this case. Another result of the massless case here is that $m_{l\bar{\nu}_l}^2 = (p_l + p_{\bar{\nu}_l})^2 = q^2$. Note from Equation D.9 that $dm_{l\bar{\nu}_l}^2 = -2M_H dE_{H'}$ and $dm_{H'\bar{\nu}_l}^2 = -2M_H dE_l$ and thus the three body phase space D.8 can be written as

$$d\Phi_3 = \frac{dm_{l\bar{\nu}_l}^2 dm_{H'\bar{\nu}_l}^2}{16(2\pi)^3 M_H^2}. \tag{D.11}$$

For a particular $m_{l\bar{\nu}_l}^2$ the term $m_{H'\bar{\nu}_l}^2$ has a maximum and minimum depending on if $p_{\bar{\nu}_l}$ is parallel or anti-parallel to $p_{H'}$ [192]. The energies of the daughter hyperon and the neutrino in the rest frame of $m_{l\bar{\nu}_l}^2$ can be written as

$$E_{H'} = \frac{M_H^2 - q^2 - M_{H'}^2}{2q} \qquad \text{and} \qquad E_{\bar{\nu}_l} = \frac{q}{2}. \tag{D.12}$$

The kinematical maximum (+) and minimum (−) of $m_{H'\bar{\nu}_l}^2$ is given by

$$m_{H'\bar{\nu}_l}^2 = \left(\frac{q}{2} + \frac{M_H^2 - q^2 - M_{H'}^2}{2q}\right)^2 - \left(\frac{q}{2} \pm \sqrt{\left(\frac{M_H^2 - q^2 - M_{H'}^2}{2q}\right)^2 - M_{H'}}\right)^2. \tag{D.13}$$

Now one can integrate over the invariant mass squared $m^2_{H'\bar{\nu}_l}$, and also make the replacement $dm^2_{l\bar{\nu}_l} = dq^2$ to find that the phase space becomes

$$\begin{aligned} d\Phi_3 &= \frac{1}{16(2\pi)^3 M_H^2} dq^2 2q \sqrt{\left(\frac{M_H^2 - q^2 - M_{H'}^2}{2q}\right)^2 - M_{H'}^2} \\ &= \frac{1}{16(2\pi)^3 M_H^2} dq^2 \sqrt{\left(M_H^2 - q^2 - M_{H'}^2\right)^2 - 4M_{H'}^2 q^2} \end{aligned} \tag{D.14}$$

which can be algebraically manipulated to a more convenient form with

$$d\Phi_3 = \frac{1}{16(2\pi)^3 M_H^2} dq^2 (M^2 - q^2)^{\frac{1}{2}} (\Delta^2 - q^2)^{\frac{1}{2}}, \tag{D.15}$$

where the terms M and Δ have been introduced; $M = M_H + M_{H'}$ and $\Delta = M_H - M_{H'}$. The differential decay rate D.1 can now be written in terms of the matrix element, both hyperon masses and the transferred momenta as

$$d\Gamma = \frac{1}{(2\pi)^3} |\mathcal{M}|^2 (M^2 - q^2)^{\frac{1}{2}} (\Delta^2 - q^2)^{\frac{1}{2}} \frac{dq^2}{32 M_H^3}, \tag{D.16}$$

where the square of the spin-averaged matrix element, $|\mathcal{M}|$, has been abbreviated by dropping the decay label, and is calculated with Equation 5.9. The lepton part is calculated from

$$L^{\alpha\beta} = \left[\bar{u}_l \gamma^\alpha (1 - \gamma_5) v_{\bar{\nu}_l}\right] \left[\bar{v}_{\bar{\nu}_l} \gamma^\beta (1 - \gamma_5) u_l\right], \tag{D.17}$$

and the hadron part from

$$H_{\alpha\beta} = \left[\bar{u}_{H'} (\mathcal{V}_\alpha + \mathcal{A}_\alpha) u_H\right] \left[\bar{u}_H (\mathcal{V}_\beta + \mathcal{A}_\beta)^\dagger u_{H'}\right], \tag{D.18}$$

along with the use of the 'Casimir trick' [193], where for arbitrary Dirac structures

Γ_1 and Γ_2;

$$\sum_{\text{spins}} [\bar{u}_a \Gamma_1 u_b] [\bar{u}_b \Gamma_2 u_a] = Tr \left[\Gamma_1 (\not{p}_b + m_b) \bar{\Gamma}_2 (\not{p}_a + m_a) \right]. \tag{D.19}$$

The spin averaged matrix element squared (again with a massless lepton), calculated from the lepton and hadron tensors, can then be written as

$$\begin{aligned} |\mathcal{M}|^2 = \frac{4}{3} G_F^2 |V_{us}|^2 \Bigg\{ & (\Delta^2 - q^2) \left[M^2 \left| f_1(q^2) + \frac{q^2}{M^2} f_2(q^2) \right|^2 + 2q^2 \left| f_1(q^2) + f_2(q^2) \right|^2 \right] \\ & + (M^2 - q^2) \left[\left| \Delta g_1(q^2) - \frac{q^2}{M} g_2(q^2) \right|^2 + 2q^2 \left| g_1(q^2) - \frac{\Delta}{M} g_2(q^2) \right|^2 \right] \Bigg\}, \end{aligned} \tag{D.20}$$

which is combined with the phase space (Equation D.16) and integrated over the phase space momentum range $0 \leq q^2 \leq (M_H - M_{H'})^2$ to lead to

$$\begin{aligned} \Gamma = & \frac{G_F^2 |V_{us}|^2}{24(2\pi)^3} \Bigg\{ \int_0^{\Delta^2} (\Delta^2 - q^2)^{\frac{3}{2}} (M^2 - q^2)^{\frac{1}{2}} \times \\ & \left[M^2 \left| f_1(q^2) + \frac{q^2}{M^2} f_2(q^2) \right|^2 + 2q^2 \left| f_1(q^2) + f_2(q^2) \right|^2 \right] \frac{dq^2}{M_H^3} \\ & + \int_0^{\Delta^2} (\Delta^2 - q^2)^{\frac{1}{2}} (M^2 - q^2)^{\frac{3}{2}} \times \\ & \left[\left| \Delta g_1(q^2) - \frac{q^2}{M} g_2(q^2) \right|^2 + 2q^2 \left| g_1(q^2) - \frac{\Delta}{M} g_2(q^2) \right|^2 \right] \frac{dq^2}{M_H^3} \Bigg\}. \end{aligned} \tag{D.21}$$

We define $\delta = \Delta / M$ and we make the substitution $q^2 = \Delta^2 x$ leading to $dq^2 = \Delta^2 dx$. The phase space covers a small momentum range and so the momentum dependence can be accounted for by modifying the f_1 and g_1 form factors with a dipole type expansion [106]:

$$f_1(q^2) \approx f_1(0) \left(1 + \frac{q^2}{M^2} \lambda_f \right) \quad \text{and} \quad g_1(q^2) \approx g_1(0) \left(1 + \frac{q^2}{M^2} \lambda_g \right). \tag{D.22}$$

This integral is easier to deal with by looking first at parts related to the vector

form factors, which we will term Γ_V. Suppressing momentum dependence,

$$\begin{aligned}\Gamma_V &= \int_0^1 \Delta^3(1-x)^{\frac{3}{2}} M \left(1-\frac{\Delta^2}{M^2}x\right)^{\frac{1}{2}} M^2 \Bigg[\left(f_1 + \frac{\Delta^2}{M^2}x(f_2+\lambda_f f_1)\right)^2 \\ &\qquad + 2\frac{\Delta^2}{M^2}x\left(f_1+f_2+\frac{\Delta^2}{M^2}\lambda_f f_1\right)^2 \Bigg] \frac{\Delta^2}{M_H^3}dx \\ &= \Delta^5 \frac{M^3}{M_H^3}\int_0^1 dx(1-x)^{\frac{3}{2}}\left(1-\frac{1}{2}\delta^2 x\right)\Bigg[f_1^2 + 2\delta^2 x f_1(f_2+\lambda_f f_1) \\ &\qquad + 2\delta^2 x\left(f_1^2+f_2^2+2f_1f_2\right)\Bigg],\end{aligned} \tag{D.23}$$

where we have expanded $(1-\delta^2)^{\frac{1}{2}} \approx 1 - \frac{1}{2}\delta^2 - \frac{1}{8}\delta^4$ and then neglected terms of higher than $\mathcal{O}(\delta^2)$ so now

$$\Gamma_V = \Delta^5 \frac{M^3}{M_H^3}\int_0^1 dx(1-x)^{\frac{3}{2}}\left[f_1^2 + \delta^2 x\left(\frac{3}{2}f_1^2 + 6f_1f_2 + 2f_2^2 + 2f_1^2\lambda_f\right)\right]. \tag{D.24}$$

Furthermore,

$$\begin{aligned}\frac{M^3}{M_H^3} &= \left(\frac{M}{\frac{1}{2}(M+\Delta)}\right)^3 = 8\left(\frac{\frac{1}{2}M+\frac{1}{2}\Delta}{\frac{1}{2}M}\right)^{-3} = 8(1+\delta)^{-3} \\ &\approx 8(1-3\delta+6\delta^2)\end{aligned} \tag{D.25}$$

to second order in δ. The necessary integrals are

$$\int_0^1 (1-x)^{\frac{3}{2}} = \left[-\frac{2}{5}(1-x)^{\frac{5}{2}}\right]_0^1 = \frac{2}{5} \tag{D.26}$$

and

$$\int_0^1 (1-x)^{\frac{3}{2}}x = \int_0^1 (1-x)^{\frac{3}{2}}(1-(1-x)) = \left[-\frac{2}{5}(1-x)^{\frac{5}{2}} + \frac{2}{7}(1-x)^{\frac{7}{2}}\right]_0^1 = \frac{4}{35}. \tag{D.27}$$

So for the vector part we find

$$\begin{aligned}\Gamma_V &= \Delta^5 8(1-3\delta+6\delta^2)\left[\frac{2}{5}f_1^2+\frac{4}{35}\delta^2\left(\frac{3}{2}f_1^2+6f_1f_2+2f_2^2+2f_1\lambda_f\right)\right] \\ &= \frac{16}{5}\Delta^5\left[(1-3\delta)f_1^2+\delta^2\left(\frac{45}{7}f_1^2+\frac{12}{7}f_1f_2+\frac{4}{7}f_2^2+\frac{4}{7}f_1^2\lambda_f\right)\right].\end{aligned} \tag{D.28}$$

Now the axial part can be done in a similar way to the vector part,

$$\begin{aligned}\Gamma_A &= \int_0^1 \Delta(1-x)^{\frac{1}{2}}M^3\left(1-\frac{\Delta^2}{M^2}x\right)^{\frac{3}{2}}\left[\Delta^2\left|g_1+\frac{\Delta^2}{M^2}x\lambda_g g_1-\frac{\Delta^2 x}{\Delta M}g_2\right|^2\right. \\ &\qquad \left.+2\Delta^2 x\left|g_1+\frac{\Delta^2}{M^2}x\lambda_g g_1-\frac{\Delta}{M}g_2\right|^2\right]\frac{\Delta^2}{M_H^2}dx \\ &= \Delta^5\frac{M^3}{M_H^3}\int_0^1 dx(1-x)^{\frac{1}{2}}\left(1-\frac{3}{2}\delta^2 x\right)\left[g_1^2+2\delta^2 x\lambda_g g_1^2-2\delta x g_1 g_2\right. \\ &\qquad \left.+\delta^2x^2g_1g_2+2xg_1^2+2x\delta^2g_2^2+4\delta x^2g_1^2\lambda_g-4\delta x g_1g_2\right],\end{aligned} \tag{D.29}$$

where we have expanded $(1-\delta^2)^{\frac{3}{2}} \approx 1-\frac{3}{2}\delta^2+\frac{3}{8}\delta^4$ and then neglected terms of higher than $\mathcal{O}(\delta^2)$;

$$\begin{aligned}\Gamma_A &= \Delta^5\frac{M^3}{M_H^3}\int_0^1 dx(1-x)^{\frac{1}{2}}\left[g_1^2-\frac{3}{2}\delta^2 x g_1^2+2\delta^2 x g_1^2\lambda_g-2\delta x g_1g_2\right. \\ &\quad \left.+\delta^2x^2g_2^2+2xg_1^2-3\delta^2x^2g_1^2+2\delta^2g_2^2x+4\delta^2x^2g_1^2\lambda_g-4\delta x g_1g_2\right].\end{aligned} \tag{D.30}$$

We now use the same procedure to write $\frac{M^3}{M_H^3} \approx 8(1-3\delta+6\delta^2)$ and calculate the relevant integrals,

$$\int_0^1 (1-x)^{\frac{1}{2}} = \left[-\frac{2}{3}(1-x)^{\frac{3}{2}}\right]_0^1 = \frac{2}{3}, \tag{D.31}$$

$$\int_0^1 x(1-x)^{\frac{1}{2}} = \int_0^1 (1-x)^{\frac{1}{2}}(1-(1-x)) = \frac{2}{3}+\left[\frac{2}{5}(1-x)^{\frac{5}{2}}\right]_0^1 = \frac{4}{15}, \tag{D.32}$$

and

$$\int_0^1 x^2(1-x)^{\frac{1}{2}} = \int_0^1 (1-x)^{\frac{1}{2}}(1-(1-x))^2 = \frac{2}{3}-\frac{4}{5}-\left[\frac{2}{7}(1-x)^{\frac{7}{2}}\right]_0^1 = \frac{16}{105}, \quad \text{(D.33)}$$

so that the axial part can finally be written as

$$\Gamma_A = \Delta^5 \frac{16}{5}\left[3g_1^2 - \delta(9g_1^2+4g_1g_2) + \delta^2\left(\frac{111}{7}g_1^2 + 12g_1g_2 + \frac{12}{7}g_2^2 + \frac{20}{7}g_1^2\lambda_g\right)\right]. \quad \text{(D.34)}$$

By combining Γ_V and Γ_A the total decay rate at second order in δ can be written down,

$$\begin{aligned}\Gamma =& \frac{G_F^2|V_{us}|^2}{60\pi^3}\Delta^5\left[\left(1-3\delta+\frac{45}{7}\delta^2\right)f_1^2 + 3\left(1-3\delta+\frac{37}{7}\delta^2\right)g_1^2 + \frac{12}{7}\delta^2 f_1 f_2\right. \\ &\left. - (4\delta - 12\delta^2)g_1g_2 + \frac{4}{7}\delta^2 f_2^2 + \frac{12}{7}\delta^2 g_2^2 + \frac{4}{7}\delta^2 f_1^2\lambda_f + \frac{20}{7}\delta^2 g_1^2\lambda_g\right]. \end{aligned} \quad \text{(D.35)}$$

Note that this appears different to the decay rate found by others [101,173] which is due to a different definitions, first of δ which is sometimes given as $\delta' = \Delta/M_H$. Our convention can be related to this by

$$\delta = \frac{1}{2}\delta' + \frac{1}{4}\delta'^2 + \mathcal{O}(\delta'^3). \quad \text{(D.36)}$$

Secondly, keeping the primed notation for the other convention we note that

$$\frac{f_2}{M} = \frac{f_2'}{M_H}. \quad \text{(D.37)}$$

To recover Equations 8.4 and 8.5 one must set $g_2 = 0$ and, for the former, discard terms of higher than $\mathcal{O}(\delta)$, which will be smaller than leading order terms.

Bibliography

[1] W. N. Cottingham and D. A. Greenwood. *An Introduction to the Standard Model of Particle Physics*. Cambridge University Press, 2 edition, 2007.

[2] Atlas Collaboration (G. Aad et al.). Observation of a new particle in the search for the Standard Model Higgs boson with the ATLAS detector at the LHC. *Phys. Lett. B*, 716:1, 2012. [arXiv:1207.7214 [hep-ex]].

[3] CMS Collaboration (S. Chatrchyan et al.). Observation of a new particle in the search for the Standard Model Higgs boson with the ATLAS detector at the LHC. *Phys. Lett. B*, 716:30, 2012. [arXiv:1207.7235 [hep-ex]].

[4] Particle Data Group (J. Beringer et al.). Review of particle physics. *Phys. Rev. D*, 86:010001, 2012.

[5] M. Gell-Mann. A schematic model of baryons and mesons. *Phys. Lett.*, 8:214–215, 1964.

[6] G. Zweig. An SU(3) model for strong interaction symmetry and its breaking. *CERN-TH-401 (Developments in the Quark Theory of Hadrons)*, 1:22–101, 1964.

[7] E. D. Bloom et al. High-energy inelastic $e - p$ scattering at 6° and 10°. *Phys. Rev. Lett.*, 23:930–934, 1969.

[8] M. Breidenbach et al. Observed behavior of highly inelastic electron-proton scattering. *Phys. Rev. Lett.*, 23:935–939, Oct 1969.

[9] O. W. Greenberg. Spin and unitary-spin independence in a paraquark model of baryons and mesons. *Phys. Rev. Lett.*, 13:598–602, 1964.

[10] LHCb collaboration (R. Aaij et al.). Observation of the resonant character of the $Z(4430)^-$ state. *Phys. Rev. Lett.*, 112:222002, 2014. [arXiv:1404.1903 [hep-ex]].

[11] D. Gross and F. Wilczek. Asymptotically Free Guage Theories. *Phys. Rev. D.*, 8:3633–3652, 1973.

[12] H. D. Politzer. Reliable Perturbative Results for Strong Interactions? *Phys. Rev. Lett.*, 30:1346–1349, 1973.

[13] R. D. Peccei. The Strong CP problem and axions. *Lect. Notes Phys.*, 741:3–17, 2008. [arXiv:hep-ph/0607268].

[14] R. P. Feynman. Space-time approach to non-relativistic quantum mechanics. *Rev. Mod. Phys.*, 20:367–387, 1948.

[15] J. J. de Swart. The octet model and its Clebsch-Gordan coefficients. *Rev. Mod. Phys.*, 35:916–939, 1963.

[16] G. D. Rochester and C. C. Butler. Evidence for the existence of new unstable elementary particles. *Nature*, 160:855–857, 1947.

[17] M. Gell-Mann and Y. Ne'eman. *The Eightfold Way.* Westview Press, 1 edition, 2000.

[18] K. G. Wilson. Confinement of quarks. *Phys. Rev. D*, 10:24452459, 1974.

[19] H. J. Rothe. *Lattice Guage Theories: An Introduction.* World Scientific Lecture Notes in Physics - Vol. 74, 3 edition, 2005.

[20] C. Gattringer and C. B. Lang. *Quantum Chromodynamics on the Lattice.* Springer, 1 edition, 2010.

[21] I. Montvay and G. Münster. *Quantum Fields on a Lattice.* Cambridge University Press, 1 edition, 1994.

[22] J. W. Negele, H. W. Griesshammer, and D. Lehmann. *Lectures on QCD: Foundations - Lattice Guage Theory and the structure of the vacuum and hadrons*. Springer, 1 edition, 1997.

[23] H. B. Nielsen and M. Ninomiya. Absence of neutrinos on a lattice. 1. proof by homotopy theory. *Nucl. Phys. B*, 185:20–40, 1981.

[24] D. Friedan. A proof of the Nielsen-Ninomiya theorem. *Commun. Math. Phys.*, 85:481–490, 1982.

[25] F. Niedermayer. Exact chiral symmetry, topological charge and related topics. *Nucl. Phys. Proc. Suppl.*, 73:105–119, 1999. [arXiv:hep-lat/9810026].

[26] L. Susskind. Lattice fermions. *Phys. Rev. D*, 16:3031–3039, 1977.

[27] P. H. Ginsparg and K. G. Wilson. A remnant of chiral symmetry on the lattice. *Phys. Rev. D*, 25:2649–2657, 1982.

[28] K. Symanzik. Continuum limit and improved action in lattice theories. 1. principles and ϕ^4 theory. *Nucl. Phys. B*, 226:187, 1983.

[29] K. Symanzik. Continuum limit and improved action in lattice theories. 2. $O(N)$ non-linear sigma model in perturbation theory. *Nucl. Phys. B*, 226:205, 1983.

[30] B. Sheikholeslami and R. Wohlert. Improved continuum limit lattice action for QCD with Wilson fermions. *Nucl. Phys. B*, 259:572, 1985.

[31] N. Cundy et al. Clover improvement for stout-smeared 2 + 1 flavour SLiNC fermions: Non-perturbative results. *PoS*, LATTICE2008:132, 2008. [arXiv:0811.2355 [hep-lat]].

[32] M. Lüscher and P. Weisz. On-shell improved lattice gauge theories. *Commun. Math. Phys.*, 97:59, 1985.

[33] M. Creutz. *Quarks, Gluons and Lattices*. Cambridge University Press, 1 edition, 1983.

[34] M. Creutz. Overrelaxation and Monte Carlo simulations. *Phys. Rev. D*, 36:515–519, 1987. [arXiv:hep-lat/9507010].

[35] S. Duane et al. Hybrid Monte Carlo. *Phys. Lett. B*, 195:216–222, 1987.

[36] M. A. Clark. The Rational Hybrid Monte Carlo Algorithm. *PoS*, LAT2006:004, 2006. [arXiv:hep-lat/0610048].

[37] P. F. Bedaque. Aharonov-Bohm effect and nucleon nucleon phase shifts on the lattice. *Phys. Lett. B*, 593:82–88, 2004. [arXiv:nucl-th/0402051].

[38] G. M. de Divitiis, R. Petronzio, and N. Tantalo. On the discretization of physical momenta in lattice QCD. *Phys. Lett. B*, 595:408–413, 2004. [arXiv:hep-lat/0405002].

[39] C. T. Sachrajda and G. Villadoro. Twisted boundary conditions in lattice simulations. *Phys. Lett. B*, 609:73–85, 2005. [arXiv:hep-lat/0411033].

[40] J. M. Flynn et al. Partially twisted boundary conditions in lattice simulations. *PoS*, LAT2005:352, 2006. [arXiv:hep-lat/0509093].

[41] J. M. Flynn, A. Juttner, and C. T. Sachrajda. A numerical study of partially twisted boundary conditions. *Phys. Lett. B*, 632:313–318, 2006. [arXiv:hep-lat/0506016].

[42] S. Durr et al. Lattice QCD at the physical point: light quark masses. *Phys. Lett. B*, 701:265–268, 2011. [arXiv:1011.2403 [hep-lat]].

[43] G. S. Bali et al. $\langle x \rangle_{u-d}$ from lattice QCD at nearly physical quark masses. *Phys. Rev. D*, 86:054504, 2012. [arXiv:1207.1110 [hep-lat]].

[44] M. Göckeler et al. A lattice determination of moments of unpolarised nucleon structure functions using improved Wilson fermions. *Phys. Rev. D*, 71:114511, 2005. [arXiv:hep-ph/0410187].

[45] M. Göckeler et al. A Lattice study of the spin structure of the Lambda hyperon. *Phys. Lett. B*, 545:112–118, 2002. [arXiv:hep-lat/0208017].

[46] K. Bitar et al. The QCD finite temperature transition and hybrid Monte Carlo. *Nucl. Phys. B*, 313:348–376, 1989.

[47] M. Göckeler et al. Hyperon Form Factors from $N_f = 2 + 1$ QCD. *PoS*, LATTICE2010:165, 2010. [arXiv:1101.2806 [hep-lat]].

[48] C. Morningstar and M. J. Peardon. Analytic smearing of SU(3) link variables in lattice QCD. *Phys. Rev. D*, 69:054501, 2004. [arXiv:hep-lat/0311018].

[49] N. Cundy et al. Non-perturbative improvement of stout-smeared three flavour clover fermions. *Phys. Rev. D*, 79:094507, 2009. [arXiv:0901.3302 [hep-lat]].

[50] W. Bietenholz et al. Results from $2 + 1$ flavours of SLiNC fermions. *PoS*, LAT2009:102, 2009. [arXiv:0910.2963 [hep-lat]].

[51] T. Bhattacharya et al. Improved bilinears in lattice QCD with non-degenerate quarks. *Phys. Rev. D*, 73:034504, 2006. [arXiv:hep-lat/0511014].

[52] W. Bietenholz et al. Flavour blindness and patterns of flavour symmetry breaking in lattice simulations of up, down and strange quarks. *Phys. Rev. D*, 84:054509, 2011. [arXiv:1102.5300 [hep-lat]].

[53] C. R. Allton et al. Gauge invariant smearing and matrix correlators using Wilson fermions at Beta = 6.2. *Phys. Rev. D*, 47:5128–5137, 1993. [arXiv:hep-lat/9303009].

[54] C. Best et al. Pion and rho structure functions from lattice QCD. *Phys. Rev. D*, 56:2743–2754, 1997. [arXiv:hep-lat/9703014].

[55] P. A. Boyle et al. Hadronic form factors in Lattice QCD at small and vanishing momentum transfer. *JHEP*, 0705:016, 2007. [arXiv:hep-lat/0703005].

[56] P. A. Boyle et al. The kaon semileptonic form factor with near physical domain wall quarks. *JHEP*, 1308:132, 2013. [arXiv:1305.7217 [hep-lat]].

[57] F. J. Jiang and B. C. Tiburzi. Flavor Twisted Boundary Conditions and the Nucleon Vector Current. *Phys. Rev. D*, 78:114505, 2008. [arXiv:0810.1495 [hep-lat]].

[58] P. A. Boyle et al. The Pion's electromagnetic form-factor at small momentum transfer in full lattice QCD. *JHEP*, 0807:112, 2008. [arXiv:0804.3971 [hep-lat]].

[59] M. Göckeler et al. Perturbative and Nonperturbative Renormalization in Lattice QCD. *Phys. Rev. D*, 82:114511, 2010. [arXiv:1003.5756 [hep-lat]].

[60] G. Martinelli et al. A general method for non-perturbative renormalization of lattice operators. *Nucl. Phys. B*, 445:81–105, 1995. [arXiv:hep-lat/9411010].

[61] M. Luscher et al. The Schrödinger functional: A Renormalizable probe for non-Abelian gauge theories. *Nucl. Phys. B*, 384:168–228, 1992. [arXiv:hep-lat/9207009].

[62] R. G. Edwards B. Joo. The Chroma software system for lattice QCD. *Nucl. Phys. Proc. Suppl.*, 140:832, 2005. [arXiv:hep-lat/0409003].

[63] C. McClendon. Optimized Lattice QCD Kernels for a Pentium 4 cluster. *Jlab preprint*, JLAB-THY-01-29, 2001. `http://www.jlab.org/~edwards/qcdapi/reports/dslash_p4.pdf`.

[64] P. A. Boyle. The BAGEL assembler generation library. *Comp. Phys. Comm*, 180:2739, 2009.

[65] C. S. Wu et al. Experimental test of parity conservation in beta decay. *Phys. Rev.*, 105:1413–1415, 1957.

[66] J. H. Christenson et al. Evidence for the 2π Decay of the K_2^0 Meson. *Phys. Rev. Lett.*, 13:138–140, 1964.

[67] E. Fermi. Versuch einer Theorie der B-Strahlen. I. *Zeitschrift für Physik*, 88, issue 3-4:161–177, 1934.

[68] S. L. Glashow, J. Iliopoulos, and L. Maiani. Weak Interactions with Lepton-Hadron Symmetry. *Phys. Rev. D*, 2:12851292, 1970.

[69] J. J. Aubert et al. Experimental Observation of a Heavy Particle J. *Phys. Rev. Lett.*, 33:1404–1406, 1974.

[70] J. E. Augustin et al. Discovery of a Narrow Resonance in e^+e^- Annihilation. *Phys. Rev. Lett.*, 33:1406–1408, 1974.

[71] R. P. Feynman and M. Gell-Mann. Theory of the Fermi Interaction. *Phys. Rev.*, 109:193–198, 1958.

[72] E. C. G. Sudarshan and R. E. Marshak. Chirality Invariance and the Universal Fermi Interaction. *Phys. Rev.*, 109:1860–1862, 1958.

[73] P. Langacker. *The Standard Model and Beyond*. Taylor and Francis, 1 edition, 2009.

[74] R. Flores-Mendieta, E. Jenkins, and A. V. Manohar. SU(3) symmetry breaking in hyperon semileptonic decays. *Phys. Rev. D*, 58:094028, 1998. [arXiv:hep-ph/9805416].

[75] N. Cabibbo. Unitary symmetry and leptonic decays. *Phys. Rev. Lett.*, 10:531–533, 1963.

[76] E. Blucher et al. Status of the cabibbo angle. In *3rd Workshop on the Unitarity Triangle : CKM 2005*, 2005.

[77] M. Kobayashi and T. Maskawa. CP-violation in the renormalizable theory of weak interaction. *Prog. Theor. Phys.*, 49(2):652–657, 1973.

[78] E. Blucher and W. J. Marciano. V_{ud}, V_{us}, the Cabibbo angle and CKM unitarity. *PDG*, 2012.

[79] A. Ceccucci, Z. Ligeti, and Y. Sakai. The CKM quark-mixing matrix. *PDG*, 2012.

[80] L. Wolfenstein. Parametrization of the Kobayashi Maskawa matrix. *Phys. Rev. Lett.*, 51(1):1945–1947, 1983.

[81] C. Jarlskog. Matrix Representation of Symmetries in Flavor Space, Invariant Functions of Mass Matrices and Applications. *Phys. Rev. D*, 35:1685, 1987.

[82] CKMfitter Group (J. Charles et al.). CP Violation and the CKM Matrix: Assessing the Impact of the Asymmetric B Factories. *Eur. Phys. J.*, C41:1–131, 2005. arXiv:[hep-ph/0406184], updated results and plots available at: `http://ckmfitter.in2p3.fr`.

[83] S. Boinepalli et al. Precision Electromagnetic Structure of Octet Baryons in the Chiral Regime. *Phys. Rev. D.*, 74:093005, 2006. [arXiv:hep-lat/0604022].

[84] H-W. Linn and K. Orginos. Strange Baryon Electromagnetic Form Factors and $SU(3)$ Flavor Symmetry Breaking. *Phys. Rev. D*, 79:074507, 2009. [arXiv:0812.4456 [hep-lat]].

[85] H-W. Linn and K. Orginos. First Calculation of Hyperon Axial Couplings from Lattice QCD. *Phys. Rev. D*, 79:034507, 2009. arXiv:0712.1214 [hep-lat].

[86] G. Engel. Baryon axial charges from chirally improved fermions - first results. *PoS*, LAT2009:135, 2009. arXiv:0910.4190 [hep-lat].

[87] P. A. Boyle et al. K_{l3} semileptonic form factor from $2+1$ avor lattice QCD. *Phys. Rev. Lett*, 100:141601, 2008. [arXiv:0710.5136 [hep-lat]].

[88] N. Cabibbo, E. C. Swallow, and R. Winston. Semileptonic hyperon decays and CKM unitarity. *Phys. Rev. Lett.*, 92:251803, 2004. [arXiv:hep-ph/0307214].

[89] A. Walker-Loud. Octet baryon masses in partially quenched chiral perturbation theory. *Nucl. Phys. A*, 747:476–507, 2005. [arXiv:hep-lat/0405007].

[90] H-C. Kim et al. Semileptonic decay constants of octet baryons in the chiral quark-soliton model. *Phys.Rev. D*, 57:299–307, 1998. [arXiv:hep-ph/9709221].

[91] V. Linke. Leptonic decays of polarised baryons. *Nucl. Phys. B*, 12:669–693, 1969.

[92] H. Leutwyler and M. Roos. Determination of the Elements v_{us} and v_{ud} of the Kobayashi-Maskawa Matrix. *Z. Phys. C*, 25:91–101, 1984.

[93] S. Weinberg. Charge Symmetry of Weak Interactions. *Phys. Rev.*, 112:1375–1379, 1958.

[94] J-M. Gaillard and G. Sauvage. Hyperon Beta Decays. *Ann. Rev. Nucl. Part. Sci.*, 34, 1984.

[95] S. Eliezer and P. Singer. Second-class vector currents and scalar mesons. *Il Nuovo Cimento A Series 11*, 4(3):638–646, 1971.

[96] L. Wolfenstein and E. M. Henley. Second class currents and mirror beta decays. *Phys. Lett. B*, 36(1):28 – 31, 1971.

[97] S. Sasaki and T. Yamazaki. Lattice study of flavor $SU(3)$ breaking in hyperon beta decay. *Phys. Rev. D*, 79:074508, 2009. [arXiv:0811.1406 [hep-lat]].

[98] D. Guadagnoli et al. First lattice QCD study of the $\Sigma^- \to n$ axial and vector form factors with SU(3) breaking corrections. *Nucl. Phys. B*, 761:63, 2007. [arXiv:hep-ph/0606181].

[99] N. Solomey. Importance of Future Hyperon Beta Decay Experiments. [arXiv:hep-ex/0011074].

[100] K.-S. Choi, W. Plessas, and R. F. Wagenbrunn. Axial charges of octet and decuplet baryons. *Phys. Rev. D*, 82, 2010. [arXiv:1005.0337 [hep-ph]].

[101] N. Cabibbo, E. C. Swallow, and R. Winston. Semileptonic hyperon decays. *Ann. Rev. Nucl. Part. Sci.*, 53:39–75, 2003. [arXiv:hep-ph/0307298].

[102] M. Ademollo and R. Gatto. Nonrenormalization Theorem for the Strangeness-Violating Vector Currents. *Phys. Rev. Lett.*, 13:264–266, 1964.

[103] R. E. Behrends and A. Sirlin. Effect of mass splittings on the conserved vector current. *Phys. Rev. Lett.*, 4:186–187, 1960.

[104] J. Anderson and M. A. Luty. Chiral corrections to hyperon vector form-factors. *Phys. Rev. D*, 47:4975–4980, 1993. [arXiv:hep-ph/9301219].

[105] D. Bećirević, G. Martinelli, and G. Villadoro. The Ademollo-Gatto theorem for lattice semileptonic decays. *Phys. Lett. B*, 633:84–88, 2006. [arXiv:hep-lat/0508013].

[106] V. Mateu and A. Pich. V_{us} determination from hyperon semileptonic decays. *JHEP*, 10:041, 2005. [arXiv:hep-ph/0509045].

[107] A. Sirlin. A class of first-order $SU(3)$ theorems and their possible application to the analysis of the semileptonic decays of the baryon octet. *Nucl. Phys. B*, 161:301–310, 1979.

[108] F. Schlumpf. Beta decay of hyperons in a relativistic quark model. *Phys. Rev. D*, 51:2262–2270, 1995. [arXiv:hep-ph/9409272].

[109] H. Dahiya et al. Semi-leptonic Octet Baryon Weak Axial-Vector Form Factors in the Chiral Constitutent Quark Model. *AIP Conf.Proc.*, 1149:361–364, 2009. [arXiv:0812.3735 [hep-ph]].

[110] S. N. Syritsyn et al. Nucleon Electromagnetic Form Factors from Lattice QCD using $2+1$ Flavor Domain Wall Fermions on Fine Lattices and Chiral Perturbation Theory. *Phys. Rev. D*, 81:034507, 2010. [arXiv:0907.4194 [hep-lat]].

[111] M. Göckeler et al. Baryon Axial Charges and Momentum Fractions with $N_f = 2 + 1$ Dynamical Fermions. *PoS*, LATTICE2010:163, 2010. [arXiv:1102.3407 [hep-lat]].

[112] European Muon Collaboration (J. Ashman et al.). A measurement of the spin asymmetry and determination of the structure function g_1 in deep inelastic muon-proton scattering. *Phys. Lett. B*, 206:364–370, 1988.

[113] C. A. Aidala et al. The spin structure of the nucleon. *Rev. Mod. Phys.*, 85:655–691, 2013.

[114] M. Göckeler et al. A Lattice study of the spin structure of the Lambda hyperon. *Phys. Lett. B*, 545:112–118, 2002. [arXiv:hep-lat/0208017].

[115] Bristol - Geneva - Heidelberg - Orsay - Rutherford - Strasbourg Collaboration (M. Bourquin et al.). Measurements of hyperon semileptonic decays at the CERN super proton synchrotron. 2. the $\Lambda \to pe^-\bar{\nu}$, $\Xi^- \to \Lambda e^-\bar{\nu}$, and $\Xi^- \to \Sigma^0 e^-\bar{\nu}$ decay modes. *Z. Phys. C*, 21:1, 1983.

[116] S. Y. Hsueh et al. A high precision measurement of polarized-Σ^- beta decay. *Phys. Rev. D*, 38:2056, 1988.

[117] KTeV Collaboration (A. Alavi-Harati et al.). First measurement of form-factors of the decay $\Xi^0 \to \Sigma^+ e^-\bar{\nu}$. *Phys. Rev. Lett.*, 87:132001, 2001. [arXiv:hep-ex/0105016].

[118] O. Naviliat-Cuncic and M. Gonzlez-Alonso. Prospects for precision measurements in nuclear beta decay at the LHC era. *Annalen Phys.*, 525(8-9):600–619, 2013. [arXiv:1304.1759 [hep-lat]].

[119] S. Sasaki. Hyperon vector form factor from $2+1$ flavor lattice QCD. *Phys. Rev. D*, 86:114502, 2012. [arXiv:1209.6115 [hep-lat]].

[120] G. Martinelli and C. T. Sachrajda. A Lattice Study of Nucleon Structure. *Nucl. Phys. B*, 316:355, 1989.

[121] W. Wilcox, T. Draper, and K-F. Liu. Chiral limit of nucleon lattice electromagnetic form-factors. *Phys. Rev. D*, 46:1109–1122, 1992. [arXiv:hep-lat/9205015].

[122] K-F. Liu et al. Nucleon axial form-factor from lattice QCD. *Phys. Rev. D*, 49:4755–4761, 1994. [arXiv:hep-lat/9305025].

[123] S. Collins et al. Dirac and pauli form factors from lattice QCD. *Phys. Rev. D*, 84:074507, 2011. [arXiv:1106.3580 [hep-lat]].

[124] S. Capitani et al. Nucleon axial charge in lattice QCD with controlled errors. *Phys. Rev. D*, 86:074502, 2012. [arXiv:1205.0180 [hep-lat]].

[125] H-W. Lin et al. Nucleon structure with two flavors of dynamical domain-wall fermions. *Phys. Rev. D*, 78:014505, 2008. [arXiv:0802.0863 [hep-lat]].

[126] T. Yamazaki et al. Nucleon form factors with 2+1 flavor dynamical domain-wall fermions. *Phys. Rev. D*, 79:114505, 2009. [arXiv:0904.2039 [hep-lat]].

[127] J. D. Bratt et al. Nucleon structure from mixed action calculations using $2+1$ flavors of asqtad sea and domain wall valence fermions. *Phys. Rev. D*, 82:094502, 2010. [arXiv:1001.3620 [hep-lat]].

[128] C. Alexandrou et al. Axial nucleon form factors from lattice QCD. *Phys. Rev. D*, 83:045010, 2011. [arXiv:1012.0857 [hep-lat]].

[129] S. Sasaki and T. Yamazaki. Nucleon form factors from quenched lattice QCD with domain wall fermions. *Phys. Rev. D*, 78:014510, 2008. [arXiv:0709.3150 [hep-lat]].

[130] J. J. Kelly. Simple parametrization of nucleon form factors. *Phys. Rev. C*, 70:068202, 2004.

[131] P. E. Shanahan et al. Magnetic form factors of the octet baryons from lattice QCD and chiral extrapolation. *Phys. Rev. D*, 89:074511, 2014. [arXiv:1401.5862 [hep-lat]].

[132] T. Bhattacharya et al. Nucleon Charges and Electromagnetic Form Factors from 2 + 1 + 1-Flavor Lattice QCD. *Phys. Rev. D*, 89:094502, 2014. [arXiv:1306.5435 [hep-lat]].

[133] M. J. Savage and J. Walden. SU(3) breaking in neutral current axial matrix elements and the spin content of the nucleon. *Phys. Rev. D*, 55:5376, 1997. [arXiv:hep-ph/9611210].

[134] P. E. Shanahan et al. Octet Spin Fractions and the Proton Spin Problem. *Phys. Rev. Lett.*, 110(20):202001, 2013. [arXiv:1302.6300 [nucl-th]].

[135] G. S. Bali et al. Strangeness Contribution to the Proton Spin from Lattice QCD. *Phys.Rev.Lett.*, 108:222001, 2012. [arXiv:1112.3354 [hep-lat]].

[136] R. Babich et al. Exploring strange nucleon form factors on the lattice. *Phys. Rev. D*, 85:054510, 2012. [arXiv:1012.0562 [hep-lat]].

[137] ATLAS Collaboration (G. Aad et al.). Determination of the strange quark density of the proton from ATLAS measurements of the $W \to l\nu$ and $Z \to ll$ cross sections. *Phys. Rev. Lett.*, 109:012001, 2012. [arXiv:1203.4051 [hep-ex]].

[138] R. D. Ball et al. Parton distributions with LHC data. *Nucl. Phys. B*, 867:244–289, 2013. [arXiv:1207.1303 [hep-ph]].

[139] N. Hartland. LHC data and the proton strangeness. 2012. [arXiv:1205.3508 [hep-ph]].

[140] D. Ashery and H. J. Lipkin. Expected polarization of Lambda particles produced in deep inelastic polarized lepton scattering. *Phys. Lett. B*, 469:263–269, 1999. [arXiv:hep-ph/9908355].

[141] A. J. Chambers et al. A Feynman-Hellmann approach to the spin structure of hadrons. 2014. [arXiv:1405.3019 [hep=lat]].

[142] P. E. Shanahan, A. W. Thomas, and R. D. Young. Chiral expansion of moments of quark distributions. *Phys. Rev. D*, 87(11):114515, 2013. [arXiv:1301.6861 [nucl-th]].

[143] T. Yamanishi. F and D values with explicit flavor symmetry breaking and Δs contents of nucleons. *Phys. Rev. D*, 76:014006, 2007. [arXiv:0705.4340 [hep-ph]].

[144] A. Ali Khan et al. Axial coupling constant of the nucleon for two flavours of dynamical quarks in finite and infinite volume. *Phys. Rev.*, D74:094508, 2006. [arXiv:hep-lat/0603028].

[145] U. Mosel. *Fields, Symmetries, and Quarks*. Springer, 2 edition, 1999.

[146] S. Okubo. Note on Unitary Symmetry in Strong Interactions. *Prog. Theor. Phys.*, 27:5, 1962.

[147] A. N. Cooke et al. The effects of flavour symmetry breaking on hadron matrix elements. *PoS*, LATTICE2012:116, 2012. [arXiv:1212.2564 [hep-lat]].

[148] A. N. Cooke et al. SU(3) flavour breaking and baryon structure. *PoS*, LATTICE2013:278, 2013. [arXiv:1311.4916 [hep-lat]].

[149] P. E. L. Rakow. Private communication.

[150] Wolfram Research Inc. *Mathematica, Version 8.0.* Champaign, Illinois, 2010.

[151] S. Sasaki et al. Nucleon axial charge from quenched lattice QCD with domain wall fermions. *Phys. Rev. D*, 68:054509, 2003. [arXiv:hep-lat/0306007].

[152] P. G. Ratcliffe. SU(3) breaking in hyperon beta decays: A prediction for $\Xi^0 \to \Sigma^+ e^- \bar{\nu}$. *Phys. Rev. D*, 59:014038, 1998.

[153] T. N. Pham. Test of SU(3) Symmetry in Hyperon Semileptonic Decays. *Phys. Rev. D*, 87:016002, 2013. [arXiv:1210.3981 [hep-ex]].

[154] R. Flores-Mendieta, A. Garcia, and G. Sanchez-Colon. Determination of the Kobayashi-Maskawa-Cabibbo matrix element V_{us} under various flavor symmetry breaking models in hyperon semileptonic decays. *Phys. Rev. D*, 54:6855–6860, 1996. [arXiv:hep-ph/9603256].

[155] J. F. Donoghue, B. R. Holstein, and S. W. Klimt. Kobayashi-Maskawa angles and SU(3) breaking in hyperon beta decay. *Phys. Rev. D*, 35:934–938, 1987.

[156] J. C. Hardy and I. S. Towner. New limit on fundamental weak-interaction parameters from superallowed beta decay. *Phys.Rev.Lett.*, 94:092502, 2005. [arXiv:nucl-th/0412050].

[157] A. Czarnecki, W. J. Marciano, and A. Sirlin. Precision measurements and CKM unitarity. *Phys. Rev. D*, 70:093006, 2004. [arXiv:hep-ph/0406324].

[158] W. J. Marciano and A. Sirlin. Improved calculation of electroweak radiative corrections and the value of $|V_{ud}|$. *Phys. Rev. Lett.*, 96:032002, 2006. [arXiv:hep-ph/0510099].

[159] H. Liang, N. V. Giai, and J. Meng. Isospin corrections for superallowed Fermi beta decay in self-consistent relativistic random-phase approximation approaches. *Phys. Rev. C*, 79:064316, 2009.

[160] G. A. Miller and A. Schwenk. Isospin-symmetry-breaking corrections to superallowed Fermi beta decay: Formalism and schematic models. *Phys. Rev. C*, 78:035501, 2008. [arXiv:0805.0603 [nucl-th]].

[161] A. Bornheim et al. Improved measurement of $|V_{ub}|$ with inclusive semileptonic B decays. *Phys. Rev. Lett.*, 88:231803, 2002. [arXiv:hep-ex/0202019].

[162] BaBar Collaboration (B. Aubert et al.). Measurements of Charged Current Lepton Universality and $|V_{us}|$ using Tau Lepton Decays to $e^-\bar{\nu}_e\nu_\tau$, $\mu^-\bar{\nu}_\mu\nu_\tau$, $\pi^-\nu_\tau$ and $K^-\nu_\tau$. *Phys. Rev. Lett.*, 105:051602, 2010. [arXiv:0912.0242 [hep-ex]].

[163] KLOE Collaboration (F. Ambrosino et al.). Measurement of the K_L meson lifetime with the KLOE detector. *Phys. Lett. B*, 626:15–23, 2005. [arXiv:hep-ex/0507088].

[164] M. Antonelli et al. An Evaluation of V_{us} and precise tests of the Standard Model from world data on leptonic and semileptonic kaon decays. *Eur. Phys. J.*, C69:399–424, 2010. [arXiv:1005.2323[hep-ph]].

[165] P. A. Boyle et al. $K \to \pi$ form factors with reduced model dependence. *Eur. Phys. J.*, C69:159–167, 2010. [arXiv:1004.0886 [hep-lat]].

[166] S. Aoki et al. Review of lattice results concerning low energy particle physics. 2013. [arXiv:1310.8555 [hep-lat]].

[167] V. Cirigliano and H. Neufeld. A note on isospin violation in $P_{l2(\gamma)}$ decays. *Phys. Lett. B*, 700:7–10, 2011. [arXiv:1102.0563 [hep-ph]].

[168] W. J. Marciano. Precise determination of $|V_{us}|$ from lattice calculations of pseudoscalar decay constants. *Phys. Rev. Lett.*, 93:231803, 2004. [arXiv:hep-ph/0402299].

[169] I. M. Nugent. Determination of $|V_{us}|$ from tau Decays. 2013. [arXiv:1301.0637 [hep-ex]].

[170] E. Gamiz. $|V_us|$ from hadronic τ decays. 2013. [arXiv:1301.2206 [hep-ph]].

[171] E. Gamiz et al. $|V_{us}|$ and m_s from hadronic τ decays. *Nucl. Phys. Proc. Suppl.*, 169:85–89, 2007. [arXiv:hep-ph/0612154].

[172] E. Gamiz et al. Determination of m_s and $|V_{us}|$ from hadronic τ decays. *JHEP*, 0301:060, 2003. [arXiv:hep-ph/0212230].

[173] A. Garcia and P. Kielanowski. *The Beta Decay of Hyperons - Lecture Notes in Physics Vol. 222*. Springer-Verlag, 1985.

[174] D. Chang. Challenges in hyperon decays. 2000. [arXiv:hep-ph/0011163].

[175] A. Garcia and P. Kielanowski. Cabibbo theory and hyperon semileptonic decays. *Phys. Rev. D*, 26:1090–1102, 1982.

[176] A. Sirlin and A. Ferroglia. Radiative Corrections in Precision Electroweak Physics: a Historical Perspective. *Rev. Mod. Phys.*, 85(1):263297, 2013. [arXiv:1210.5296 [hep-ph]].

[177] I. Bender, V. Linke, and H.J. Rothe. Leptonic decays of baryons. *Z. Phys.*, 212(2):190–212, 1968.

[178] R. Flores-Mendieta. V_{us} from hyperon semileptonic decays. *Phys. Rev. D.*, 70:114036, 2004. [arXiv:hep-ph/0410171].

[179] N. Sharma, H. Dahiya, and P. K. Chatley. Extraction of the CKM matrix element V_{us} from the hyperon semileptonic decays. *Eur. Phys. J.*, A44:125–128, 2010.

[180] A. Sirlin. General Properties of the Electromagnetic Corrections to the Beta Decay of a Physical Nucleon. *Phys. Rev.*, 164:1767, 1967.

[181] Felix Schlumpf. Relativistic constituent quark model for baryons. 1992. [arXiv:hep-ph/9211255].

[182] A. Sirlin. Radiative Corrections in the $SU(2)_L \times U(1)$ theory: A simple renormalization framework. *Phys. Rev. D.*, 22(4):971981, 1980.

[183] A. Garcia. Electromagnetic corrections to the semileptonic decays of polarized neutral and charged hyperons. *Phys. Rev. D*, 25:1348–1354, 1982.

[184] Bristol - Geneva - Heidelberg - Orsay - Rutherford - Strasbourg Collaboration (M. Bourquin et al.). Measurements of Hyperon Semileptonic Decays at the CERN Super Proton Synchrotron. 4. Tests of the Cabibbo Model. *Z. Phys. C*, 21:27, 1983.

[185] K. Toth, K. Szego, and T. Margaritisz. Radiative Corrections for Semileptonic Decays of Hyperons: The 'Model Independent' Part. *Phys. Rev. D*, 33:3306, 1986.

[186] V. Mateu. Private communication.

[187] J. Lach and L. G. Pondrom. Hyperon beam physics. *Annu. Rev. Nucl. Part. Sci.*, 29:203, 1979.

[188] S. Sasaki. Status of Semileptonic Hyperon Decays from Lattice QCD using $2 + 1$ flavour Domain Wall Fermions. *PoS*, LATTICE2013:388, 2013.

[189] KTeV Collaboration (A. Affolder et al.). Observation of the decay $\Xi \to \Sigma$. *Phys. Rev. Lett.*, 82:3751–3754, 1999.

[190] R. Horsley et al. Nucleon axial charge and pion decay constant from two-flavor lattice QCD. *Phys. Lett. B*, 732:41–48, 2014. [arXiv:1302.2233 [hep-lat]].

[191] W. Pfeifer. *The Lie Algebras SU(N): An Introduction*. Birkhäuser Verlag AG, 1 edition, 2003.

[192] J. D. Jackson and D.R. Tovey. *Particle Physics Booklet - Kinematics*. Particle Data Group, 2012.

[193] D. Griffiths. *Introduction to Elementary Particles*. Wiley-VCH, 2 edition, 2008.

Glossary

BNL	Brookhaven National Laboratory.
BSM	beyond the standard model.
CERN	European Organization for Nuclear Research.
CKM	Cabibbo-Kobayashi-Maskawa.
CP	Charge Parity.
CVC	generalised conserved vector current.
EMC	European Muon Collaboration.
FCNC	Flavour Changing Neutral Current.
GIM	Glashow-Iliopoulos-Maiani.
HSL	hyperon semi-leptonic.
IVB	intermediate vector boson theory.
LHC	Large Hadron Collider.
LQCD	Lattice QCD.

PDG Particle Data Group.

QCD Quantum Chromodynamics.

QED Quantum Electrodynamics.

QFT Quantum Field Theory.

SLAC Stanford Linear Accelerator Center.

SM Standard Model.